Nonreciprocal Vibration Transmission in Discrete Periodic Systems with Spatiotemporal Modulations

Jiuda Wu

A Thesis

In the Department of

Mechanical, Industrial and Aerospace Engineering

Presented in Partial Fulfillment of the Requirements

For the Degree of

Doctor of Philosophy (Mechanical Engineering) at

Concordia University

Montreal, Quebec, Canada

March 2025

CONCORDIA UNIVERSITY
SCHOOL OF GRADUATE STUDIES

This is to certify that the thesis

prepared By: Jiuda Wu

Entitled: Nonreciprocal Vibration Transmission in Discrete Periodic Systems with Spatiotemporal Modulations

and submitted in partial fulfillment of the requirements for the degree of

DOCTOR OF PHILOSOPHY (Mechanical Engineering)

complies with the regulations of the University and meets the accepted standards with respect to originality and quality.

Signed by the final examining committee:

______________________________ Chair
Dr. Pawel Gora

______________________________ External Examiner
Dr. Kefu Liu

______________________________ Arm's Length Examiner
Dr. Pablo Bianucci

______________________________ Examiner
Dr. Ramin Sedaghati

______________________________ Examiner
Dr. Subhash Rakheja

______________________________ Thesis Supervisor
Dr. Behrooz Yousefzadeh

Approved by ______________________________
Dr. Ramin Sedaghati, Graduate Program Director

March 25, 2025 ______________________________
Dr. Mourad Debbabi
Dean, Gina Cody School of Engineering and Computer Science

Abstract

Nonreciprocal Vibration Transmission in Discrete Periodic Systems with Spatiotemporal Modulations

Jiuda Wu, Ph.D.
Concordia University, 2025

Materials with time-varying properties enable direction-dependent vibration transmission, meaning that interchanging the source and receiver changes transmission characteristics such as amplitude, phase, or wave speed, resulting in nonreciprocal behavior. While unidirectional transmission in long, weakly modulated systems has been widely studied, the transmission characteristics of short, strongly modulated systems remain underexplored. This thesis addresses this gap, aiming to expand the application of materials and devices with time-varying mechanical properties. The focus is on discrete models of spatiotemporally modulated systems, where effective elasticity changes harmonically in time and space.

A methodology is developed to accurately predict the steady-state response of spatiotemporally modulated systems in response to external harmonic drive. The formulation is valid for strongly modulated systems of an arbitrary number of units. Using this methodology, vibration transmission characteristics of both weakly and strongly modulated systems are investigated. Contributions of primary and sideband resonances, and their overlaps, to nonreciprocity are clarified. The effects of modulation amplitude and wavenumber on the resonance frequencies are discussed.

The contribution of phase to nonreciprocity is highlighted, a feature that is often overlooked in the literature. It is shown that the difference between the transmitted phases is the primary contributor to nonreciprocity in short systems. To further emphasize the significant role of phase, a nonreciprocal response regime is introduced which is characterized by equal transmitted amplitudes in opposite directions. A nonreciprocal phase shift is the sole contributor to nonreciprocity in this case. A methodology is developed for achieving nonreciprocal phase shifts in short, weakly modulated systems based on the envelope of the response. A formulation is also presented that ensures the shapes of the transmitted response envelopes have the same shape but different phases.

Parametric stability is analyzed using Floquet theory, revealing the influence of key system parameters, including modulation phase, wavenumber, amplitude, frequency, damping, and system size. Perturbation theory shows that parametric instability occurs at specific frequency combinations of the unmodulated system. Instability is more likely at higher modulation frequencies, whereas lower modulation frequencies provide wide stable amplitude ranges. These insights enhance the design and safe operation of spatiotemporally modulated systems, potentially broadening their applications.

Dedication

This thesis is lovingly dedicated to my beloved wife, Lan Wu.

For her unwavering love, patience, trust,
understanding, and steadfast support,
which have been my greatest strength throughout this journey.

Acknowledgments

Firstly, I would like to express my deepest gratitude to my supervisor, Dr. Behrooz Yousefzadeh, for his invaluable guidance, support, and encouragement throughout the course of my research. His expertise, insightful feedback, and dedication to my academic growth have been a constant source of motivation and inspiration. I am truly fortunate to have had the opportunity to study and work under his mentorship.

I am deeply appreciative of the time and effort Dr. Yousefzadeh dedicated to reviewing my work, offering constructive suggestions, and helping me navigate the challenges I faced during this academic journey. His patience and commitment have played a pivotal role in the completion of this thesis, and I will always be grateful for his unwavering support.

Secondly, I would also like to thank all my colleagues in Concordia WAVE Lab: Ali Kogani, Hooman Zoka, Will Sze, Seyed Mojtaba Mousavi, Nikolas Hartadi, Payam Azadian and Temitope Akinpelu, for their valuable assistance and collaboration. Their contributions have made a significant impact on the progress of this research.

Finally, I wish to acknowledge Concordia University, Natural Science and Engineering Research Council of Canada, Centre de Recherches Mathématique, School of Graduate Studies, Gina Cody School of Concordia University, Technical Committee of Vibration and Sound (TCVS) of the American Society of Mechanical Engineers (ASME) and School of the Acoustical Society of America (ASA) for their financial support, which has been essential in helping me stay focused and motivated.

Contribution of Authors

To comply with the manuscript-based format outlined in the *Thesis Preparation Guide* provided by the Thesis Office of the School of Graduate Studies, this thesis has been prepared in alignment with the specified regulations. Coauthored works are presented in Chapters 2, 3, 4, and the Appendices, with the abstracts of these manuscripts excluded from the chapters. The contributions of each coauthor are detailed below.

Chapter 2, manuscript "Linear Nonreciprocal Dynamics of Coupled Modulated Systems", which is reprinted from the published journal article in *The Journal of the Acoustical Society of America* (DOI: https://doi.org/10.1121/10.0035882). Contributions of the Authors:

Jiuda Wu: Conceptualization, all the mathematical modeling, result acquisition, validation, analysis, and manuscript preparation, including drafting and writing.

Behrooz Yousefzadeh: Conceptualization, manuscript review and editing, supervision, and funding acquisition.

Chapter 3, manuscript "Nonreciprocal Phase Shifts in Spatiotemporally Modulated Systems", which has been submitted to *Physical Review B*, currently under revision. Contributions of the Authors:

Jiuda Wu: Conceptualization, all the mathematical modeling, result acquisition, validation, analysis, and manuscript preparation, including drafting and writing.

Behrooz Yousefzadeh: Conceptualization, manuscript review and editing, supervision, and funding acquisition.

Chapter 4, manuscript "Parametric Instability in Discrete Models of Spatiotemporally Modulated Materials", which is ready to be submitted to *Physical Review E.* Contributions of the Authors:

Jiuda Wu: Conceptualization, all the mathematical modeling, result acquisition, validation, analysis, and manuscript preparation, including drafting and writing.

Behrooz Yousefzadeh: Conceptualization, manuscript review and editing, supervision, and funding acquisition.

Appendix A "Computation of response envelopes in a lattice material with spatiotemporal modulations", which is reprinted from the published conference proceeding with the DOI of https://doi.org/10.17118/11143/21144. Contributions of the Authors:

Jiuda Wu: Conceptualization, all the mathematical modeling, result acquisition, validation, analysis, and manuscript preparation, including drafting and writing.

Behrooz Yousefzadeh: Conceptualization, manuscript review and editing, supervision, and funding acquisition.

Appendix B "Numerical analysis of phase nonreciprocity in a linear spatiotemporally modulated system", which is reprinted from the published conference proceeding with the DOI of https://doi.org/10.1115/DETC2023-110347. Contributions of the Authors:

Jiuda Wu: Conceptualization, all the mathematical modeling, result acquisition, validation, analysis, and manuscript preparation, including drafting and writing.

Behrooz Yousefzadeh: Conceptualization, manuscript review and editing, supervision, and funding acquisition.

Appendix C "Nonreciprocal dynamics of spatiotemporally varying materials: strong modulations", which was presented at "The 2024 edition of the CSME International Congress". Contributions of the Authors:

Jiuda Wu: Conceptualization, all the mathematical modeling, result acquisition, validation, analysis, and manuscript preparation, including drafting and writing.

Behrooz Yousefzadeh: Conceptualization, manuscript review and editing, supervision, and funding acquisition.

Appendix D "On vibration transmission reciprocity in modulated materials", which is reprinted from the published conference proceeding with the DOI of https://doi.org/10.7939/r3-excb-c769. Contributions of the Authors:

Jiuda Wu: Conceptualization, all the mathematical modeling, result acquisition, validation, analysis, and manuscript preparation, including drafting and writing.

Behrooz Yousefzadeh: Conceptualization, manuscript review and editing, supervision, and funding acquisition.

Contents

List of Figures

List of Tables

Nomenclature

u, v	Dimensional displacement
x	Dimensionless displacement
$\underline{x}$	Column matrix composed of x
$\underline{X}$	Column matrix composed of x and $\dot{x}$
Δ^2, δ^2	Difference terms which represent coupling in the system
y, η, ξ	Complex amplitude of harmonic term in the Fourier series of x
$\mathbf{y}$	Time-varying term in the Fourier series of x
$\{Y\}$	Column matrix composed of y
ψ	Phase angle of a harmonic term in the Fourier series of x in cosine notation
w	Subset of the Fourier series of x
W	Complex amplitude of a harmonic term in the Fourier series of w
$\underline{w}$	Column matrix which consists of w
$\underline{\mathrm{W}}$	Unmodulated mode shape of the equations of motion in terms of y
w	Element in vector $\underline{\mathrm{W}}$
z	Decoupled displacement of the equations of motion in terms of w
n	Number of modulated units
$\mathcal{F}$	Number of sideband-pairs
$\mathbb{N}$	The set of natural numbers
$\mathbb{Z}$	The set of integers
$\mathbb{R}$	The set of real numbers
$\underline{\underline{I}}$	Identity matrix
$\underline{\underline{O}}$	Zero matrix
Ω_n	Unmodulated natural frequency
G	Effective property of a system, can be elastic modulus, density, stiffness coefficient, or mass
m	Mass
c	Damping coefficient
ζ	Damping ratio

$\underline{\underline{D}}$	Damping matrix
s	Coordinate along a one-dimensional waveguide
l	Distance between two adjacent modulated units in a periodic system
t	Dimensional time
τ, μ, ν	Dimensionless time
k_c	Dimensional stiffness coefficient of the linear coupling spring
K_c	Dimensionless stiffness of the linear coupling spring
$k_{g,DC}$	Constant term in the stiffness coefficient of the grounding spring
ω_0	Constant term determined by $k_{g,DC}$ and m
$k_{g,AC}$	Amplitude of the time-varying term in the stiffness coefficient of the grounding spring
K_m	Dimensionless amplitude of the time-varying term in the stiffness coefficient of the grounding spring; Modulation amplitude
ϵ	Modulation amplitude with an infinitesimal value
k	Wavenumber of a traveling wave
ω	Angular frequency of a traveling wave
k_m	Wavenumber of the spatiotemporal modulation
ω_m	Dimensional angular frequency of the spatiotemporal modulation
Ω_m	Dimensionless angular frequency of the spatiotemporal modulation
f	Harmonic force
ω_f	Dimensional angular frequency of the harmonic force
Ω_f	Dimensionless angular frequency of the harmonic force
F	Dimensional amplitude of the harmonic force
P	Dimensionless amplitude of the harmonic force
$\{F\}$	Column matrix composed of P
$\underline{p}$	Column matrix which represents external forces
ϕ	Phase shift between two adjacent modulations; Spatial modulation
N	Output norm
N_{df}	Difference between two output norms
R	Reciprocity bias
R_N	Norm bias
R_A	Amplitude bias

$\underline{\underline{D}}$, $[D]$	Matrix obtained from the equations of motion
A	Diagonal term in $\underline{\underline{D}}$
$\mathcal{D}$	Term in $\lvert\underline{\underline{D}}\rvert$
M	Minor of $\underline{\underline{D}}$
$\underline{\underline{\mathsf{A}}}$	Matrix in the first order differential equation obtained from the equations of motion
$\underline{\underline{\mathsf{C}}}$	Time-varying submatrix of $\underline{\underline{\mathsf{A}}}$
B	Diagonal term in $\underline{\underline{\mathsf{C}}}$
E	Response envelope
T_E, T_{ev}	Period of response envelope
A_{ev}	Maximum displacement of response envelope
$\mathcal{S}_{dc}$	Time-independent bias portion of response envelope
$\mathcal{S}_{ac}$	Time-varying portion of response envelope
θ, ϑ	Phase angle of a harmonic term in the expression of $\mathcal{S}_{ac}$
$\mathcal{A}$, $\mathcal{B}$, $\mathcal{E}$, $\mathcal{Y}$	Amplitude of a harmonic term in the expression of $\mathcal{S}_{ac}$
C	Carrier wave
φ	Phase angle of approximated harmonic carrier wave
$\mathcal{R}_{em}$	Remainder of dividing an angle by 2π
$c.c.$	Corresponding complex conjugate terms
$\underline{\underline{\Psi}}$, $\underline{\underline{\mathsf{E}}}$	Principle matrix

Chapter 1

Introduction and Literature Review

1.1. Background

In time-invariant structures and materials, transmission of small-amplitude (linear) vibrations between two points remains unchanged when the locations of the source and the receiver are interchanged. This invariance property is called reciprocity. Reciprocity has led to development of various wave processing techniques and industrial applications, for instance, calibration of hydrophones and crack identification [1–3]. However, vibration transmission properties (speed, amplitude, phase, etc.) that are dependent on the direction of transmission cannot be realized in reciprocal systems. Many researchers have recently focused on developing methods to break the reciprocity invariance and realize direction-dependent vibration transmission [4, 5].

Nonreciprocal vibration transmission can occur in a structure that has one or more of its properties (e.g. effective mass or stiffness) change in both time and space [6]. We refer to a structure or material with such properties as a system subject to spatiotemporal modulations, or more simply as a (spatiotemporally) modulated system. In this context, modulation refers to a time-periodic (typically harmonic) variation in an effective property of the system, most commonly the stiffness of the material. Discrete and continuous models of periodic modulated materials are commonly used in the studies on nonreciprocal vibration transmission. The smallest repetitive substructure with modulation in a periodic system is called its modulated unit. The characteristics in each modulated unit determine how vibrations transmit differently in opposite directions within the modulated system.

1.2. Theoretical studies on nonreciprocal vibration transmission in modulated materials

1.2.1. Various systems with spatiotemporal modulations

Nonreciprocal wave propagation has been extensively studied using various theoretical models of spatiotemporally modulated materials. Examples include one-dimensional (1-D) uniform media with spatiotemporal modulations in their elastic modulus [7–13], density [14] or both density and elasticity [15–18]. Other examples include membrane systems with spatiotemporally modulated density [19], time-invariant media featuring local modulated patches [20], or local modulated resonators [21–23]. Additionally, discrete spring-mass chains with modulations in their spring stiffness [24, 25], masses [26] or both [27, 28] have been explored, as well as metamaterials with modulated resonant springs [29] or modulated resonant and coupling springs [30]. A periodic material featuring modulations in all its springs and dampers, including both coupling and grounding connections, has also been proposed [31].

In some theoretical studies, innovative designs have been introduced to realize spatiotemporal modulations. For instance, magnetoelastic materials, whose elastic modulus can be modulated spatiotemporally by an external magnetic field varying in both time and space, have been proposed for achieving nonreciprocal vibration transmission [8]. Fully mechanical structures have also been designed as modulated units in discrete waveguides. One such design uses a rigid rotating element attached to each mass in the main structure, enabling temporal modulation of the effective mass [26]. Similar designs utilizing rotary mechanisms have demonstrated modulations in both mass and coupling stiffness [27] or in both mass and grounding stiffness [28].

Another approach involves attaching each mass in the primary structure to a local resonator and a levered mass that slides freely along an axis perpendicular to the transverse axis, achieving modulations in both equivalent mass and coupling stiffness [20, 31]. A simpler design for modulating coupling stiffness employs a triangular arrangement of three linear springs, where one spring acts as the coupling spring between two masses, and the hinged node of the other two springs slides freely along a fixed axis perpendicular to the transverse axis [32]. Finally, time-modulated inerters featuring a levered mass connected to a modulated base have been proposed as periodic attachments to achieve nonreciprocal vibration transmission [23].

1.2.2. Research methodologies

If one of the effective material properties of a system, denoted by parameter G, is spatiotemporally modulated, then we have $G(s+\lambda, t+T) = G(s,t)$, where s is the spatial coordinate system, t is time, and λ and T represent the periodicity in space and time, respectively. In developing a mathematical framework for studying wave propagation in modulated materials, it is common to express the spatiotemporal modulations in terms of a plane-wave (Fourier) expansion. In 1-D systems, these expansions are:

$$G_{con}\left(s,t\right) = \sum_{q=-\infty}^{\infty} [\mathring{G}_{con;q} e^{iq(\omega_m t - k_m s)} + c.c.], \tag{1.1}$$

and

$$G_{dsc;p}\left(t\right) = \sum_{q=-\infty}^{\infty} [\mathring{G}_{dsc;p;q} e^{i(q\omega_m t - \phi p)} + c.c.], \tag{1.2}$$

for continuous and discrete systems, respectively. Parameter p denotes the ordinal number of a modulated unit in a discrete system (to replace a continuous spatial coordinate). The term $c.c.$ indicates the complex conjugate terms. The parameters ω_m and k_m are the modulation frequency and wavenumber, respectively, while ϕ represents a constant phase shift between modulations in adjacent units, equivalent to spatial modulation. In continuous systems, G_{con} can represent Young's modulus [7, 10, 12], density [14], or both [15, 16, 18]. For discrete systems, G_{dsc} may correspond to the stiffness coefficient [24, 25], mass [26], or a combination of stiffness and mass [27, 28].

When the spatiotemporal modulation is harmonic, Eqs. 1.1 and 1.2 simplify to:

$$G_{con}\left(s,t\right) = G_{con,DC} + G_{con,AC}\cos\left(\omega_m t - k_m s\right), \tag{1.3}$$

and

$$G_{dsc;p}\left(t\right) = G_{dsc,DC;p} + G_{dsc,AC;p}\cos\left(\omega_m t - \phi p\right), \tag{1.4}$$

respectively [8, 29]. In these equations, $G_{con,DC}$, $G_{con,AC}$, $G_{dsc,DC;p}$ and $G_{dsc,AC;p}$ are constants. The spatial modulation terms in Eqs. (1.3) and (1.4) are related by $k_m l = \phi$, where l is the distance between adjacent modulated units in a discrete system. This relation is crucial for transforming waveguide models of continuous and discrete systems when the wavelength is much larger than l [29].

The motion of a uniform medium with modulation is governed by a second-order linear partial differential equation. Solutions to this equation, because of the imposed periodic modulations in Eq. (1.1), take the form of Bloch waves [10, 24]:

$$\mathbf{u}\left(s,t\right) = \sum_{q=-\infty}^{\infty} [\mathring{\mathbf{u}}_q e^{i[(\omega+q\omega_m)t-(k+qk_m)s]} + c.c.], \tag{1.5}$$

where $\mathbf{u}\left(s,t\right)$ represents the displacement of the modulated medium. Eq. (1.5) is also referred to as the generalized Floquet wave [33] or Floquet-Bloch wave [25, 29]. Substitution of Eq. (1.5) into the governing equations leads to the derivation of dispersion relations as a compatibility condition. Several methodologies exist for this calculation such as the plane-wave expansion method [33–35], multiple scattering method [22], or scattering matrix method [10].

For discrete modulated systems, the equations of motion are coupled second-order differential equations with time-varying coefficients. Exact closed-form solutions are unavailable for this type of equations. Instead, a Bloch-based approach is employed, seeking solutions in the Fourier series form [22, 26, 28, 30, 32, 36, 37]:

$$u\left(t\right) = \sum_{q=-\infty}^{\infty} [\mathring{u}_q e^{i(\omega+q\omega_m)t} + c.c.], \tag{1.6}$$

which is supported by the fact that sideband resonance appears at $\omega_n \pm \kappa\omega_m$ in the frequency spectrum of a modulated oscillator, with ω_n representing the natural frequency of the unmodulated system and $\kappa \in \mathbb{N}$ [38]. Typically, the infinite summation in Eq. (1.6) is truncated to a finite range for q, usually $-1 \leq q \leq 1$ [26, 28, 29, 36, 37]. Substitution of Eq. (1.6) into the equations of motion, along with the application of the harmonic-balance or averaging methods, yields a set of linear algebraic equations, from which the complex-valued amplitudes $\mathring{u}_q$ are determined [26, 28, 36, 37].

Other methodologies have also been utilized to obtain the response of modulated systems in the literature. Examples include direct numerical simulations using the finite difference method [15, 25, 29, 31], the method of multiple scales [24], a method based on coupled-mode theory [29], plane-wave expansion [16, 31, 39], finite-element method [18] and the transfer-matrix method [8, 27].

1.2.3. Demonstration of nonreciprocity

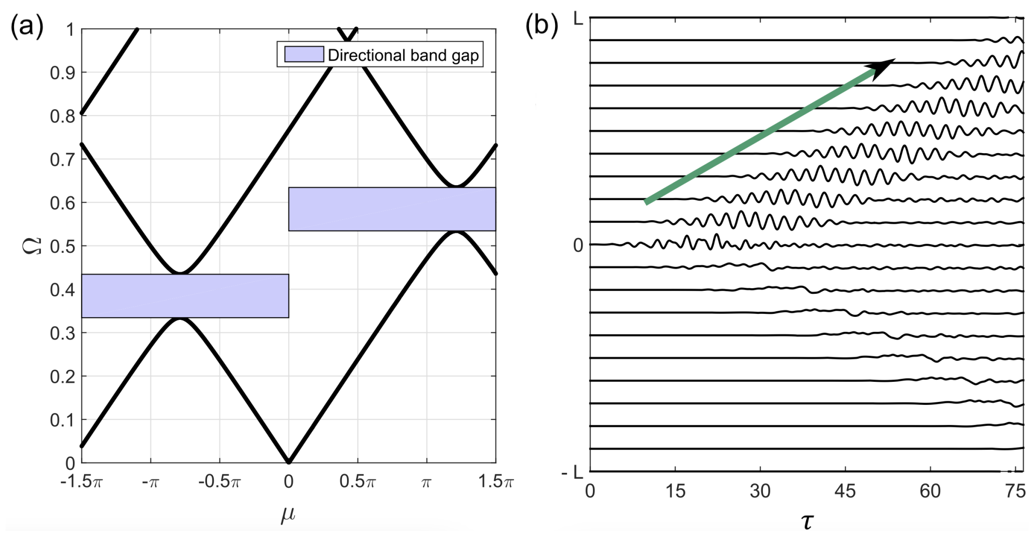

Figure 1.1: Illustration of nonreciprocal wave propagation in a 1-D modulated medium.[1] (a) A dispersion curve with directional bandgaps, where Ω and μ represent frequency and wavenumber, respectively. (b) A waterfall plot representing the transient response when the excitation frequency falls within a directional bandgap [7].

Wave propagation through materials is characterized by properties such as amplitude, phase, wavelength, group velocity, and phase velocity. Nonreciprocity in wave propagation can be

[1]These two figures are taken from G. Trainiti & M. Ruzzene, Non-reciprocal elastic wave propagation in spatiotemporal periodic structures, *New Journal of Physics* **18** 083047, (2016).

established by demonstrating that any of these properties depends on the direction of propagation. Probably the most obvious indicator of nonreciprocity is the difference in transmitted amplitudes between opposite directions, known as amplitude bias. A notable manifestation of amplitude bias is unidirectional wave propagation in one-dimensional (1-D) continuously modulated media, which is identified by directional bandgaps in their dispersion curves. In a 1-D modulated system, spatiotemporal modulation introduces scattered waves into the waveguide, with frequencies and wavenumbers that are direction-dependent. This results in dispersion curves for the scattered waves being asymmetric about the line 'wavenumber = 0' [29]. Consequently, the interaction between an incident wave and a scattered wave with opposite group velocities leads to a directional bandgap. Fig. 1.1(a) shows a dispersion curve with directional bandgaps. Fig. 1.1(b) displays a waterfall plot showing the response of a $2L$-long bar following excitation at its midpoint, where the excitation frequency falls within a directional bandgap.

Additionally, other methods have been employed to graphically represent amplitude bias, and to demonstrate nonreciprocity. The frequency spectra of transmitted vibrations in opposite directions can reveal the amplitude bias of each harmonic component within the transmitted vibrations [9, 37]. When vibrations pass through a modulated system in two opposite directions, comparing the amplitudes of temporal responses in different scenarios makes it straightforward to identify nonreciprocity [7, 23].

1.3. Experimental studies on nonreciprocal vibration transmission in modulated materials

Unlike the early theoretical studies, experimental demonstrations of nonreciprocal vibration transmission caused in modulated materials are necessarily conducted on systems with a finite length. In these systems, modulations (parametric excitation) are typically applied at discrete points along the structure, with each modulated unit exhibiting temporal modulation. Collectively, these modulated units can represent spatial modulation provided that there is a phase shift (ϕ) between modulations in adjacent units.

1.3.1. Realization of spatiotemporal modulations

A variety of techniques, including electromagnetism, piezoelectricity, and mechanical methods, have been used in experimental setups to introduce spatiotemporal modulations within waveguides. Fig. 1.2 shows some illustrative examples.

The experimental setups in Figs. 1.2(a) and 1.2(b) used piezoelectricity to realize nonreciprocal wave propagation. Fig. 1.2(a) shows a uniform thin-beam waveguide equipped with

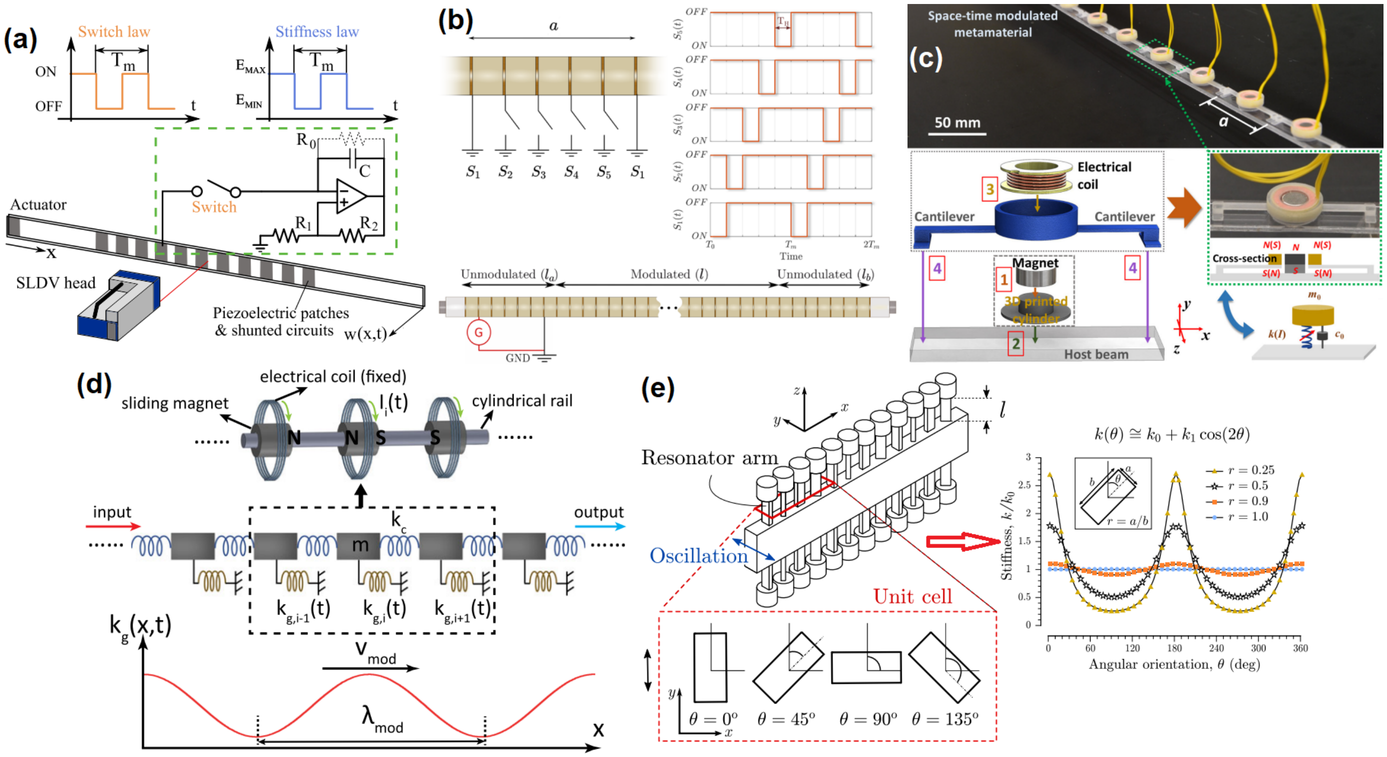

Figure 1.2: Experimental setups to study nonreciprocal vibration transmission realized by spatiotemporal modulations. (a) A thin beam with piezoelectric patches [40].[1] (b) A periodic material consisting of piezoelectric cells [41].[2] (c) A thin beam with electromagnetically modulated resonators [42].[3] (d) A ring-magnet chain with electromagnetically modulated grounding stiffness [43].[4] (e) A periodic system with geometrically modulated resonators [44].[5]

piezoelectric patches periodically adhered along its length, utilized for transmitting transverse waves nonreciprocally [40, 45–47]. The local elasticity of the waveguide was tuned by

[1]This figure is taken from G. Trainiti *et al*, Time-Periodic Stiffness Modulation in Elastic Metamaterials for Selective Wave Filtering: Theory and Experiment, *Physical Review Letters* **122** 124301, (2019). Copyright (2025) by American Physical Society.

[2]This figure is taken from S. Tessier Brothelande *et al*, Experimental evidence of nonreciprocal propagation in space-time modulated piezoelectric phononic crystals, *Applied Physics Letters* **123** no. 20, (2023). Copyright (2025) by AIP Publishing.

[3]This figure is taken from Y. Chen *et al*, Nonreciprocal wave propagation in a continuum-based metamaterial with space-time modulated resonators, *Physical Review Applied* **11** 064052, (2019). Copyright (2025) by American Physical Society.

[4]This figure is taken from Y. Wang *et al*, Observation of nonreciprocal wave propagation in a dynamic phononic lattice, *Physical Review Letters* **121** 194301, (2018). Copyright (2025) by American Physical Society.

[5]This figure is taken from M. Attarzadeh *et al*, Experimental observation of nonreciprocal waves in a resonant metamaterial beam, *Physical Review Applied* **13** 021001, (2020). Copyright (2025) by American Physical Society.

changing the voltage applied to each patch, thereby realizing spatiotemporal modulations in the equivalent elastic modulus through pre-programmed periodic voltages. Fig. 1.2(b) shows a periodic material made of cylindrical piezoelectric cells with thin electrodes in-between, it was used as a modulated waveguide [41, 48]. By tuning the voltage difference between the two boundaries of each piezoelectric cell, directional elastic waves were generated, which resulted in nonreciprocal propagation of incident waves.

The setups in Figs. 1.2(c) and 1.2(d) utilized electromagnetism. Fig. 1.2(c) shows a thin beam with magnets equidistantly fixed on it. The electrical coils which are coaxial with the magnets are connected to the thin beam by elastic rods, they function as local modulated resonators [42, 49]. Periodic change of current in an electrical coil brings a magnetic field which changes accordingly at the same frequency, and a time-varying magnetic force is generated between the coil and the coaxial magnet. The time-varying magnetic force is equivalent to an elastic force of a spring with modulated stiffness coefficient. Fig. 1.2(d) shows another design that used magnets and electrical coils to construct a waveguide, where modulations were introduced to the equivalent stiffness of the grounding springs [43, 50].

A purely mechanical method was employed in the setup shown in Fig. 1.2(e). It is a periodic system with beam-like rotary resonators in which modulations were introduced to the effective stiffness [44]. The resonators have the same rectangular cross-section but different preset orientation angles. By rotating the resonators at the same speed, the second moment of area of every arm cross-section which is calculated perpendicular to the vibration direction changes periodically. Thus, the rotation leads to modulation added to the effective stiffness of each resonator.

1.3.2. Observation of nonreciprocity

The amplitude bias (the difference between the transmitted amplitudes in opposite directions) remains the main indicator of nonreciprocity in the literature. This is also the most straightforward measure to use in experiments. Fig. 1.3 shows examples of amplitude bias used to demonstrate nonreciprocity. Similar to the theoretical studies, observations of the differences in frequency spectra, results from space-time Fourier transforms, and plots of the transient response are widely used as other pieces of evidence to demonstrate nonreciprocity.

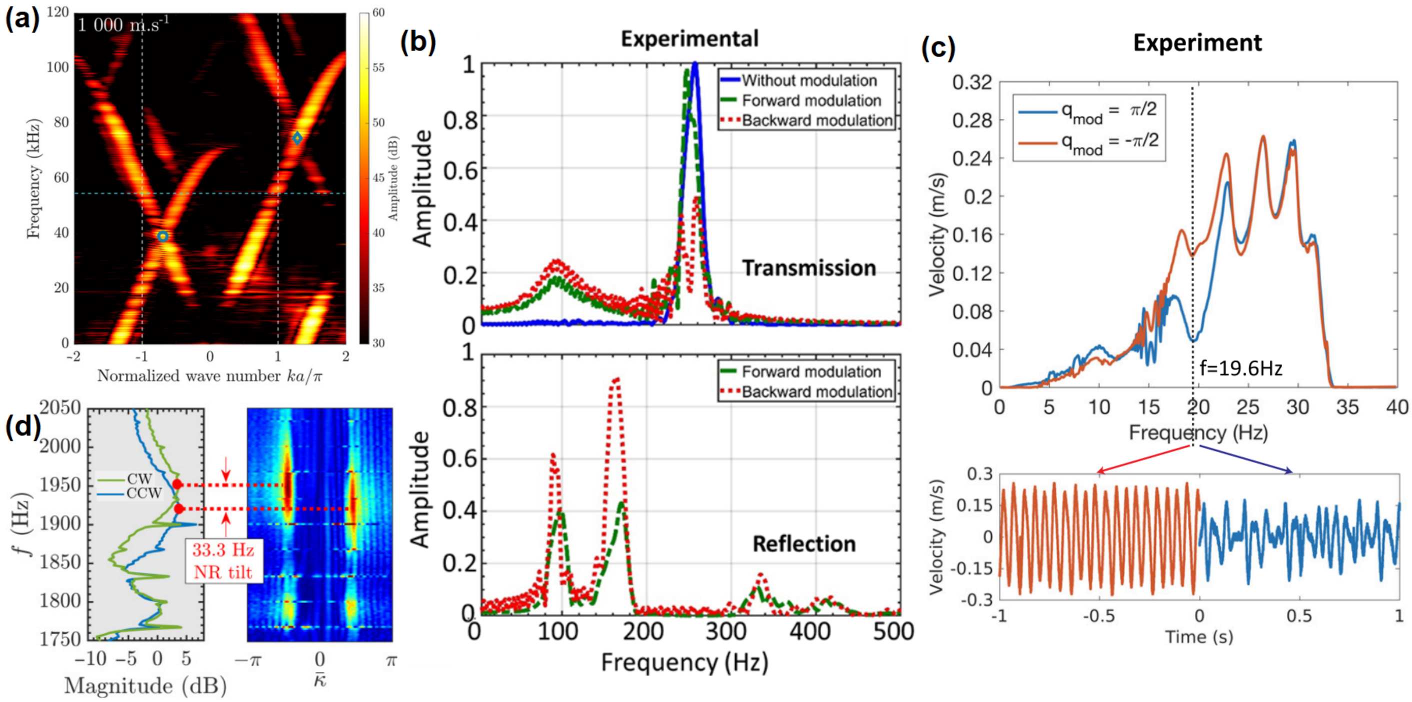

Figure 1.3: Observations of nonreciprocity in experiments on vibration transmission in spatiotemporally modulated systems in opposite directions. (a) Space-time Fourier transform of the response of the modulated system [41].[1] (b) Frequency spectrum of transmitted vibrations [42].[2] (c) Frequency spectrum and measured steady-state response [43].[3] (d) Frequency spectrum and space-time Fourier transform of the measured response of the system [44].[4]

1.4. Contributions of phase to nonreciprocity

The difference between transmitted phases in opposite directions can also be a contributor to nonreciprocity as well. Under certain conditions, phase can even be the only contributor to nonreciprocity [51, 52]. Phase difference as a measure of nonreciprocity is often used in the literature on electromagnetic waves [53–56]. However, in studies on acoustic and mechanical

[1]This figure is taken from S. Tessier Brothelande *et al*, Experimental evidence of nonreciprocal propagation in space-time modulated piezoelectric phononic crystals, *Applied Physics Letters* **123** no. 20, (2023). Copyright (2025) by AIP Publishing.

[2]This figure is taken from Y. Chen *et al*, Nonreciprocal wave propagation in a continuum-based metamaterial with space-time modulated resonators, *Physical Review Applied* **11** 064052, (2019). Copyright (2025) by American Physical Society.

[3]This figure is taken from Y. Wang *et al*, Observation of nonreciprocal wave propagation in a dynamic phononic lattice, *Physical Review Letters* **121** 194301, (2018). Copyright (2025) by American Physical Society.

[4]This figure is taken from M. Attarzadeh *et al*, Experimental observation of nonreciprocal waves in a resonant metamaterial beam, *Physical Review Applied* **13** 021001, (2020). Copyright (2025) by American Physical Society.

systems, contributions of phase to nonreciprocity have been rarely investigated.

In short modulated systems (only a few modulated units), preliminary results indicate that the norm bias is typically very small because nonreciprocity is primarily caused by the difference between the transmitted phases (not energies) in opposite directions [57]. The role of phase in nonreciprocal vibration transmission in systems with spatiotemporal modulations remains unexplored, to the best of our knowledge.

1.5. Parametric instability and strong modulations

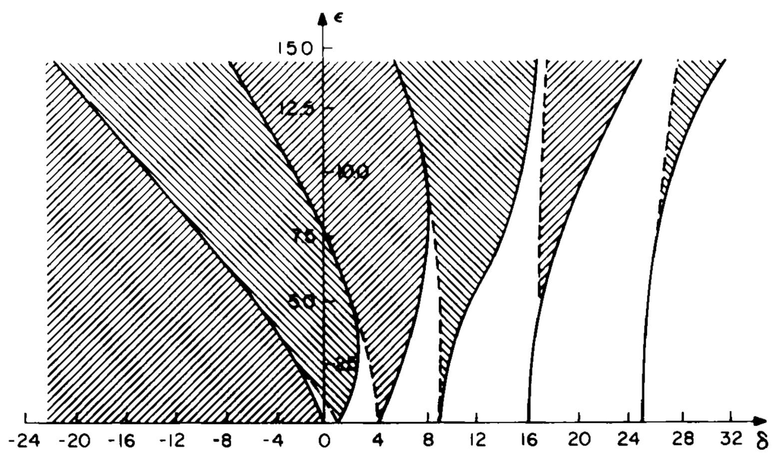

Figure 1.4: Stability diagram of Mathieu's equation.[1] White and shaded regions indicate the combinations of δ and ϵ that result in stable and unstable motion, respectively [58].

Modulations (usually harmonic) in stiffness bring parametric excitations, which are forces dependent on displacements. Such forces may lead to parametric instability to the modulated system, *i.e.* the amplitude of response grows exponentially in time. Studies on boundedness of the solutions for Mathieu's equations have demonstrated this phenomenon. Fig. 1.4 shows a stability diagram, a graphical illustration of stability results, for an oscillator with a modulation in the stiffness coefficient of the spring. Its equation of motion can be expressed by the classical Mathieu's equation [58]:

$$\frac{\mathrm{d}^2}{\mathrm{d}t^2}u + (\delta + \epsilon \cos 2t)\, u = 0. \tag{1.7}$$

Parametric instability can occur even when the modulation amplitude is very low. This instability also extends to coupled Mathieu's equations, which are equations of motion for a modulated system with multiple degrees of freedom (DoF). Figure 1.5 displays the stability diagrams for a modulated system governed by a set of two coupled Mathieu's equations [59]:

[1]This figure is taken from A. H. Nayfeh & D. T. Mook *Nonlinear Oscillations* (John Wiley & Sons, 1979), p. 21. Copyright (2025) by John Wiley & Sons, Inc.

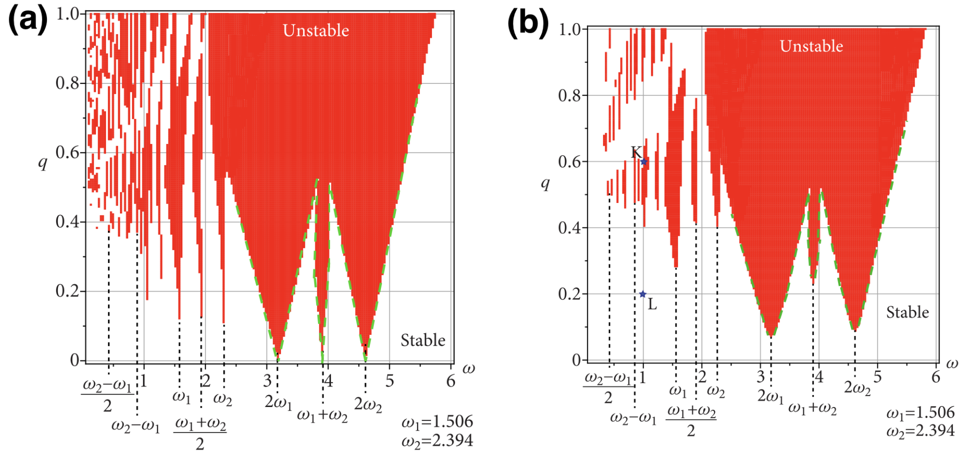

Figure 1.5: Stability diagrams of Eq. (1.8).[1] White and red regions indicate the combinations of δ and ϵ that result in stable and unstable motion, respectively [59]. (a) $c = 0$; (b) $c = 0.1$.

$$\begin{Bmatrix} \mathrm{d}^2u_1/\mathrm{d}t^2 \\ \mathrm{d}^2u_2/\mathrm{d}t^2 \end{Bmatrix} + \begin{bmatrix} c & 0 \\ 0 & c \end{bmatrix} \begin{Bmatrix} \mathrm{d}u_1/\mathrm{d}t \\ \mathrm{d}u_2/\mathrm{d}t \end{Bmatrix} + \left(\begin{bmatrix} 3 & 1 \\ 1 & 5 \end{bmatrix} + 2q \begin{bmatrix} 3 & 1 \\ 0.5 & 2 \end{bmatrix} \cos \omega t \right) \begin{Bmatrix} u_1 \\ u_2 \end{Bmatrix} = \begin{Bmatrix} 0 \\ 0 \end{Bmatrix}, \quad (1.8)$$[2]

where all harmonic coefficients that represent modulations are in-phase with the same frequency ω. The shapes of the unstable regions in Figure 1.5(a) are more complex than those depicted in Figure 1.4. Despite the presence of damping, parametric instability can still occur, as seen in Figure 1.5(b). Therefore, determining the stability of modulated systems is critical for analyzing their response and investigating the nonreciprocal dynamics. A systematic analysis on the effects of system parameters, especially modulation parameters, is essential for understanding their roles on parametric instability.

There are two established methods to increase the amplitude bias in a finite modulated system: one is to increase the number of modulated units; the other one is to increase the amplitudes of modulation. The transmission characteristics of long systems with low-amplitude (weak) modulations have been well investigated and stated in the literature. High-amplitude (strong) modulations lead to more complex spectral contents of the response, and tend to result in unstable response.

The existing formulations in the literature, such as those based on various perturbation

[1] These two figures are taken from J. Deng, Numerical simulation of stability and responses of dynamic systems under parametric excitation, *Applied Mathematical Modelling* **119**, 648-676 (2023). Copyright (2025) by Elsevier.

[2] This equation is taken from J. Deng, Numerical simulation of stability and responses of dynamic systems under parametric excitation, *Applied Mathematical Modelling* **119**, 648-676 (2023). Copyright (2025) by Elsevier.

methods [24, 25, 29], have primarily been developed for weakly modulated systems. Strong modulations are rarely explored in the literature, despite their ability to significantly increase the amplitude bias in short systems. In strongly modulated systems, however, the existing methodologies fail to accurately capture the response of the system. In addition, the natural frequencies of the unmodulated system are no longer helpful in describing the resonance frequencies of strongly modulated systems. As a result, the analysis of strongly modulated systems typically involves direct numerical computations, which are particularly inefficient for a parametric study of the response. In addition, a formulation is needed that can accurately predict the steady-state response of strongly modulated systems.

1.6. Thesis objectives

The ability to accurately predict the response of modulated systems with arbitrary number of units and arbitrary modulation amplitude is critical for development of practical implementation of devices that operate based on spatiotemporal modulations. The analysis of parametric stability is a critical factor for the safe operation of such devices. Moreover, understanding the role of phase in transmitted vibrations will bring a complete analysis of nonreciprocal vibration transmission. With these factors in mind, the three overarching objectives of this thesis are:

1. Development of a semi-analytical methodology for accurately predicting the steady-state response of spatiotemporally modulated systems that is valid for any strength of modulation. This is addressed in Chapter 2.

2. Investigating the role of transmitted phase in nonreciprocal vibration transmission. This is addressed in Chapter 3.

3. Analyzing the stability of spatiotemporally modulated systems. This is addressed in Chapter 4.

Inspired by the experimental studies on nonreciprocal vibration transmission in modulated systems, specifically the corresponding mathematical models used in their analysis, this thesis will exclusively focus on a discrete model of spatiotemporally modulated systems. Fig. 1.6 shows a schematic representation of the discrete model used in this thesis. The research methodologies developed herein are applicable to discrete modulated systems in various designs.

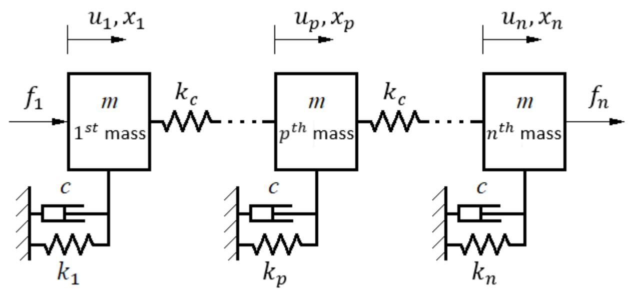

Figure 1.6: Scheme of the modulated system. It is composed of n identical masses which are connected by the same linear springs. Each mass is connected to the ground by a viscous damper and a modulated spring with stiffness coefficient $k_p = k_{g,DC} + k_{g,AC} \cos(\omega_m t - \phi_p)$, $\phi_p = (p-1)\,\phi$, $(p = 1, 2, \cdots, n)$. Two harmonic forces are $f_1 = F_1 \cos\omega_f t$ and $f_n = F_n \cos\omega_f t$. The only degree of freedom considered is the longitudinal rectilinear motion of each mass.

1.7. Thesis layout

This thesis is organized in five chapters and is written according to the manuscript-based thesis regulations stated in the *Thesis Preparation Guide*.

The purpose of Chapter 1 is to present the basic background information on nonreciprocal vibration transmission in systems subject to spatiotemporal modulations, and to present the main objectives of the thesis.

In Chapter 2, nonreciprocal vibration transmission in a modulated system with only 2-DoF is analyzed. Nonreciprocity is quantified using a measure that can account for contributions from both amplitude and phase. The averaging method, introduced in detail, is employed to approximate the steady-state response. The methodology is applicable to systems with any number of modulated units. The spectral contents of the non-periodic response and their contributions to nonreciprocity are analyzed. Additionally, the influence of increasing the modulation amplitude on the steady-state response, nonreciprocity, and resonant frequencies are investigated.

Chapter 3 presents phase nonreciprocity, a regime where transmitted amplitudes are the same in opposite directions. This analysis provides a systematic examination of this scenario, in which nonreciprocal phase shifts are highlighted as the sole contributors to nonreciprocity. To realize nonreciprocal phase shifts, a numerical methodology is developed based on the envelope of the output displacement. A formulation is also introduced to enforce identical shapes for the envelopes of the transmitted waves in opposite directions. Two special cases of nonreciprocal phase shift are introduced, and the limitations of the methodology are discussed as well.

Chapter 4 focuses on investigating the parametric instability of the response of the modulated system in Fig. 1.6, whose motion is governed by coupled Mathieu's equations. A perturbation method is used to identify unstable modulation frequencies (UMFs). Stability diagrams in different parameter planes are computed numerically based on the Floquet theory. By analyzing the stability diagrams, the effects of various system parameters on stability are investigated, with a particular focus on the effects of modulation phase and the number of modulated units.

The appendices consist of four conference proceeding papers that provide additional information to make this thesis coherent.

Appendix A complements Chapter 2, demonstrating that amplitude bias increases with the number of modulated units while keeping all other system parameters unchanged. Unidirectional vibration transmission, the extreme case of transmission with amplitude bias, can be realized in very long modulated systems.

Appendix B complements Chapter 3 by presenting a study on nonreciprocal vibration transmission cases where equal energy is transmitted in opposite directions. These cases are categorized into two types based on the properties of the response envelopes in the opposite configurations. Notably, the cases exhibiting nonreciprocal phase shifts, as discussed in Chapter 3, form a subset of those with equal transmitted energies in opposite directions.

Appendix C serves as supplementary material for Chapter 4, presenting the design of a short system with strong modulations targeted at achieving unidirectional vibration transmission. During this design process, because of the strong modulation amplitudes required, it was necessary to conduct a stability analysis to identify stable regions from which system parameters favorable for unidirectional transmission were selected.

Appendix D serves as a pilot study in two coupled modulated oscillators to indicate the potential role of nonlinearity on nonreciprocity in spatiotemporally modulated systems. It complements the discussions in Chapters 2 and 5.

Chapter 2

Linear Nonreciprocal Dynamics of Coupled Modulated Systems

2.1. Introduction

The principle of reciprocity states that propagation of elastic or acoustic waves in a medium remains invariant upon interchanging the positions of the source and receiver [1]. The reciprocity invariance generally holds in time-invariant materials functioning in the linear (small-amplitude) operating regime. This property has led to the development of various wave processing techniques and industrial applications, such as calibration of hydrophones and crack identification [2, 3].

In situations where reciprocity holds, the wave propagation properties (speed, amplitude, phase, etc.) cannot be controlled or tuned by changing the direction of propagation. Therefore, one way to enable direction-dependent vibration transmission is to circumvent reciprocity. Understanding the underlying mechanism for nonreciprocal propagation can enable the design and development of novel devices for energy harvesting, vibration isolation and signal processing. The theories and applications of nonreciprocal wave propagation have drawn the attention of many researcher in recent years [4].

Nonlinearity can break the reciprocity invariance in systems with broken mirror symmetry [60–63]. In linear systems, changing one or more of the effective properties of the system as a function of time *and* space is an effective approach to break the time-reversal symmetry and enable nonreciprocal transmission [6]. The time- and space-varying term within an effective property of the system is called spatiotemporal modulation.

Continuous media with wavelike spatiotemporal modulations in elasticity were used to study nonreciprocal wave propagation [7, 11, 16, 18, 64]. Here, nonreciprocity manifests as directional bandgaps in the dispersion curves, which indicates unidirectional transmission of energy through the system [25]. Inerters mounted on a vibrating base have been demonstrated to enable nonreciprocal transmission in a fully mechanical waveguide [23]. Nonreciprocal transmission of bending and longitudinal vibrations were analyzed for beams with local modulated attachments [9, 44, 47]. Nonreciprocal wave propagation also occurs in a medium with two-phase modulation; *i.e.* when both elastic modulus and density change spatiotemporally [15]. Moving media exhibit asymmetric dispersion characteristics too, including directional bandgaps [11, 13].

Nonreciprocity has been explored in discrete models of modulated materials as well. Unidirectional wave propagation can happen in metamaterials in which modulations are introduced to the stiffness of resonant springs [29], grounding springs [65], or springs of surface oscillators [22, 37]. Unidirectional wave propagation also occurs in a piezoelectric phononic lattice in which incident waves couple with directional elastic waves generated by applying spatiotemporally modulated voltages on the boundaries of piezoelectric cells [41, 48]. A study on a modulated system with only two degrees of freedom highlighted the role of phase as a contributor to nonreciprocity [57]. Experimental studies on nonreciprocal vibration transmission due to spatiotemporal modulations were performed on setups that are discrete and finite in length, for example by using piezoelectric materials to change stiffness [66, 67] and tuning electromagnet forces on magnetic masses [42, 43, 49, 68].

In this work, our objective is to systematically investigate the influence of different system parameters on steady-state vibration transmission in very short modulated systems under weak or strong modulation amplitudes. We focus exclusively on a system with two degrees of freedom (2-DoF). This is the smallest possible system for investigating nonreciprocity, and has the advantage of possessing well separated modes. Within this framework, we aim to understand the role of different parameters, particularly the modulation amplitude and phase, on nonreciprocal vibration transmission characteristics. The evaluation of (non)reciprocity in vibration transmission involves comparing both transmitted amplitudes (energies) and transmitted phases. Notably, the impact of strong modulations on the steady-state response of discrete systems is explored here for the first time.

Section 2.2 provides an analysis of a 2-DoF modulated system, along with an introduction to the solution methodology utilized throughout the paper. In Section 2.3, we delve into the characteristics of weakly modulated systems with a specific focus on nonreciprocity. Section 2.4 presents the study of vibration transmission in strongly modulated systems. Phase nonreciprocity, identified in both weakly and strongly modulated systems, is introduced in Section 2.5. Section 2.6 summarizes our findings.

2.2. Analysis of a 2-DoF modulated system

2.2.1. Formulation of the problem

Fig. 2.1 shows the schematic of the 2-DoF model of the coupled modulated systems studied in this work. The model consists of two identical masses, m, that are connected by a linear spring of stiffness k_c. $u(t)$ and $v(t)$ denote the rectilinear displacement of each mass from its static equilibrium position. Each mass is grounded by a spring with a temporally modulated stiffness, as well as a linear viscous damper. The modulated stiffness coefficients are $k_1(t) = k_{g,DC} + k_{g,AC}\cos(\omega_m t)$ and $k_1'(t) = k_{g,DC} + k_{g,AC}\cos(\omega_m t - \phi)$, each with a constant component $k_{g,DC}$ and a time-dependent modulation of amplitude $k_{g,AC}$ and frequency ω_m. The parameter ϕ represents the phase difference between the modulations of the two grounding springs. This is equivalent to the modulation wavenumber in a spatiotemporally modulated lattice. External harmonic forces are applied on each mass, expressed by $f_1(t) = F_1\cos(\omega_f t)$ and $f_2(t) = F_2\cos(\omega_f t)$.

We start by nondimensionalizing the governing equations, as detailed in Appendix 2A. In terms of nondimensional parameters, the equations of motion for the 2-DoF modulated system are:

$$\ddot{x}_1 + 2\zeta\dot{x}_1 + [1 + K_m\cos(\Omega_m\tau)]x_1 + K_c(x_1 - x_2) = P_1\cos(\Omega_f\tau), \tag{2.1a}$$

$$\ddot{x}_2 + 2\zeta\dot{x}_2 + [1 + K_m\cos(\Omega_m\tau - \phi)]x_2 + K_c(x_2 - x_1) = P_2\cos(\Omega_f\tau). \tag{2.1b}$$

Note that Eqs. (2.1a) and (2.1b) are identical when $\phi = 0$.

To investigate reciprocity, we need two configurations: (i) the *forward* configuration (or left-to-right, L2R) with $P_1 = P$ and $P_2 = 0$, where the output is the steady-state response of the second mass, $x_2^F(\tau)$; (ii) the *backward* configuration (or right-to-left, R2L) with $P_1 = 0$ and $P_2 = P$, where the output is the steady-state response of the first mass, $x_1^B(\tau)$. A reciprocal response is then characterized by $x_2^F(\tau)/P_1 = x_1^B(\tau)/P_2$ in this case, or simply $x_2^F(\tau) = x_1^B(\tau)$ because we use the same forcing amplitude for the *forward* and *backward* configurations.

The response of the modulated system is characterized by two frequencies Ω_f and Ω_m. Because these frequencies are independent from each other (incommensurate), the steady-state response of the system is neither harmonic nor periodic; it is quasi-periodic. To characterize the quasi-periodic response in the *forward* and *backward* configurations, we use the output

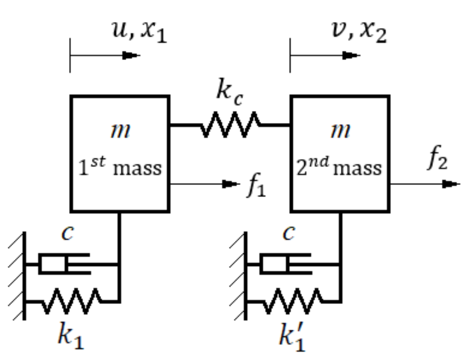

Figure 2.1: Schematic of the 2-DoF model of coupled modulated systems.

norms N^F and N^B, respectively, which are defined as:

$$N^{F,B} \quad = \lim_{T\to\infty} \sqrt{\tfrac{1}{T}\int_0^T [x_{2,1}^{F,B}(\tau)]^2 d\tau}, \tag{2.2a}$$

$$R \quad = \lim_{T\to\infty} \sqrt{\tfrac{1}{T}\int_0^T [x_2^F(\tau) - x_1^B(\tau)]^2 d\tau}. \tag{2.2b}$$

R is called the reciprocity bias, which quantifies the degree of (non)reciprocity of the system. By definition, $R = 0$ if and only if vibration transmission through the system is reciprocal.

2.2.2. Solution methodology

In the absence of a tractable exact analytical solution to Eq. (2.1), we use approximate methods to obtain analytical expressions for the steady-state response of the system. Informed by the numerical observations made in Appendix 2B, we write the steady-state response of the system in the *forward* and *backward* configurations as follows:

$$x_j^{F,B}(\tau) = \sum_{q=-\infty}^{\infty} [y_{j,q}^{F,B} e^{i(\Omega_f + q\Omega_m)\tau} + c.c.] = \sum_{q=-\infty}^{\infty} 2|y_{j,q}^{F,B}| \cos[(\Omega_f + q\Omega_m)\tau + \Psi_{j,q}^{F,B}] \tag{2.3}$$

where $j \in \{1, 2\}$ indicates the 1^{st} mass or the 2^{nd} mass, *c.c.* denotes the complex conjugate terms, and i is the imaginary unit. $y_{j,q}^F$ and $y_{j,q}^B$ are the complex-valued amplitudes of the harmonic components in the steady-state response in the two configurations. The phase angles are $\Psi_{j,q}^F$ =atan2 (imag ($y_{j,q}^F$), real ($y_{j,q}^F$)) and $\Psi_{j,q}^B$ =atan2 (imag ($y_{j,q}^B$), real ($y_{j,q}^B$)). The modal expansion in Eq. (2.3), in addition to satisfying the numerical observations in Appendix 2B, is the correct asymptotic solution for either weak or strong modulations, and it has been used extensively in the literature on modulated materials [17, 23, 32, 40, 64, 69, 70].

To calculate the complex-valued amplitudes $y_{2,q}^F$ and $y_{1,q}^B$, we use the method of averaging [58]. The full details of this procedure are provided in Appendix 2C. The outcome is a linear system of algebraic equations for the unknown amplitudes in Eq. (2.3); see Eq. (2C.3) in Appendix 2C. Subsequently, the expressions for the output norms and reciprocity bias in Eq. (2.2) can be rewritten in terms of the complex-valued amplitudes as:

$$N^{F,B} = \sqrt{2 \sum_{q=-\infty}^{\infty} |y_{2,1,q}^{F,B}|^2}, \tag{2.4a}$$

$$R = \sqrt{2 \sum_{q=-\infty}^{\infty} |y_{2,q}^F - y_{1,q}^B|^2}. \tag{2.4b}$$

In practice, the infinite summation in Eq. (2.4) needs to be truncated at a finite value of q, for example $q \in [-\mathcal{F}, \mathcal{F}]$ with $\mathcal{F} \in \mathbb{N}$, to approximate the response of the system and the output norms in Eq. (2.4). In general, the magnitude $|y_{j,q}|$ of a harmonic component (its participation in the steady-state response x_j) becomes smaller as q increases, and the accuracy of the overall approximation improves by increasing the value of $\mathcal{F}$. We choose higher values of $\mathcal{F}$ for systems with strong modulations than systems with weak modulations. Appendix 2C provides examples of the comparison between the results obtained from this approximation and direct numerical integration of the equations of motion.

The approximate solution developed here provides the convenience that the non-periodic steady-state response of a modulated system can be obtained by solving a linear algebraic system. We expect a similar methodology to apply to systems that have local resonators attached to them through springs of spatiotemporally modulated constants. Moreover, nonreciprocity can be investigated and understood by focusing on the differences between each pair of harmonic components in the two outputs: $2|y^F_{2,q}|\cos[(\Omega_f + q\Omega_m)\tau - \Psi^F_{2,q}]$ and $2|y^B_{1,q}|\cos[(\Omega_f + q\Omega_m)\tau - \Psi^B_{1,q}]$. We refer to such pair as a component-pair for ease of reference. For a given q, the frequencies of a component-pair are the same. Either $|y^F_{2,q}| \neq |y^B_{1,q}|$ or $\Psi^F_{2,q} \neq \Psi^B_{1,q}$ can indicate a nonreciprocal response.

2.3. Vibration transmission in weakly modulated systems

In this section, we provide a parametric study of the steady-state nonreciprocal dynamics for weak modulations, characterized by $K_m \leq 0.1$. In the absence of a universal definition of weak modulation, we consider weakly modulated systems to be those for which including one sideband resonance is sufficient for accurately capturing the steady-state response of the system; *i.e.* $\mathcal{F} = 1$ in Eq. (2.3). This allows us to distinguish between weak and strong modulations based on the influence of K_m on the resonance frequencies and the steady-state frequency response of the system. We discuss this in more detail in Section 2.4.

We start with investigating the effects of K_c and Ω_m, followed by the role of the symmetry-breaking parameter ϕ in breaking reciprocity.

2.3.1. Primary bands and sidebands

Fig. 2.2(a) shows the response of the system in the *forward* and *backward* configurations as a function of the forcing frequency, Ω_f. The response of the unmodulated system ($K_m = 0$) is included for comparison. The natural frequencies of the unmodulated system are $\Omega_{n1} = 1$ and $\Omega_{n2} = \sqrt{1 + 2K_c}$. We observe primary resonances of the modulated system occurring at $\Omega_{n1,2}$, accompanied by sideband (secondary) resonances at $\Omega_{n1} \pm \Omega_m$ and $\Omega_{n2} \pm \Omega_m$. Except at the sideband resonances, the response curves of the modulated and unmodulated systems are the same. Within a sideband, the significant difference between the modulated response

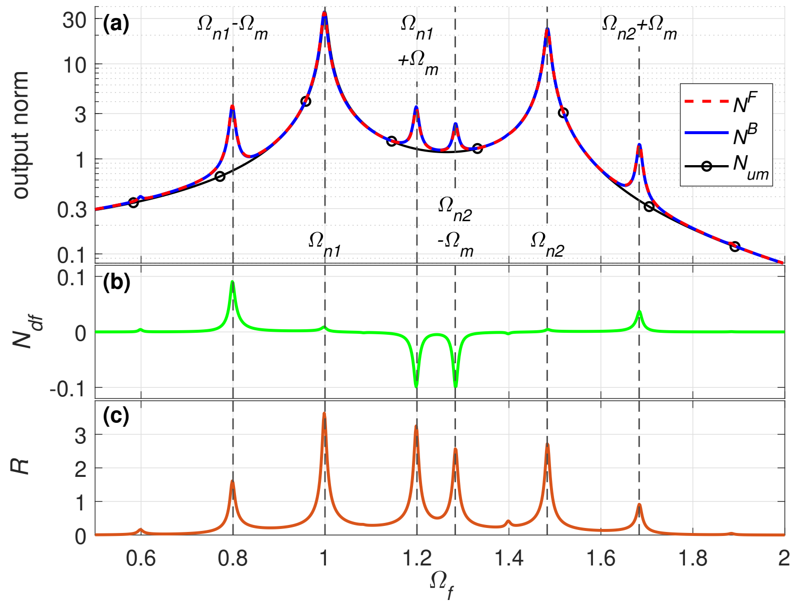

Figure 2.2: Variations of (a) output norms, (b) difference between output norms and (c) reciprocity bias as functions of Ω_f. System parameters: $K_c = 0.6$, $\zeta = 0.005$, $K_m = 0.1$, $\Omega_m = 0.2$, $\phi = \pi/2$ and $P = 1$. The black curve with circles in Panel (a) represents the output norm of the unmodulated system, which is denoted by N_{um}.

and the unmodulated response is due to the spatiotemporal modulations. The values of K_c and Ω_m are chosen such that there is no overlap between sideband resonances; we consider overlap in Section 2.3.3. The sidebands further from the primary resonances ($\Omega_{n1} \pm 2\Omega_m$, $\Omega_{n2} \pm 2\Omega_m$, etc.) have a negligible influence on the response in weakly modulated systems and have been ignored.

We emphasize that parametric amplification does not occur in the response regime that we investigate in this work. Parametric amplification occurs when the modulation frequency is locked to the forcing frequency (typically $\Omega_m = 2\Omega_f$), and is often characterized by unbounded response even in the presence of damping [71]. In this work, however, Ω_m and Ω_f are independent of each other. If we had fixed the frequencies such that $\Omega_m = 2\Omega_f$, we would have observed parametric amplification (unbounded response) at $\Omega_f = \Omega_{n1}, \Omega_{n2}$ and $(\Omega_{n1} + \Omega_{n1})/2$ for both configurations.

Although we do not expect the response to be reciprocal (because $\phi \neq 0$), the output norms in Fig. 2.2(a) seem to indicate a reciprocal response. Fig. 2.2(b) shows the difference between the two output norms (transmitted energies),

$$N_{df} = N^F - N^B. \tag{2.5}$$

We see that the transmitted energies are almost equal in the two directions, with a small difference that occurs predominantly at the sideband resonances.

Fig. 2.2(c) shows the reciprocity bias, R. It shows that despite equal energies transmitted in the opposite directions (small N_{df}), the transmission of vibrations is nonreciprocal ($R > 0$) throughout the entire range of forcing frequencies considered. Notably, the value of R is much larger than the value of N_{df}. Furthermore, the reciprocity bias is large not only at sideband resonances, but also at the primary resonances.

This difference between the values of R and N_{df} indicates that the phase difference between output displacements is the main contributor to breaking reciprocity in this system. In other words, the phase difference between the two outputs makes a much greater contribution to nonreciprocity than the amplitude difference between them.

To better understand the contribution of phase to breaking reciprocity, we consider the amplitudes and phases of the main three harmonic components of the response; $q \in \{-1, 0, 1\}$ in Eq. (2.3). Recall that because K_m is small (weak modulation), the magnitudes of the outer sidebands ($|q| > 1$) are increasingly small and their contribution to the overall response is negligible.

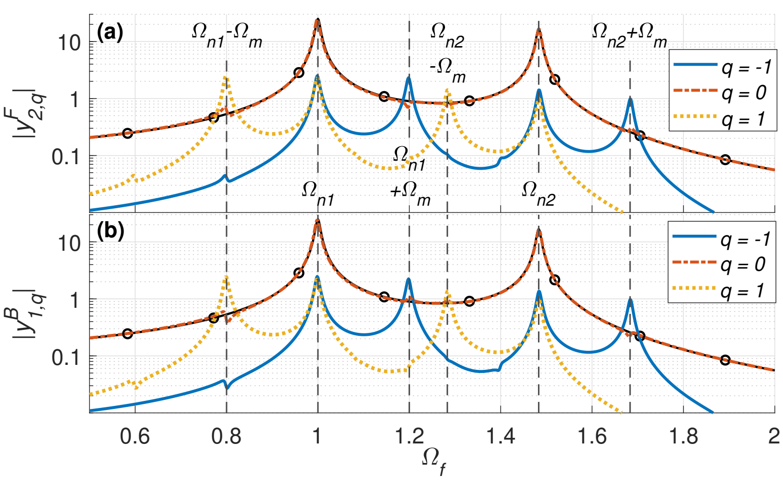

Figure 2.3: Plots of the amplitudes of three components ($q \in \{-1, 0, 1\}$) of (a) *forward* output and (b) *backward* output. The black curves with circles show the amplitude of the unmodulated system.

Fig. 2.3 shows the amplitudes of the three harmonic components of the response for the *forward* and *backward* configurations; *i.e.* the component-pairs. The black curves with circles represent the amplitude of the harmonic response of the unmodulated system for comparison. The amplitude of the component $q = 0$ (primary resonance), which almost coincides with the unmodulated response, has the highest amplitudes at Ω_{n1} and Ω_{n2}, as expected, and shows negligible amplification near the sideband resonances. At the upper

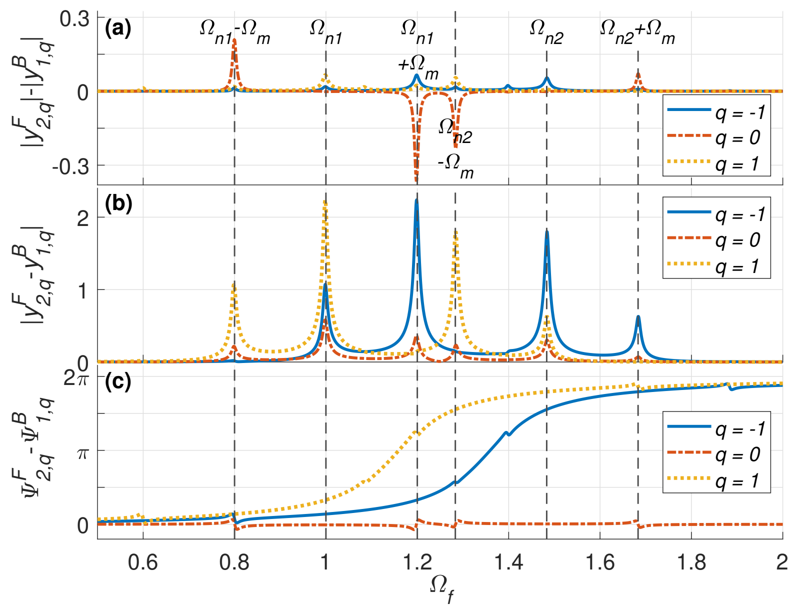

Figure 2.4: Plots of (a) the amplitude difference, (b) the contribution of each component-pair to the reciprocity bias and (c) the phase difference.

sideband resonances, $\Omega_{n1}+\Omega_m$ and $\Omega_{n2}+\Omega_m$, the largest component is $q=-1$ for both the *forward* and *backward* configurations. Similarly, the largest component is $q=1$ at the lower sideband resonances, $\Omega_f=\Omega_{n1,2}-\Omega_m$.

Fig. 2.4(a) shows the difference in the amplitudes of the component-pairs; *cf.* Fig. 2.3. As expected, the differences in the amplitudes are too small to account for the reciprocity bias observed in Fig. 2.2(c).

Fig. 2.4(b) shows the magnitude of the amplitude difference, $|y^F_{2,q}-y^B_{1,q}|$, which accounts for contributions from phase. We see that the component-pairs $q=\pm 1$ make the biggest contributions to reciprocity bias. Consistent with Fig. 2.3, the component-pair with $q=1$ contributes most strongly at the lower sideband resonances, while the component-pair with $q=-1$ contributes most strongly at the upper sidebands. Notably, this is in contrast to Fig. 2.4(a), in which the contributions from phase were ignored.

The role of phase is also observed in the primary component-pair $q=0$: although the difference between the amplitudes is relatively large near the sideband resonances in Fig. 2.4(a), their contribution to reciprocity bias is relatively small in Fig. 2.4(b) where the phase effect is taken into account.

To complete the picture, Fig. 2.4(c) shows the phase difference for each component-pair. The phase difference in the component-pair $q=0$ agrees with the contrasting behavior observed in panels (a) and (b). The component-pairs $q \pm 1$ undergo significant phase changes, which contributes to the reciprocity bias. Note, also, that the three curves in Fig. 2.4(c) never intersect with the horizontal line ($\Psi^F_{2,q} - \Psi^B_{1,q} = 0$) at the same Ω_f. This implies that the difference between transmitted phases always contributes to the reciprocity bias.

In summary, we found the transmitted phase to be the main contributor to nonreciprocity in short system with weak modulation. The largest contribution to phase was associated to component-pairs $q = \pm 1$.

2.3.2. The Role of ϕ

The parameter ϕ represents a relative phase shift between the modulations of the two grounding springs in Fig. 2.1. This phase shift represents a spatial modulation in the grounding stiffness coefficient of the system. It is the same as the modulation wavenumber in a spatiotemporally modulated system. However, we do not refer to ϕ as the modulation wavenumber because the system we study has only two units. Note that the modulation phase, ϕ, is the only difference between the two oscillators. Thus, it takes on the role of breaking the mirror-symmetry of the system: if $\phi = 0$, the response of the system remain reciprocal by virtue of mirror symmetry.

Fig. 2.5 shows the surface plots of N_{df} and R as functions of Ω_f and ϕ for the same parameters used in Fig. 2.2. We observe that N_{df} changes sign along $\phi = \pi$. This is also a line of symmetry for R, implying that R has a local maximum when $\phi = \pi$. We will discuss this behavior in more detail in Section 2.5.

To explain the symmetries observed in Fig. 2.5, we consider the complex-valued amplitudes $y^F_{2,q}$ and $y^B_{1,q}$. It can be obtained from Eqs. (2C.6) and (2C.7), that:

$$y^F_{2,0}(\phi) = y^B_{1,0}(2\pi - \phi), \;\; |y^F_{2,q}(\phi)| = |y^B_{1,q}(2\pi - \phi)|, \tag{2.6}$$

where $q \in [-\mathcal{F}, \mathcal{F}]$. The plot of N_{df} is therefore odd-symmetric about the line $(\phi, N_{df}) = (\pi, 0)$, as seen in Fig. 2.5(a). Furthermore, $N^F = N^B$ when $\phi = \pi$, regardless of the value of Ω_f. For the corresponding phases, we have:

$$\Psi^F_{2,q}(\phi) - \Psi^B_{1,q}(\phi) = \Psi^B_{1,q}(2\pi - \phi) - \Psi^F_{2,q}(2\pi - \phi). \tag{2.7}$$

The plot of R is therefore symmetric about the plane $\phi = \pi$, as shown in Fig. 2.5(b).

The relations in Eq. (2.6) and Eq. (2.7) are valid regardless of the values of all other system parameters; they hold even in systems with more units [72]. Thus, the odd-symmetry of N_{df} and the symmetry of R persist with the change of system parameters.

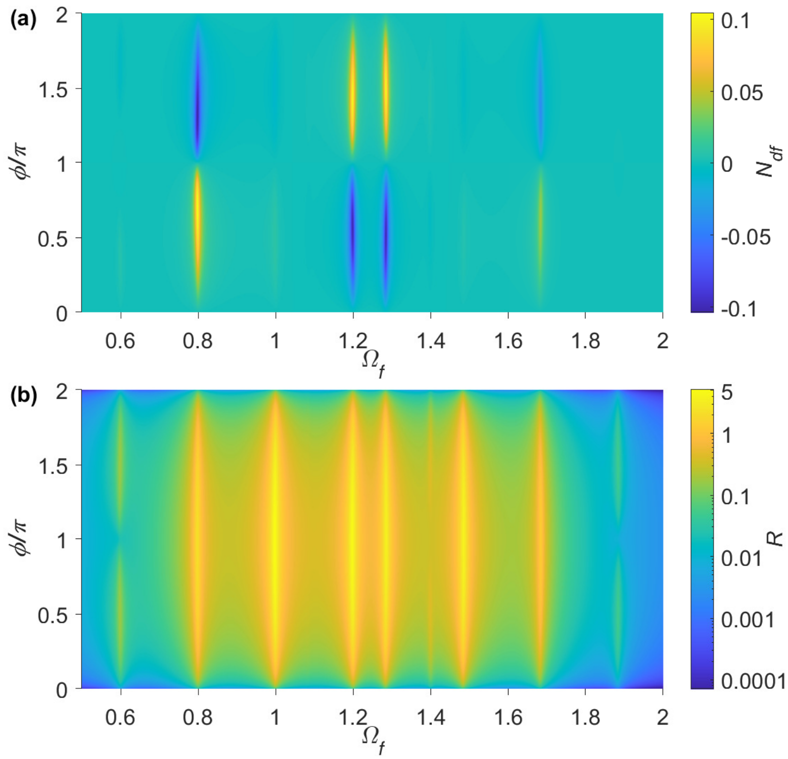

Figure 2.5: Plots of (a) N_{df} and (b) R as functions of Ω_f and ϕ.

The six resonant frequencies of a weakly modulated system correspond to the zeros of the determinant of matrix $\underline{\underline{D}}$ in Eq. (2C.3) with $\zeta = 0$ and $\mathcal{F} = 1$. This determinant can be expanded as:

$$|\underline{\underline{D}}| = \mathcal{D}_0 + \epsilon^2 \mathcal{D}_2 + O(\epsilon^4) \tag{2.8}$$

where

$$\begin{aligned}
\mathcal{D}_0 =& A_{-1}^2 A_0^2 A_1^2 - K_c^2 (A_{-1}^2 A_0^2 + A_{-1}^2 A_1^2 + A_0^2 A_1^2) \\
&+ K_c^4 (A_{-1}^2 + A_0^2 + A_1^2) - K_c^6, \\
\mathcal{D}_2 =& 2A_0 (K_c^2 - A_{-1} A_1)(A_{-1} + A_1) \\
&- 2K_c^2 (A_{-1}^2 + A_1^2 - 2K_c^2) \cos\phi, \\
\epsilon =& K_m/2,
\end{aligned}$$

and A_{-1}, A_0 and A_1 can be obtained from Eq. (2C.4). For the weakly modulated system studied in this section, we have $\epsilon \leq 0.05$. Therefore, $|\underline{\underline{D}}| \approx \mathcal{D}_0$ throughout the frequency range considered, $0.5 \leq \Omega_f \leq 2$. The six resonant frequencies can be approximated by solving $\mathcal{D}_0(\Omega_f) = 0$, which gives $\Omega_{n1,2}$ and $\Omega_{n1,2} \pm \Omega_m$. These six frequencies do not depend on the modulation phase, ϕ. This is why the regions of high amplitude in Fig. 2.5 appear as vertical stripes. We will see in Section 2.4 that this is not true in strongly modulated systems.

2.3.3. Overlap of two resonant frequencies

The primary ($\Omega_{n1,2}$) and sideband ($\Omega_{n1,2} \pm \Omega_m$) frequencies can be tuned by changing the values of coupling stiffness, K_c, and modulation frequency, Ω_m. In this section, we keep $K_c = 0.6$ and change Ω_m to investigate the influence of frequency overlaps.

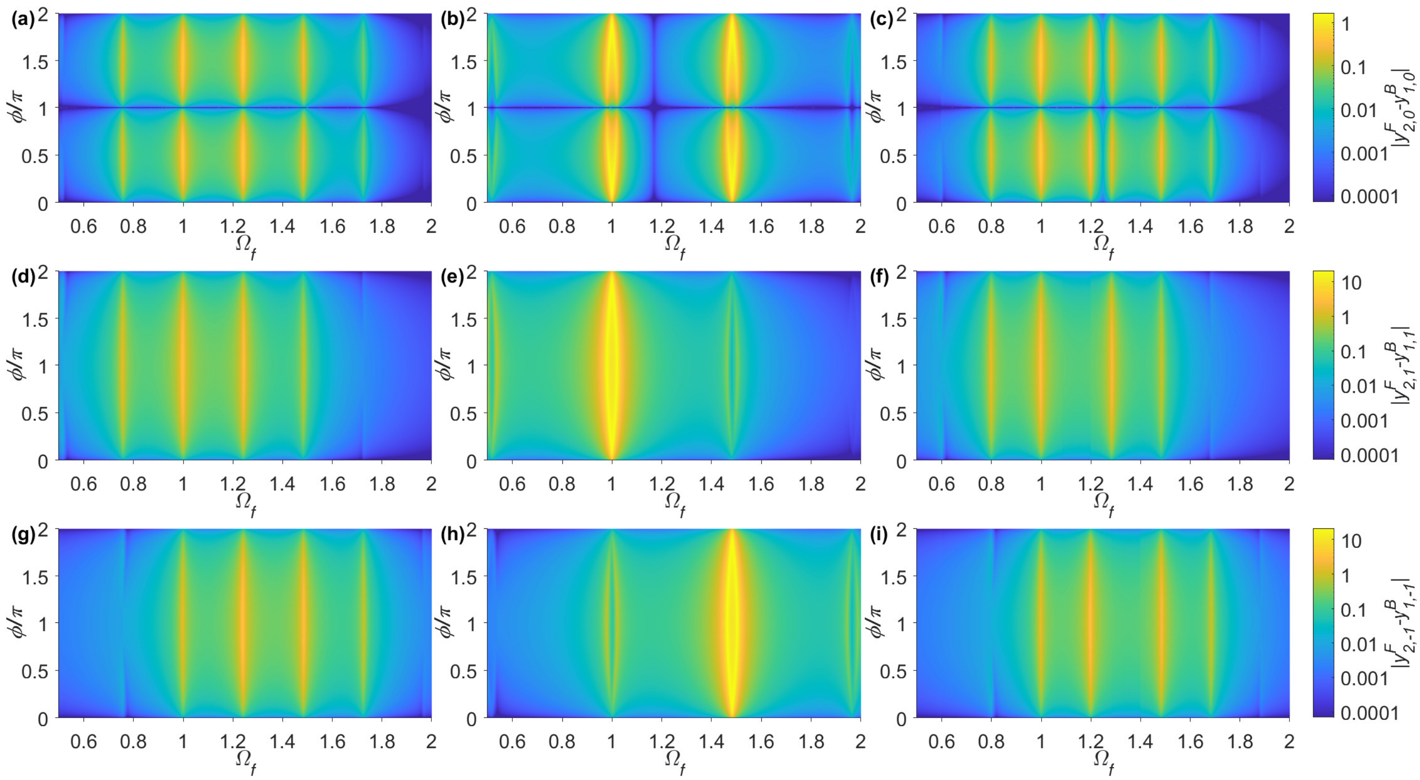

Figure 2.6: Plots of $|y^F_{2,q} - y^B_{1,q}|$ for $q \in \{-1, 0, 1\}$ as functions of Ω_f and ϕ for three systems with different values of Ω_m: (a,d,g) *Case A* with $\Omega_m = (\Omega_{n2} - \Omega_{n1})/2$; (b,e,h) *Case B* with $\Omega_m = \Omega_{n2} - \Omega_{n1}$; (c,f,i) *Case C* with $\Omega_m = 0.2$.

Fig. 2.6 shows the variation of $|y^F_{2,q} - y^B_{1,q}|$ as functions of Ω_f and ϕ for component-pairs with $q = 0$ (first row), $q = 1$ (second row) and $q = -1$ (third row). We consider two scenarios with resonant frequency overlaps: (i) *Case A*: a system with $\Omega_m = (\Omega_{n2} - \Omega_{n1})/2$, where two sidebands overlap (left column in Fig. 2.6); (ii) *Case B*: a system with $\Omega_m = \Omega_{n2} - \Omega_{n1}$, where each primary band overlaps with a sideband (middle column in Fig. 2.6). A third scenario, *Case C*, is shown in the right column of Fig. 2.6, where there is no frequency overlap (the same as Fig. 2.5). Except for Ω_m, all system parameters are the same in these three scenarios. The same logarithmic scale is used in each row.

We observe in Fig. 2.6 that the magnitude of $|y^F_{2,q} - y^B_{1,q}|$ in *Case B* is significantly higher than those in *Case A* and *Case C* for all component pairs, $q = -1, 0, 1$. Accordingly, the magnitude of reciprocity bias in *Case B* is the highest among the three (not shown). We also observe that the component-pairs $q = \pm 1$ have a more significant contribution to reciprocity bias than the component-pair $q = 0$. We observe in the top row of Fig. 2.6 that $|y^F_{2,0} - y^B_{1,0}| = 0$ when $\phi = \pi$, as predited by Eq. (2.6).

In *Case B* (middle column in Fig. 2.6), we observe that the regions of high amplitude no longer appear as vertical stripes, as they do in *Case A* and *Case C*. This means that the resonant frequencies have a weak dependence on the modulation phase, ϕ. This happens because $\mathcal{D}_0$ and $\epsilon^2 \mathcal{D}_2$ in Eq. (2.8) have the same order of magnitude when a primary band and a sideband overlap ($\Omega_m = \Omega_{n2} - \Omega_{n1}$).

2.4. Vibration transmission in strongly modulated systems

Strong modulations ($K_m > 0.1$) bring about different vibration characteristics in spatiotemporally modulated systems. We investigate some of these characteristics in this section.

Note that increasing the modulation amplitude can result in parametric instabilities, which lead to unbounded response [73]. We have computed the stability bounds for our system, and further ensured that all the results presented in this work are stable and remain bounded by direct numerical integration of the governing equations. However, a detailed analysis of parametric instabilities falls outside the scope of the current work and will be presented separately elsewhere.

2.4.1. Steady-state response

Fig. 2.7 shows the response of a strongly modulated system with $K_m = 0.8$ in the *forward* and *backward* configurations; *cf.* Fig. 2.2. All other system parameters are the same as those used in Section 2.3.1.

The number and frequencies of resonance peaks in Fig. 2.7(a) are very different from what we observed in weakly modulated systems. The peaks no longer appear at Ω_{n1}, Ω_{n2}, $\Omega_{n1} \pm \Omega_m$ and $\Omega_{n2} \pm \Omega_m$. Sideband resonances are no longer limited to $q \in \{-1, 0, 1\}$ because the amplitudes of higher-order sidebands ($q > 1$) do not diminish as significantly. And it is difficult to distinguish primary and sideband resonances by their relative peak amplitudes. Even though the values of the peak amplitudes are similar to those in the weakly modulated system, there is clearly more energy in the strongly modulated system; compare the areas under the frequency response functions in Figs. 2.7(a) and 2.2(a).

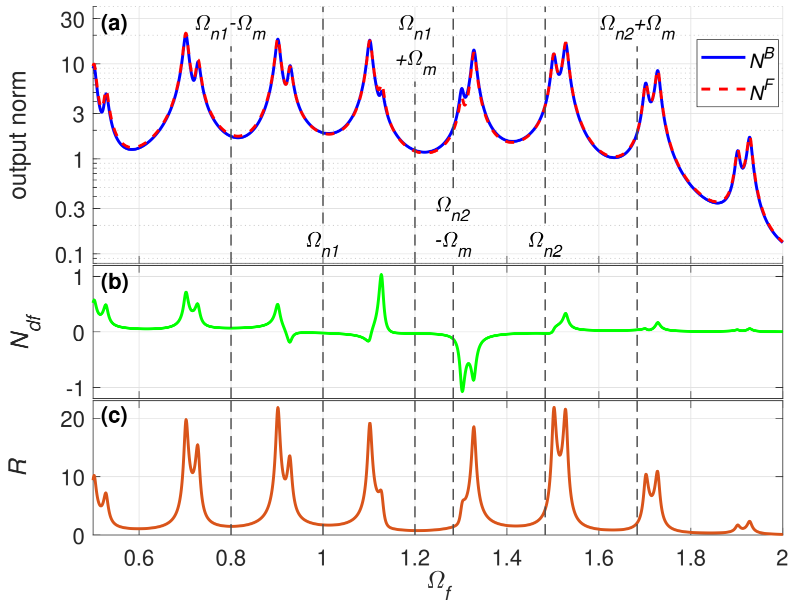

Figure 2.7: Plots of (a) output norms, (b) difference between output norms and (c) reciprocity bias as functions of forcing frequency.

Despite these key differences between weakly and strongly modulated systems, the transmitted phase remains a signficant contributor to the reciprocity bias. Figs. 2.7(b) and 2.7(c) show the difference between transmitted energies, N_{df}, and reciprocity bias, R, respectively. We observe that although the difference in transmitted energies is relatively small, reciprocity bias is very large in comparison. This indicates the important role of phase in breaking reciprocity.

Fig. 2.8 shows the variation of N_{df} and R as functions of Ω_f and ϕ. The symmetry properties discussed in Section 2.3.2 still hold because they do not depend on the strength of modulation. Most notably, we observe that the peak frequencies depend on the modulation phase, ϕ, in stark contrast to weakly modulated systems; *cf.* Fig. 2.5. We explore this phenomenon in the next section.

2.4.2. Resonant frequencies

We calculate the resonant frequencies of the modulated system based on the formulation developed in Appendix 2C. The resonant frequencies of the systems are the zeros of the determinant of the matrix $\underline{\underline{D}}$ in Eq. (2C.3) when $\zeta = 0$; *i.e.*, $|\underline{\underline{D}}| = 0$. The response amplitude in this case becomes infinite, as expected.

In weakly modulated systems (small K_m), the first superdiagonal and the first subdiagonal of $\underline{\underline{D}}$ are negligible compared to its main diagonal. Because the modulation parameters

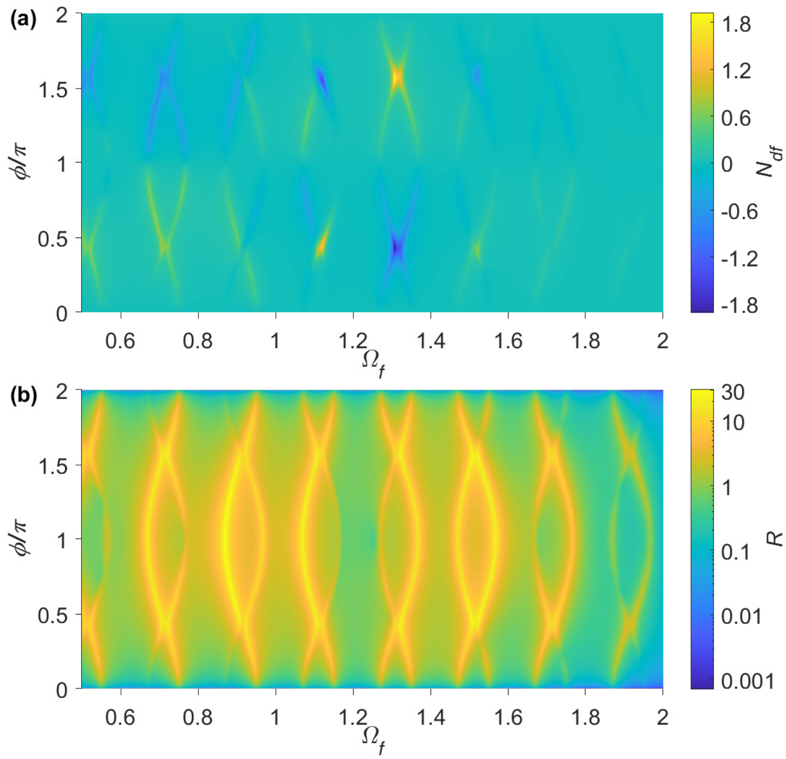

Figure 2.8: Plots of (a) N_{df} and (b) R as functions of Ω_f and ϕ.

K_m and ϕ do not appear on the main diagonal, they have little influence on the solutions of $|\underline{\underline{D}}(\Omega_f)| = 0$. Therefore, the resonant frequencies of the weakly modulated system are mainly determined by K_c and Ω_m; see Eq. (2.8). In strongly modulated systems, the entries on the first super diagonal and the first subdiagonal of $\underline{\underline{D}}$ are no longer negligible. Therefore, the resonant frequencies of the system depend on the values of K_m and ϕ too.

Fig. 2.9 shows the natural frequencies of the strongly modulated systems as a function of ϕ for $K_m \in \{0.3, 0.5, 0.8\}$, $K_c = 0.6$ and $\Omega_m = 0.2$. The horizontal dashed lines denote $\Omega_{n1} \pm q\Omega_m$ and $\Omega_{n2} \pm q\Omega_m$ with $q = 0, \cdots, 4$. We observe that all the loci in Fig. 2.9 have local maxima at $\phi \in \{0, \pi, 2\pi\}$, a property that stems from the symmetries of the cosine function in the modulation term. As K_m increases to 0.3 and 0.5, the deviations in natural frequencies are largest near $\phi = \pi$, and decrease monotonically away from this point. The variations in the natural frequencies are no longer monotonic for higher strengths of modulation, as observed for $K_m = 0.8$. We also observe avoided crossing between adjacent branches; see the loci of Ω_{n2} to $\Omega_{n1}+3\Omega_m$ for an example of this.

Fig. 2.10 shows the variation of the primary natural frequencies, Ω_{n1} and Ω_{n2}, as a function of modulation phase for $\Omega_m \in \{0.2, 0.33, 0.4\}$. We observe that at larger values of the

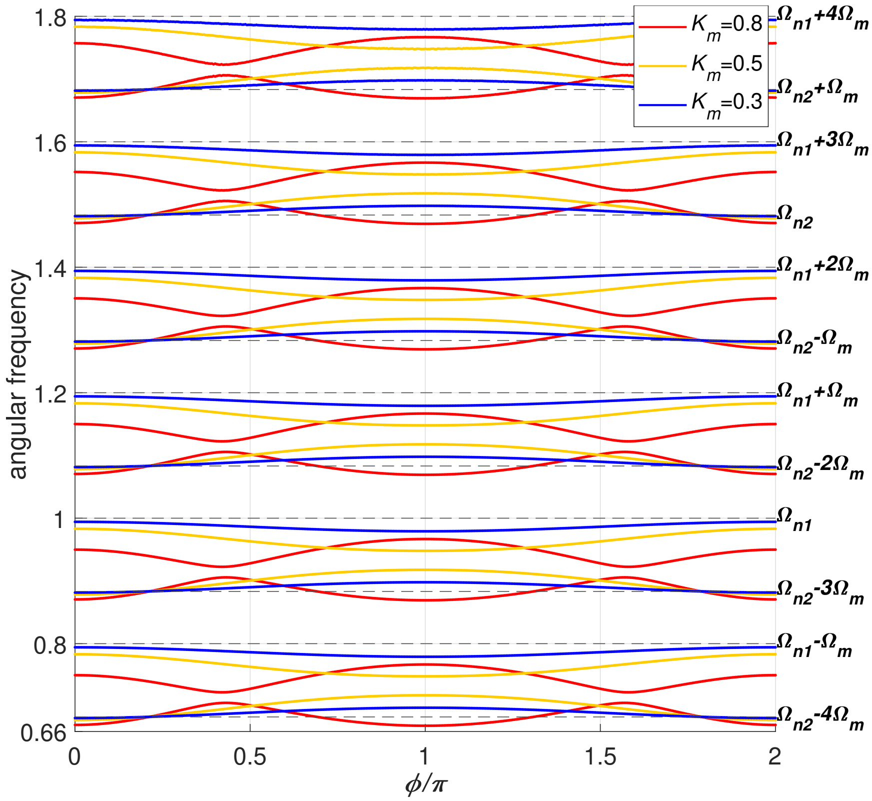

Figure 2.9: Resonant frequencies of a strongly modulated system as functions of ϕ.

modulation frequency, the range of variation in Ω_{n1} and Ω_{n2} is larger as well.

2.5. Phase nonreciprocity

Looking back at Eq. (2.2), if $R = 0$ then it is obvious that $N^F = N^B$; *i.e.*, if the response is reciprocal then the transmitted energies in the *forward* and *backward* directions are identical. However, $N^F = N^B$ cannot guarantee a reciprocal response. This means that it is possible to have nonreciprocal response ($R \neq 0$) that is accompanied by equal energies transmitted in opposite directions ($N^F = N^B$). We refer to this scenario as *phase nonreciprocity* because a difference in the transmitted phases is the sole contributor to nonreciprocity. Phase nonreciprocity in vibration transmission has been reported in time-invariant nonlinear systems [51, 52].

Due to the odd-symmetry of N_{df} about the line $(\phi, N_{df}) = (\pi, 0)$, a trivial case of phase nonreciprocity occurs when $\phi = \pi$, regardless of the values of other system parameters. This is because the matrix $\underline{\underline{D}}$ in Eq. (2C.3) becomes symmetric for $\phi = \pi$. Therefore, the amplitudes of each pair of harmonic components, $|y^F_{2,q}|$ and $|y^B_{1,q}|$, become equal for $q = 0, \pm 1, \pm 2, \cdots$. Meanwhile, $\Psi^F_{2,q} - \Psi^B_{1,q} = \pi$ if q is an odd number; $\Psi^F_{2,q} - \Psi^B_{1,q} = 0$ if q is

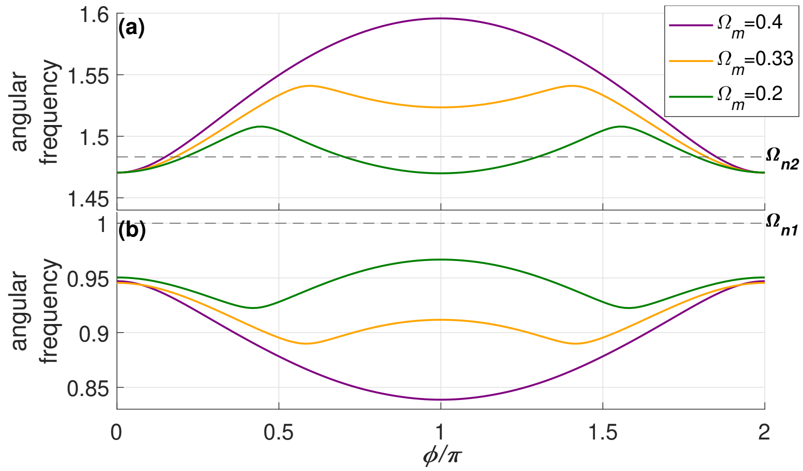

Figure 2.10: resonant frequencies nearby (a) Ω_{n1} and (b) Ω_{n2} as functions of ϕ.

an even number.

If $\phi \neq \pi$, there exist combinations of Ω_f and ϕ which can lead to $N_{df} = 0$. Because $R > 0$ throughout the ranges of Ω_f and ϕ considered, the response at these combinations of Ω_f and ϕ is therefore phase nonreciprocal. Fig. 2.11 shows the outputs in the time domain for two examples of phase nonreciprocity with $\phi = \pi$ and $\phi \neq \pi$. While it is obvious that $x_2^F(\tau) \neq x_1^B(\tau)$, the transmitted vibrations have the same amount of energy, $N^F = N^B$.

For the non-trivial case of $\phi \neq \pi$, a more stringent requirement than equal transmitted energies ($N^F = N^B$) is to have nonreciprocal transmission with the same waveform. We were only able to find parameters that lead to this scenario in systems with more than two degrees of freedom. The methodology involved for these calculations falls beyond the scope of this paper and is presented elsewhere [74].

2.6. Conclusions

We investigated nonreciprocal vibration transmission in a system of coupled mechanical oscillators subject to spatiotemporal stiffness modulations. The temporal modulation appeared as harmonic modulation of the grounding stiffness of each oscillator. The phase difference between the two temporal modulations (ϕ) acts as the spatial modulation, equivalent to the modulation wavenumber in a longer system. The modulation phase, ϕ, acts as the symmetry-breaking parameter that is necessary to break reciprocity. We used the averaging method to develop an analytical framework to obtain the steady-state quasi-periodic response of the system to harmonic external excitation. These results were validated against direct numerical simulation of the response of the system for both weak and strong modulations.

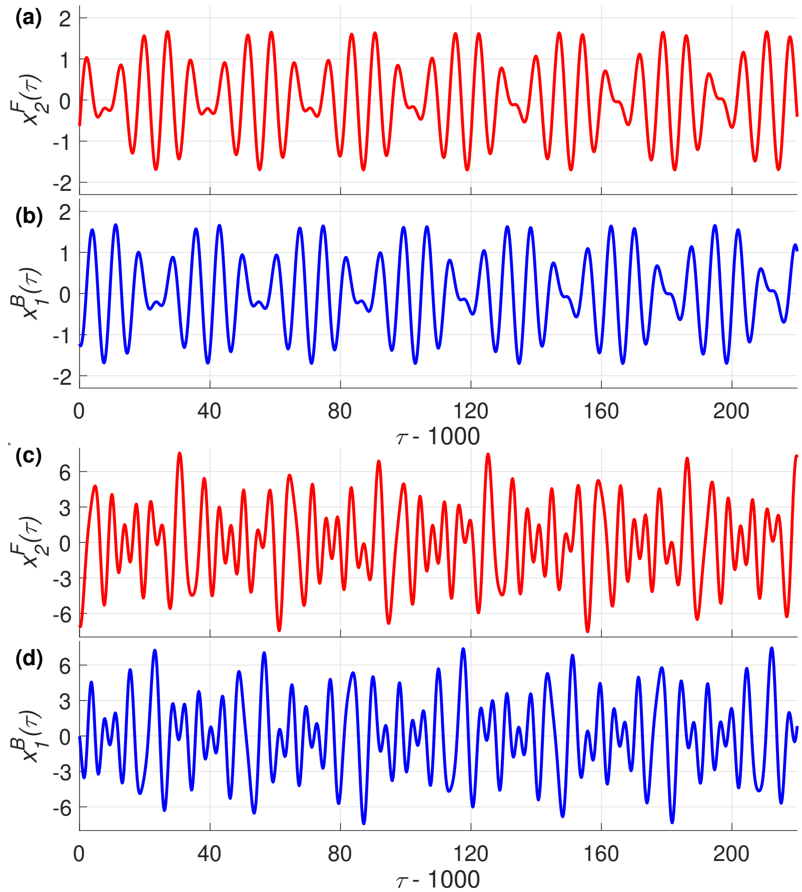

Figure 2.11: Plots of *forward* and *backward* outputs. Common parameters in these two examples: $K_c = 0.6$, $\zeta = 0.005$, $\Omega_m = 0.2$ and $P = 1$. (a,b) $\phi = \pi$, $\Omega_f = 0.79$ and $K_m = 0.1$; (c,d) $\phi = 0.75\pi$, $\Omega_f = 0.93$ and $K_m = 0.8$.

We found the response to be nonreciprocal when $\phi \neq 0$, as expected. However, the transmitted energies in the forward and backward configurations were similar in most cases, meaning that the difference between the transmitted phases is the main contributor to breaking reciprocity in short systems. This was the case for both weak and strong modulations.

In weakly modulated systems, we found only one pair of sideband resonances to be sufficient to capture the response of the system accurately. The pairs of harmonic components of the response (primary and sideband) contribute differently to the reciprocity bias. We found that an overlap of a primary and sideband resonance results in stronger nonreciprocity than an overlap of two sideband frequencies.

Increasing the strength of modulations significantly increases the reciprocity bias because there is more energy provided to the system. Increasing the modulation amplitude also makes the resonance frequencies dependent on the modulation phase and amplitude. The frequency contents of the response of strongly modulated systems are richer due to contributions from additional (higher-order) sideband frequencies.

The exclusive focus on modulated systems with two units was motivated by the system having well separated modes. This enabled us to elucidate the roles of the primary and side-band resonances of the system, and their overlaps, in breaking reciprocity. We provided a detailed analysis of the primary and sideband resonances, and component-pairs, in how they contribute to nonreciprocity for both weakly and strongly modulated systems. An equally technical discussion of the influence of the number of units falls outside the scope of this work. However, the methodology we presented holds for modulated systems of any number of units. For example, one can increase the reciprocity bias by including more units in the system. This is accompanied by an increasing difference between the transmitted amplitudes, and can ultimately lead to unidirectional transmission. This intuitive attribute of nonreciprocity is demonstrated numerically elsewhere [75].

We found two types of nonreciprocal response in which equal amounts of energy is transmitted in the forward and backward configurations. In one case, the two output displacements are distinguished by just a phase shift, whereas in the other the two waveforms are different while maintaining the same energy. This feature will be addressed in detail in the near future, along with an analysis of parametric instabilities for strongly modulated systems. The analytical framework developed here paves the way for these studies.

Appendices

2A. Non-dimensionalization

The equations of motion which govern the 2-DoF modulated system in Fig. 2.1 read:

$$m\frac{d^2u}{dt^2}+c\frac{du}{dt}+k_1u+k_c(u-v)=F_1\cos(\omega_f t), \tag{2A.1a}$$

$$m\frac{d^2v}{dt^2}+c\frac{dv}{dt}+k_1'v+k_c(v-u)=F_2\cos(\omega_f t), \tag{2A.1b}$$

where $k_1 = k_{g,DC} + k_{g,AC}\cos(\omega_m t)$ and $k_1' = k_{g,DC} + k_{g,AC}\cos(\omega_m t - \phi)$. We define $\tau = \omega_0 t$, where $\omega_0 = \sqrt{k_{g,DC}/m}$. Therefore, $d/dt = \omega_0 d/d\tau$, $d^2/dt^2 = \omega_0^2 d^2/d\tau^2$.

To non-dimensionalize, we define $\zeta = c/(2m\omega_0)$, $\Omega_m = \omega_m/\omega_0$, $\Omega_f = \omega_f/\omega_0$, $K_c = k_c/k_{g,DC}$, $K_m = k_{g,AC}/k_{g,DC}$, $P_1 = F_1/(ak_{g,DC})$, $P_2 = F_2/(ak_{g,DC})$, $x_1 = u/a$ and $x_2 = v/a$, where a is a representative length. After substituting them into Eq. (2A.1), we obtain:

$$m a \omega_0^2 \ddot{x}_1 + 2\zeta m a \omega_0^2 \dot{x}_1 + k_{g,DC} a x_1 \left[1 + K_m \cos(\Omega_m \tau)\right] + K_c k_{g,DC} a (x_1 - x_2) = P_1 a k_{g,DC} \cos(\Omega_f \tau), \tag{2A.2a}$$

$$m a \omega_0^2 \ddot{x}_2 + 2\zeta m a \omega_0^2 \dot{x}_2 + k_{g,DC} a x_2 \left[1 + K_m \cos(\Omega_m \tau - \phi)\right] + K_c k_{g,DC} a (x_2 - x_1) = P_2 a k_{g,DC} \cos(\Omega_f \tau), \tag{2A.2b}$$

where $\ddot{x}$ and $\dot{x}$ represent $\frac{d^2x}{d\tau^2}$ and $\frac{dx}{d\tau}$, respectively. Eq. (2A.2) can be further simplified as:

$$\ddot{x}_1 + 2\zeta \dot{x}_1 + [1 + K_m \cos(\Omega_m \tau)] x_1 + K_c (x_1 - x_2) = P_1 \cos(\Omega_f \tau), \tag{2A.3a}$$

$$\ddot{x}_2 + 2\zeta \dot{x}_2 + [1 + K_m \cos(\Omega_m \tau - \phi)] x_2 + K_c (x_2 - x_1) = P_2 \cos(\Omega_f \tau). \tag{2A.3b}$$

In this paper, calculations and analysis of the response of the 2-DoF modulated system are all based on Eq. (2A.3), which is the same as Eq. (2.1).

2B. Frequency contents of the outputs

Due to the simultaneous presence of external and parametric excitations of incommensurate frequencies, it is not straightforward to guess the frequency spectrum of the steady-state output of modulated systems. Here, we use the Runge-Kutta method to obtain the transient response of the modulated system numerically. The output displacement of the system is then recorded after the steady state is reached. We do this for the *forward* configuration with weak modulation and the *backward* configuration with strong modulation. We then obtain the Fast Fourier Transform (FFT) of the steady-state outputs, shown in Fig. 2B.1.

We observe in Fig. 2B.1 that all the response is dominated by the frequencies $\Omega_f + q\Omega_m$ where $q \in \{\cdots, -2, -1, 0, 1, 2, \cdots\}$. In the case of weak modulations, Fig. 2B.1(a), the magnitudes (heights) of the peaks decrease rapidly as the frequency moves away from Ω_f (notice the logarithmic scale for the amplitude). For a strongly modulated system, however, the height of a peak is not directly related to its distance to Ω_f, as shown in Fig. 2B.1(b).

We conclude for both weakly and strongly modulated systems, that the output can be reasonably approximated using a truncated harmonic expansion with a set of frequencies determined by Ω_f and Ω_m. This leads to the expressions used in Eq. (2.3).

2C. Application of the averaging method

We use the system in the *forward* configuration to show the application of the averaging method to approximate the steady-state response of the 2-DoF modulated system. The same procedure can be used for the *backward* configuration.

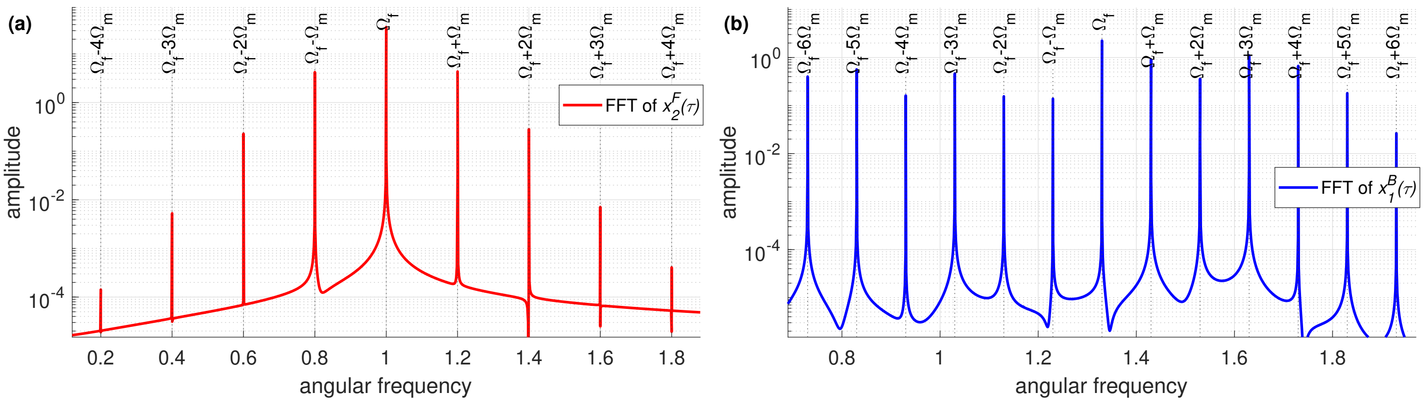

Figure 2B.1: Frequency spectrum of the steady-state response. Parameters in these examples: (a) $K_c = 0.6$, $K_m = 0.1$, $\zeta = 0.005$, $\Omega_m = 0.2$, $\phi = 0.5\pi$, $P = 1$ and $\Omega_f = 1$, in *forward* configuration; (b) $K_c = 0.7$, $K_m = 0.6$, $\zeta = 0.005$, $\Omega_m = 0.1$, $\phi = 0.3\pi$, $P = 1$ and $\Omega_f = 1.33$, in *backward* configuration.

We start by substituting Eq. (2.3), the complex Fourier series of the steady-state response, into Eq. (2.1), the equations of motion of the system. We use Euler's formula to rewrite the harmonic modulation terms within Eq. (2.1) in the complex exponential form. After algebraic simplifications, we arrive at the following equations:

$$\sum_{q=-\infty}^{\infty}\left[1+K_c-(\Omega_f+q\Omega_m)^2+i2\zeta(\Omega_f+q\Omega_m)\right]y_{1,q}^F e^{iq\Omega_m\tau}-K_c\sum_{q=-\infty}^{\infty}y_{2,q}^F e^{iq\Omega_m\tau}$$
$$+\frac{K_m}{2}\sum_{q=-\infty}^{\infty}y_{1,q}^F e^{i(q+1)\Omega_m\tau}+\frac{K_m}{2}\sum_{q=-\infty}^{\infty}y_{1,q}^F e^{i(q-1)\Omega_m\tau}=\frac{P}{2}\,, \quad \text{(2C.1a)}$$

$$\sum_{q=-\infty}^{\infty}\left[1+K_c-(\Omega_f+q\Omega_m)^2+i2\zeta(\Omega_f+q\Omega_m)\right]y_{2,q}^F e^{iq\Omega_m\tau}-K_c\sum_{q=-\infty}^{\infty}y_{1,q}^F e^{iq\Omega_m\tau}$$
$$+\frac{K_m}{2}e^{-i\phi}\sum_{q=-\infty}^{\infty}y_{2,q}^F e^{i(q+1)\Omega_m\tau}+\frac{K_m}{2}e^{i\phi}\sum_{q=-\infty}^{\infty}y_{2,q}^F e^{i(q-1)\Omega_m\tau}=0\,. \quad \text{(2C.1b)}$$

We then multiply each term in Eq. (2C.1) by $e^{-ik\Omega_m\tau}\Omega_m/(2\pi)$, where $k\in[-\mathcal{F},\mathcal{F}]$, and integrate them over one modulation period, from $-\pi/\Omega_m$ to π/Ω_m. After integration, only one non-zero term remains in each equation. Thus, a set of complex-valued linear equations can be obtained:

$$\left[1+K_c-(\Omega_f+k\Omega_m)^2+i2\zeta(\Omega_f+k\Omega_m)\right]x_{1,k}^F-K_c x_{2,k}^F+\frac{K_m}{2}x_{1,k-1}^F+\frac{K_m}{2}x_{1,k+1}^F=\frac{P}{2}\delta_{k,0}\,, \quad \text{(2C.2a)}$$

$$\left[1+K_c-(\Omega_f+k\Omega_m)^2+i2\zeta(\Omega_f+k\Omega_m)\right]x_{2,k}^F-K_c x_{1,k}^F+\frac{K_m}{2}e^{-i\phi}x_{2,k-1}^F+\frac{K_m}{2}e^{i\phi}x_{2,k+1}^F=0\,. \quad \text{(2C.2b)}$$

Here, $\delta_{k,0}$, the Kronecker delta, is non-zero (with value 1) if and only if $k = 0$; this term determines the location where the external force is applied in the *forward* configuration. We can write Eq. (2C.2) in matrix form as follows:

$$\begin{bmatrix} \vdots & \vdots & \vdots & \vdots & \vdots & \vdots & \vdots & \vdots & \vdots & \vdots \\ \cdots & A_{-1} & K_m/2 & 0 & \cdots & \cdots & -K_c & 0 & 0 & \cdots \\ \cdots & K_m/2 & A_0 & K_m/2 & \cdots & \cdots & 0 & -K_c & 0 & \cdots \\ \cdots & 0 & K_m/2 & A_1 & \cdots & \cdots & 0 & 0 & -K_c & \cdots \\ \vdots & \vdots & \vdots & \vdots & \vdots & \vdots & \vdots & \vdots & \vdots & \vdots \\ \vdots & \vdots & \vdots & \vdots & \vdots & \vdots & \vdots & \vdots & \vdots & \vdots \\ \cdots & -K_c & 0 & 0 & \cdots & \cdots & A_{-1} & K_m e^{i\phi}/2 & 0 & \cdots \\ \cdots & 0 & -K_c & 0 & \cdots & \cdots & K_m e^{-i\phi}/2 & A_0 & K_m e^{i\phi}/2 & \cdots \\ \cdots & 0 & 0 & -K_c & \cdots & \cdots & 0 & K_m e^{-i\phi}/2 & A_1 & \cdots \\ \vdots & \vdots & \vdots & \vdots & \vdots & \vdots & \vdots & \vdots & \vdots & \vdots \end{bmatrix} \begin{Bmatrix} \vdots \\ y^F_{1,-1} \\ y^F_{1,0} \\ y^F_{1,1} \\ \vdots \\ \vdots \\ y^F_{2,-1} \\ y^F_{2,0} \\ y^F_{2,1} \\ \vdots \end{Bmatrix} = \begin{Bmatrix} \vdots \\ 0 \\ P/2 \\ 0 \\ \vdots \\ \vdots \\ 0 \\ 0 \\ 0 \\ \vdots \end{Bmatrix} \quad (2C.3)$$

where

$$A_j = 1 + K_c - (\Omega_f + j\Omega_m)^2 + i2\zeta(\Omega_f + j\Omega_m) \quad (2C.4)$$

for $j = 0, \pm1, \pm2, \cdots$. Eq. (2C.3) can be written in a compact notation as:

$$\underline{\underline{D}}\; \underline{y^F} = \underline{p^F} \quad (2C.5)$$

Thus, the complex-valued amplitudes of the harmonic terms in the output $x_2^F(\tau)$ can be formally calculated as $\underline{y^F} = \underline{\underline{D}}^{-1}\, \underline{p^F}$.

The size of matrix $\underline{\underline{D}}$ is $4\mathcal{F}+2$ by $4\mathcal{F}+2$. With the exception of the elements in its main diagonal, first super diagonal, first subdiagonal, $(2\mathcal{F}+1)^{th}$ super diagonal and $(2\mathcal{F}+1)^{th}$ subdiagonal, all the elements in matrix $\underline{\underline{D}}$ are zero.

The only difference between the *forward* and *backward* configurations is the location where the external force is applied. The matrix $\underline{\underline{D}}$ is therefore the same for the two configurations. The force vector $\underline{p^F}$ has only one non-zero element, which is in the $(\mathcal{F}{+}1)^{th}$ row. This greatly simplifies the matrix inversion: $y^F_{2,p}$, an arbitrary complex-valued amplitude of a harmonic term in $x_2^F(\tau)$, can be calculated from:

$$y^F_{2,p} = (-1)^{p+1}\, M_{\mathcal{F}+1, 3\mathcal{F}+2+p}\, \frac{P}{2\,|\underline{\underline{D}}|} \quad (2C.6)$$

where M_{j_1,j_2} is the minor of matrix $\underline{\underline{D}}$ for the element in j_1^{th} row and j_2^{th} column.

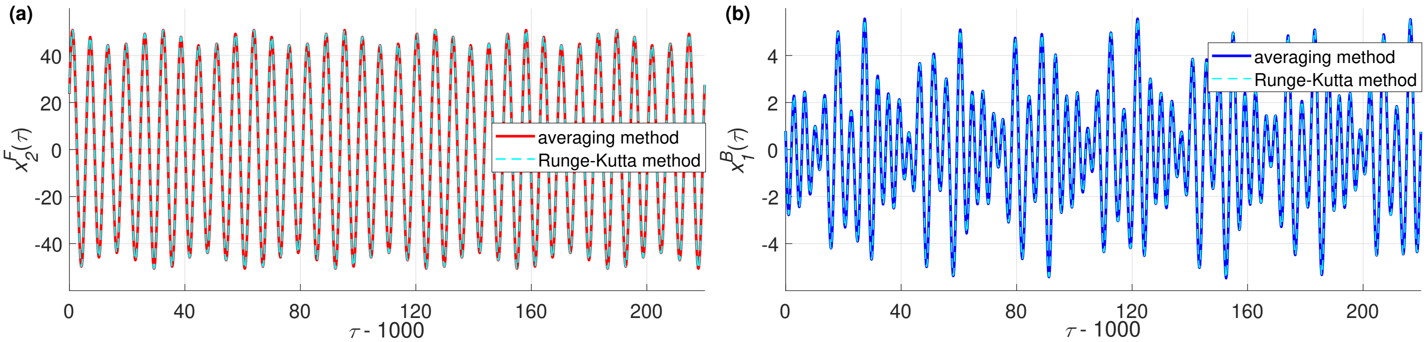

Figure 2C.1: Comparison of steady-state response calculated using the averaging method (red and blue solid curves) and the Runge-Kutta method (cyan dashed curves). (a) $K_c = 0.6$, $K_m = 0.1$, $\zeta = 0.005$, $\Omega_m = 0.2$, $\phi = 0.5\pi$, $P = 1$, $\Omega_f = 1$ and $\mathcal{F} = 2$, in *forward* configuration; (b) $K_c = 0.7$, $K_m = 0.6$, $\zeta = 0.005$, $\Omega_m = 0.1$, $\phi = 0.3\pi$, $P = 1$, $\Omega_f = 1.33$ and $\mathcal{F} = 6$, in *backward* configuration.

Similarly, for the 2-DoF modulated system in the *backward* configuration, the complex-valued amplitudes of all harmonic components in the output $x_1^B(\tau)$ can be formally calculated from $\underline{y}^B = \underline{\underline{D}}^{-1}\,\underline{p}^B$. The force vector $\underline{p}^B$ has only one nonzero element, which lies in the $(3\mathcal{F}+2)^{th}$ row. $y_{1,p}^B$, an element in $\underline{y}^B$, can then be written as:

$$y_{1,p}^B = (-1)^{p+1}\, M_{3\mathcal{F}+2,\mathcal{F}+1+p}\, \frac{P}{2\,|\underline{\underline{D}}|}. \tag{2C.7}$$

Fig. 2C.1 shows the steady-state output displacements calculated for Eq. (2.1) for the following parameters: $K_c = 0.6$, $\zeta = 0.005$, $\Omega_m = 0.2$, $\phi = \pi/2$ and $P = 1$. To validate the predictions made with the averaging method, the outputs of Eq. 2.1a is computed using the Runge-Kutta method. The predictions made from the averaging method match very well the results obtained from direct numerical integration.

The same methodology based on the averaging method can be used to obtain the steady-state response of longer discrete modulated systems [70, 72].

Chapter 3

Nonreciprocal Phase Shifts in Spatiotemporally Modulated Systems

3.1. Introduction

Reciprocity theorems state that wave propagation in a material is independent of the direction of transmission: the transmitted wave remains unchanged if the locations of the source and receiver are interchanged [1]. In analysis of the steady-state response, reciprocity manifests as the symmetry of the transfer matrix between the input and output [76]. This property has laid the foundation for several measurement techniques and industrial applications [2, 3, 77–79]. Recently, however, there has been a surge of interest in realizing direction-dependent transmission properties in acoustic and mechanical systems, a feat that is impossible within the framework of reciprocity [4, 80].

In linear systems, one way to realize nonreciprocal wave transmission is through *spatiotemporal modulations*: periodic changes in the effective properties of the medium in both space and time [6]. To enable nonreciprocity, spatiotemporal modulations are usually introduced to the effective elasticity (stiffness) in various models of waveguides. Examples include a uniform bar with wavelike spatiotemporal modulation in its elastic modulus [7, 11, 16] or with local modulated attachments [9, 20, 23], discrete periodic materials with spatiotemporally modulated coupling springs [24] or grounding springs [31, 43], and metamaterials with spatiotemporal modulations in the stiffness of the local resonant springs [29, 42] or springs of surface oscillators [22, 37]. Nonreciprocal vibration transmission can also occur in systems with spatiotemporal modulations in the effective inertia (masses) [26] or in systems with two-phase modulations, *i.e.* in both masses and springs [28] or in both density and elastic modulus [15, 18]. By introducing spatiotemporal modulations to the electrical boundary conditions of each cells in piezoelectric media, directional elastic waves can be generated and result in direction-dependent propagation of incident waves [41, 81].

Successful realization of nonreciprocal dynamics leads to the dependence of at least one of the transmission characteristics (amplitude, phase, phase or group velocity, etc.) on the direction of transmission. The difference between the transmitted amplitudes or energies in the opposite directions is almost universally used as the indicator of nonreciprocity. Typical ways to illustrate this effect are directional bandgaps [7, 16, 26, 31, 46], frequency spectra of transmitted vibrations [9, 37, 42–44] or the temporal response of the system [7, 43, 67].

The difference between the transmitted phases can also contribute to nonreciprocity. Phase has played an important role in nonreciprocal propagation of electromagnetic waves [53, 82]. When the propagation direction is reversed, significant phase difference can be observed in electromagnetic waves that propagate through a time-invariant waveguide inside a magnetic field [54–56, 83] or a spatiotemporally modulated waveguide [84]. Several techniques have been developed to realize direction-dependent phases of electromagnetic waves, with current or potential applications in industries such as telecommunications [85–87], radar systems [88] and medical magnetic resonance imaging [89]. In acoustic and mechanical systems, however, this attribute of nonreciprocity (contributions of phase) remains unexplored in comparison.

One way to highlight the role of phase in breaking reciprocity is to identify nonreciprocal response regimes that are characterized by equal energies transmitted in opposite directions. In this case, because the transmitted energies are the same, the difference between the phases of the transmitted waves is the only contributor to nonreciprocity. We refer to this scenario as *phase nonreciprocity*, and to the corresponding difference between the transmitted phases as the *nonreciprocal phase shift*. Phase nonreciprocity has been reported in the steady-state response of nonlinear systems to harmonic excitation [51, 52], where the nonreciprocal phase shift can be controlled by varying system parameters. In spatiotemporally modulated materials, nonreciprocal phase shifts have been identified as the main contributor to nonreciprocity in systems with a small number of modulated units [90]. A detailed analysis of nonreciprocal phase shifts for modulated systems, however, remains to be presented.

In this work, our goal is to systematically characterize nonreciprocal phase shifts in discrete, spatiotemporally modulated systems. We focus on the steady-state response of a one-dimensional (1-D) systems subject to simultaneous spatiotemporal modulation and external harmonic drive. Due to the scattering effects of the modulations, the response of a modulated system is not periodic in nature (characterized by two incommensurate frequencies). Therefore, the analysis of the response, and thereby the direction-dependent propagation of phase, is not straightforward and the methodology used for nonlinear systems [51] is not directly applicable here. We therefore develop a methodology based on the envelopes of the transmitted vibrations in order to enable a systematic search for and realization of nonreciprocal phase shifts in spatiotemporally modulated systems. This includes a near-zero nonreciprocal phase shift and retrieval of reciprocal response. While the primary focus of the work is on weakly modulated systems with a small number of units, we also present a special case of the phenomenon for systems of arbitrary length and strength of modulation.

Section 3.2 provides a derivation of response envelopes for the steady-state response of the system, along with a short overview of nonreciprocity. In Section 3.3, we present our methodology for obtaining response that exhibits nonreciprocal phase shifts, followed by a constraint that ensures the same shapes for the two response envelopes. Section 3.4 provides two special cases of nonreciprocal phase shifts: systems with arbitrary length and strength of modulation, and near-reciprocal transmission. We discuss the limitations of our methodology for obtaining nonreciprocal phase shifts in Section 3.5. Section 3.6 summarizes our findings.

3.2. Steady-state response of the modulated systems

3.2.1. Equations of motion

Fig. 3.1 shows the schematic of the discrete model of the spatiotemporally modulated material that we study in this work. The model consists of n identical masses, viscous dampers, coupling springs and modulated grounding springs. The longitudinal rectilinear movement of each mass is considered as its only degree of freedom (DoF). External harmonic forces are applied on the first mass and the last mass, $f_1(t) = F_1 \cos(\omega_f t)$ and $f_n(t) = F_n \cos(\omega_f t)$. The stiffness coefficient of each grounding spring is composed of a constant term and a time-periodic term, expressed as $k_p(t) = k_{g,DC} + k_{g,AC} \cos(\omega_m t - \phi_p)$, where $\phi_p = (p-1)\phi$ and $p = 1, 2, \cdots, n$. Parameter ω_m is the modulation frequency and ϕ is the phase shift between the modulations in two adjacent units.

Parameter ϕ represents the spatial variation of the grounding stiffness along the length of the system. This is the same as the modulation wavenumber in long systems. Nevertheless, we continue referring to ϕ as the modulation phase in this work (instead of modulation wavenumber) because we consider systems that can often be too short to even contain one full modulation wavelength within them. The modulation phase is the only parameter that breaks the mirror symmetry of the model and enables nonreciprocity; *i.e.*, the end-to-end transmission is always reciprocal for $\phi = 0$ by virtue of mirror symmetry.

We start by nondimensionalizing the governing equations, as detailed in Appendix 3A. The

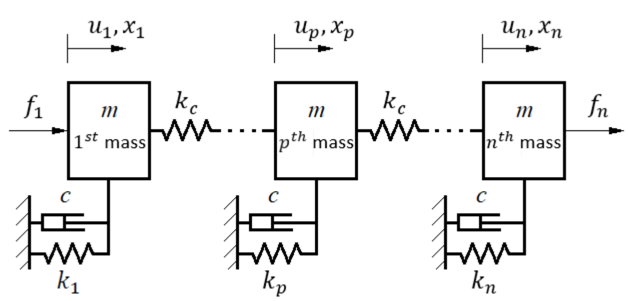

Figure 3.1: Schematic of the modulated system with n DoF.

nondimensional equation of motion for the p-th mass of the system shown in Fig. 3.1 is:

$$\ddot{x}_p + 2\zeta\dot{x}_p + [1 + K_m \cos(\Omega_m\tau - \phi_p)]x_p + K_c\Delta_p^2 = P_p \cos(\Omega_f\tau) \tag{3.1}$$

where the overdot represents differentiation with respect to nondimensional time τ. The difference term $\Delta_p^2 = 2x_p - x_{p-1} - x_{p+1}$ everywhere except at the two ends where $\Delta_1^2 = x_1 - x_2$ and $\Delta_n^2 = x_n - x_{n-1}$. The external forces are only applied at the two ends: $P_p = P$ for $p \in \{1, n\}$ and zero everywhere else. Only one of the two ends is subject to an external force at a time, as explained in Section 3.2.3.

3.2.2. Response envelopes

The response of the modulated system is characterized by two independent frequencies Ω_f and Ω_m. The steady-state displacement is therefore not periodic in time (called *quasi-periodic*), except for the rare cases when the ratio of the two frequencies is a rational number. However, the envelope of the response is in fact periodic in time [72]. In this section, we develop an expression for the response envelope to simplify the ensuing analysis and computation.

The steady-state response of the system can be expressed in general as a combination of harmonic components in complex or real notation as:

$$\begin{aligned} x_p(\tau) &= \textstyle\sum_{q=-\infty}^{\infty} [y_{p;q} e^{i(\Omega_f + q\Omega_m)\tau} + c.c.] \\ &= \textstyle\sum_{q=-\infty}^{\infty} 2|y_{p;q}| \cos\left[\left(\Omega_f + q\Omega_m\right)\tau + \psi_{p;q}\right]. \end{aligned} \tag{3.2}$$

where $y_{p;q}$ is the complex amplitude of each harmonic component and *c.c.* represents the corresponding complex conjugate terms. The phase in the real representation, $\psi_{p;q}$, can be expressed as:

$$\psi_{p;q} = \text{atan2}\left(\text{Im}\left(y_{p;q}\right), \text{Re}\left(y_{p;q}\right)\right), \tag{3.3}$$

where Re( ) and Im( ) indicate the real part and imaginary parts of the complex amplitudes, respectively. For a given Ω_f and a set of system parameters, the complex amplitudes $y_{p;q}$ can be calculated using the averaging method. This results in a linear system of algebraic equations in the complex amplitudes

$$[D]\{Y\} = \{F\} \tag{3.4}$$

where the matrix $[D]$ contains the system parameters, $\{Y\}$ is the vector of unknown complex amplitudes and $\{F\}$ contains information about the location and amplitude of the external force. The details of this well established methodology are discussed elsewhere [36, 70, 90] and are not repeated here. Instead, we directly proceed with obtaining the envelope equations.

The steady-state displacements can alternatively be rewritten as:

$$x_p(\tau) = E_p(\tau)\ C_p(\tau), \tag{3.5}$$

where $E_p(\tau)$ represents the response envelope and $C_p(\tau)$ represents the corresponding carrier wave of unit amplitude. $E_p(\tau)$ is expressed as:

$$E_p(\tau) = 2\Big|\sum_{q=-\infty}^{\infty} y_{p;q} e^{iq\Omega_m\tau}\Big|. \tag{3.6}$$

When $\Omega_m < \Omega_f$ and $K_m \leq 0.1$, $C_p(\tau)$ can be approximated by a harmonic wave of the same frequency as the external excitation:

$$C_p(\tau) = \cos\left(\Omega_f\tau + \psi_{p;0}\right), \tag{3.7}$$

where $\psi_{p;0} = \operatorname{atan2}\left(\operatorname{Im}\left(y_{p;0}\right), \operatorname{Re}\left(y_{p;0}\right)\right)$. Otherwise, $C_p(\tau)$ is not periodic but its amplitude remains equal to 1.

We emphasize that although the steady-state displacements $x_p(\tau)$ are not periodic in time, their envelopes, $E_p(\tau)$, remain periodic with period $T_E = 2\pi/\Omega_m$. Regardless, the displacement function $x_p(\tau)$ remains bounded by its envelopes $\pm\, E_p(\tau)$.

The infinite summations in Eqs. (3.2) and (3.6) need to be truncated at a finite value of q. We take an expansion with $q \in [-\mathcal{F}, \mathcal{F}]$ and $\mathcal{F} \in \mathbf{N}$. We restrict our attention to short systems with weak modulations, *i.e.* $n \leq 5$ and $K_m \leq 0.1$. Under these assumptions, the response envelope is nearly harmonic. Thus, we use $\mathcal{F} = 1$ to approximate the steady-state response of the system.

To validate the solution predicted by Eq. (3.2) with $q \in [-1, 1]$, the response of Eq. (3.1) is computed using the Runge-Kutta method until the steady state is reached. We arbitrarily choose two sets of system parameters, then calculate the displacements of two masses using both the averaging and Runge-Kutta methods, as shown in Fig. 3.2. We observe that the averaging method predicts the steady-state response well, $\pm\, E_5(\tau)$ and $\pm\, E_1(\tau)$ following the response envelopes of the outputs accurately in both cases. The response envelope for a system with stronger modulation amplitude remains periodic but it is no longer harmonic [72]. The formulation in Eq. (3.6) can still accurately predict the response envelopes provided that more terms are included in the expansion ($\mathcal{F} > 1$). In contrast, more conventional methods of computing the response envelopes based on the method of multiple scales or rotating wave approximation are typically limited to harmonic envelopes [91].

3.2.3. Nonreciprocity

Before presenting the special case of nonreciprocal phase shifts, we briefly review the typical scenario for nonreciprocal vibration transmission in our system. The response of an exter-

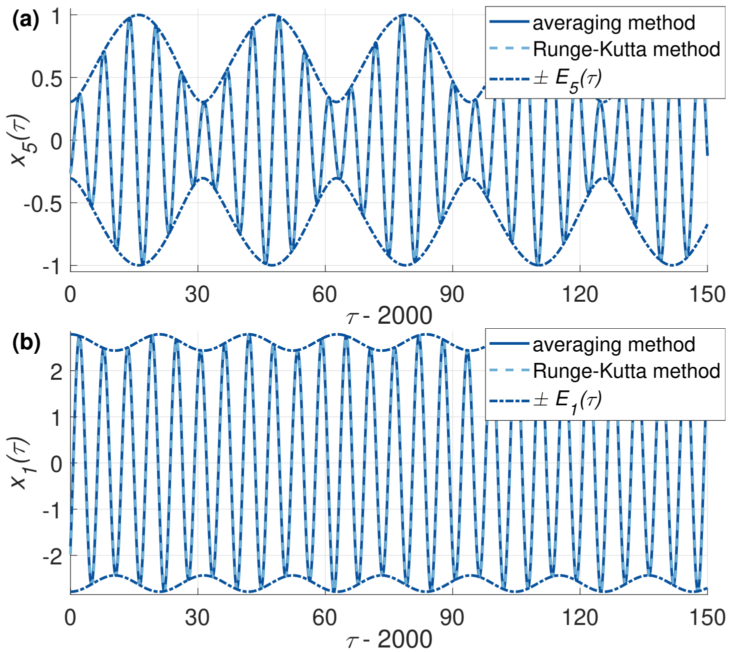

Figure 3.2: Comparison between the output displacements computed using the averaging method (solid curves) and the Runge-Kutta method (dashed curves). Dash-dotted curves are plots of $\pm E_5(\tau)$ and $\pm E_1(\tau)$ in panels (a) and (b), respectively. (a) $n = 5$, $\Omega_m = 0.2$, $\phi = 0.42\pi$, $\Omega_f = 0.88$, $K_c = 0.6$, $K_m = 0.1$, $\zeta = 0.02$, $P_1 = 1$ and $P_5 = 0$; (b) $n = 4$, $\Omega_m = 0.3$, $\phi = 0.95\pi$, $\Omega_f = 1.1$, $K_c = 0.8$, $K_m = 0.1$, $\zeta = 0.02$, $P_1 = 0$ and $P_4 = 1$.

nally forced system is reciprocal if it remains invariant upon interchanging the locations of the input (source) and output (receiver). To test for reciprocity, therefore, we define two configurations to distinguish between the two directions of vibration transmission: (i) the *forward* (from left to right) configuration with $P_1 = P$ and $P_n = 0$, where the output is the steady-state displacement of the rightmost (last) mass, $x_n^F(\tau)$; (ii) the *backward* (from right to left) configuration with $P_1 = 0$ and $P_n = P$, where the output is the steady-state displacement of the leftmost (first) mass, $x_1^B(\tau)$. The superscripts F and B denote the response in the *forward* and *backward* configurations, respectively. Vibration transmission is then reciprocal if and only if $x_n^F(\tau) = x_1^B(\tau)$.

We introduce the reciprocity bias, R, to quantify the degree of nonreciprocity of the response:

$$R = \lim_{T\to\infty} \sqrt{\frac{\int_0^T \left[x_n^F(\tau) - x_1^B(\tau)\right]^2 \,\mathrm{d}\tau}{2\int_0^T \left[x_n^F(\tau)\right]^2 + \left[x_1^B(\tau)\right]^2 \,\mathrm{d}\tau}} = \sqrt{\frac{\sum_{q=-\mathcal{F}}^{\mathcal{F}} \left|y_{n;q}^F - y_{1;q}^B\right|^2}{2\sum_{q=-\mathcal{F}}^{\mathcal{F}} \left|y_{n;q}^F\right|^2 + \left|y_{1;q}^B\right|^2}}. \tag{3.8}$$

By definition, $0 \leq R \leq 1$, and $R = 0$ if and only if vibration transmission through the system is reciprocal. The case of $R = 1$ corresponds to unilateral transmission, which is not relevant in this work. The denominator in Eq. (3.8) is introduced to remove the apparent increase in the degree of nonreciprocity due to P. Because we study a linear system in this work, the reported value of R hold for any choice of P.

To demonstrate the influence of ϕ on nonreciprocity, we compute R as a function of ϕ and Ω_f for two sets of system parameters; see Fig. 3.3. In general, the response remains nonreciprocal ($R > 0$) over the entire range $0 < \phi < 2\pi$. A prominent exception is for systems with an odd number of units, for which the response is reciprocal ($R = 0$) for $\phi = \pi$; see Fig. 3.3(a). This is because the time-reversal symmetry is retained when $\phi = \pi$ and n is an odd number. The role of phase on nonreciprocity in coupled spatiotemporally modulated systems is explored in detail elsewhere [90].

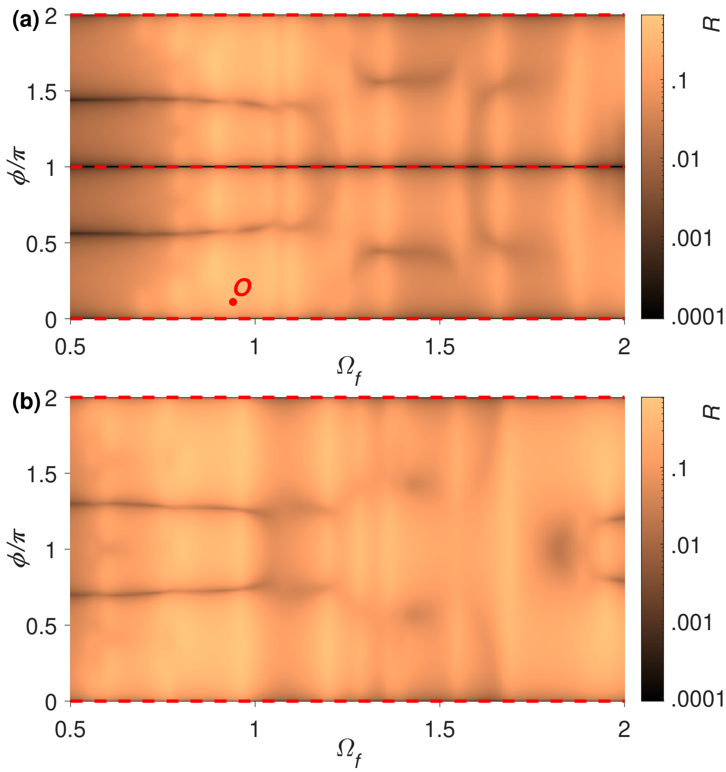

Figure 3.3: Surface plots of reciprocity bias as a function of Ω_f and ϕ for $K_m = 0.1$, $\zeta = 0.02$ and $P = 1$. Red dashed lines indicate the combinations of Ω_f and ϕ that lead to $R = 0$. (a) $n = 5$, $\Omega_m = 0.1$ and $K_c = 0.8$; (b) $n = 4$, $\Omega_m = 0.2$ and $K_c = 0.6$.

Fig. 3.4 shows the response of the system at point O of Fig. 3.3(a) with $\Omega_f = 0.94$ and $\phi = 0.11\pi$. Vibration transmission is clearly nonreciprocal, as seen in panels (a) and (b). The difference in the transmitted amplitudes is also evident in the response envelopes in panel (c). Panel (d) shows that, in addition to the response envelopes, the two carrier waves are also different between the two configurations, thus contributing to nonreciprocity. The carrier waves are harmonic in weakly modulated systems; recall Eq. (3.7).

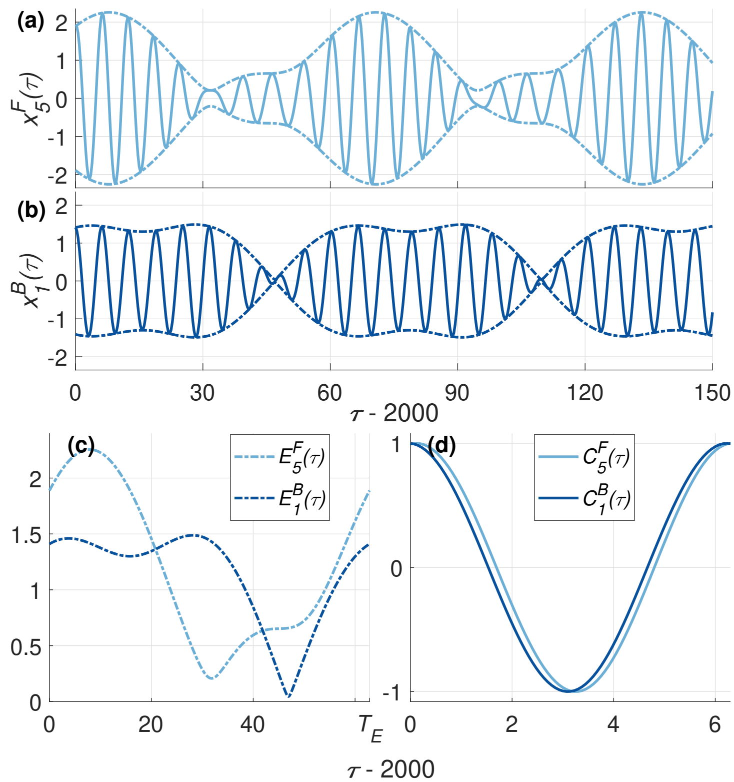

Figure 3.4: Plots of (a,b) output displacements, (c) response envelopes and (d) carrier waves for point O. Dash-dotted curves are plots of $\pm E_5^F(\tau)$ and $\pm E_1^B(\tau)$ in panels (a) and (b), respectively. System parameters: $n = 5$, $\Omega_m = 0.1$, $\phi = 0.11\pi$, $\Omega_f = 0.94$, $K_c = 0.8$, $K_m = 0.1$, $\zeta = 0.02$ and $P = 1$.

The primary focus of this work is to investigate nonreciprocal response with equal amplitudes transmitted in the opposite directions. Because the amplitudes are the same, nonreciprocity is caused merely by the phase difference between the transmitted vibrations: nonreciprocal phase shift. In time-invariant nonlinear systems, it is possible to realize nonreciprocal phase shifts in the steady-state response to external harmonic excitation [51, 52]. Nonreciprocal phase shifts occur when the two outputs have the same amplitudes but different phases, where the amount of the nonreciprocal phase shift can be controlled using a system parameter. In spatiotemporally modulated systems, however, a similarly systematic investigation of nonreciprocal phase shifts is more challenging due to the non-periodic nature of the response. We will take advantage of the periodicity of the response envelopes to obtain a vibration transmission scenario that exhibits nonreciprocal phase shifts.

3.3. Nonreciprocal phase shifts

Because the steady-state response of an externally driven modulated system is quasi-periodic, the definition of its phase is not as straightforward as in systems without modulation. This further complicates the search for parameters that lead to nonreciprocal phase shifts in the response of the system. Given that the envelope of the response remains periodic, it is much more feasible to investigate nonreciprocal phase shifts based on the response envelopes. We expect that the steady-state displacements exhibit a nonreciprocal phase shift if the corresponding response envelopes exhibit a nonreciprocal phase shift. We discuss this approach here.

3.3.1. Formulation

The displacement response of the system oscillates in time with two incommensurate frequencies around the static equilibrium point; *i.e.*, there is no bias (DC shift with respect to $x_p = 0$) in the response. As a result, the envelope equations appear as a pair located symmetrically with respect to $x_p = 0$; see the envelopes in Fig. 3.2. We can therefore express the envelope equation as

$$E_p(\tau) = \sqrt{\mathcal{S}_{dc;p} + \mathcal{S}_{ac;p}(\tau)}, \tag{3.9}$$

where $\mathcal{S}_{dc;p}$ represent time-independent bias portions (DC shifts) and $\mathcal{S}_{ac;p}$ represent the time-varying portions of the amplitude equation. The square root is included in Eq. (3.9) because we will be working with the square of envelope, $E_p^2(\tau)$. With $\mathcal{F} = 1$, the envelope bias terms are defined as:

$$\mathcal{S}_{dc;p} = \frac{1}{T_E} \int_0^{T_E} \left(E_p\left(\tau\right)\right)^2 \, \mathrm{d}\tau = 4\left(\left|y_{p;-1}\right|^2 + \left|y_{p;0}\right|^2 + \left|y_{p;1}\right|^2\right). \tag{3.10}$$

And the time-varying portion of the envelopes are defined as:

$$\mathcal{S}_{ac;p}(\tau) = \mathcal{A}_p \cos\left(\Omega_m \tau - \theta_{a;p}\right) + \mathcal{B}_p \cos\left(2\Omega_m \tau - \theta_{b;p}\right), \tag{3.11}$$

See Appendix 3B for the expressions for the envelope amplitudes, $\mathcal{A}_p$ and $\mathcal{B}_p$, and envelope phases, $\theta_{a;p}$ and $\theta_{b;p}$, in terms of the response amplitudes.

In terms of the envelope parameters $\mathcal{S}_{dc;n,1}^{F,B}$, $\mathcal{A}_{n,1}^{F,B}$ and $\mathcal{B}_{n,1}^{F,B}$, nonreciprocal phase shift between response envelopes is characterized by the following three constraints:

$$\mathcal{S}_{dc;n}^{F} = \mathcal{S}_{dc;1}^{B}, \tag{3.12a}$$

$$\mathcal{A}_{n}^{F} = \mathcal{A}_{1}^{B}, \tag{3.12b}$$

$$\mathcal{B}_{n}^{F} = \mathcal{B}_{1}^{B}. \tag{3.12c}$$

If the three constraints in Eq. (3.12) are satisfied, it is still possible that the two envelopes are not the same, $E_n^F(\tau) \neq E_1^B(\tau)$. This can happen because of the phase terms in Eq. (3.11); *i.e.*, $\theta_{a,n}^F \neq \theta_{a,1}^B$ or $\theta_{b,n}^F \neq \theta_{b,1}^B$. The envelopes $E_n^F(\tau)$ and $E_1^B(\tau)$ would exhibit a nonreciprocal phase shift in this case, which corresponds to a nonreciprocal phase shift in the displacement as well. Therefore, we use Eq. (3.12) as the constraints that need to be satisfied for nonreciprocal phase shifts.

We note that satisfying Eq. (3.12) provides a necessary but insufficient condition for the occurrence of nonreciprocal phase shifts. Having equal *forward* and *backward* response envelopes, $E_n^F(\tau) = E_1^B(\tau)$, may not necessarily be equivalent to $x_n^F(\tau) = x_1^B(\tau)$ due to the possible phase difference between two carrier waves. We have not encountered this particular scenario in our simulations, however. See Section 3.5.2 for the extension of the formulation to $\mathcal{F} \geq 1$.

3.3.2. Solution methodology and results

To find system parameters that lead to nonreciprocal phase shifts, we first need to calculate the steady-state response amplitudes of the system, $y_{p;q}$. Truncating the expansion in Eq. (3.1) at $\mathcal{F}$ sideband frequencies, $q \in [-\mathcal{F}, \mathcal{F}]$, there will be $2\mathcal{F} + 1$ amplitudes for each degree of freedom. For a system with n masses, considering both the *forward* and *backward* configurations, the solution process involves calculating $2n(2\mathcal{F}+1)$ complex amplitudes. The averaging method outlined in Section 3.2.2 provides the required linear system of $2n(2\mathcal{F}+1)$ algebraic equations in the complex amplitudes.

In addition, the three constraints in Eq. (3.12) need to be satisfied in order to ensure the envelope equations exhibit nonreciprocal phase shifts. This requires three of the system parameters to vary independently (free parameters). Not all the system parameters are suitable for this purpose, however. For example, n does not change continuously, P scales the amplitudes linearly and has no effect on the nature of the response (because of linearity), K_m is limited to the range of weak modulations ($K_m \leq 0.1$) to ensure $\mathcal{F} = 1$ provides sufficient accuracy, and ζ is limited to small values to ensure light damping. We choose ϕ, Ω_f and K_c as the free parameters. The modulation frequency, Ω_m, has a smaller permissible range of variation in comparison and is therefore left unchanged in this section – we use Ω_m in Section 3.3.3 to control the shape of the envelopes after nonreciprocal phase shift is achieved.

This procedure results in a system of $6n$ nonlinear algebraic equations for $\mathcal{F} = 1$. Solving this system of equations results in sets of the free system parameters ϕ, Ω_f and K_c that lead to nonreciprocal phase shifts. To demonstrate the methodology, we fix the other system

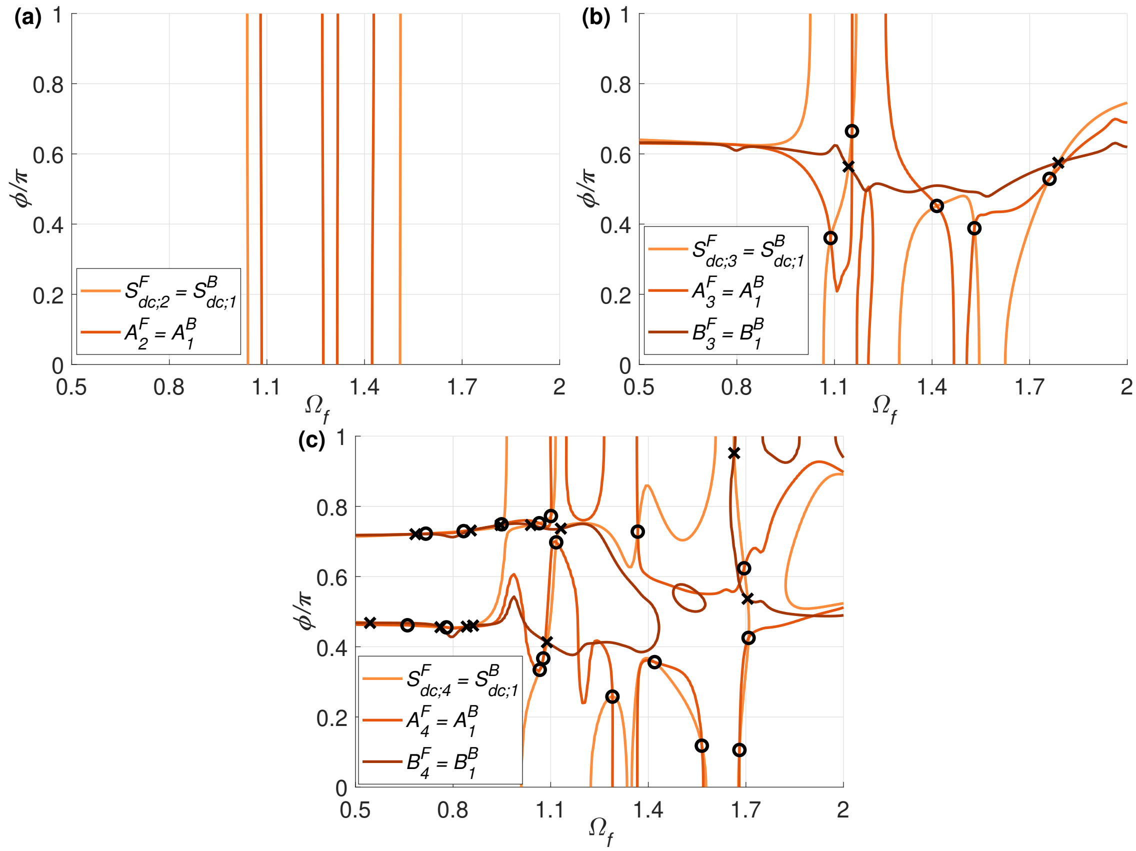

Figure 3.5: The curves in each panel show the locus of system parameters that satisfy one of the three constraints in Eq. (3.12). (a) $n = 2$, (b) $n = 3$ and (c) $n = 4$.

parameter to $\Omega_m = 0.2$, $K_m = 0.1$, $\zeta = 0.02$ and $P = 1$. We focus on short systems with $n \in \{2, 3, 4\}$ in this section – we discuss longer systems in Sections 3.4.1 and 3.5.2.

To satisfy the three constraints in Eq. (3.12), we first fix $K_c = 0.7$ and perform an exhaustive search to find combinations of ϕ and Ω_f that satisfy each pair of the constraint equations over the range $0 < \phi < \pi$ and $0.5 < \Omega_f < 2$. Because of the symmetries of trigonometric functions, the interval from 0 to π covers the entire range of variation for ϕ. We also note that the interval chosen for the forcing frequency covers the primary resonances and sidebands; the frequency range beyond this interval is off-resonance and therefore of limited practical interest.

Fig. 3.5 shows the combinations of ϕ and Ω_f that satisfy different constraints in Eq. (3.12). For the system with $n = 2$, panel (a), there are no intersections between the loci of $\mathcal{S}^F_{dc;2} = \mathcal{S}^B_{dc;1}$ and $\mathcal{A}^F_2 = \mathcal{A}^B_1$, and no parameter values that result in $\mathcal{B}^F_2 = \mathcal{B}^B_1$. Thus, a system with $n = 2$ cannot exhibit nonreciprocal phase shifts.

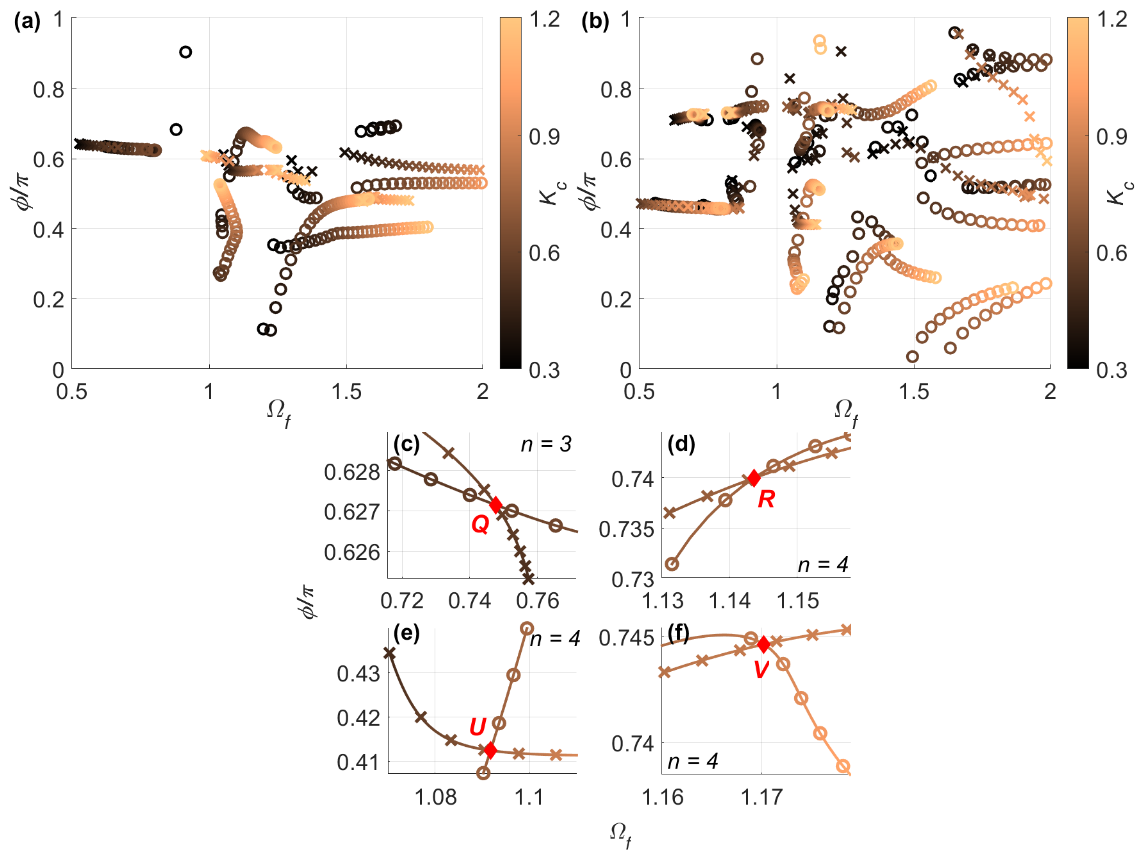

Figure 3.6: Locus of the intersection points from Fig. 3.5 as a function of K_c. (a,c) $n = 3$, (b,d-f) $n = 4$. Panels (c-f) are zoomed-in views of the intersections points between loci of circles and crosses. The color along each locus indicates the corresponding value of K_c, using the same color scale as in (a,b). The intersection points indicated by red diamonds satisfy Eq. (3.12).

In systems with more modulated units, the loci of the constraint equations are more complex and several intersection points are possible. Figs. 3.5(b) and 3.5(c) show these intersection points for systems with $n = 3$ and $n = 4$, respectively. The circle markers indicate intersections points that satisfy both Eq. (3.12a) and Eq. (3.12b), and cross markers indicate intersection points that satisfy both Eq. (3.12a) and Eq. (3.12c).

Having found pairs of (Ω_f,ϕ) that satisfy two of the three constraints (circles and crosses in Fig. 3.5), we allow K_c to vary and track how the intersection points (circles and crosses) evolve. Figs. 3.6(a,b) show the results of this search for systems with $n = 3$ and $n = 4$, respectively. For better clarity, we have used a colormap in K_c instead of showing the three-dimensional plots. There are several intersection points between the loci of circles and

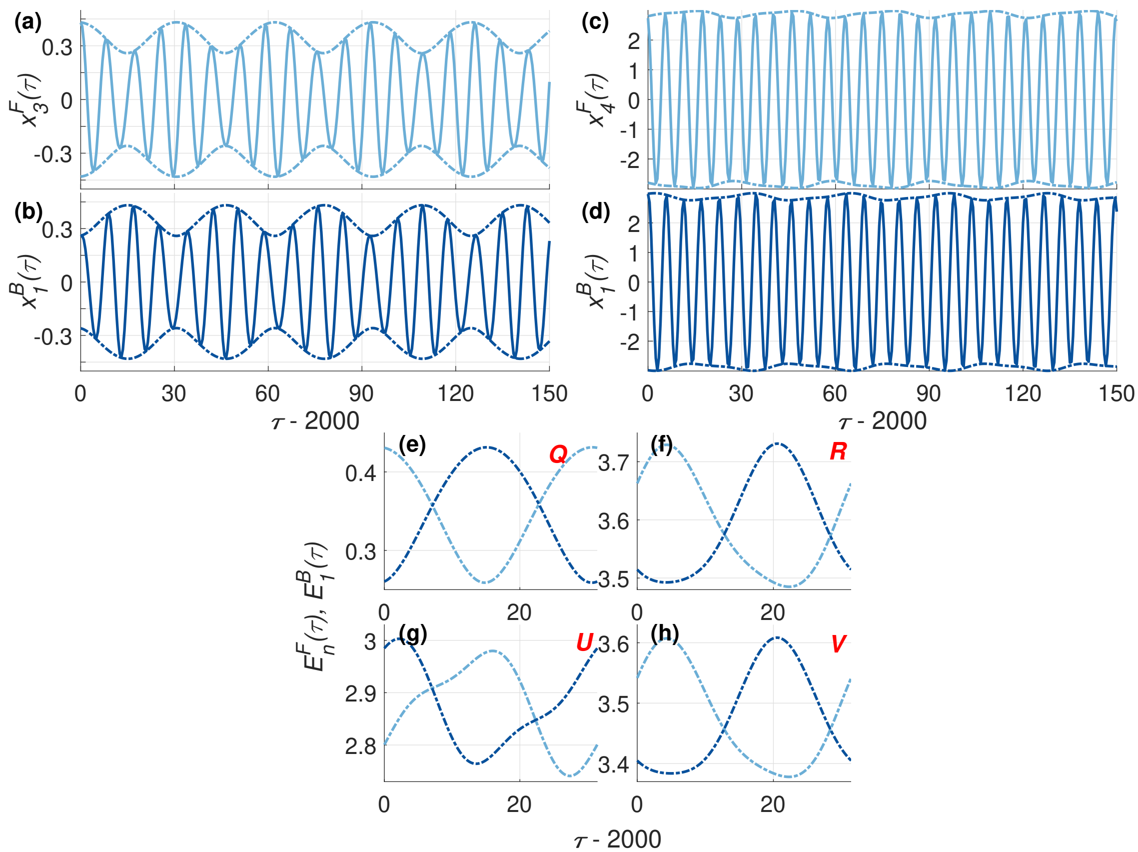

Figure 3.7: Displacement outputs and response envelopes exhibiting nonreciprocal phase shift for (a,b) point Q, (c,d) point U. (e-h) Response envelopes for points Q, R, U and V, respectively.

crosses. Figs. 3.6(c-f) show closeup views of four of these intersection points, labeled Q, R, U and V. These points represent parameters that satisfy the three constraints in Eq. (3.12) and lead to nonreciprocal phase shifts.

Figs. 3.7(a-d) show the output displacements and the corresponding response envelopes in the time domain for intersection points Q and U. As expected, the nonreciprocal phase shift in the response envelopes corresponds to nonreciprocal phase shifts in the displacement outputs. Figs. 3.7(e-h) show the response envelopes, $E_n^F(\tau)$ and $E_1^B(\tau)$, for all the four intersections points identified in Fig. 3.6(c-f). None of the four response envelopes in these examples is harmonic, a feature that is particularly visible for point U, Fig. 3.7(g). These points were chosen because they result in significant phase difference between the *forward* and *backward* configurations. The nonrecipocal phase shift can sometimes be small for other intersection points.

3.3.3. Enforcing the same envelope shapes

The constraints for nonreciprocal phase shift, Eq. (3.12), do not impose any restrictions on the shape of the response envelopes. The corresponding response envelopes can therefore satisfy the constraints while having different shapes; this is particularly obvious for point U, shown in Fig. 3.7(g). To enforce the same shape for the *forward* and *backward* response envelopes, we can introduce the following constraint:

$$\mathcal{R}_{em} = \mathrm{rem}\Big(2\big(\theta^F_{a;n} - \theta^B_{a;1}\big) - \big(\theta^F_{b;n} - \theta^B_{b;1}\big) + 2\hat{z}\pi, 2\pi\Big) = 0, \quad (3.13)$$

where rem (α, β) is the remainder of dividing α by β, and $\hat{z}$ is an integer introduced to ensure the continuity of $\mathcal{R}_{em}$.

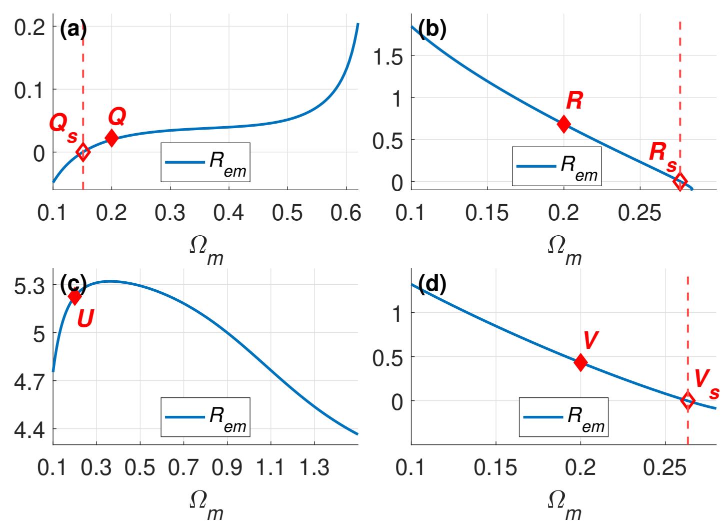

Figure 3.8: Variation of $\mathcal{R}_{em}$ as a function of Ω_m for points Q (a), R (b), U (c) and V (d), all exhibiting nonreciprocal phase shifts. Q_s, R_s and V_s represent points at which $E^F_n(\tau)$ and $E^B_1(\tau)$ have the same shape.

To satisfy the additional constraint in Eq. (3.13), we allow the modulation frequency Ω_m to vary as a free parameter and monitor $\mathcal{R}_{em}$ for zero crossings. The other system parameters need to vary during this computation to ensure the constraints in Eq. (3.12) remain satisfied. We note that it may not necessarily be possible to satisfy the additional constraint in Eq. (3.13) within a reasonable range of Ω_m.

Fig. 3.8 shows the variation of $\mathcal{R}_{em}$ as a function of Ω_m for points Q, R, U and V. A set of system parameters exist for which $\mathcal{R}_{em} = 0$ for points Q, R and V, but not for point U. We have therefore identified three points, named Q_s, R_s and V_s, that satisfy all the constraints in Eqs. (3.6) and (3.13). Fig. 3.9 shows the displacement outputs and the corresponding

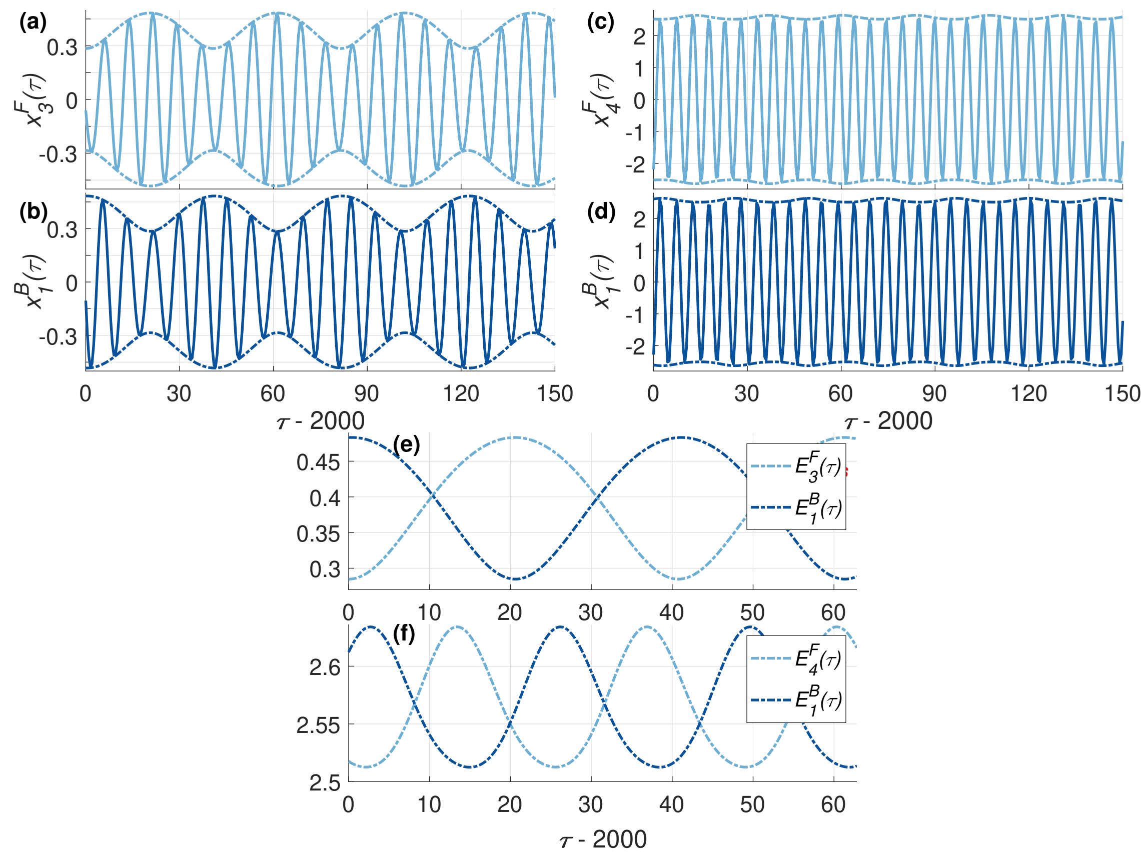

Figure 3.9: Displacement outputs for points Q_s (a,b) and V_s (c,d) that exhibit nonreciprocal phase shift with the same envelope shapes. The corresponding response envelopes are shown in (e) and (f) respectively.

response envelopes for points Q_s and V_s. As expected, the response envelopes have the same shape and exhibit nonreciprocal phase shift in both cases.

The results presented in this section were obtained for a fixed set of parameters n, K_m and ζ. It is, of course, possible to use the same methodology to find many other sets of parameters at which the response of the system exhibits nonreciprocal phase shifts, potentially with the same envelope shape.

3.4. Special cases

3.4.1. Systems with $\phi = \pi$ and even n

A trivial case of nonreciprocity with equal transmitted amplitudes in the opposite directions occurs when $\phi = \pi$ and n is an even number [90]. In this scenario, $|y^F_{n;q}| = |y^B_{1;q}|$ for any integer q, regardless of the values of other system parameters. Moreover, $\psi^F_{n;q} = \psi^B_{1;q}$ when q is an even number and $\psi^F_{n;q} = \psi^B_{1;q} \pm \pi$ when q is an odd number. This leads to the following relation between the two response envelopes: $E^F_n(\tau) = E^B_1(\tau \pm T_E/2)$. In other words, the two response envelopes have the same shape with a temporal shift equal to half a period. Therefore, we can obtain response that is characterized by nonreciprocal phase shifts with the same envelope shapes without applying the methodology described in Section 3.3. More importantly, this special case of nonreciprocal phase shifts can be realized at any strength of modulation and for a system of arbitrary length.

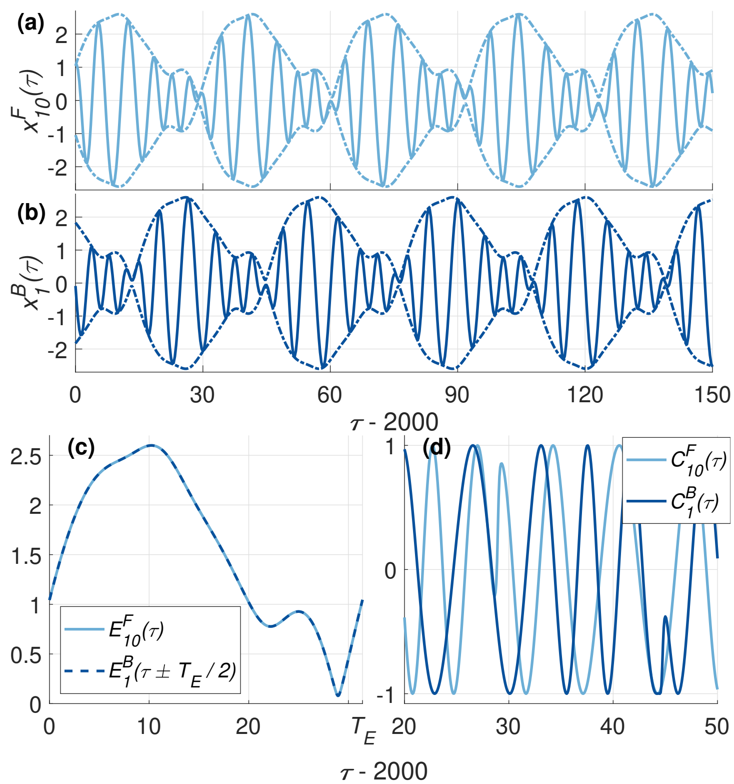

Figure 3.10: Displacement outputs (a,b), shifted response envelopes (c) and carrier waves (d) calculated with parameters: $n = 10$, $\Omega_m = 0.2$, $\phi = \pi$, $\Omega_f = 0.89$, $K_c = 0.7$, $K_m = 0.8$, $\zeta = 0.02$, $P = 1$ and $\mathcal{F} = 7$.

Fig. 3.10 shows the displacement outputs $x(\tau)$, the response envelopes $E(\tau)$ and the carrier waves $C(\tau)$ for a strongly modulated system ($K_m = 0.8$) with $\phi = \pi$ and $n = 10$; recall Eq. (3.5). We use $\mathcal{F} = 7$ in Eq. (3.2) to approximate the response accurately. Panels (a,b) show that the anharmonic envelopes of the output displacements are captured well. Panel (c) shows that the plots of $E^F(\tau)$ and $E^B(\tau \pm T_E/2)$ coincide, confirming the half-period phase shift between the two envelopes. As shown in panel (d), the carrier waves are no longer periodic in strongly modulated systems, in contrast to the harmonic carrier waves of weakly modulated systems; *cf.* Fig. 3.4. Thus, nonreciprocity in strongly modulated systems manifests in both the envelopes and carrier waves.

3.4.2. Near-reciprocal transmission

The constraints in Eq. (3.13) are applied to the response envelopes and do not directly control the properties of the carrier waves. Interestingly, we have observed that enforcing the constraint for the same envelope shapes can occasionally result in a near-reciprocal response.

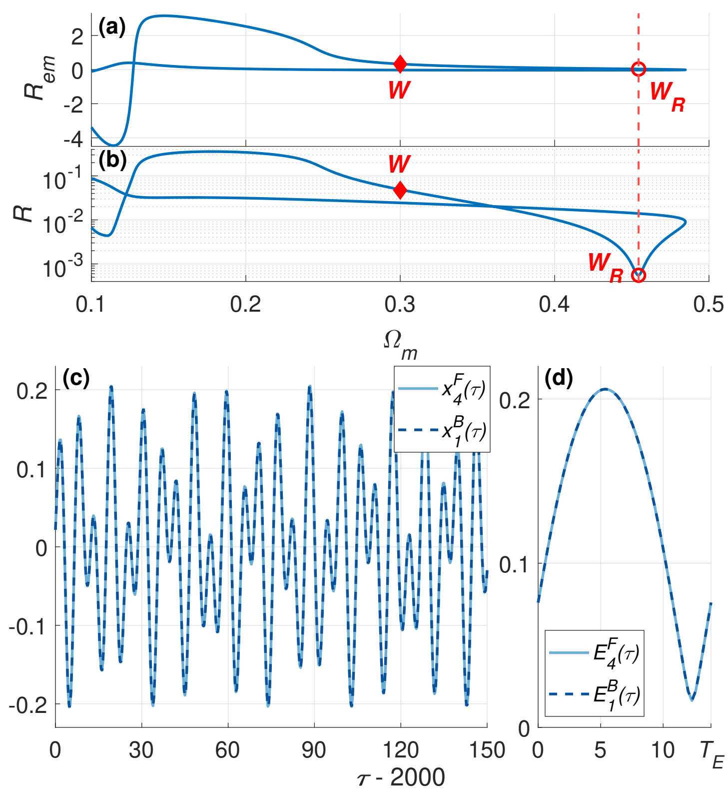

Figure 3.11: Variation of $\mathcal{R}_{em}$ (a) and R (b) as functions of Ω_m for point W that exhibits nonreciprocal phase shift. Displacement outputs (c) and response envelopes (d) for point W_R.

Fig. 3.11(a) shows the variation of $\mathcal{R}_{em}$ as a function of Ω_m for point W, representing a set of system parameters that satisfy the constraints in Eq. (3.12) for nonreciprocal phase shifts: $\Omega_m = 0.3$, $\Omega_f = 0.753$, $\phi = 0.703\pi$, $K_c = 0.415$, $K_m = 0.1$, $n = 4$, $\zeta = 0.02$ and $P = 1$. In Fig. 3.11(a), $\mathcal{R}_{em} \approx 0$ over a large portion of the curve, especially starting from the portion leading to the turning point near $\Omega_m \approx 0.48$ and extending to $\Omega_m \approx 0.2$. The *forward* and *backward* response envelopes have very similar shapes throughout this range of Ω_m. Fig. 3.11(b) shows the variation of the reciprocity bias, R, along the same locus. We have $R < 0.04$ throughout the range of Ω_m where $\mathcal{R}_{em} \simeq 0$, implying that the degree of nonrecpirocity is small. The minimum value of R, indicated by point W_R, occurs near a zero crossing of $\mathcal{R}_{em}$ for $\Omega_m = 0.454$, $\Omega_f = 0.638$, $\phi = 0.715\pi$ and $K_c = 0.713$. We have $R = 5.52 \times 10^{-4}$ at this point, which means that the two response envelopes almost coincide. Figs. 3.11(c,d) show the output displacements and response envelopes at point W_R. Neither the two output displacements nor the two response envelopes can be visibly distinguished. Vibration transmission is therefore nearly reciprocal for this set of system parameters.

The near-reciprocal response reported here is reminiscent of the restoring of reciprocity in nonlinear systems with broken mirror symmetry [52, 92]. While restoring reciprocity in nonlinear systems, the reciprocity bias can be made arbitrarily small to ensure reciprocity [92]. We do not expect the same property to hold in the present work because there is only one symmetry-breaking parameter in our system. Nevertheless, given the small value of R for the example in Fig. 3.11, it is unlikely that the output displacements could be distinguished in an experimental realization of the system in this case.

3.5. Limitations of the methodology

3.5.1. Systems with $\Omega_f < \Omega_m$

In analogy to audio communication systems [93, Ch. 3], the response envelopes can be viewed as the message signals in the amplitude modulation (AM) technique and the output displacement as the resultant waves after AM. A successful AM process requires that the carrier wave has a much higher frequency than the message signal. Upon receiving the signal, the frequency contents of the signal (peaks at equally distanced frequencies) are used during the demodulation process to retrieve the original message signal. When the frequency of the carrier waves is high enough, the receiver can obtain sufficient peaks within every period of the message signal to reconstruct the original message with high quality. Similarly, if $\Omega_f < \Omega_m$ in our system, there will be less than one intersection point of output displacement and its response envelope within a period $T_E = 2\pi/\omega_m$. Thus, the response envelope fails to capture the profile of the output displacement.

In Section 3.3.2, we used parameter sets with $0.5 \leq \Omega_f \leq 2$ and $\Omega_m = 0.2$. The frequency of the response envelopes was therefore lower than the frequencies of the carrier waves, and Eq. (3.6) captured the response envelopes well, as a result; recall Fig. 3.7. In Section 3.3.3, Ω_m was allowed to vary as a free parameter to satisfy the additional constraint on envelope shapes, $\mathcal{R}_{em} = 0$ in Eq. (3.13). It is possible that the additional constraint is sometimes satisfied with $\Omega_m > \Omega_f$. Here, we present an example of this scenario that leads to inaccurate prediction of nonreciprocal phase shifts.

Fig. 3.12(a) shows the variation of $\mathcal{R}_{em}$ as a function of Ω_m for a set of parameters that satisfies the constraints in Eq. (3.12) for nonreciprocal phase shifts: $\Omega_m = 0.2$, $\Omega_f = 0.753$, $\phi = 0.458\pi$, $K_c = 0.969$, $K_m = 0.1$, $n = 4$, $\zeta = 0.02$ and $P = 1$. We refer to this initial point as H. As Ω_m varies, $\mathcal{R}_{em}$ has three zero crossings, indicated by the empty diamond markers. Fig. 3.12(b) shows that $\Omega_m < \Omega_f$ for the first two zero crossings; they fall above the oblique dashed line that indicates $\Omega_m = \Omega_f$. As expected, the response at these two points exhibits nonreciprocal phase shift with the same envelope shape (not shown). However, $\Omega_m > \Omega_f$ at the third zero crossing, indicated by point H_s where $\Omega_m = 0.901$, $\Omega_f = 0.177$, $\phi = 0.473\pi$ and $K_c = 4.747$. Figs. 3.12(c,d) show the output displacements and response envelopes for point H_s. The predicted response envelopes have low-amplitude fluctuations of high frequency with large DC shifts ($\mathcal{S}^F_{dc;4}$, $\mathcal{S}^B_{dc;1}$) while the displacements have high-amplitude fluctuations of low frequency. The predicted envelopes do not capture the actual envelope of the response because $\Omega_f < \Omega_m$.

3.5.2. Long systems with strong modulation

Except for the special case presented in Section 3.4.1, all the calculations for nonreciprocal phase shifts in this work are conducted with $\mathcal{F} = 1$. We have the same number of free system parameters in this case as the constraint equations, which makes the search for nonreciprocal phase shifts feasible. Nevertheless, the assumption of $\mathcal{F} = 1$ restricts the analysis to short, weakly modulated systems [90].

A higher value of $\mathcal{F}$ is required to accurately capture the steady-state response envelopes in systems with $K_m > 0.1$ or $n > 5$. To update the formulation of response envelopes from Section 3.2.2 to a general value of $\mathcal{F}$, we need to use:

$$\begin{aligned} E^{F,B}_{n,1}(\tau) &= \sqrt{\mathcal{S}^{F,B}_{dc;n,1} + \mathcal{S}^{F,B}_{ac;n,1}(\tau)}, \\ \mathcal{S}^{F,B}_{dc;n,1} &= 4\sum_{q=-\mathcal{F}}^{\mathcal{F}} \left|y^{F,B}_{n,1;q}\right|^2, \\ \mathcal{S}^{F,B}_{ac;n,1}(\tau) &= \sum_{j=1}^{2\mathcal{F}} \mathcal{E}^{F,B}_{j;n,1} \cos\left(j\Omega_m\tau - \vartheta^{F,B}_{j;n,1}\right), \end{aligned} \tag{3.14}$$

which replaces Eqs. (3.9-3.11). The following constraints replace Eq. (3.12) to enforce a nonreciprocal phase shift between the response envelopes:

$$\begin{aligned} \mathcal{S}^F_{dc;n} &= \mathcal{S}^B_{dc;1}, \\ \mathcal{E}^F_{1;n} &= \mathcal{E}^B_{1;1}, \\ &\vdots \\ \mathcal{E}^F_{2\mathcal{F};n} &= \mathcal{E}^B_{2\mathcal{F};1}. \end{aligned} \tag{3.15}$$

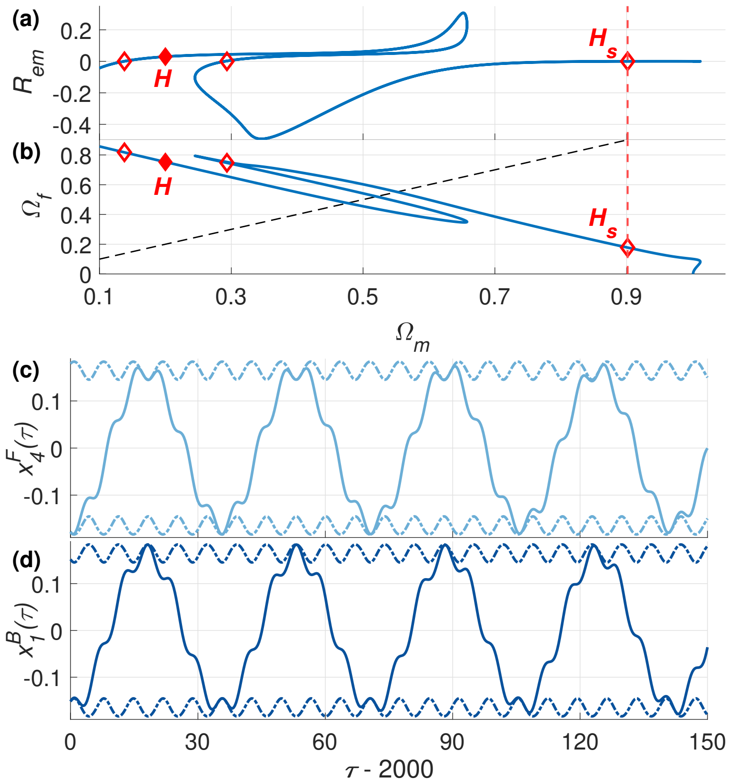

Figure 3.12: Variation of $\mathcal{R}_{em}$ (a) and Ω_f (b) as functions of Ω_m for point H that exhibits nonreciprocal phase shift. The black dashed line in panel (b) represent $\Omega_f = \Omega_m$. (c,d) Displacement outputs and response envelopes for point H_s.

There are $2\mathcal{F} + 1$ constraints in Eq. (3.15). A larger value of $\mathcal{F}$ increases the number of constraints, but it does not change the number of available system parameters that can be used to satisfy the additional constraints. As discussed in Section 3.3, only 4 system parameters can be changed as free (control) parameters: Ω_f, ϕ, K_c and Ω_m. If $\mathcal{F} > 1$, the number of equations exceed the number of unknowns (overdetermined system) and it becomes no longer possible to satisfy all the constraints in Eq. (3.15). Thus, the methodology introduced in Section 3.3, in its current form, is limited to $\mathcal{F} = 1$, which corresponds to short systems ($n < 5$) subject to weak modulations ($K_m \leq 0.1$).

This is not an insurmountable limitation, however. Within the framework of the present work, one potential way to overcome this limitation is to allow more system parameters to vary (increasing the number of free parameters). Currently, parameter ϕ makes the only difference between the units. It is possible to allow for variation in the system parameters across units (mass, stiffness, etc.) to make up for the required number of control parameters. Alternatively, it may be possible to develop an alternative formulation to find nonreciprocal phase shifts in strongly modulated systems with more number of units.

3.6. Conclusions

We reported on the existence of response regimes in spatiotemporally modulated systems that are characterized by nonreciprocal phase shifts. This is a special case of nonreciprocal dynamics in which the transmitted vibrations have the same amplitude and the only contributor to nonreciprocity is the difference between the transmitted phases in opposite directions. This attribute of nonreciprocity is rarely discussed in the context of spatiotemporally modulated systems.

We presented a methodology for obtaining nonreciprocal phase shifts that takes advantage of the time-periodic nature of the envelopes of the response in the steady state. This circumvents the complexities of the non-periodic nature of the response caused by the presence of two incommensurate frequencies (modulation and external drive). While we primarily focused on weakly modulated systems with a small number of units, we also presented a special case of nonreciprocal phase shifts in a system of arbitrary length and strength of modulation. In addition, we provided a formulation that ensures the same transmitted waveforms in opposite directions, which also helped us obtain a special case of near-reciprocal transmission of vibrations.

In summary, we extended the phenomenon of phase nonreciprocity from nonlinear systems (passive) to spatiotemporally modulated systems (active). We discussed the main limitations of our methodology in its current form: systems with modulation that is faster than the external drive, and long systems subject to strong modulation. We point out a potential way to overcome the second limitation to motivate further research on the topic. We hope that our findings can enable new developments in wave processing techniques such as phase shift keying and communication devices.

Appendices

3A. Non-dimensionalization

The equations of motion which govern the n-DoF modulated system in Fig. 3.1 are:

$$\begin{gathered}
m\frac{\mathrm{d}^2u_1}{\mathrm{d}t^2}+c\frac{\mathrm{d}u_1}{\mathrm{d}t}+k_1u_1+k_c\delta_1^2=F_1\cos(\omega_f t),\\
\vdots\\
m\frac{\mathrm{d}^2u_p}{\mathrm{d}t^2}+c\frac{\mathrm{d}u_p}{\mathrm{d}t}+k_pu_p+k_c\delta_p^2=0,\\
\vdots\\
m\frac{\mathrm{d}^2u_n}{\mathrm{d}t^2}+c\frac{\mathrm{d}u_n}{\mathrm{d}t}+k_nu_n+k_c\delta_n^2=F_n\cos(\omega_f t),
\end{gathered}\tag{3A.1}$$

where $k_p = k_{g,DC} + k_{g,AC}\cos(\omega_m t - \phi_p)$ and $\phi_p = (p-1)\phi$ $(p = 1, 2, \cdots, n)$. The difference term $\delta_p^2 = 2u_p - u_{p-1} - u_{p+1}$ everywhere, except at the two ends where $\delta_1^2 = u_1 - u_2$ and $\delta_n^2 = u_n - u_{n-1}$. We use $\tau = \omega_0 t$ as the nondimensional time with $\omega_0 = \sqrt{k_{g,DC}/m}$. We define $\zeta = c/(2m\omega_0)$, $\Omega_m = \omega_m/\omega_0$, $\Omega_f = \omega_f/\omega_0$, $K_c = k_c/k_{g,DC}$, $K_m = k_{g,AC}/k_{g,DC}$, $P_1 = F_1/(ak_{g,DC})$, $P_n = F_n/(ak_{g,DC})$ and $x_p = u_p/a$, where a is a representative length. After substituting these parameters into Eq. (3A.1), we obtain:

$$\begin{gathered}
ma\omega_0^2\ddot{x}_1+2\zeta ma\omega_0^2\dot{x}_1+k_{g,DC}ax_1\left[1+K_m\cos(\Omega_m\tau)\right]\\
+K_ck_{g,DC}a\left(x_1-x_2\right)=P_1ak_{g,DC}\cos(\Omega_f\tau),\\
\vdots\\
ma\omega_0^2\ddot{x}_p+2\zeta ma\omega_0^2\dot{x}_p+k_{g,DC}ax_p\left[1+K_m\cos(\Omega_m\tau-\phi_p)\right]\\
+K_ck_{g,DC}a\left(2x_p-x_{p+1}-x_{p-1}\right)=0,\\
\vdots\\
ma\omega_0^2\ddot{x}_n+2\zeta ma\omega_0^2\dot{x}_n+k_{g,DC}ax_n\left[1+K_m\cos(\Omega_m\tau-\phi_n)\right]\\
+K_ck_{g,DC}a\left(x_n-x_{n-1}\right)=P_nak_{g,DC}\cos(\Omega_f\tau),
\end{gathered}\tag{3A.2}$$

where $\ddot{x}_p$ and $\dot{x}_p$ represent $\mathrm{d}^2x_p\,/\,\mathrm{d}^2\tau$ and $\mathrm{d}x_p\,/\,\mathrm{d}\tau$ respectively. Eq. (3A.2) can be further simplified as:

$$\begin{gathered}
\ddot{x}_1+2\zeta\dot{x}_1+x_1\left[1+K_m\cos(\Omega_m\tau)\right]+K_c\left(x_1-x_2\right)=P_1\cos(\Omega_f\tau),\\
\vdots\\
\ddot{x}_p+2\zeta\dot{x}_p+x_p\left[1+K_m\cos(\Omega_m\tau-\phi_p)\right]+K_c\left(2x_p-x_{p+1}-x_{p-1}\right)=0,\\
\vdots\\
\ddot{x}_n+2\zeta\dot{x}_n+x_n\left[1+K_m\cos(\Omega_m\tau-\phi_n)\right]+K_c\left(x_n-x_{n-1}\right)=P_n\cos(\Omega_f\tau),
\end{gathered}\tag{3A.3}$$

In this paper, calculations and analysis of the response of the n-DoF modulated system are all based on Eq. (3A.3), which is the same as Eq. (3.1).

3B. Response envelope: Amplitude terms

The envelope amplitudes ($\mathcal{A}_p$ and $\mathcal{B}_p$) and envelope phases ($\theta_{a;p}$ and $\theta_{b;p}$) in Eq. (3.11) can be calculated from:

$$\begin{aligned}\mathcal{A}_p =& 8\sqrt{\left(Q_{c;a;p}\right)^2 + \left(Q_{s;a;p}\right)^2},\ \ \theta_{a;p} = \operatorname{atan2}\left(Q_{s;a;p}, Q_{c;a;p}\right),\\ \mathcal{B}_p =& 8\sqrt{\left(Q_{c;b;p}\right)^2 + \left(Q_{s;b;p}\right)^2},\ \ \theta_{b;p} = \operatorname{atan2}\left(Q_{s;b;p}, Q_{c;b;p}\right),\end{aligned}$$

where $Q_{c,s;a,b;p}$ are defined as:

$$\begin{aligned}Q_{c;a;p} =& \operatorname{Re}(y_{p,0})\left(\operatorname{Re}(y_{p,-1}) + \operatorname{Re}(y_{p,1})\right)\\ &+ \operatorname{Im}(y_{p,0})\left(\operatorname{Im}(y_{p,-1}) + \operatorname{Im}(y_{p,1})\right),\\ Q_{s;a;p} =& \operatorname{Re}(y_{p,0})\left(\operatorname{Im}(y_{p,-1}) - \operatorname{Im}(y_{p,1})\right)\\ &- \operatorname{Im}(y_{p,0})\left(\operatorname{Re}(y_{p,-1}) - \operatorname{Re}(y_{p,1})\right),\\ Q_{c;b;p} =& \operatorname{Re}(y_{p,-1})\operatorname{Re}(y_{p,1}) + \operatorname{Im}(y_{p,-1})\operatorname{Im}(y_{p,1}),\\ Q_{s;b;p} =& \operatorname{Re}(y_{p,1})\operatorname{Im}(y_{p,-1}) - \operatorname{Re}(y_{p,-1})\operatorname{Im}(y_{p,1}).\end{aligned}$$

Chapter 4

Parametric Instability in Discrete Models of Spatiotemporally Modulated Materials

4.1. Introduction

Spatiotemporal modulation of the effective material properties of a system is one established way to realize nonreciprocal transmission of mechanical or acoustic waves [4, 6]. In this context, spatiotemporal modulation refers to periodic changes (often harmonic) in the material properties of a waveguide, material or device in both space and time. The nonreciprocal transmission characteristics of spatiotemporally modulated materials have been a key factor in the great attention they have received in recent years.

The underlying mechanisms that lead to nonreciprocal propagation in spatiotemporally modulated materials are relatively well understood by now [7, 17, 25, 94]. A widely featured dynamic characteristic of these systems is the appearance of direction-dependent frequency gaps in the dispersion diagram, which leads to unidirectional propagation of waves through the system. In finite systems, this leads to a large difference between the energies transmitted in opposite directions: a large energy bias.

In systems with very few spatiotemporally modulated units, the energy bias is often very small and nonreciprocity manifests primarily as a difference in the transmitted phases instead [90]. To increase the energy bias in short systems, one can increase the number of modulated units or the modulation amplitude. The influence of adding more modulated units on the transmission characteristics can be investigated using the theoretical frameworks that already exist in the literature. This is no longer the case for strongly modulated systems.

Increasing the strength of modulations can change the spectral contents of the response, specifically by making the contributions from sidebands more significant and by shifting the resonance frequencies; a detailed analysis of these effects is available elsewhere [90]. More importantly, strong modulations can result in parametric instability, which leads to unbounded growth of the response amplitude in time [73, 95]. This is a critical feature of strongly modulated systems because it can compromise safe operation of modulated devices or cause device failure.

The objective of this work is to investigate the phenomenon of parametric instability in spatiotemporally modulated systems. We focus exclusively on discrete models of spatiotemporally modulated materials. To a great extent, this choice is motivated by the models associated with experimental realization of spatiotemporal modulations. Spatiotemporal modulation, a type of parametric excitation, is often achieved at discrete points throughout the structure, for example by piezoelectric patches [40, 47] or magnetic forces [43, 49]. Discrete models are therefore developed for their analysis, especially in the case of finite systems.

Parametric excitation occurs in numerous mechanical systems when a displacement-dependent forcing is present, perhaps most famously in a pendulum with a moving base [58, Ch. 5] or used to explain how to get a swing in motion [96]. The study of parametrically excited systems dates back to the nineteenth century [97], with the works of Mathieu [98] and Rayleigh [99] among the early contributions in mechanical vibrations. In the present century, parametric excitation and the associated amplification effect are widely utilized in the operation of MEMS sensors and actuators [71, 100].

Parametric instabilities occur when the system can no longer maintain a bounded response amplitude above a threshold of modulation amplitude – this threshold can be infinitesimally small under certain conditions. The ensuing exponential growth of the response amplitude is detrimental to a system's ability to carry out its intended operation and often leads to failure. Understanding of parametric stability is therefore crucial in applications ranging from aerospace rotors [101, 102] and wind turbines [103] to machining chatter [104, 105] and control systems [106].

Spatiotemporally modulated materials can be modeled as coupled oscillators subject to parametric excitation. The corresponding mathematical model is a system of coupled Mathieu equations, with a phase term that corresponds to spatial modulation. Despite the vast literature on the Mathieu equation, there are relatively fewer studies on coupled Mathieu equations, and we have found that parametric stability is rarely discussed in the context of spatiotemporally modulated systems [107, 108]. In particular, the influence of spatial modulations (modulation wavenumber) on parametric stability remains to be investigated. Our goal in this work is to contribute to filling this gap in the literature.

We refer to the modulation frequencies that can lead to unstable response for infinitesimally small modulation amplitudes as the unstable modulation frequencies (UMFs) – this only occurs in the absence of energy dissipation. One of the early studies on parametric stability in a system of n undamped Mathieu equations found that the response remains stable for sufficiently small modulation amplitudes unless the modulation frequency is equal to a combination of any two natural frequencies of the system in the absence of modulations [109, Ch. 4]. Specifically, $|\Omega_{n,j_1} \pm \Omega_{n,j_2}|/\beta > 0$ are identified as potential UMFs , where $j_{1,2} \in \{1, 2, \cdots, n\}$, $\beta \in \mathbb{N}$, and $\Omega_{n,j_{1,2}}$ denotes an unmodulated natural frequency. An independent study based on perturbation analysis reported the same result [110].

It has been long established to use stability diagrams (stability charts) to graphically present the dependence of parametric stability on modulation amplitude and frequency [111]. Despite the extensive research on parametric stability of Mathieu's equation and its various extended forms, systems with more degrees of freedom (DoF) have received much less attention in comparison. For example, the UMFs have been studied in coupled modulated systems (2-DoF) [59, 112], for which the presence of a phase shift between the two modulations influences the stability but not the UMFs [112]. When the parametric excitation terms are uncoupled in the equations of motion, only $\Omega_{2,j_1} + \Omega_{2,j_2}$ are identified as UMFs [113]. In a study on a 3-DoF system, the stability diagram shows an increase in the number of unstable regions, with the UMFs located at $(\Omega_{3,j_1} + \Omega_{3,j_2})/\beta$ [59]. Nevertheless, we could not find a systematic study of parametric instability that can be readily applied in the context of spatiotemporally modulated systems. In particular, the influence of spatial modulations and the number of modulated units on parametric stability remains unexplored for the most part.

In this work, we present a detailed computational analysis of parametric instability in spatiotemporally modulated systems. We use Floquet theory to determine the stability of response of the system. We also perform a perturbation analysis of the UMFs that incorporates the influence of modulation phase (wavenumber). The stability of long modulated systems is investigated and discussed in more detail than we could find in the literature. Additionally, we highlight the wide continuous stable ranges of modulation amplitude that appear at low values of modulation frequency in stability diagrams for both short and long systems. These wide ranges of modulation amplitude support the design of slowly modulated systems with high modulation amplitudes.

Finally, it is important to note that when a vibrating system is subject to simultaneous external and parametric excitation with the modulation frequency locked at twice the frequency of the external drive, we can observe unbounded amplitude in the steady-state response of the system even in the presence of damping. This phenomenon is called parametric amplification [71], and is distinct from the scenario we explore in this work. We also note that wavenumber bandgaps may appear in dispersion curves, indicating the appearance of standing waves with exponentially growing amplitudes, especially when the modulation frequency is high [40, 50, 114].

We present the discrete model of a one-dimensional spatiotemporally modulated system in Section 4.2. Section 4.3 introduces the approaches used to determine the stability of the response: Floquet theory and perturbation analysis. Stability diagrams for short systems are presented in Section 4.4. In Section 4.5, we investigate the influence of spatial modulation on parametric stability. Stability of long modulated systems is explored in Section 4.6. The influence of damping on stability is analyzed in Section 4.7. Section 4.8 summarizes our findings.

4.2. Problem formulation

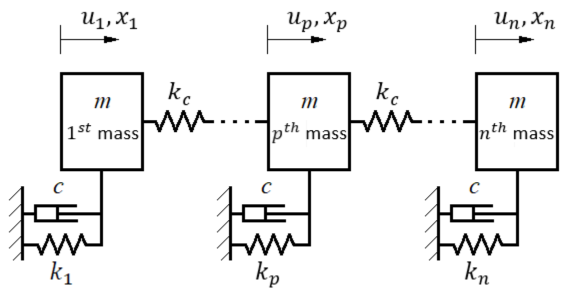

Figure 4.1: Schematic representation of the modulated system with n DoFs.

We consider a discrete model of one-dimensional spatiotemporally modulated materials in this work. Fig. 4.1 shows the schematic of this model. The system is composed of identical masses, linear coupling springs, viscous dampers, and modulated grounding springs. For each mass, only the longitudinal rectilinear motion is considered as a degree of freedom (DoF). The stiffness coefficient of the grounding spring in the p-th modulated unit is expressed as $k_p(t) = k_{g,DC} + k_{g,AC} \cos(\omega_m t - \phi_p)$, where $\phi_p = (p-1)\,\phi$ for $p = 1, 2, \cdots, n$. Parameters ω_m and $k_{g,AC}$ are the modulation frequency and amplitude, respectively. Parameter ϕ represents the spatial modulation along the system. This is the same as the modulation wavenumber. We refer to ϕ as the modulation phase in this work because of our emphasis on short systems.

The equations of motion for the modulated system in Fig. 4.1 are first nondimensionalized; see 4A. The nondimensional equations of motion for the p-th mass of the system are:

$$\ddot{x}_p + 2\zeta\dot{x}_p + x_p\left[1 + K_m \cos(\Omega_m \tau - \phi_p)\right] + K_c \Delta_p^2 = 0, \tag{4.1}$$

where the overdot represents differentiation with respect to nondimentional time τ. The difference terms representing coupling are $\Delta_1^2 = x_1 - x_2$ and $\Delta_n^2 = x_n - x_{n-1}$ at two ends of the system; $\Delta_p^2 = 2x_p - x_{p+1} - x_{p-1}$ elsewhere. We will continue with the nondimensional equations.

Fig. 4.2 shows the time-domain response of Eq.(4.1) for two different sets of system parameters. Panel (a) shows a typical stable response, characterized by its quasiperiodic nature and constant amplitude (energy). Panel (b) shows a typical unstable response, which is characterized by an exponentially growing amplitude.

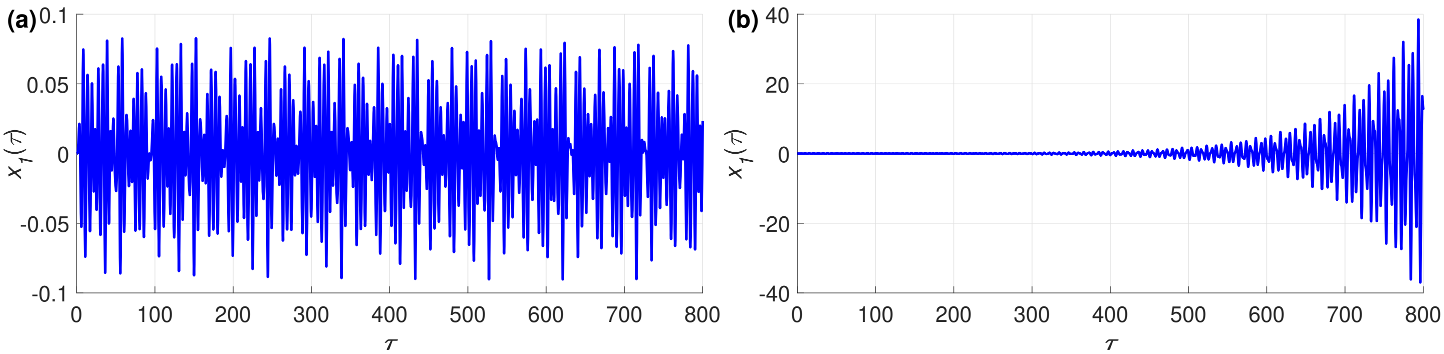

Figure 4.2: Displacements of the first masses in two modulated systems with $K_c = 0.6$, $\phi = 0.5\pi$ and $\zeta = 0$. (a) $n = 3$, $\Omega_m = 2.6$ and $K_m = 0.2$; this scenario falls inside a stable region in Fig. 4.3(b). (b) $n = 5$, $\Omega_m = 2.6$ and $K_m = 0.1$; this scenario falls inside an unstable region in Fig. 4.3(b). The initial conditions for both examples are: $\dot{x}_n(0) = 0.1$, $x_n(0) = x_p(0) = \dot{x}_p(0) = 0$ for $1 \leq p \leq n-1$.

4.3. Approaches to determine parametric stability

4.3.1. Floquet theory: Direct computation

Eq.(4.1) can be recast as a system of linear ordinary differential equations:

$$\frac{\mathrm{d}}{\mathrm{d}\tau} \underline{X}(\tau) = \underline{\underline{\mathsf{A}}}(\tau)\ \underline{X}(\tau), \tag{4.2}$$

where $\underline{X} = \{\dot{\underline{x}}, \underline{x}\}^T$ and $\underline{x} = \{x_1, x_2, \cdots, x_n\}^T$. The matrix of coefficients is periodic in time, $\underline{\underline{\mathsf{A}}}(\tau) = \underline{\underline{\mathsf{A}}}(\tau + T_E)$, with $T_E = 2\pi/\Omega_m$ in this case. Vector and matrix variables are indicated with single and double underlines. Floquet theory describes the conditions for stability (boundedness) of the solutions, $X(\tau)$, based on the principal matrix of the system [115].

The principal matrix of Eq.(4.1), denoted by $\underline{\underline{\Psi}}$, satisfies $\underline{\underline{X}}(T_E) = \underline{\underline{\Psi}}\,\underline{\underline{X}}(0)$, where $\underline{\underline{X}}(0)$ contains an independent set of initial conditions (the identity matrix is the most common choice). The eigenvalues of the principal matrix are crucial to determine the stability of the response of the system. Because there is no explicit analytical solution for Eq. (4.2), or for Mathieu's equation, the stability of the solutions are typically computed numerically. Several approximation methods have also been developed to obtain the principal matrix [58, 116, 117]. In addition to approaches that focus on the principal matrix, the stability of Mathieu's equation can be determined by the harmonic-balance method and the method of multiple scales [73, 118].

The $2n \times 2n$ matrix of coefficients in Eq. (4.2) is:

$$\underline{\underline{\mathsf{A}}}(\tau) = \begin{bmatrix} \underline{\underline{\mathsf{D}}} & \underline{\underline{\mathsf{C}}}(\tau) \\ \underline{\underline{I}} & \underline{\underline{O}} \end{bmatrix} \tag{4.3}$$

where $\underline{\underline{\mathsf{D}}}$, $\underline{\underline{\mathsf{C}}}(\tau)$, $\underline{\underline{I}}$ and $\underline{\underline{O}}$ are all $n \times n$ matrices. $\underline{\underline{O}}$ is a zero matrix, $\underline{\underline{I}}$ is an identity matrix and $\underline{\underline{\mathsf{D}}} = -2\zeta\underline{\underline{I}}$. Matrix $\underline{\underline{\mathsf{C}}}(\tau)$ can be written as:

$$\underline{\underline{\mathsf{C}}}(\tau) = \begin{bmatrix} \mathsf{B}_1(\tau) & K_c & 0 & \cdots & 0 \\ K_c & \mathsf{B}_2(\tau) & K_c & \cdots & 0 \\ 0 & K_c & \mathsf{B}_3(\tau) & \cdots & 0 \\ \vdots & \vdots & \vdots & \ddots & \vdots \\ 0 & 0 & 0 & \cdots & \mathsf{B}_n(\tau) \end{bmatrix} \tag{4.4}$$

where the diagonal terms $\mathsf{B}_p(\tau) = -2K_c - [1 + K_m \cos(\Omega_m \tau - \phi_p)]$ for any value of p, except at the two ends where $\mathsf{B}_1(\tau) = -K_c - [1 + K_m \cos(\Omega_m \tau)]$ and $\mathsf{B}_n(\tau) = -K_c - [1 + K_m \cos(\Omega_m \tau - \phi_n)]$. The elements in the first super diagonal and the first subdiagonal of $\underline{\underline{\mathsf{C}}}(\tau)$ are equal to K_c. The remaining elements of $\underline{\underline{\mathsf{C}}}(\tau)$ are zero.

We define $2n$ vectors of initial conditions that can form an identity matrix:

$$\begin{bmatrix} \underline{X}_1(0) & \underline{X}_2(0) & \cdots & \underline{X}_{2n}(0) \end{bmatrix} = \underline{\underline{I}}. \tag{4.5}$$

The response of the modulated system at $\tau = T_E$, computed for each set of initial conditions, forms a matrix called the principal matrix:

$$\underline{\underline{\mathsf{E}}} = \begin{bmatrix} \underline{X}_1(T_E) & \underline{X}_2(T_E) & \cdots & \underline{X}_{2n}(T_E) \end{bmatrix}. \tag{4.6}$$

Floquet theory states that the response of the system becomes unstable (unbounded) if any eigenvalue of $\underline{\underline{\mathsf{E}}}$ has its modulus larger than unity. In this work, we compute the principal matrices using the fourth-order Runge-Kutta method with Gill coefficients [119, 120]. All the stability diagrams reported in subsequent sections are computed in this way.

4.3.2. Perturbation method: Predicting unstable modulation frequencies

Our goal in this section is to obtain analytical expressions for modulation frequencies that lead to unbounded response in the presence of (infinitesimally) small modulation amplitude. We refer to these frequencies as the unstable modulation frequencies, UMFs. We decompose the steady-state response of the system into its constituent modes to facilitate the analysis based on the method of multiple scales.

In the absence of energy loss ($\zeta = 0$), the response of the modulated system governed by Eq. (4.1) can be expressed as a Fourier series:

$$x_p(\tau) = \sum_{q=1}^{n} \sum_{\kappa=-\infty}^{\infty} X_{p;q;\kappa}(\tau)\, e^{i(\Omega_{n,q}+\kappa\Omega_m)\tau}, \tag{4.7}$$

where $\Omega_{n,q}$ is the q-th natural frequency of the unmodulated system. To keep track of the parametric instabilities that occur at lower modulation frequencies more easily, we introduce the parameter β and rewrite $x_p(\tau)$ as:

$$x_p(\tau) = \sum_{\beta=1}^{\infty} w_{p;\beta}(\tau), \tag{4.8}$$

$$w_{p;\beta}(\tau) = \sum_{q=1}^{n} \sum_{\kappa=-\infty}^{\infty} W_{p;\beta;q;\kappa}(\tau)\, e^{i(\Omega_{n,q}+\kappa\beta\Omega_m)\tau}, \tag{4.9}$$

where $\beta \in \mathbb{N}$. If any $w_{p;\beta}(\tau)$ is unbounded, then $x_p(\tau)$ becomes unbounded too. Therefore, we check the boundedness of $w_{p;\beta}(\tau)$ to determine the parametric stability of $x_p(\tau)$. $w_{p;\beta}(\tau)$ satisfies the equation:

$$\ddot{w}_{p;\beta} + w_{p;\beta}\left[1 + \epsilon\cos\left(\beta\Omega_m\tau - \phi_p\right)\right] + K_c\delta_p^2 = 0, \tag{4.10}$$

where $\delta_1^2 = w_{1;\beta} - w_{2;\beta}$ and $\delta_n^2 = w_{n;\beta} - w_{n-1;\beta}$ at the two ends, and $\delta_p^2 = 2w_{p;\beta} - w_{p-1;\beta} - w_{p+1;\beta}$ elsewhere. Parameter $\epsilon = K_m$ is used here to indicate a small value of K_m. We note that the unmodulated natural frequencies of Eq. (4.10) are the same as those of Eq. (4.1).

We first decouple the unmodulated terms in Eq. (4.10). The mode shape for $\Omega_{n,q}$ is denoted by the vector $\underline{\mathrm{W}}_{q;\beta} = \left\{\mathrm{w}_{q;\beta;1}, \mathrm{w}_{q;\beta;2}, \cdots, \mathrm{w}_{q;\beta;n}\right\}^T$, where $q = 1, 2, \cdots, n$. In the decoupled (modal) space, the displacement is expressed as $z_{p;\beta} = \underline{\mathrm{W}}_{p;\beta}^T \underline{w}_\beta$, where $\underline{w}_\beta = \left\{w_{1;\beta}, w_{2;\beta}, \cdots, w_{n;\beta}\right\}^T$. The p-th decoupled (modal) equation of motion to replace Eq. (4.10) is:

$$\ddot{z}_{p;\beta} + \Omega_{n,p}^2 z_{p;\beta} + \epsilon\sum_{q=1}^{n} \mathrm{w}_{p;\beta;q} w_{q;\beta}\cos\left(\beta\Omega_m\tau - \phi_q\right) = 0. \tag{4.11}$$

Here, $w_{q;\beta}$ can be written out using the inverse transformation $\underline{w}_\beta = \underline{\underline{\mathrm{W}}}_\beta^{-1}\underline{Z}_\beta$, where $\underline{Z}_\beta = \left\{z_{1;\beta}, z_{2;\beta}, \cdots, z_{n;\beta}\right\}^T$ and $\underline{\underline{\mathrm{W}}}_\beta = \left[\underline{\mathrm{W}}_{1;\beta}^T; \underline{\mathrm{W}}_{2;\beta}^T; \cdots; \underline{\mathrm{W}}_{n;\beta}^T\right]$.

The stability of the response of the system is determined by whether the amplitude of $z_{p;\beta}$ becomes unbounded. We present this analysis in detail for the 2-DoF system. Hereafter, we will drop the subscript β in $z_{p;\beta}$ for simplicity.

4.3.2.1. 2-DoF modulated systems

The decoupled equations of motion for the 2-DoF system are:

$$\ddot{z}_1 + \Omega_{2,1}^2 z_1 + \frac{\epsilon}{2}\left(z_1 + z_2\right)\cos\beta\Omega_m\tau + \frac{\epsilon}{2}\left(z_1 - z_2\right)\cos\left(\beta\Omega_m\tau - \phi\right) = 0, \tag{4.12a}$$

$$\ddot{z}_2 + \Omega_{2,2}^2 z_2 + \frac{\epsilon}{2}\left(z_1 + z_2\right)\cos\beta\Omega_m\tau - \frac{\epsilon}{2}\left(z_1 - z_2\right)\cos\left(\beta\Omega_m\tau - \phi\right) = 0, \tag{4.12b}$$

where $\Omega_{2,1} = 1$ and $\Omega_{2,2} = \sqrt{1+2K_c}$. To employ the method of multiple scales, we define two (slow and fast) time variables, $\mu = \Omega_m\tau$ and $\nu = \epsilon\Omega_m\tau$. Eq. (4.12) is therefore rewritten in the new time variables as:

$$\begin{aligned}\Omega_m^2\frac{\partial^2 z_1}{\partial\mu^2} + 2\epsilon\Omega_m^2\frac{\partial^2 z_1}{\partial\mu\partial\nu} + \epsilon^2\Omega_m^2\frac{\partial^2 z_1}{\partial\nu^2} + \Omega_{2,1}^2 z_1&\\ + \frac{\epsilon}{2}\left(z_1 + z_2\right)\cos\beta\mu + \frac{\epsilon}{2}\left(z_1 - z_2\right)\cos\left(\beta\mu - \phi\right) &= 0,\end{aligned} \tag{4.13a}$$

$$\begin{aligned}\Omega_m^2\frac{\partial^2 z_2}{\partial\mu^2} + 2\epsilon\Omega_m^2\frac{\partial^2 z_2}{\partial\mu\partial\nu} + \epsilon^2\Omega_m^2\frac{\partial^2 z_2}{\partial\nu^2} + \Omega_{2,2}^2 z_2&\\ + \frac{\epsilon}{2}\left(z_1 + z_2\right)\cos\beta\mu - \frac{\epsilon}{2}\left(z_1 - z_2\right)\cos\left(\beta\mu - \phi\right) &= 0.\end{aligned} \tag{4.13b}$$

z_p is expanded into a power series of ϵ:

$$z_p\left(\mu,\nu\right) = z_{p,0}\left(\mu,\nu\right) + \epsilon z_{p,1}\left(\mu,\nu\right) + O\left(\epsilon^2\right). \tag{4.14}$$

We substitute Eq. (4.14) into Eq. (4.13) and neglect the terms of $O\left(\epsilon^2\right)$. Equating the coefficients of ϵ^0 and ϵ^1 gives two sets of equations:

$$\frac{\partial^2 z_{j,0}}{\partial\mu^2} + \left(\frac{\Omega_{2,j}}{\Omega_m}\right)^2 z_{j,0} = 0, \tag{4.15}$$

where $j \in \{1,2\}$, and

$$\begin{aligned}\frac{\partial^2 z_{1,1}}{\partial\mu^2} + \left(\frac{\Omega_{2,1}}{\Omega_m}\right)^2 z_{1,1} =& -2\frac{\partial^2 z_{1,0}}{\partial\mu\partial\nu} - \frac{1}{2\Omega_m^2}\left(z_{1,0} + z_{2,0}\right)\cos\beta\mu\\ &- \frac{1}{2\Omega_m^2}\left(z_{1,0} - z_{2,0}\right)\cos\left(\beta\mu - \phi\right),\end{aligned} \tag{4.16a}$$

$$\begin{aligned}\frac{\partial^2 z_{2,1}}{\partial\mu^2} + \left(\frac{\Omega_{2,2}}{\Omega_m}\right)^2 z_{2,1} =& -2\frac{\partial^2 z_{2,0}}{\partial\mu\partial\nu} - \frac{1}{2\Omega_m^2}\left(z_{1,0} + z_{2,0}\right)\cos\beta\mu\\ &+ \frac{1}{2\Omega_m^2}\left(z_{1,0} - z_{2,0}\right)\cos\left(\beta\mu - \phi\right).\end{aligned} \tag{4.16b}$$

The general solution for Eq. (4.15) is:

$$z_{j,0}\left(\mu,\nu\right) = A_j\left(\nu\right)\cos\frac{\Omega_{2,j}}{\Omega_m}\mu + B_j\left(\nu\right)\sin\frac{\Omega_{2,j}}{\Omega_m}\mu. \tag{4.17}$$

Substituting Eq. (4.17) into Eq. (4.16) gives:

$$
\begin{aligned}
\frac{\partial^2 z_{j,1}}{\partial \mu^2} + \left(\frac{\Omega_{2,j}}{\Omega_m}\right)^2 z_{j,1} =& \mathcal{T}_j\left[\frac{\Omega_{2,j}}{\Omega_m}\right] + \mathcal{T}_j\left[\beta + \frac{\Omega_{2,1}}{\Omega_m}\right] + \mathcal{T}_j\left[\beta - \frac{\Omega_{2,1}}{\Omega_m}\right] \\
&+ \mathcal{T}_j\left[\beta + \frac{\Omega_{2,2}}{\Omega_m}\right] + \mathcal{T}_j\left[\beta - \frac{\Omega_{2,2}}{\Omega_m}\right],
\end{aligned} \tag{4.18}
$$

where $\mathcal{T}_j[\omega]$ represents the sum of all harmonic terms at frequency ω in the j-th equation. See 4B for the expressions of each $\mathcal{T}_j[\omega]$.

The forcing terms in Eq. (4.18) can result in unbounded growth of $z_{i,1}$, which leads to unstable response of the system. Therefore, stability is determined by considering the resonance condition of these terms. In perturbation theory, this process is known as removing the *secular* terms.

If neither $|\beta \pm \Omega_{2,1}/\Omega_m|$ nor $|\beta \pm \Omega_{2,2}/\Omega_m|$ is equal to $\Omega_{2,j}/\Omega_m$ for both $j = 1$ and $j = 2$, then $\mathcal{T}_j[\Omega_{2,j}/\Omega_m]$ is the only secular term in Eq. (4.18). Removing this term results in:

$$
\frac{\mathrm{d}A_j}{\mathrm{d}\nu} = \frac{\mathrm{d}B_j}{\mathrm{d}\nu} = 0. \tag{4.19}
$$

Both $z_{j,0}$ and $z_{j,1}$ are bounded when $A_j(\nu)$ and $B_j(\nu)$ are constant. Thus, parametric instability may occur when one of $|\beta \pm \Omega_{2,j_1}/\Omega_m|$ is equal to $\Omega_{2,j_2}/\Omega_m$, where $j_{1,2} \in \{1, 2\}$.

When $\Omega_m = 2\Omega_{2,j}/\beta$, both $\mathcal{T}_j[\Omega_{2,j}/\Omega_m]$ and $\mathcal{T}_j[\beta - \Omega_{2,j}/\Omega_m]$ include secular terms in the j-th equation of Eq. (4.18). The removal of these two sets of resonance terms gives:

$$
\frac{\mathrm{d}A_j}{\mathrm{d}\nu} = -\frac{1+\cos\phi}{8\Omega_{2,j}\Omega_m}B_j + \frac{\sin\phi}{8\Omega_{2,j}\Omega_m}A_j, \quad \frac{\mathrm{d}B_j}{\mathrm{d}\nu} = -\frac{1+\cos\phi}{8\Omega_{2,j}\Omega_m}A_j - \frac{\sin\phi}{8\Omega_{2,j}\Omega_m}B_j,
$$

and

$$
\frac{\mathrm{d}^2A_j}{\mathrm{d}\nu^2} = \frac{1+\cos\phi}{32\Omega_{2,j}^2\Omega_m^2}A_j, \quad \frac{\mathrm{d}^2B_j}{\mathrm{d}\nu^2} = \frac{1+\cos\phi}{32\Omega_{2,j}^2\Omega_m^2}B_j. \tag{4.20}
$$

When $\cos\phi > -1$, both $A_j(\nu)$ and $B_j(\nu)$ grow exponentially, making $\Omega_m = 2\Omega_{2,j}/\beta$ a UMF. Otherwise, both $A_j(\nu)$ and $B_j(\nu)$ are constant when $\cos\phi = -1$ and the response remains stable.

When $\Omega_m = (\Omega_{2,1} + \Omega_{2,2})/\beta$, we have $\Omega_{2,1}/\Omega_m = \beta - \Omega_{2,2}/\Omega_m$ and $\Omega_{2,2}/\Omega_m = \beta - \Omega_{2,1}/\Omega_m$. Thus, both $\mathcal{T}_1[\Omega_{2,1}/\Omega_m]$ and $\mathcal{T}_1[\beta - \Omega_{2,2}/\Omega_m]$ include resonant terms in Eq. (4.18) with $j = 1$. In addition, both $\mathcal{T}_2[\Omega_{2,2}/\Omega_m]$ and $\mathcal{T}_2[\beta - \Omega_{2,1}/\Omega_m]$ include resonance terms in Eq. (4.18) with $j = 2$. The removal of these four sets of resonance terms gives:

$$
\frac{\mathrm{d}A_1}{\mathrm{d}\nu} = -\frac{1-\cos\phi}{8\Omega_{2,1}\Omega_m}B_2 - \frac{\sin\phi}{8\Omega_{2,1}\Omega_m}A_2, \quad \frac{\mathrm{d}B_1}{\mathrm{d}\nu} = -\frac{1-\cos\phi}{8\Omega_{2,1}\Omega_m}A_2 + \frac{\sin\phi}{8\Omega_{2,1}\Omega_m}B_2,
$$

$$\frac{\mathrm{d}A_2}{\mathrm{d}\nu} = \frac{-1+\cos\phi}{8\Omega_{2,2}\Omega_m}B_1 - \frac{\sin\phi}{8\Omega_{2,2}\Omega_m}A_1, \quad \frac{\mathrm{d}B_2}{\mathrm{d}\nu} = \frac{-1+\cos\phi}{8\Omega_{2,2}\Omega_m}A_1 + \frac{\sin\phi}{8\Omega_{2,2}\Omega_m}B_1,$$

and

$$\frac{\mathrm{d}^2A_j}{\mathrm{d}\nu^2} = \frac{1-\cos\phi}{32\Omega_{2,1}\Omega_{2,2}\Omega_m^2}A_j, \quad \frac{\mathrm{d}^2B_j}{\mathrm{d}\nu^2} = \frac{1-\cos\phi}{32\Omega_{2,1}\Omega_{2,2}\Omega_m^2}B_j. \tag{4.21}$$

When $-1 \leq \cos\phi < 1$, both $A_j(\nu)$ and $B_j(\nu)$ grow exponentially, making $\Omega_m = (\Omega_{2,1} + \Omega_{2,2})/\beta$ a UMF. Otherwise, both $A_j(\nu)$ and $B_j(\nu)$ are constant when $\cos\phi = 1$ and the response remains stable.

When $\Omega_m = (\Omega_{2,2} - \Omega_{2,1})/\beta$, we have $\Omega_{2,1}/\Omega_m = \Omega_{2,2}/\Omega_m - \beta$ and $\Omega_{2,2}/\Omega_m = \beta + \Omega_{2,1}/\Omega_m$. Thus, both $\mathcal{T}_1[\Omega_{2,1}/\Omega_m]$ and $\mathcal{T}_1[\beta - \Omega_{2,2}/\Omega_m]$ include resonance terms in Eq. (4.18) with $j = 1$. Meanwhile, both $\mathcal{T}_2[\Omega_{2,2}/\Omega_m]$ and $\mathcal{T}_2[\beta + \Omega_{2,1}/\Omega_m]$ include resonance terms in Eq. (4.18) with $j = 2$. The removal of these four sets of resonance terms gives:

$$\frac{\mathrm{d}A_1}{\mathrm{d}\nu} = \frac{1-\cos\phi}{8\Omega_{2,1}\Omega_m}B_2 + \frac{\sin\phi}{8\Omega_{2,1}\Omega_m}A_2, \quad \frac{\mathrm{d}B_1}{\mathrm{d}\nu} = -\frac{1-\cos\phi}{8\Omega_{2,1}\Omega_m}A_2 + \frac{\sin\phi}{8\Omega_{2,1}\Omega_m}B_2,$$

$$\frac{\mathrm{d}A_2}{\mathrm{d}\nu} = \frac{1-\cos\phi}{8\Omega_{2,2}\Omega_m}B_1 - \frac{\sin\phi}{8\Omega_{2,2}\Omega_m}A_1, \quad \frac{\mathrm{d}B_2}{\mathrm{d}\nu} = \frac{-1+\cos\phi}{8\Omega_{2,2}\Omega_m}A_1 - \frac{\sin\phi}{8\Omega_{2,2}\Omega_m}B_1,$$

and

$$\frac{\mathrm{d}^2A_j}{\mathrm{d}\nu^2} = \frac{\cos\phi-1}{32\Omega_{2,1}\Omega_{2,2}\Omega_m^2}A_j, \quad \frac{\mathrm{d}^2B_j}{\mathrm{d}\nu^2} = \frac{\cos\phi-1}{32\Omega_{2,1}\Omega_{2,2}\Omega_m^2}B_j. \tag{4.22}$$

Modulation frequency $\Omega_m = (\Omega_{2,2} - \Omega_{2,1})/\beta$ is not a UMF in this case because $\cos\phi - 1 \leq 0$.

The results of the perturbation analysis of UMFs for the 2-DoF system are summarized in Table 4.1.

Table 4.1: Summary of the perturbation analysis of UMF for the 2-DoF system.

Ω_m	$\frac{\mathrm{d}^2A_j}{\mathrm{d}\nu^2}\Big/A_j = \frac{\mathrm{d}^2B_j}{\mathrm{d}\nu^2}\Big/B_j$	When is Ω_m a UMF?
$2\Omega_{2,1}/\beta$	$\frac{1+\cos\phi}{32\Omega_{2,1}^2\Omega_m^2}$	$\cos\phi \neq -1$
$2\Omega_{2,2}/\beta$	$\frac{1+\cos\phi}{32\Omega_{2,2}^2\Omega_m^2}$	$\cos\phi \neq -1$
$(\Omega_{2,1}+\Omega_{2,2})/\beta$	$\frac{1-\cos\phi}{32\Omega_{2,1}\Omega_{2,2}\Omega_m^2}$	$\cos\phi \neq 1$
$(\Omega_{2,2}-\Omega_{2,1})/\beta$	$\frac{\cos\phi-1}{32\Omega_{2,1}\Omega_{2,2}\Omega_m^2}$	Never.

4.3.2.2. 3-DoF modulated systems

The natural frequencies of the unmodulated 3-DoF system are $\Omega_{3,1} = 1$, $\Omega_{3,2} = \sqrt{1+K_c}$ and $\Omega_{3,3} = \sqrt{1+3K_c}$. Using the same procedure outlined in Section 4.3.2, we can obtain expressions for the UMFs of the system by removing the terms that lead to exponential growth of the response. The results of this analysis are summarized in Table 4.2. We note that the 3-DoF system has a significantly larger number of UMFs than the 2-DoF system.

Table 4.2: Summary of the perturbation analysis of UMF for the 3-DoF system.

Ω_m	$\dfrac{\mathrm{d}^2 A_j}{\mathrm{d}\nu^2}\Big/A_j = \dfrac{\mathrm{d}^2 B_j}{\mathrm{d}\nu^2}\Big/B_j$	When is Ω_m a UMF?
$2\Omega_{3,1}/\beta$	$\dfrac{(1+2\cos\phi)^2}{144\Omega_{3,1}^2\Omega_m^2}$	$\cos\phi \neq -0.5$
$2\Omega_{3,2}/\beta$	$\dfrac{\cos^2\phi}{16\Omega_{3,2}^2\Omega_m^2}$	$\cos\phi \neq 0$
$2\Omega_{3,3}/\beta$	$\dfrac{(2+\cos\phi)^2}{144\Omega_{3,3}^2\Omega_m^2}$	Always.
$(\Omega_{3,1}+\Omega_{3,2})/\beta$	$\dfrac{\sin^2\phi}{24\Omega_{3,1}\Omega_{3,2}\Omega_m^2}$	$\sin\phi \neq 0$
$(\Omega_{3,2}-\Omega_{3,1})/\beta$	$\dfrac{-\sin^2\phi}{24\Omega_{3,1}\Omega_{3,2}\Omega_m^2}$	Never.
$(\Omega_{3,1}+\Omega_{3,3})/\beta$	$\dfrac{(1-\cos\phi)^2}{72\Omega_{3,1}\Omega_{3,3}\Omega_m^2}$	$\cos\phi \neq 1$
$(\Omega_{3,3}-\Omega_{3,1})/\beta$	$\dfrac{-(1-\cos\phi)^2}{72\Omega_{3,1}\Omega_{3,3}\Omega_m^2}$	Never.
$(\Omega_{3,2}+\Omega_{3,3})/\beta$	$\dfrac{\sin^2\phi}{48\Omega_{3,2}\Omega_{3,3}\Omega_m^2}$	$\sin\phi \neq 0$
$(\Omega_{3,3}-\Omega_{3,2})/\beta$	$\dfrac{-\sin^2\phi}{48\Omega_{3,2}\Omega_{3,3}\Omega_m^2}$	Never.

4.3.2.3. n-DoF modulated systems with $n \geq 4$

Using the same procedure for modulated systems with $n \geq 4$, we can obtain a general expression for the UMFs as $\left(\Omega_{n,j_1} + \Omega_{n,j_2}\right)/\beta$, where $j_{1,2} \in \{1, 2, \cdots, n\}$.

The natural frequencies of the unmodulated system are bounded within $1 \leq \Omega_{n,j_{1,2}} <$

$\sqrt{1+4K_c}$ for any value of n because of the periodicity of the system. Because the general expression for UMFs in our perturbation analysis involves a combination of two unmodulated frequencies, we can conclude that the UMFs are bounded within $0 < \Omega_m < 2\sqrt{1+4K_c}$.

4.4. Stability diagrams for short systems

We investigate the parametric instability of short systems that have well separated modes ($K_c = 0.6$). We explore the influence of modulation amplitude, K_m, on stability in the range of modulation frequency, $0.1 \leq \Omega_m \leq 4$. This frequency range is chosen to include all the UMFs for $K_c = 0.6$ and $\beta \leq 20$, as discussed in Section 4.3.2. To present the stability diagrams clearly, this frequency range is split at $\Omega_m = 1.8$ and presented separately. The parametric instabilities occurring within $1.8 \leq \Omega_m \leq 4$ correspond to $\beta = 1$, while those occurring within $0.1 \leq \Omega_m \leq 1.8$ correspond to $\beta \geq 2$. We present the latter in logarithmic scale to improve clarity. In this study, all stability diagrams are presented at a resolution of 300 dots per inch (dpi). Consequently, the limitations associated with this resolution preclude the representation of certain minute features of stability diagrams in undamped systems.

4.4.1. $1.8 \leq \Omega_m \leq 4$

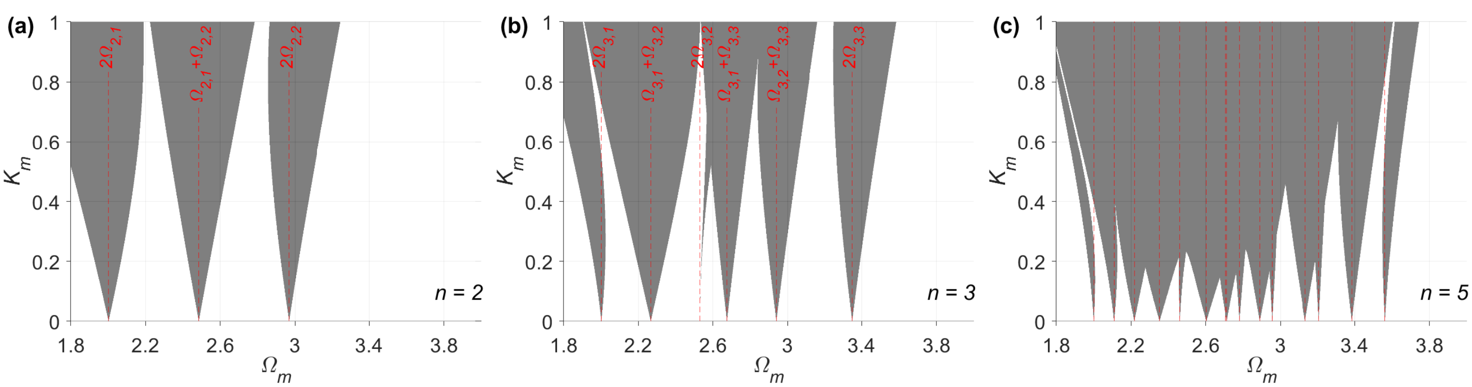

Figure 4.3: Stability diagrams for $K_c = 0.6$, $\phi = 0.5\pi$, $\zeta = 0$ and different numbers of modulated units: (a) $n = 2$, (b) $n = 3$ and (c) $n = 5$. Grey regions represent unstable response, white regions represent stable response. Red dashed lines indicate UMFs obtained from perturbation analysis.

Fig. 4.3 shows the stability diagrams in the (Ω_m, K_m) plane for $1.8 \leq \Omega_m \leq 4$. The grey regions represent the combinations of Ω_m and K_m that result in unstable response, while the white regions represent stable response. The unstable regions originate from the UMFs along $K_m = 0$. The widths of these unstable regions increase as K_m increases, giving the unstable regions an inverted triangular shape known as a *tongue*. The vertical dashed lines indicate the UMFs obtained from the perturbation analysis in Section 4.3.2. We observe an excellent match between the predicted and computed UMFs.

Many of the unstable regions have a triangular shape for small values of K_m. In the vicinity of the UMFs (near $K_m = 0$), the slopes of the transition curves are generally symmetric with respect to the vertical line. In some cases, however, the transition curves become very close to each other and appear to touch the K_m-axis almost vertically; *e.g.* near $\Omega_m = 2.53$ in Fig. 4.3(b) and near $\Omega_m = 2.46$ in Fig. 4.3(c). These points correspond to the special values of ϕ at which the expression for the UMFs did not hold in the perturbation analysis; recall the exclusion points in the right-most column in Tables 1 and 2. At higher values of modulation amplitude, typically $K_m > 0.2$, the transition curves bend and some adjacent unstable regions merge.

We note that it is possible to obtain the slopes (and higher-order approximations) of the transition curves using the perturbation method outlined in Section 4.3.2. This analysis yields good approximation of the transition curves [73], but is tractable only for $\beta = 1$ and very small values of n. We did not pursue this analysis in this work.

4.4.2. $0.1 \leq \Omega_m \leq 1.8$

Figs. 4.4 and 4.5 show the stability diagrams of the modulated systems over $0.5 \leq \Omega_m \leq 1.8$ and $0.1 \leq \Omega_m \leq 0.5$, respectively. All other parameters remain the same as those in Fig. 4.3. Within $0.1 \leq \Omega_m \leq 1.8$ ($\beta > 1$), the lowest point of each unstable region is generally found above $K_m = 0.05$. Moreover, the lowest point tends to appear at a higher value of K_m as Ω_m decreases. While the UMFs with $\beta > 1$ cannot predict an unstable response for very small modulation amplitudes, they still provide accurate approximations for the lowest points of unstable regions when $0.8 \leq \Omega_m \leq 1.8$. However, their accuracy diminishes for $\Omega_m < 0.8$, as shown in Fig. 4.4.

We observe that certain unstable regions narrow as K_m increases, leading to points where these regions converge or pinch off. This phenomenon is shown in Fig.4.4(a) near $\Omega_m = 0.54$ and in Fig.4.4(b) near $\Omega_m \in 0.58, 0.68$. At these points, the unstable regions taper and may eventually separate, forming distinct upper and lower segments.

In Fig. 4.5, numerous unstable regions are observed as isolated individuals, having separated from the unstable regions above them and appearing as detached unstable islands. The stability diagram for a longer system has more unstable islands. Within the range of $0.1 \leq \Omega_m \leq 0.2$, the vertices of some unstable regions become rounded. Moreover, we observe that large continuous stable regions emerge when Ω_m is small. For instance, no unstable

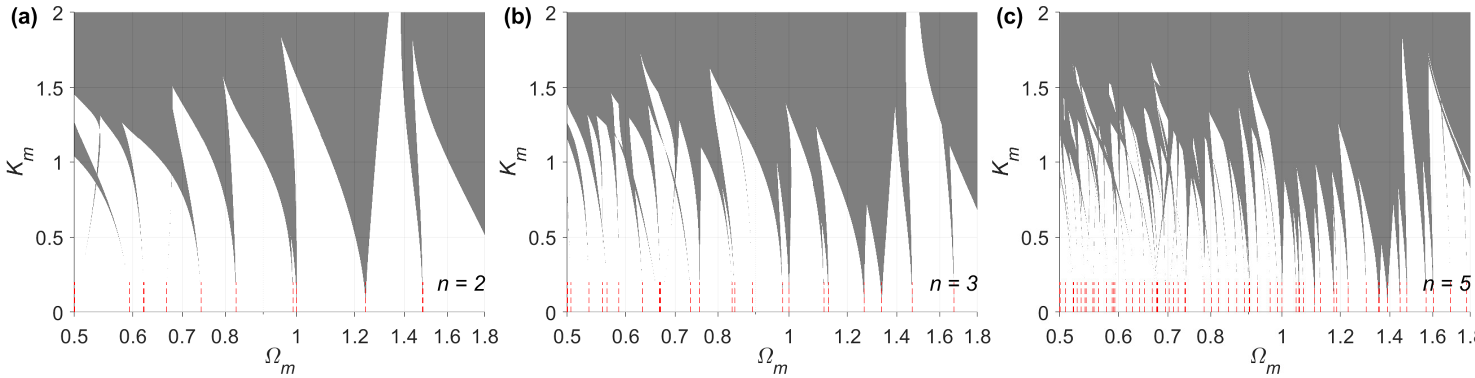

Figure 4.4: Stability diagrams for $K_c = 0.6$ and $\phi = 0.5\pi$. (a) $n = 2$, (b) $n = 3$ and (c) $n = 5$. Red dashed lines indicate UMFs with $\beta \geq 2$, predicted by perturbation analysis.

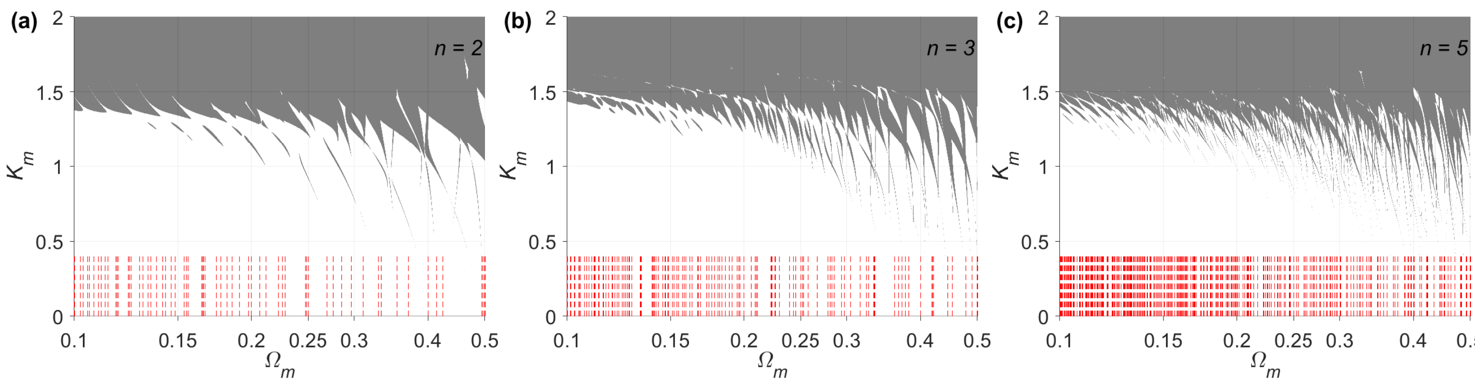

Figure 4.5: Stability diagrams for $K_c = 0.6$ and $\phi = 0.5\pi$. (a) $n = 2$, (b) $n = 3$ and (c) $n = 5$. Red dashed lines indicate the UMFs predicted by perturbation analysis.

regions appear within the domains $\{(\Omega_m, K_m) \in \mathbb{R}^2 \mid 0.1 \leq \Omega_m \leq 0.35, K_m \leq 0.5\}$ and $\{(\Omega_m, K_m) \in \mathbb{R}^2 \mid 0.1 \leq \Omega_m \leq 0.17, K_m \leq 1\}$ in all the examples shown in Fig. 4.5. These stable regions provide broad safe ranges of modulation amplitudes, offering a basis for the design of modulated systems with slow modulations.

4.5. The role of spatial modulation

4.5.1. Stability diagrams in the (Ω_m, ϕ) plane

Fig. 4.6 shows the stability diagrams in the (Ω_m, ϕ) plane for weakly modulated systems ($K_m = 0.05$) and $1.8 \leq \Omega_m \leq 3.6$. This frequency range corresponds to resonance tongues with $\beta = 1$. Most of the unstable regions do not overlap with each other, a feature that makes it easier to distinguish different features of the stability diagrams. All the stability diagrams

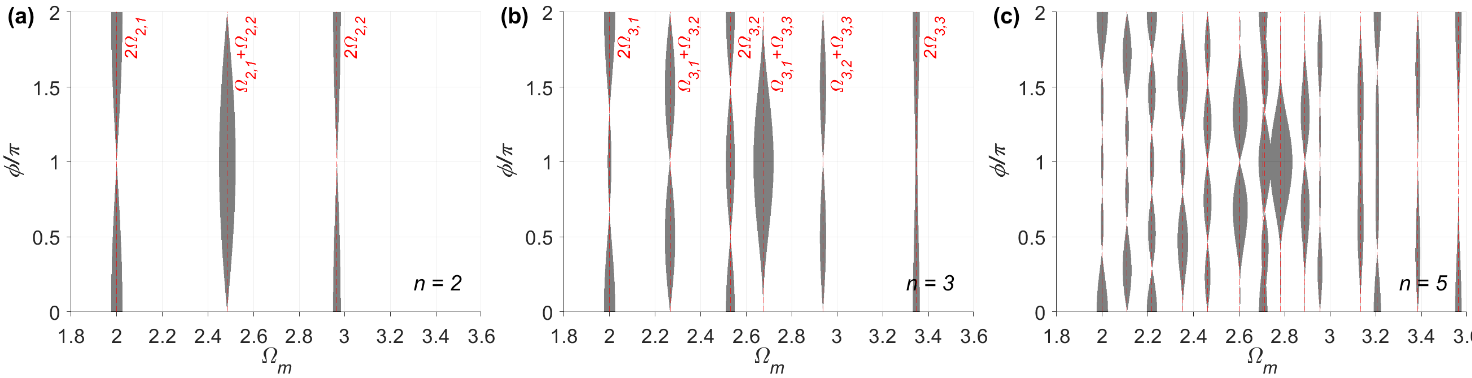

Figure 4.6: Stability diagrams for $K_c = 0.6$ and $K_m = 0.05$. (a) $n = 2$, (b) $n = 3$ and (c) $n = 5$. Red dashed lines indicate UMFs predicted by perturbation analysis.

are symmetry with respect to $\phi = \pi$ because the modulation term remains unchanged under the transformation $\phi \mapsto 2\pi - \phi$. Moreover, we have $\partial\lambda/\partial\phi = 0$ at $\phi = \pi$, where λ represents the eigenvalue of $\underline{\underline{\mathsf{E}}}$ with the largest modulus.

The unstable regions are organized around the UMFs predicted by the perturbation analysis, with their widths undulating symmetrically about the UMFs. The modulation phase at which the width of an unstable region is zero agrees well with the analysis in Section 4.3.2. An example can be seen in panel (a) for the 2-DoF system: $2\Omega_{2,j}$ is an UMF except when $\cos\phi = -1$. These properties of unstable regions may not hold, however, when two adjacent regions overlap. See the overlapping regions near $\Omega_m = 2.7$ in panel (c) for an example.

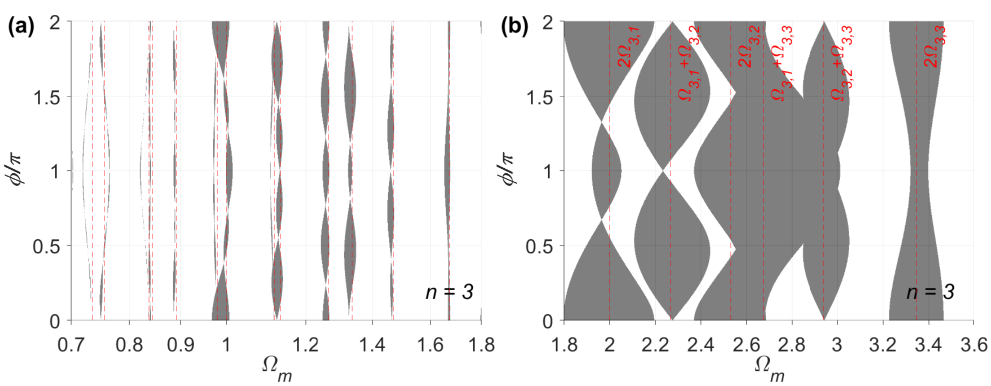

Figure 4.7: Stability diagrams for $K_c = 0.6$, $K_m = 0.4$ and $n = 3$. (a) $0.7 \leq \Omega_m \leq 1.8$ for $\beta = 1$, (b) $1.8 \leq \Omega_m \leq 3.6$ for $\beta > 1$. Red dashed lines indicate UMFs predicted by perturbation analysis.

Fig. 4.7 shows the stability diagrams in the (Ω_m, ϕ) plane for a system with$K_m = 0.4$ (strong modulation) and $n = 3$. Even though the regions of stability are still organized around the

UMFs, they are no longer symmetric about the UMFs; *cf.* Fig. 4.6(b). The unstable regions become wider with increasing the modulation amplitude, as expected. The unstable regions that correspond to $2\Omega_{3,1}$, $\Omega_{3,1} + \Omega_{3,2}$ and $2\Omega_{3,3}$ show these features clearly. The same trend is observed for $\beta > 1$ in panel (a). We also observe that the widths of the unstable regions in Fig. 4.7(a) for $\beta \geq 2$ alternate more frequently than those in Fig. 4.6(b) for $\beta = 1$.

4.5.2. Stability diagrams in the (K_m, ϕ) plane

Fig. 4.8 shows the stability diagrams for three short systems with $K_c = 0.6$ and $\Omega_m = 0.2$. For all values of ϕ, the response remains stable when $K_m \leq 0.7$ and unstable when $K_m \geq 1.7$. Thus, all the transition curves are confined within the range $0.7 < K_m < 1.7$.

The transition curves exhibit more complicated shapes when projected onto the (K_m, ϕ) plane. We observe for $n = 2$, panel (a), the reappearance of stable regions that are surrounded by regions of instability. These islands of stable (unstable) response become more numerous, fragmented and elaborate as the number of units increases; see panels (b) and (c). Despite these intricacies, the range of modulation amplitude over which the response remains stable becomes wider as the modulation phase approaches π.

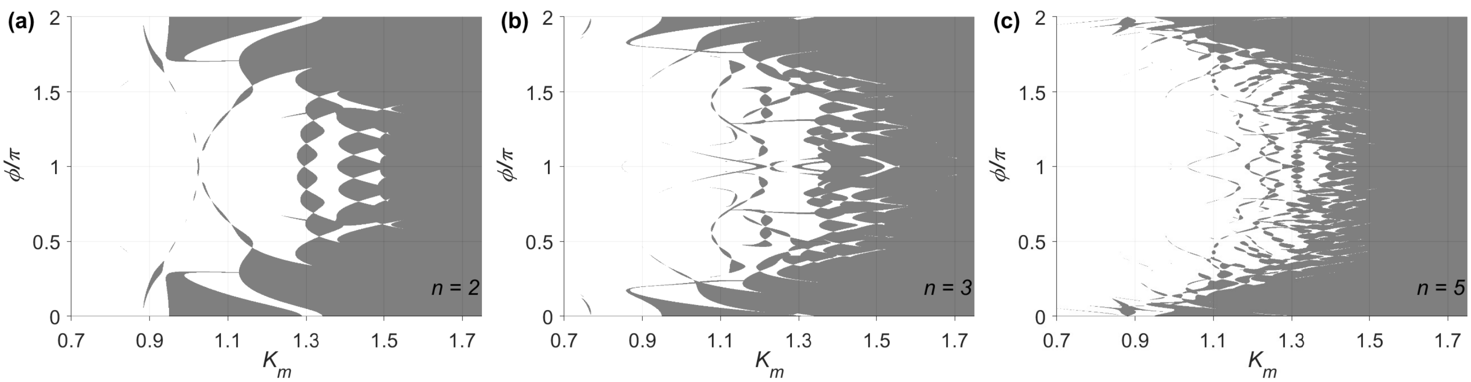

Figure 4.8: Stability diagrams for $K_c = 0.6$ and $\Omega_m = 0.2$. (a) $n = 2$, (b) $n = 3$ and (c) $n = 5$. For all values of ϕ, the response remains stable for $K_m \leq 0.7$ and unstable for $K_m \geq 1.71$.

4.6. Stability of long systems

For short systems ($n \leq 5$), Fig. 4.3 suggests that as the number of modulated units increases, there is a larger set of system parameters that leads to parametric instability: longer systems exhibit more unstable modulation frequencies for $\beta = 1$, and the widths of the unstable regions increase with K_m. A similar trend cannot be seen easily for $\beta > 1$: the stability diagrams in Figs. 4.4, 4.5 and 4.8 have an increasingly more complicated shape as n increases, but it is no longer clear how the total areas covered by the unstable regions in these figures change. To further investigate the impact of n on stability, we calculate the stability diagrams for long systems.

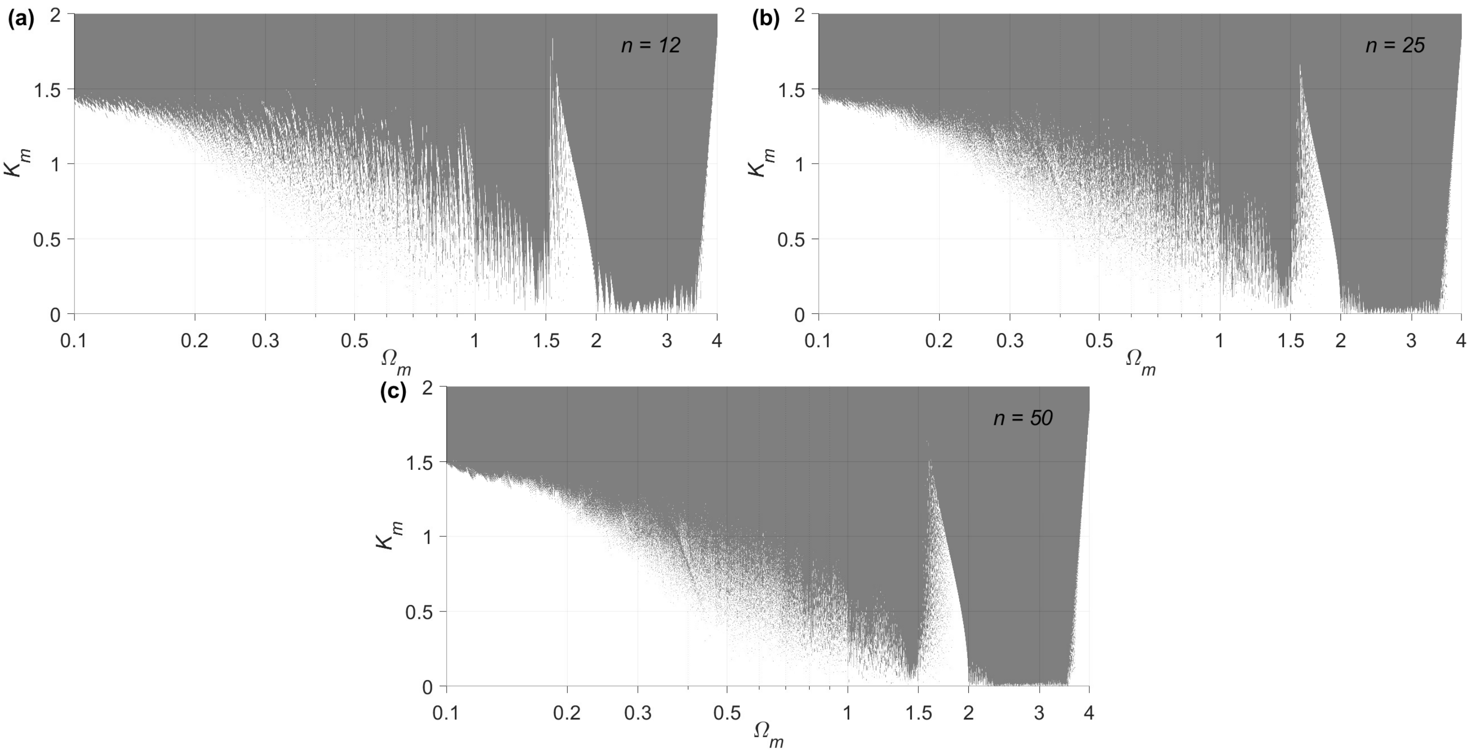

Figure 4.9: Stability diagrams of the modulated systems with $K_c = 0.6$ and $\phi = 0.5\pi$. (a) $n = 12$, (b) $n = 25$ and (c) $n = 50$. The regions bounded by the pink curves are cloudy regions.

Fig. 4.9 shows the stability diagrams in the (Ω_m, K_m) plane for three long systems with $K_c = 0.6$ and $\phi = 0.5\pi$. The unstable regions nearly cover the entire range of $2 \leq \Omega_m \leq 3.688$, within which the UMFs with $\beta = 1$ are present. At lower modulation frequencies ($\beta > 1$), where UMFs appear very densely, the unstable regions become fragmented and there is barely any clear transition curve in the range $0.1 \leq \Omega_m \leq 1.5$. For ease of reference, we refer to these regions as the *cloudy* regions of the stability diagrams.

A main consistent trend in the cloudy regions is that as Ω_m decreases from 1.5, the onset of instability occurs at a higher value of K_m. Many of the other features of the cloudy region do not seem to follow a clear pattern. There are several very small islands of stability that appear sporadically within the unstable regions at higher values of K_m. For $n = 12$, Fig. 4.9(a), two such stable regions appear above $K_m = 1.5$ near $\Omega_m = 0.4$. In contrast, the response remains unstable for $K_m \geq 1.5$ for $n = 25$. We have not explored these features in detail because they disappear in the presence of damping; see Section 4.7.

Another prominent feature of the stability diagrams in Fig. 4.9 is the presence of a semi-triangular region within $1.5 \leq \Omega_m \leq 2$, the majority of which corresponds to stable response. This frequency range falls immediately below the lowest UMF with $\beta = 1$. In these triangular regions, the system can exhibit stable response at very high values of K_m. Fragmented unstable regions are present within each triangular region, with greater density on the left side. For $0.1 \leq \Omega_m \leq \sqrt{1 + 4K_c}$, the largest value of K_m in a stable region occurs within the triangular region.

To explore this phenomenon in greater detail, we calculate the stability diagrams in the (Ω_m, ϕ) plane for $1.4 \leq \Omega_m \leq 2$. Fig. 4.10 shows the stability diagrams for three long systems with $K_c = 0.6$ and $K_m = 1$. A horizontal U-shaped region of predominantly stable response appears in each diagram within the range $0.35\pi \leq \phi \leq 1.65\pi$ and $1.55 \leq \Omega_m \leq 1.81$. Several narrow bands of unstable response appear within the stable U-shaped regions. These bands become increasingly more fragmented, narrow and dense as n increases. For $\Omega_m \geq 1.81$, no unstable regions are found within the U-shaped regions. We conjecture that the stability of this portion of the U-shaped region persists as the number of modulated units increases. We highlight the role of ϕ in the existence of such a persistence region of stable response in a strongly modulated system: the response at $\phi = 0$ remains unstable.

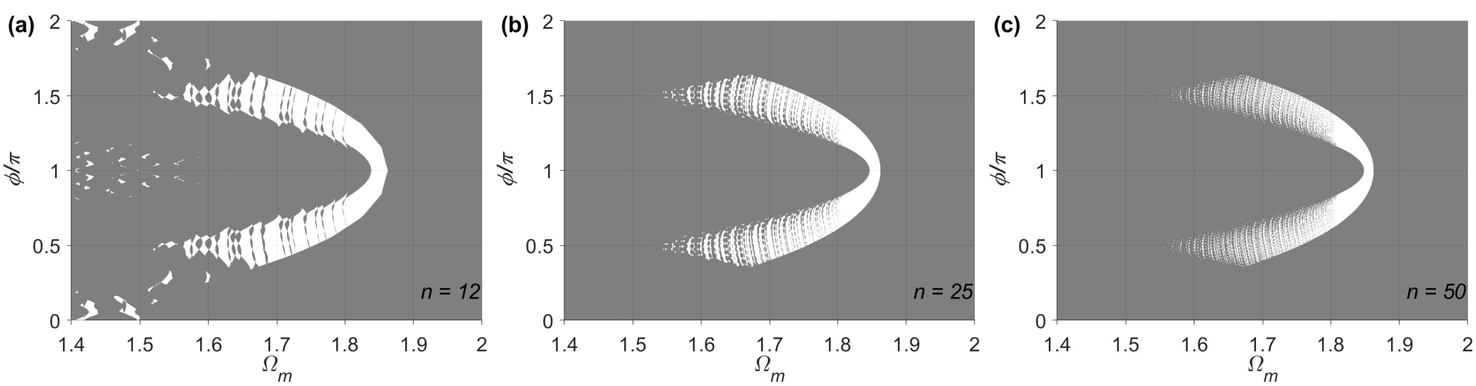

Figure 4.10: Stability diagrams for $K_c = 0.6$ and $K_m = 1$. (a) $n = 12$, (b) $n = 25$ and (c) $n = 50$.

Fig. 4.11 shows the stability diagrams in the (Ω_m, K_m) plane for three long systems with $K_c = 0.6$ and $\Omega_m = 0.2$. For these parameters, all transition curves are confined to the range $0.6 < K_m < 1.5$. In general, the range of modulation amplitudes over which the response remains stable becomes wider as the modulation phase increases from 0 to π. The fragmentation of the small regions of instability continues as n increases, though it remains

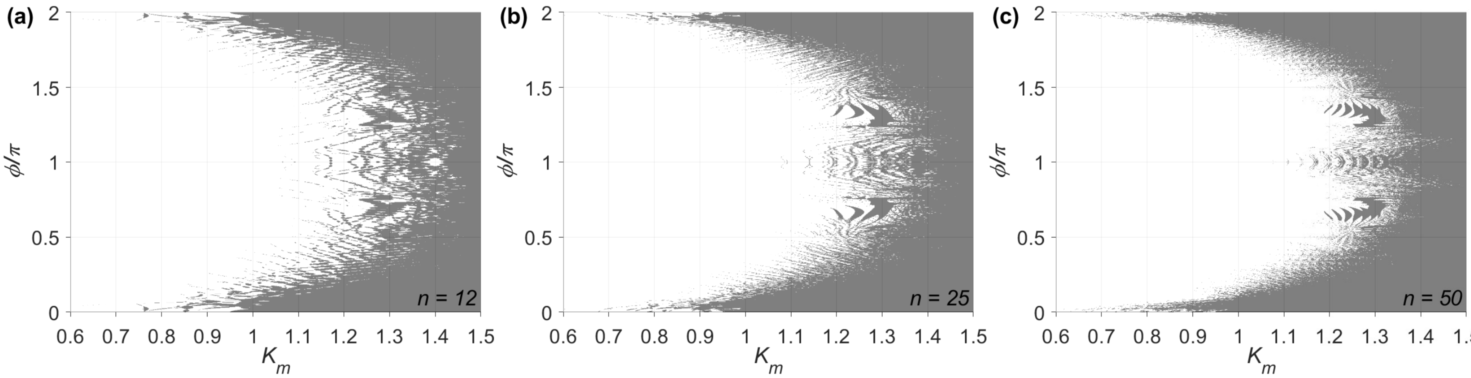

Figure 4.11: Stability diagrams for $K_c = 0.6$ and $\Omega_m = 0.2$. (a) $n = 12$, (b) $n = 25$ and (c) $n = 50$. For all values of ϕ, the response remains stable for $K_m \leq 0.6$ and unstable for $K_m \geq 1.5$.

unclear whether the total area covered by the unstable regions increases or not. These are the same trends that we observed for shorter systems in Fig. 4.8. The investigation fo the fine details of the fragmented transition between stable and unstable regions falls beyond the scope of this work.

4.7. Influence of damping

It is intuitively understood that damping enhances the stability of the response. To demonstrate this effect, Fig. 4.12 shows the stability diagrams for $n = 3$, $K_c = 0.6$ and different damping ratios. The darker grey zones indicate unstable regions corresponding to higher values of ζ. Note that Fig. 4.12(a) is plotted over the range $0 \leq K_m \leq 2$, while Fig. 4.12(c) is plotted over $0 \leq K_m \leq 1$ for better clarity.

As expected, the regions of unstable response become smaller as the damping ratio increases, with many of the smaller regions of instability disappearing; see Fig. 4.12(a). The vertices of the tongues detach from the K_m axis and become rounded, as seen in Fig. 4.12(b). Thus, a minimum modulation amplitude is now required for parametric instability to occur. The transition curves for $\beta > 1$ appear to be influenced by damping to a greater extent than those for $\beta = 1$.

The same trends are observed in the stability diagrams of a longer system ($n = 25$) in Fig. 4.13. In addition, panel (a) shows that the cloudy region of the stability diagrams has almost completely disappeared (become stable) in the damped system. The semi-triangular region of stable response in panel (a) becomes wider and extends to higher values of K_m as ζ increases, with almost all the fragmented unstable regions within it disappearing.

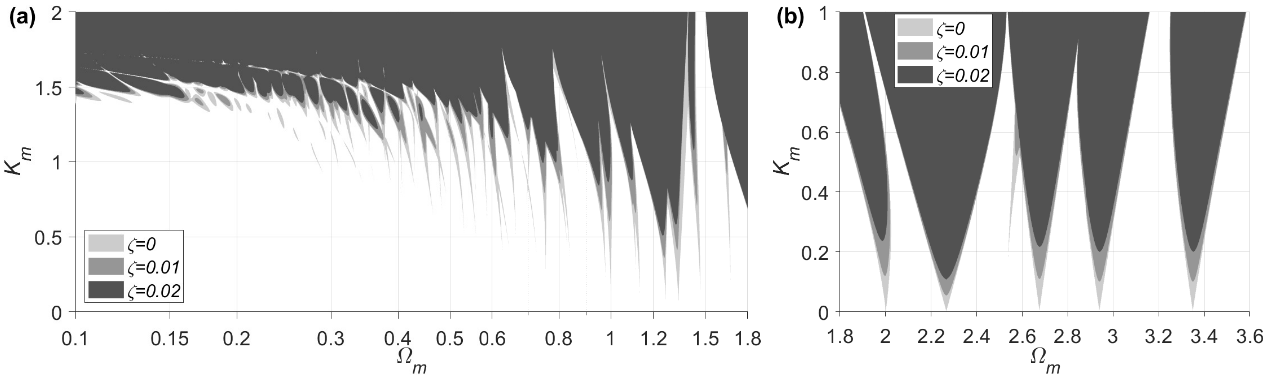

Figure 4.12: Stability diagrams of the modulated systems with $n = 3$, $K_c = 0.6$ and $\phi = 0.5\pi$. (a) $0.1 \leq \Omega_m \leq 1.8$; (b) $1.8 \leq \Omega_m \leq 3.6$. The darker grey zones indicate unstable regions corresponding to higher values of ζ.

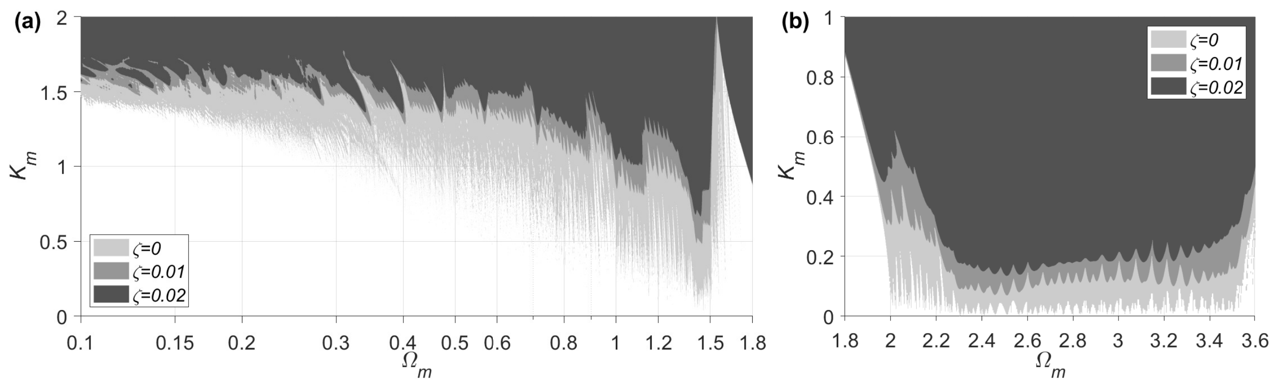

Figure 4.13: Stability diagrams of the modulated systems with $n = 25$, $K_c = 0.6$ and $\phi = 0.5\pi$. (a) $0.1 \leq \Omega_m \leq 1.8$; (b) $1.8 \leq \Omega_m \leq 3.6$. The darker grey zones indicate unstable regions corresponding to higher values of ζ.

As a quantitative indication of the overall influence of damping on parametric instability, we calculate the percentage of the total area of the unstable regions in Figs. 4.12 and 4.13; see Table 4.3. Although some of the stability diagrams use a logarithmic scale for Ω_m, the areas are calculated using a linear scale. The introduction of damping results in a significant decrease in the unstable regions. The influence of damping is greater for $\beta > 1$ than for $\beta = 1$, as previously observed. In general, increasing ζ from 0 to 0.01 results in a greater change in the area than increasing it from 0.01 to 0.02. Moreover, the influence of damping is greater on the longer system. Thus, in damped systems with slow modulations, longer systems tend to provide greater stability compared to shorter ones.

Table 4.3: Percentage of the unstable regions in the stability diagrams in Figs. 4.12 and 4.13.

		$0 \leq K_m \leq 2$ $0.1 \leq \Omega_m \leq 1.8$	$0 \leq K_m \leq 1$ $1.8 \leq \Omega_m \leq 3.6$
	$\zeta = 0$	46%	55%
$n = 3$	$\zeta = 0.01$	41%	53%
	$\zeta = 0.02$	38%	50%
	$\zeta = 0$	65%	91%
$n = 25$	$\zeta = 0.01$	40%	80%
	$\zeta = 0.02$	34%	72%

4.8. Conclusions

We presented a detailed computational investigation of parametric instability in a discrete model of a 1-D spatiotemporally modulated system. We assessed the stability of the response using direct computation based on Floquet theory. We explored the roles of several key parameters on parametric instability such as modulation parameters (modulation phase or wavenumber, amplitude, and frequency), damping and the number of units.

We used perturbation theory to show that unstable modulation frequencies (UMFs) occur at combinations of two natural frequencies of the underlying unmodulated system divided by a natural number, β. UMFs are modulation frequencies at which the response of the undamped system grows exponentially over time. Stability analysis based on Floquet theory confirmed that UMFs with $\beta = 1$ induce parametric instability in the undamped system regardless of how small the modulation amplitude is. In contrast, Floquet theory revealed that UMFs with $\beta \geq 2$ may not always lead to instability, provided that the modulation amplitude is sufficiently small. As the modulation frequency decreases, parametric instability occurs at increasingly higher modulation amplitudes. There are therefore significant regions of stable response within the stability diagram, offering a broad safe range of modulation amplitudes for designing stable modulated systems.

As a function of the modulation phase (wavenumber), the unstable regions are symmetric with response to $\phi = \pi$. At low modulation amplitudes, the unstable regions appear symmetrically about the UMFs with $\beta = 1$. The perturbation analysis accurately predicts the values of modulation phase at which the width of an unstable region is zero (typically occurs multiple times). As the modulation amplitude increases, the unstable regions become wider, are no longer symmetric with respect to the UMFs, and overlap with each other. Overall, the range of modulation amplitudes over which the response remains stable becomes wider as the modulation phase approaches π.

As the number of modulated units increases, the number of UMFs increases and the unstable region nearly covers the entire range of modulation frequencies corresponding to $\beta = 1$; *i.e.* $2 \leq \Omega_m < 2\sqrt{1 + 4K_c}$. A semi-triangular region of stable response also forms in the frequency gap between UMFs with $\beta = 1$ and $\beta = 2$. Typically, the largest value of modulation amplitude at which the response remains stable occurs within this range of modulation frequencies. At lower modulation frequencies ($\beta > 1$), several very small regions of stability appear sporadically within the unstable regions and the transition between unstable and stable regions becomes fragmented, narrow and dense. A main consistent trend within this parameter range is that the onset of instability occurs at higher modulation amplitudes as the modulation frequency decreases.

Damping has an overall stabilizing effect by increasing the threshold of modulation amplitude that leads to parametric instability. This threshold is finite even at UMFs, in contrast to undamped systems. Damping has a stronger influence on stability diagram at lower modulation frequencies ($\beta > 1$) and for longer systems. As a result, a damped system with several modulated units can remain stable at relatively high-amplitude modulations of low frequency.

We hope that our findings on the stability of spatiotemporally modulated systems encourage further stability analyses of modulated systems and inspire future research on systems with high-amplitude modulations.

Appendices

4A. Non-dimensionalization

The equations of motion which govern the system of n modulated units in Fig. 4.1 are:

$$\begin{aligned} m\frac{\mathrm{d}^2 u_1}{\mathrm{d}t^2} + c\frac{\mathrm{d}u_1}{\mathrm{d}t} + k_1 u_1 + k_c\left(u_1 - u_2\right) &= 0, \\ &\vdots \\ m\frac{\mathrm{d}^2 u_p}{\mathrm{d}t^2} + c\frac{\mathrm{d}u_p}{\mathrm{d}t} + k_p u_p + k_c\left(2u_p - u_{p-1} - u_{p+1}\right) &= 0, \\ &\vdots \\ m\frac{\mathrm{d}^2 u_n}{\mathrm{d}t^2} + c\frac{\mathrm{d}u_n}{\mathrm{d}t} + k_n u_n + k_c\left(u_n - u_{n-1}\right) &= 0, \end{aligned} \tag{4A.1}$$

where $k_p(t) = k_{g,DC} + k_{g,AC}\cos(\omega_m t - \phi_p)$ and $\phi_p = (p-1)\phi$ for $p = 1, 2, \cdots, n$. We use $\tau = \omega_0 t$ as the nondimensional time with $\omega_0 = \sqrt{k_{g,DC}/m}$. We define $\zeta = c/(2m\omega_0)$, $\Omega_m = \omega_m/\omega_0$, $\Omega_f = \omega_f/\omega_0$, $K_c = k_c/k_{g,DC}$ and $K_m = k_{g,AC}/k_{g,DC}$. The variable $x_p = u_p/a$ is used as nondimensional displacement where a is a representative length. After substituting these parameters into Eq. (4A.1), we obtain:

$$ma\omega_0^2\ddot{x}_p + 2\zeta ma\omega_0^2\dot{x}_p + ak_{g,DC}x_p\left[1 + K_m\cos\left(\Omega_m\tau - \phi_p\right)\right] + aK_ck_{g,DC}\Delta_p^2 = 0, \qquad (4A.2)$$

where $\ddot{x}_p$ and $\dot{x}_p$ represent $\mathrm{d}^2x_p\,/\,\mathrm{d}^2\tau$ and $\mathrm{d}x_p\,/\,\mathrm{d}\tau$ respectively. The difference terms are defined as $\Delta_1^2 = x_1 - x_2$ and $\Delta_n^2 = x_n - x_{n-1}$ at two ends of the system, and $\Delta_p^2 = 2x_p - x_{p+1} - x_{p-1}$ elsewhere. Dividing the two sides of Eq. (4A.2) by $ak_{g,DC}$ yields Eq. (4.1) in the main text. In this paper, calculations and analysis of the n-DoF modulated system are all based on the nondimensional form of the equations.

4B. Sets of harmonic terms at different frequencies

The sets of harmonic terms in Eq. (4.18) are:

$$\begin{aligned}
\mathcal{T}_1\left[\frac{\Omega_{2,1}}{\Omega_m}\right] &= 2\frac{\Omega_{2,1}}{\Omega_m}\frac{\mathrm{d}A_1}{\mathrm{d}\nu}\sin\frac{\Omega_{2,1}}{\Omega_m}\mu - 2\frac{\Omega_{2,1}}{\Omega_m}\frac{\mathrm{d}B_1}{\mathrm{d}\nu}\cos\frac{\Omega_{2,1}}{\Omega_m}\mu,\\
\mathcal{T}_1\left[\beta + \frac{\Omega_{2,1}}{\Omega_m}\right] &= \left[-\frac{(1+\cos\phi)\,A_1}{4\Omega_m^2} + \frac{\sin\phi B_1}{4\Omega_m^2}\right]\cos\left(\beta + \frac{\Omega_{2,1}}{\Omega_m}\right)\mu\\
&\quad - \left[\frac{(1+\cos\phi)\,B_1}{4\Omega_m^2} + \frac{\sin\phi A_1}{4\Omega_m^2}\right]\sin\left(\beta + \frac{\Omega_{2,1}}{\Omega_m}\right)\mu,\\
\mathcal{T}_1\left[\beta - \frac{\Omega_{2,1}}{\Omega_m}\right] &= -\left[\frac{(1+\cos\phi)\,A_1}{4\Omega_m^2} + \frac{\sin\phi B_1}{4\Omega_m^2}\right]\cos\left(\beta - \frac{\Omega_{2,1}}{\Omega_m}\right)\mu\\
&\quad + \left[\frac{(1+\cos\phi)\,B_1}{4\Omega_m^2} - \frac{\sin\phi A_1}{4\Omega_m^2}\right]\sin\left(\beta - \frac{\Omega_{2,1}}{\Omega_m}\right)\mu,\\
\mathcal{T}_1\left[\beta + \frac{\Omega_{2,2}}{\Omega_m}\right] &= -\left[\frac{(1-\cos\phi)\,A_2}{4\Omega_m^2} + \frac{\sin\phi B_2}{4\Omega_m^2}\right]\cos\left(\beta + \frac{\Omega_{2,2}}{\Omega_m}\right)\mu\\
&\quad + \left[-\frac{(1-\cos\phi)\,B_2}{4\Omega_m^2} + \frac{\sin\phi A_2}{4\Omega_m^2}\right]\sin\left(\beta + \frac{\Omega_{2,2}}{\Omega_m}\right)\mu,\\
\mathcal{T}_1\left[\beta - \frac{\Omega_{2,2}}{\Omega_m}\right] &= -\left[\frac{(1-\cos\phi)\,A_2}{4\Omega_m^2} - \frac{\sin\phi B_2}{4\Omega_m^2}\right]\cos\left(\beta - \frac{\Omega_{2,2}}{\Omega_m}\right)\mu\\
&\quad + \left[\frac{(1-\cos\phi)\,B_2}{4\Omega_m^2} + \frac{\sin\phi A_2}{4\Omega_m^2}\right]\sin\left(\beta - \frac{\Omega_{2,2}}{\Omega_m}\right)\mu,
\end{aligned}$$

and

$$
\begin{aligned}
\mathcal{T}_2\left[\frac{\Omega_{2,2}}{\Omega_m}\right] &= 2\frac{\Omega_{2,2}}{\Omega_m}\frac{\mathrm{d}A_2}{\mathrm{d}\nu}\sin\frac{\Omega_{2,2}}{\Omega_m}\mu - 2\frac{\Omega_{2,2}}{\Omega_m}\frac{\mathrm{d}B_2}{\mathrm{d}\nu}\cos\frac{\Omega_{2,2}}{\Omega_m}\mu, \\
\mathcal{T}_2\left[\beta+\frac{\Omega_{2,1}}{\Omega_m}\right] &= \left[\frac{(-1+\cos\phi)\,A_1}{4\Omega_m^2} - \frac{\sin\phi B_1}{4\Omega_m^2}\right]\cos\left(\beta+\frac{\Omega_{2,1}}{\Omega_m}\right)\mu \\
&+ \left[\frac{(-1+\cos\phi)\,B_1}{4\Omega_m^2} + \frac{\sin\phi A_1}{4\Omega_m^2}\right]\sin\left(\beta+\frac{\Omega_{2,1}}{\Omega_m}\right)\mu, \\
\mathcal{T}_2\left[\beta-\frac{\Omega_{2,1}}{\Omega_m}\right] &= \left[\frac{(-1+\cos\phi)\,A_1}{4\Omega_m^2} + \frac{\sin\phi B_1}{4\Omega_m^2}\right]\cos\left(\beta-\frac{\Omega_{2,1}}{\Omega_m}\right)\mu \\
&+ \left[-\frac{(-1+\cos\phi)\,B_1}{4\Omega_m^2} + \frac{\sin\phi A_1}{4\Omega_m^2}\right]\sin\left(\beta-\frac{\Omega_{2,1}}{\Omega_m}\right)\mu, \\
\mathcal{T}_2\left[\beta+\frac{\Omega_{2,2}}{\Omega_m}\right] &= \left[\frac{(-1-\cos\phi)\,A_2}{4\Omega_m^2} + \frac{\sin\phi B_2}{4\Omega_m^2}\right]\cos\left(\beta+\frac{\Omega_{2,2}}{\Omega_m}\right)\mu \\
&+ \left[\frac{(-1-\cos\phi)\,B_2}{4\Omega_m^2} - \frac{\sin\phi A_2}{4\Omega_m^2}\right]\sin\left(\beta+\frac{\Omega_{2,2}}{\Omega_m}\right)\mu, \\
\mathcal{T}_2\left[\beta-\frac{\Omega_{2,2}}{\Omega_m}\right] &= \left[\frac{(-1-\cos\phi)\,A_2}{4\Omega_m^2} - \frac{\sin\phi B_2}{4\Omega_m^2}\right]\cos\left(\beta-\frac{\Omega_{2,2}}{\Omega_m}\right)\mu \\
&+ \left[\frac{(1+\cos\phi)\,B_2}{4\Omega_m^2} + \frac{\sin\phi A_2}{4\Omega_m^2}\right]\sin\left(\beta-\frac{\Omega_{2,2}}{\Omega_m}\right)\mu,
\end{aligned}
$$

Chapter 5

Conclusions and Recommendations

5.1. Conclusions

This thesis provided a detailed investigation of the steady-state vibration transmission characteristics of spatiotemporally modulated materials. The primary focus was on the following three aspects:

- Developing a theoretical framework for predicting the steady-state output of spatiotemporally modulated systems in response to external harmonic drive, specifically valid in the presence of strong modulation amplitude and for arbitrary number of units.
- Investigating the contribution of transmitted phase to nonreciprocity, and the possibility of realizing transmission regimes that are characterized by a nonreciprocal phase shift.
- Investigating the phenomenon of parametric stability in spatiotemporally modulated systems, with a focus on understanding the influence of modulation phase (wavenumber) and the number of units.

Firstly, we studied nonreciprocal vibration transmission in a spatiotemporally modulated system with two units. The focus on modulated systems with two units was motivated by the system having well separated modes. This enabled us to elucidate the roles of the primary and side-band resonances of the system, and their overlaps, in breaking reciprocity. Temporal modulation was introduced as harmonic variations in the grounding stiffness of each oscillator, while the phase difference between the two modulations (ϕ) served as the spatial modulation. The phase difference broken the mirror symmetry of the system, which is essential for breaking the reciprocity invariance. Using the averaging method, we developed an analytical framework to predict the steady-state quasi-periodic response of the system under harmonic external excitation, for both weak and strong modulation regimes.

For weakly modulated systems, we demonstrated that a single pair of sideband resonances is able to accurately capture the system's response. The harmonic components of the response (both primary and sideband) contribute differently to the reciprocity bias, with stronger nonreciprocity observed when a primary resonance overlaps with a sideband resonance compared to overlaps between two sideband resonances. In systems with stronger modulations, the frequency spectrum of the response becomes richer and the reciprocity bias increases significantly due to the greater energy introduced into the system. Higher modulation amplitudes also influence the resonance frequencies, making them dependent on both the modulation phase and amplitude.

We found that in short systems, even though the response is nonreciprocal when $\phi \neq 0$, the transmitted energies in the opposite directions are comparable. This indicated that the difference in the transmitted phase was the primary contributor to nonreciprocity. The amplitude bias can be amplified by increasing the number of modulated units, ultimately leading to unidirectional vibration transmission in sufficiently long modulated systems.

Secondly, we explored the steady-state response regimes characterized by nonreciprocal phase shifts: equal transmitted amplitudes (energies) but different phases. The only contributor to nonreciprocity was therefore the nonreciprocal phase shift, the difference between the transmitted phases in the opposite directions. Due to the non-periodic nature of the steady-state response, a methodology was developed based on the envelope of the output displacements to identify system parameters that exhibit nonreciprocal phase shifts. While our primary focus was on weakly modulated systems with a small number of units, we also demonstrated a special case of nonreciprocal phase shifts in systems of arbitrary length and modulation strength. Additionally, we developed a formulation that ensures identical transmitted waveforms in opposite directions, enabling us to identify a special case of near-reciprocal vibration transmission.

Finally, we conducted a comprehensive analysis of parametric instability for a 1-D spatiotemporally modulated system. Stability was determined using direct computations based on Floquet theory. We investigated the effects of several critical parameters on parametric instability, including all three modulation parameters (amplitude, frequency and phase shift), damping, and the number of modulated units.

Using perturbation theory, we obtained that unstable modulation frequencies (UMFs) are combinations of two natural frequencies of the corresponding unmodulated system, divided by a natural number, β. UMFs with $\beta = 1$ represent the modulation frequencies at which the amplitude of response of an undamped system exponentially increases over time, regardless of how small the modulation amplitudes are. At lower modulation amplitudes, unstable regions appear symmetrically about the UMFs with $\beta = 1$. As the modulation amplitude increases, the unstable regions widen, lose symmetry about the UMFs, and begin to overlap. Conversely, UMFs with $\beta \geq 2$ do not necessarily cause instability if the modulation amplitudes are low enough. In general, as the modulation frequency decreases, parametric instability requires higher modulation amplitudes. Thus, substantial regions within the stability diagram remain stable, providing a large safe range of modulation amplitudes for designing stable systems with slow modulations.

With an increasing number of modulated units, the number of UMFs increases significantly, and nearly the entire frequency range corresponding to $\beta = 1$ becomes unstable. A semi-triangular region of stable response also emerges between the frequency gaps from UMFs with $\beta = 1$ to $\beta = 2$. Typically, the highest modulation amplitude that maintains stability is found within this frequency range. At lower modulation frequencies ($\beta > 1$), transitions between unstable and stable areas become fragmented, narrow, and dense. A consistent observation is that the occurrence of instability at higher modulation amplitudes occurs as the modulation frequency decreases.

Stability can be improved by increasing the damping ratio, especially at lower modulation frequencies. Notably, in the low modulation frequency range, increased damping has a stronger effect to enlarge stable regions for longer systems. Consequently, a longer damped system can exhibit greater tolerance of modulation amplitudes than a shorter system.

In summary, the main contributions of this thesis to the current research field are as follows:

1. Introduction of a theoretical framework to predict the steady-state response of discrete modulated systems subjected to external harmonic forces that is valid for strongly modulated systems of arbitrary number of units.

2. Detailed investigation of the role of transmitted phase in nonreciprocity, including the introduction of response regimes in which phase is the only contributor to nonreciprocity.

3. Systematic analysis of the influence of various system parameters, particularly modulation phase and system length, on parametric stability.

5.2. Recommendations for future work

The present research provides gateways for further exploration on nonreciprocal vibration transmission in discrete periodic systems with spatiotemporal modulations. Potential directions for future investigations are outlined below:

1. The current analytical framework enables the determination of steady-state transmitted vibrations for a given set of system parameters and external excitation. However, the inverse problem — designing system parameters and external excitations to achieve a desired response waveform or envelope — is rarely unexplored. Developing novel methodologies to address this challenge will open new avenues in system design and control.

2. When the system operates beyond the small-amplitude regime, nonlinear effects become significant. Additionally, nonlinear forces can induce nonreciprocity in systems that do not possess mirror symmetry. Investigating the interplay between nonlinearity and spatiotemporal modulation offers a promising direction for advancing our understanding of nonreciprocal dynamics and exploring potentially new applications.

3. Our analysis of nonreciprocal phase shifts was limited to response regimes in which the output displacement has a harmonic envelope. Long modulated systems and systems with high-amplitude modulations fall beyond the reach of this analysis. Developing new methodologies to address this limitation will be a critical step toward extending the concept of nonreciprocal phase shifts to strongly or long modulated system.

4. This study is entirely theoretical, emphasizing the need for experimental validation. Experimental demonstrations of these effects will provide valuable insights for designing innovative devices with potential industrial applications.

References

1. Achenbach, J. D. *Reciprocity in elastodynamics* (Cambridge University Press, 2003).
2. Andrieux, S., Abda, A. B. & Bui, H. D. Reciprocity principle and crack identification. *Inverse problems* **15,** 59 (1999).
3. Ten Wolde, T. Reciprocity measurements in acoustical and mechano-acoustical systems. Review of theory and applications. *Acta Acustica united with Acustica* **96,** 1–13 (2010).
4. Nassar, H. *et al.* Nonreciprocity in acoustic and elastic materials. *Nature Reviews Materials* **5,** 667–685 (2020).
5. Wang, Y., Wang, Y., Wu, B., Chen, W. & Wang, Y. Tunable and active phononic crystals and metamaterials. *Applied Mechanics Reviews* **72,** 040801 (2020).
6. Lurie, K. A. *An introduction to the mathematical theory of dynamic materials* (Springer, 2017).
7. Trainiti, G. & Ruzzene, M. Non-reciprocal elastic wave propagation in spatiotemporal periodic structures. *New Journal of Physics* **18,** 083047 (2016).
8. Ansari, M., Attarzadeh, M., Nouh, M. & Karami, M. A. Application of magnetoelastic materials in spatiotemporally modulated phononic crystals for nonreciprocal wave propagation. *Smart Materials and Structures* **27,** 015030 (2017).
9. Goldsberry, B. M., Wallen, S. P. & Haberman, M. R. Nonreciprocal vibrations of finite elastic structures with spatiotemporally modulated material properties. *Physical Review B* **102,** 014312 (2020).
10. Yi, K., Karkar, S. & Collet, M. One-way energy insulation using time-space modulated structures. *Journal of Sound and Vibration* **429,** 162–175 (2018).
11. Attarzadeh, M. & Nouh, M. Elastic wave propagation in moving phononic crystals and correlations with stationary spatiotemporally modulated systems. *AIP Advances* **8** (2018).
12. Goldsberry, B. M., Wallen, S. P. & Haberman, M. R. Non-reciprocity in discrete and continuous lattice systems via mechanical modulation. *Proceedings of the* 23^{rd} *International Congress on Acoustics* (2019).
13. Al Ba'ba'a, H. Brillouin-zone definition in non-reciprocal Willis monatomic lattices. *JASA Express Letters* **3,** 120001 (2023).
14. Li, J., Shen, C., Zhu, X., Xie, Y. & Cummer, S. A. Nonreciprocal sound propagation in space-time modulated media. *Physical Review B* **99,** 144311 (2019).

15. Nassar, H., Xu, X., Norris, A. & Huang, G. Modulated phononic crystals: Non-reciprocal wave propagation and Willis materials. *Journal of the Mechanics and Physics of Solids* **101,** 10–29 (2017).

16. Riva, E., Marconi, J., Cazzulani, G. & Braghin, F. Generalized plane wave expansion method for non-reciprocal discretely modulated waveguides. *Journal of Sound and Vibration* **449,** 172–181 (2019).

17. Moghaddaszadeh, M., Attarzadeh, M., Aref, A. & Nouh, M. Complex spatiotemporal modulations and non-Hermitian degeneracies in PT-symmetric phononic materials. *Physical Review Applied* **18,** 044013 (2022).

18. Kargozarfard, M. H., Sedighi, H. M., Yaghootian, A. & Valipour, A. An improved method for unidirectional mechanical wave propagation in a metamaterial beam. *Applied Physics A: Materials Science and Processing* **129** (2023).

19. Zhu, X. & Shen, C. An acoustic metamaterial with space-time modulated density. *The Journal of the Acoustical Society of America* **156,** 3984–3991 (2024).

20. Banerjee, A. & Bera, K. K. Emergence of non-reciprocity in metabeam exploiting piezoelectric sensing and actuation. *International Journal of Mechanical Sciences* **236,** 107765 (2022).

21. Nassar, H., Chen, H., Norris, A. & Huang, G. Non-reciprocal flexural wave propagation in a modulated metabeam. *Extreme Mechanics Letters* **15,** 97–102 (2017).

22. Pu, X., Marzani, A. & Palermo, A. A multiple scattering formulation for elastic wave propagation in space–time modulated metamaterials. *Journal of Sound and Vibration* **573,** 118199 (2024).

23. Celli, P. & Palermo, A. Time-modulated inerters as building blocks for nonreciprocal mechanical devices. *Journal of Sound and Vibration* **572,** 118178 (2024).

24. Swinteck, N. *et al.* Bulk elastic waves with unidirectional backscattering-immune topological states in a time-dependent superlattice. *Journal of Applied Physics* **118** (2015).

25. Nassar, H., Chen, H., Norris, A. & Huang, G. Quantization of band tilting in modulated phononic crystals. *Physical Review B* **97,** 014305 (2018).

26. Huang, J. & Zhou, X. A time-varying mass metamaterial for non-reciprocal wave propagation. *International Journal of Solids and Structures* **164,** 25–36 (2019).

27. Wen, Z., Yuan, J., Huang, Y. & Zhou, X. Underwater acoustic non-reciprocal manipulation based on dynamic-modulation structures. *Journal of Applied Mechanics* **91** (2024).

28. Huang, J. & Zhou, X. Non-reciprocal metamaterials with simultaneously time-varying stiffness and mass. *Journal of Applied Mechanics* **87,** 071003 (2020).

29. Nassar, H., Chen, H., Norris, A., Haberman, M. & Huang, G. Non-reciprocal wave propagation in modulated elastic metamaterials. *Proceedings of the Royal Society A: Mathematical, Physical and Engineering Sciences* **473,** 20170188 (2017).

30. Attarzadeh, M., Al Ba'ba'a, H. & Nouh, M. On the wave dispersion and non-reciprocal power flow in space-time traveling acoustic metamaterials. *Applied Acoustics* **133,** 210–214 (2018).

31. Karličić, D. *et al.* Non-reciprocal wave propagation in time-modulated elastic lattices with inerters. *Applied Mathematical Modelling* **117,** 316–335 (2023).

32. Wallen, S. & Haberman, M. Nonreciprocal wave phenomena in spring-mass chains with effective stiffness modulation induced by geometric nonlinearity. *Physical Review E* **99,** 013001 (2019).

33. Slater, J. C. Interaction of waves in crystals. *Reviews of modern physics* **30,** 197–222 (1958).

34. Cassedy, E. S. & Oliner, A. A. Dispersion relations in time-space periodic media: Part I—Stable interactions. *Proceedings of the IEEE* **51,** 1342–1359 (1963).

35. Cassedy, E. S. Dispersion relations in time-space periodic media part II—Unstable interactions. *Proceedings of the IEEE* **55,** 1154–1168 (1967).

36. Vila, J., Kumar Pal, R., Ruzzene, M. & Trainiti, G. A Bloch-based procedure for dispersion analysis of lattices with periodic time-varying properties. *Journal of Sound and Vibration* **406,** 363–377 (2017).

37. Palermo, A., Celli, P., Yousefzadeh, B., Daraio, C. & Marzani, A. Surface wave non-reciprocity via time-modulated metamaterials. *Journal of the Mechanics and Physics of Solids* **145,** 104181 (2020).

38. Whittaker, E. T. On the general solution of Mathieu's equation. *Proceedings of the Edinburgh Mathematical Society* **32,** 75–80 (1913).

39. Kargozarfard, M. H., Sedighi, H. M., Yaghootian, A. & Valipour, A. Nonreciprocal wave propagation in a time-space modulated metasurface using the modified plane wave expansion method. *Thin-Walled Structures* **195,** 111335 (2024).

40. Trainiti, G. *et al.* Time-periodic stiffness modulation in elastic metamaterials for selective wave filtering: theory and experiment. *Physical Review Letters* **122,** 124301 (2019).

41. Tessier Brothelande, S. *et al.* Experimental evidence of nonreciprocal propagation in space-time modulated piezoelectric phononic crystals. *Applied Physics Letters* **123** (2023).

42. Chen, Y. *et al.* Nonreciprocal wave propagation in a continuum-based metamaterial with space-time modulated resonators. *Physical Review Applied* **11,** 064052 (2019).

43. Wang, Y. *et al.* Observation of nonreciprocal wave propagation in a dynamic phononic lattice. *Physical Review Letters* **121,** 194301 (2018).

44. Attarzadeh, M., Callanan, J. & Nouh, M. Experimental observation of nonreciprocal waves in a resonant metamaterial beam. *Physical Review Applied* **13,** 021001 (2020).

45. Marconi, J. *et al.* Experimental observation of nonreciprocal band gaps in a space-time-modulated beam using a shunted piezoelectric array. *Physical Review Applied* **13,** 031001 (2020).

46. Alshaqaq, M., Sugino, C. & Erturk, A. Digital programming of reciprocity breaking in resonant piezoelectric metamaterials. *Physical Review Research* **5,** 043003 (2023).

47. Thomes, R. L., Beli, D., Sugino, C., Erturk, A. & Junior, C. D. M. Programmable moving defect for spatiotemporal wave localization in piezoelectric metamaterials. *Physical Review Applied* **19,** 064031 (2023).

48. Croënne, C., Vasseur, J. O., Bou Matar, O., Hladky-Hennion, A.-C. & Dubus, B. Non-reciprocal behavior of one-dimensional piezoelectric structures with space-time modulated electrical boundary conditions. *Journal of Applied Physics* **126** (2019).

49. Wan, S. *et al.* Low-frequency nonreciprocal flexural wave propagation via compact cascaded time-modulated resonators. *Applied Physics Letters* **120** (2022).

50. Kim, B. L., Chong, C., Hajarolasvadi, S., Wang, Y. & Daraio, C. Dynamics of time-modulated, nonlinear phononic lattices. *Physical Review E* **107,** 034211 (2023).

51. Yousefzadeh, B. Computation of nonreciprocal dynamics in nonlinear materials. *Journal of Computational Dynamics* **9,** 451–464 (2022).

52. Kogani, A. & Yousefzadeh, B. Nonreciprocal phase shifts in a nonlinear periodic waveguide. *Nonlinear Dynamics* **112,** 13379–13391 (2024).

53. Caloz, C. *et al.* Electromagnetic nonreciprocity. *Physical Review Applied* **10,** 047001 (2018).

54. Mizumoto, T. & Naito, Y. Nonreciprocal propagation characteristics of YIG thin film. *IEEE Transactions on Microwave Theory and Techniques* **30,** 922–925 (1982).

55. Marcuse, D. Influence of position of magnetooptic layer on differential phase shift of slab waveguide. *IEEE journal of quantum electronics* **23,** 1268–1272 (1987).

56. Dumelow, T., Camley, R., Abraha, K. & Tilley, D. Nonreciprocal phase behavior in reflection of electromagnetic waves from magnetic materials. *Physical Review B (Condensed Matter)* **58,** 897–908 (1998).

57. Wu, J. & Yousefzadeh, B. On vibration transmission reciprocity in modulated materials. *Proceedings of the Canadian Society for Mechanical Engineering International Congress 2022* (2022).

58. Nayfeh, A. H. & Mook, D. T. *Nonlinear Oscillations* (John Wiley & Sons, 1979).

59. Deng, J. Numerical simulation of stability and responses of dynamic systems under parametric excitation. *Applied Mathematical Modelling* **119,** 648–676 (2023).

60. Darabi, A. *et al.* Broadband passive nonlinear acoustic diode. *Physical Review B* **99,** 214305 (21 2019).

61. Fronk, M. D. *et al.* Acoustic non-reciprocity in lattices with nonlinearity, internal hierarchy and asymmetry: Computational study. *Journal of Vibration and Acoustics* **141,** 051011 (2019).

62. Liang, B., Yuan, B. & Cheng, J.-C. Acoustic diode: Rectification of acoustic energy flux in one-dimensional systems. *Physical Review Letters* **103,** 104301 (2009).

63. Lepri, S. & Casati, G. Asymmetric Wave Propagation in Nonlinear Systems. *Physical Review Letters* **106,** 164101 (2011).

64. Bou Matar, O. *et al.* Band gap tunability of magneto-elastic phononic crystal. *Journal of Applied Physics* **111** (2012).

65. Karličić, D. *et al.* Non-reciprocal wave propagation in time-modulated elastic lattices with inerters. *Applied Mathematical Modelling* **117,** 316–335 (2023).

66. Chen, Y., Zhu, R., Barnhart, M. & Huang, G. Enhanced flexural wave sensing by adaptive gradient-index metamaterials. *Scientific Reports,* 35048 (2016).

67. Sugino, C., Ruzzene, M. & Erturk, A. Nonreciprocal piezoelectric metamaterial framework and circuit strategies. *Physical Review B* **102,** 014304 (2020).

68. Kang, J. & Haberman, M. R. Experimental demonstration of a spatiotemporally modulated sound diffusing metasurfaces. *The Journal of the Acoustical Society of America* **153,** A120–A120 (2023).

69. Goldsberry, B. M., Wallen, S. P. & Haberman, M. R. Non-reciprocal wave propagation in mechanically-modulated continuous elastic metamaterials. *Journal of the Acoustical Society of America* **146,** 782–788 (2019).

70. Rosa, M. I., Leamy, M. J. & Ruzzene, M. Amplitude-dependent edge states and discrete breathers in nonlinear modulated phononic lattices. *New Journal of Physics* **25,** 103053 (2023).

71. Rhoads, J. F., Miller, N. J., Shaw, S. W. & Feeny, B. F. Mechanical domain parametric amplification. *Journal of Vibration and Acoustics* **130,** 061006 (2008).

72. Wu, J. & Yousefzadeh, B. Numerical analysis of phase nonreciprocity in a linear spatiotemporally modulated system. *Proceedings of the International Design Engineering Technical Conferences 2023,* V012T12A001 (2023).

73. Kovacic, I., Rand, R. & Sah, S. M. Mathieu's equation and its generalizations: Overview of stability charts and their features. *Applied Mechanics Reviews* **70** (2018).

74. Wu, J. & Yousefzadeh, B. Nonreciprocal phase shifts in spatiotemporally modulated systems. *arXiv:2411.18734* (2024).

75. Wu, J. & Yousefzadeh, B. Computation of response envelopes in a lattice material with spatiotemporal modulations. *Proceedings of the Canadian Society for Mechanical Engineering International Congress 2023* (2023).

76. Newland, D. E. *Mechanical Vibration Analysis and Computation* (Courier Corporation, 2013).

77. Ewins, D. J. *Modal testing: Theory, practice and application* (John Wiley & Sons, 2009).

78. Doebling, S. W., Peterson, L. D. & Alvin, K. F. Estimation of reciprocal residual flexibility from experimental modal data. *AIAA journal* **34,** 1678–1685 (1996).

79. Fahy, F. J. The vibro-acoustic reciprocity principle and applications to noise control. *Acta Acustica united with Acustica* **81,** 544–558 (1995).

80. Bandaru, P. *Non-Reciprocal Materials and Systems: An Engineering Approach to the Control of Light, Sound, and Heat* (Elsevier, 2024).

81. Croënne, C., Vasseur, J. O., Bou Matar, O., Hladky-Hennion, A.-C. & Dubus, B. Non-reciprocal behavior of one-dimensional piezoelectric structures with space-time modulated electrical boundary conditions. *Journal of Applied Physics* **126** (2019).

82. Dötsch, H. *et al.* Applications of magneto-optical waveguides in integrated optics: review. *Journal of the Optical Society of America B* **22,** 240–253 (2005).

83. Remer, L., Mohler, E., Grill, W. & Lüthi, B. Nonreciprocity in the optical reflection of magnetoplasmas. *Physical Review B* **30,** 3277 (1984).

84. Taravati, S. & Eleftheriades, G. V. Magnet-Free Nonreciprocal Phase-Shifter Based on Time Modulation. *arXiv preprint arXiv:2210.13243* (2022).

85. Palomba, M., Palombini, D., Colangeli, S., Ciccognani, W. & Limiti, E. Broadband nonreciprocal phase shifter design technique. *IEEE Transactions on Microwave Theory and Techniques* **66,** 1964–1972 (2018).

86. Karimian, R., Taravati, S., Ardakani, M. D., Ahmadi, S. & Zaghloul, M. E. Nonreciprocal-beam phased-array antennas based on transistor-loaded phase shifters. *IEEE Transactions on Antennas and Propagation* **69,** 7572–7581 (2021).

87. Dutta, P., Kumar, G. A. & Ram, G. Numerical design of non-reciprocal bandpass filters with the aid of 3D coupling matrix for 5G bands. *IEEE Transactions on Circuits and Systems II: Express Briefs* **69,** 3334–3338 (2022).

88. Zang, J., Alvarez-Melcon, A. & Gomez-Diaz, J. Nonreciprocal phased-array antennas. *Physical review applied* **12,** 054008 (2019).

89. Kord, A., Sounas, D. L. & Alu, A. Microwave nonreciprocity. *Proceedings of the IEEE* **108,** 1728–1758 (2020).

90. Wu, J. & Yousefzadeh, B. Linear nonreciprocal dynamics of coupled modulated systems. *arXiv:2410.08533* (2024).

91. Yang, F. *et al.* Mechanically Modulated Sideband and Squeezing Effects of Membrane Resonators. *Physical Review Letters* **127** (2021).

92. Giraldo, A. & Yousefzadeh, B. Restoring the reciprocity invariance in nonlinear systems with broken mirror symmetry. *Extreme Mechanics Letters* **61,** 102008 (2023).

93. Haykin, S. S. & Moher, M. *Communication Systems* 5th ed. (Wiley, 2009).

94. Hasan, M. A., Calderin, L., Lucas, P., Runge, K. & Deymier, P. A. Geometric phase invariance in spatiotemporal modulated elastic system. *Journal of Sound and Vibration* **459,** 114843 (2019).

95. Champneys, A. in *Mathematics of Complexity and Dynamical Systems* (ed Meyers, R. A.) 183–204 (Springer, New York, 2011).

96. Curry, S. M. How children swing. *American Journal of Physics* **44,** 924–926 (1976).

97. Brimacombe, C., Corless, R. M. & Zamir, M. Computation and Applications of Mathieu Functions: A Historical Perspective. *SIAM Review* **63,** 653–720 (2021).

98. Mathieu, É. Mémoire sur le mouvement vibratoire d'une membrane de forme elliptique. *Journal de mathématiques pures et appliquées* **13,** 137–203 (1868).

99. Rayleigh, J. W. S. On maintained vibrations. *The London, Edinburgh, and Dublin Philosophical Magazine and Journal of Science* **15,** 229–235 (1883).

100. Moran, K., Burgner, C., Shaw, S. & Turner, K. A review of parametric resonance in microelectromechanical systems. *Nonlinear theory and its applications, IEICE* **4,** 198–224 (2013).

101. De Felice, A. & Sorrentino, S. Effects of anisotropic supports on the stability of parametrically excited slender rotors. English. *Nonlinear Dynamics,* 793–813 (2022).

102. De Felice, A. & Sorrentino, S. Damping and gyroscopic effects on the stability of parametrically excited continuous rotor systems. *Nonlinear Dynamics* **103,** 3529–3555 (2021).

103. Acar, G. D., Acar, M. A. & Feeny, B. F. Parametric resonances of a three-blade-rotor system with reference to wind turbines. *Journal of Vibration and Acoustics* **142,** 021013 (2020).

104. Yao, Z., Mei, D. & Chen, Z. Chatter suppression by parametric excitation: Model and experiments. *Journal of Sound and Vibration* **330,** 2995–3005 (2011).

105. Turkes, E., Orak, S., Neeli, S., Sahin, M. & Selvi, S. Modelling of dynamic cutting force coefficients and chatter stability dependent on shear angle oscillation. *International Journal of Advanced Manufacturing Technology* **91,** 679–686 (2017).

106. Stepan, G. & Insperger, T. Stability of time-periodic and delayed systems - a route to act-and-wait control. *Annual Reviews in Control* **30,** 159–168 (2006).

107. Nassar, H., Norris, A. N. & Huang, G. in *Acoustic Metamaterials: Absorption, Cloaking, Imaging, Time-Modulated Media, and Topological Crystals* 505–533 (Springer, 2024).

108. Jin, Y. *et al.* Exceptional points in time-varying oscillators with enhanced sensing sensitivity. *Physical Review Applied* **22,** 034026 (2024).

109. Cesari, L. *Asymptotic behavior and stability problems in ordinary differential equations* 2nd ed. (Academic Press Inc., 1963).

110. Hsu, C. S. On the Parametric Excitation of a Dynamic System Having Multiple Degrees of Freedom. *Journal of Applied Mechanics* **30,** 367–372 (1963).

111. Ince, E. L. Researches into the Characteristic Numbers of the Mathieu Equation. *Proceedings of the Royal Society of Edinburgh* **46,** 20–29 (1927).

112. Barakat, A. A., Weig, E. M. & Hagedorn, P. Non-trivial solutions and their stability in a two-degree-of-freedom Mathieu–Duffing system. *Nonlinear Dynamics* **111,** 22119–22136 (2023).

113. Ramirez-Barrios, M., Collado, J. & Dohnal, F. Stability of periodic Hamiltonian systems with equal dissipation. *Nonlinear Dynamics* (2024).

114. Chong, C., Kim, B., Wallace, E. & Daraio, C. Modulation instability and wavenumber bandgap breathers in a time layered phononic lattice. *Physical Review Research* **6,** 023045 (2024).

115. Floquet, G. *Sur les équations différentielles linéaires à coefficients périodiques* in *Annales scientifiques de l'École normale supérieure* **12** (1883), 47–88.

116. Rayleigh (Strutt), J. W. On the maintenance of vibrations by forces of double frequency, and on the propagation of waves through a medium endowed with a periodic structure. *The London, Edinburgh, and Dublin Philosophical Magazine and Journal of Science* **24,** 145–159 (1887).

117. Sinha, S. C. & Wu, D.-H. An efficient computational scheme for the analysis of periodic systems. *Journal of Sound and Vibration* **151,** 91–117 (1991).

118. Insperger, T. & Stépán, G. Stability chart for the delayed Mathieu equation. *Proceedings of the Royal Society of London. Series A* **458,** 1989–1998 (2002).

119. Gill, S. A process for the step-by-step integration of differential equations in an automatic digital computing machine. *Cambridge Philosophical Society* **47,** 96–108 (1951).

120. Carnahan, B., Luther, H. A., Wilkes, J. O., *et al. Applied numerical methods* (Wiley New York, 1969).

Appendices

A. Computation of response envelopes in a lattice material with spatiotemporal modulations

A.1. Introduction

Reciprocity invariance is a property of regular materials with constant density and elastic modulus, functioning in the linear operating regime. When the reciprocity invariance holds, the wave propagation between two arbitrary points in the material remains unchanged after interchanging the locations of the vibration source and receiver in a material. There exist many established applications of the principle of reciprocity, for instance, calibration of hydrophones and crack identification [1-2]. Despite its usefulness, this invariance is accompanied by limitations: for example, it is impossible to send waves along a reciprocal transmission channel such that transmission properties (speed, amplitude, phase, etc.) depend on the direction of travel. In order to realize direction-dependent wave propagation, the reciprocity invariance needs to be broken. The physics and applications of nonreciprocal propagation of mechanical waves have drawn the attention of many researchers in recent decades [3].

One strategy to realize nonreciprocal wave propagation is to use a medium in which one or more of the effective properties change with time [4]. In this context, periodic materials have been often used for investigating nonreciprocal wave propagation, in the form of discrete or continuous models with modulation. The smallest repetitive sub-structure in a periodic material, known as the unit cell, determines the properties of the periodic material acting as a waveguide. Modulation is a time- varying term within an effective property of the material, usually the stiffness coefficient or elastic modulus. Unidirectional propagation was studied in an infinite-long modulated metamaterial, in which there is a wave-like spatiotemporal modulation in the elastic coefficient of the resonant spring in every discrete unit cell [5]. Nonreciprocal wave propagation can also appear in uniform continuous media after introducing spatiotemporal modulation to the elastic modulus only [6-8], or both elastic modulus and density which is known as two-phase modulation [9]. Spatiotemporal modulations are often realized in experiments with controllable external magnetic forces [10-13]. A well-established method is to generate time-varying magnetic field by tuning the current flowing through a coil, in the center of which a magnet can move along the axis of the coil. The magnet is seen as a mass in a discrete modulated system.

In contrast to the initial theoretical studies, experimental demonstrations of nonreciprocal vibration transmission due to spatiotemporal modulation were performed on setups that are necessarily finite in length [10-13]. The influence of the finite length of the system is a relevant factor when considering device implementation. At the limit of finite length, nonreciprocal vibration transmission was investigated numerically in a system with just two degrees of freedom [14]. Nonreciprocity was attributed in that system to the phase difference between the modulation properties of the two units. In this work, we investigate the influence of the length of the system (number of modulated cells) on the vibration transmission properties. Furthermore, we present a methodology for identifying nonreciprocal phase shifts in the transmitted waves. These are response regimes in which only the phase (and not the amplitude) of the transmitted wave depends on the direction of travel.

We introduce the problem formulation and solution methodology in Section A.2. In Section A.3, we perform a parametric study to identify the influence of system parameters on the nonreciprocal response of the system. We highlight phase nonreciprocity in Section A.4. Our findings are summarized in Section A.5.

A.2. Analysis of a coupled system with modulation

We consider a system with n degrees of freedom (n DoF) which is composed of n identical masses, dampers, coupling springs and modulated grounding springs whose stiffness coefficients are time-dependent. Only the longitudinal rectilinear movement of each mass is considered as a degree of freedom. See Fig. A.1.

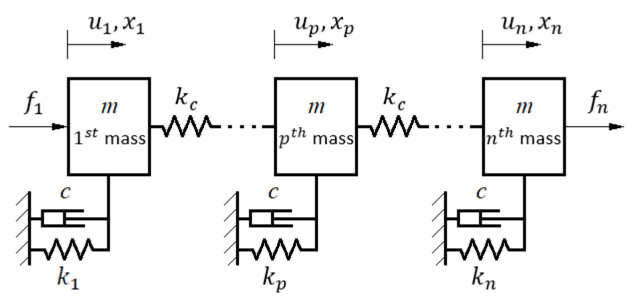

Figure A.1: Scheme of the n DoF system. Stiffness coefficient of each grounding spring has two components: a constant term and a periodic term.

A.2.1. Formulation of the problem

In the modulated system shown in Fig. A.1, each coupling spring is linear and each damper is a linear viscous damper. Two external harmonic forces of the same frequency are applied on the first mass and the last mass: $f_1(t) = F_1 \cos(\omega_f t)$ and $f_n(t) = F_n \cos(\omega_f t)$. Stiffness coefficient of the grounding spring connected to the p^{th} ($p = 1, 2, \cdots, n$) mass is: $k_p(t) =$

$k_{g,DC} + k_{g,AC}\cos(\omega_m t - \phi_p)$, where $\phi_p = (p-1)\phi$, $k_{g,DC}$, $k_{g,DC}$ and ϕ are constant. and ω_m represents the modulation frequency. The phase shift between the modulation in k_p and k_{p+1}, ϕ, represents a spatial modulation along the length of the system. A non-zero ϕ in the modulated system is the key factor in breaking the reciprocity invariance [14]. We define the following dimensionless variables to replace the dimensional terms in the governing equations: $\tau = t\omega_0$, $\omega_0^2 = k_{g,DC}/m$, $\Omega_m = \omega_m/\omega_0$, $\Omega_f = \omega_f/\omega_0$, $\zeta = c/(2m\omega_0)$, $K_c = k_c/k_{g,DC}$, $K_m = k_{g,AC}/k_{g,DC}$, $P_1 = F_1/(k_{g,DC}a)$, $P_n = F_n/(k_{g,DC}a)$ and $x_p = u_p/a$, where a is a representative length. The non-dimensionalized equations of motion for the system in Fig. A.1 are:

$$
\begin{gathered}
\frac{\mathrm{d}^2}{\mathrm{d}\tau^2}x_1 + 2\zeta\frac{\mathrm{d}}{\mathrm{d}\tau}x_1 + [1 + K_m\cos(\Omega_m\tau)]x_1 + K_c(x_1 - x_2) = P_1\cos(\Omega_f\tau),\\
\vdots\\
\frac{\mathrm{d}^2}{\mathrm{d}\tau^2}x_p + 2\zeta\frac{\mathrm{d}}{\mathrm{d}\tau}x_p + [1 + K_m\cos(\Omega_m\tau - \phi_p)]x_p + K_c(2x_p - x_{p-1} - x_{p+1}) = 0,\\
\vdots\\
\frac{\mathrm{d}^2}{\mathrm{d}\tau^2}x_n + 2\zeta\frac{\mathrm{d}}{\mathrm{d}\tau}x_n + [1 + K_m\cos(\Omega_m\tau - \phi_n)]x_n + K_c(x_n - x_{n-1}) = P_n\cos(\Omega_f\tau).
\end{gathered}
\tag{A.1}
$$

In this study, we focus on investigating nonreciprocity in the steady-state response of the system. In order to distinguish two opposite directions of vibration transmission, two configurations are defined: (i) the *forward* (left to right) configuration with $P_1 = P$, $P_n = 0$ where the output is the steady-state response of the last mass $x_n^F(\tau)$; (ii) the *backward* (right to left) configuration with $P_1 = 0$, $P_n = P$ where the output is the steady-state displacement of the first mass $x_1^B(\tau)$. If and only if $x_n^F(\tau) = x_1^B(\tau)$, the reciprocity invariance holds in vibration transmission through the system.

A.2.2. Solution methodology and envelopes for outputs

Using the averaging method, we can obtain the approximated solution for the steady-state response of a modulated system [14]. The approximated solutions for outputs in forward and backward configurations read:

$$
\begin{aligned}
x_n^F(\tau) &= \mathbf{y}_n^F(\tau)e^{i\Omega_f\tau} + c.c.\ ,\\
x_1^B(\tau) &= \mathbf{y}_1^B(\tau)e^{i\Omega_f\tau} + c.c.\ ,
\end{aligned}
\tag{A.2}
$$

where $c.c.$ represents the corresponding complex conjugate. $\mathbf{y}_n^F$ and $\mathbf{y}_1^B$ are both functions of τ:

$$
\mathbf{y}_n^F(\tau) = \sum_{q=-\infty}^{\infty}\eta e^{iq\Omega_m\tau}, \mathbf{y}_1^B(\tau) = \sum_{q=-\infty}^{\infty}\xi e^{iq\Omega_m\tau},
$$

where η and ξ are complex amplitudes for a given Ω_f, which need to be calculated. Because of the quasi-periodic form of the approximated solution in Eq. (A.2), $x_n^F(\tau)$ and $x_1^B(\tau)$ can be rewritten as:

$$\begin{aligned} x_n^F(\tau) &= 2\left|\mathbf{y}_n^F(\tau)\right|\cos\left(\Omega_f\tau - \varphi_n^F\right), \\ x_1^B(\tau) &= 2\left|\mathbf{y}_1^B(\tau)\right|\cos\left(\Omega_f\tau - \varphi_1^B\right). \end{aligned} \tag{A.3}$$

The cosine parts in equations of Eq. (A.3) have same frequency as the external excitation. These terms can be viewed as carrier waves; their amplitudes are both equal to unity but their phases can be different. Therefore, $\pm 2\left|\mathbf{y}_n^F(\tau)\right|$ and $\pm 2\left|\mathbf{y}_1^B(\tau)\right|$ are the envelopes of $x_n^F(\tau)$ and $x_1^B(\tau)$, respectively. The expressions for $\pm 2\left|\mathbf{y}_n^F(\tau)\right|$ and $\pm 2\left|\mathbf{y}_1^B(\tau)\right|$ can be written as:

$$\begin{aligned} 2\left|\mathbf{y}_n^F(\tau)\right| &= \sqrt{\textstyle\sum_{r=0}^{\infty}\mathcal{Y}_{n,r}^F\cos\left(r\Omega_m\tau - \theta_{n,r}^F\right)}, \\ 2\left|\mathbf{y}_1^B(\tau)\right| &= \sqrt{\textstyle\sum_{r=0}^{\infty}\mathcal{Y}_{1,r}^B\cos\left(r\Omega_m\tau - \theta_{1,r}^B\right)}, \end{aligned}$$

where r is an integer. $\mathcal{Y}_{n,r}^F$,$\mathcal{Y}_{1,r}^B$,$\theta_{n,r}^F$ and $\theta_{1,r}^B$ are all real numbers, which can be calculated from η and ξ. While $x_n^F(\tau)$ and $x_1^B(\tau)$ are not periodic, $2\left|\mathbf{y}_n^F(\tau)\right|$ and $2\left|\mathbf{y}_1^B(\tau)\right|$ are periodic with the same dimensionless period $T_{ev} = 2\pi/\Omega_m$. This periodicity of envelope equations brings convenience for analyzing $x_n^F(\tau)$ and $x_1^B(\tau)$. The necessary and sufficient condition for reciprocity can be written in the following <u>two</u> equations: $\left|\mathbf{y}_n^F(\tau)\right| = \left|\mathbf{y}_1^B(\tau)\right|$ and $\varphi_n^F = \varphi_1^B$.

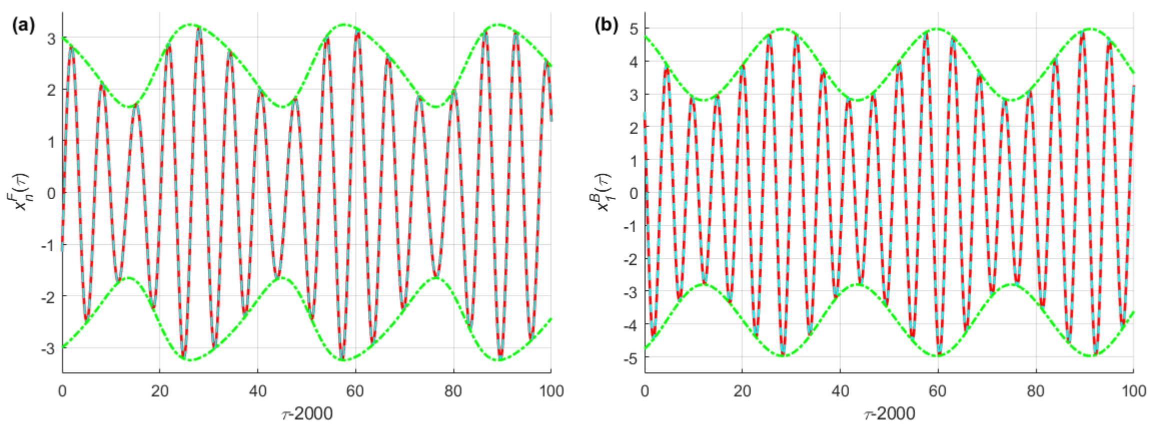

Figure A.2: Comparison between the results of averaging method and direct numerical simulation. (a): $n = 5$, $\Omega_f = 0.97$ in forward configuration; (b): $n = 8$, $\Omega_f = 1.18$ in backward configuration. Outputs calculated with the averaging method and the Runge-Kutta method are indicated by red curves and cyan dashed curves, respectively. The green curves are the plots of $\pm 2\left|\mathbf{y}_n^F(\tau)\right|$ and $\pm 2\left|\mathbf{y}_1^B(\tau)\right|$.

Fig. A.2 shows the displacements and envelopes calculated for (1) for the following parameters: $K_c = 0.6$, $\zeta = 0.01$, $K_m = 0.1$, $\Omega_m = 0.2$, $\phi = 0.5\pi$ and $P = 1$, in the steady-state with respect to time τ. In order to validate the predictions made by the averaging method, the response of Eq. (A.1) is computed using the Runge-Kutta method until the steady state is reached. The predictions of the steady-state response from analytical and numerical methods match with each other very well. Plots of $\pm 2\left|\mathbf{y}_n^F(\tau)\right|$ and $\pm 2\left|\mathbf{y}_1^B(\tau)\right|$ follow the envelopes of outputs in forward and backward configurations, respectively. Having validated the accuracy of the envelope equations, results from the averaging method are used hereafter to analyze the steady-state response and nonreciprocity of the system.

Because $x_n^F(\tau)$ and $x_1^B(\tau)$ are non-periodic, it is very difficult to obtain their maximum displacements. The maximum displacements of $2\left|\mathbf{y}_n^F(\tau)\right|$ and $2\left|\mathbf{y}_1^B(\tau)\right|$ over a period, denoted as $A_{ev,n}^F$ and $A_{ev,1}^B$ respectively, can be seen as approximations of the maximum steady-state displacements of $x_n^F(\tau)$ and $x_1^B(\tau)$. $A_{ev,n}^F$ and $A_{ev,1}^B$ can be approximated by:

$$A_{ev,n}^F = A_{ev,n,DC}^F + A_{ev,n,AC}^F, A_{ev,1}^B = A_{ev,1,DC}^B + A_{ev,1,AC}^B,$$

where,

$$\begin{aligned}
A_{ev,n,DC}^F &= \frac{2}{T_{ev}} \int_0^{T_{ev}} \left|\mathbf{y}_n^F(\tau)\right| \mathrm{d}\tau, \\
A_{ev,1,DC}^B &= \frac{2}{T_{ev}} \int_0^{T_{ev}} \left|\mathbf{y}_1^B(\tau)\right| \mathrm{d}\tau, \\
A_{ev,n,AC}^F &= \sqrt{\frac{2}{T_{ev}} \int_0^{T_{ev}} \left[2\left|\mathbf{y}_n^F(\tau)\right| - A_{ev,n,DC}^F\right]^2 \mathrm{d}\tau}, \\
A_{ev,1,AC}^B &= \sqrt{\frac{2}{T_{ev}} \int_0^{T_{ev}} \left[2\left|\mathbf{y}_1^B(\tau)\right| - A_{ev,1,DC}^B\right]^2 \mathrm{d}\tau}.
\end{aligned}$$

The amplitude bias R_A is defined to quantify the degree of nonreciprocity in terms of amplitude, without considering the difference in phases:

$$R_A = \frac{A_{ev,n}^F - A_{ev,1}^B}{A_{ev,n}^F + A_{ev,1}^B}. \tag{A.4}$$

A zero amplitude bias, $R_A = 0$, corresponds to equal amplitudes for the forward and backward configurations and the upper limit of $R_A = \pm 1$ indicates that the amplitude in one of the configurations is much larger than the other one. Furthermore, we can use $R_A = 0$ to identify response regimes where the forward and backward configurations have equal amplitudes but (possibly) different phases – see Section A.4.

A.3. Nonreciprocal vibration transmission in modulated n DoF systems

We first investigate nonreciprocity by exploring the effects of ϕ and Ω_f on maximum displacements of the outputs in the forward and backward configurations. In this section, we

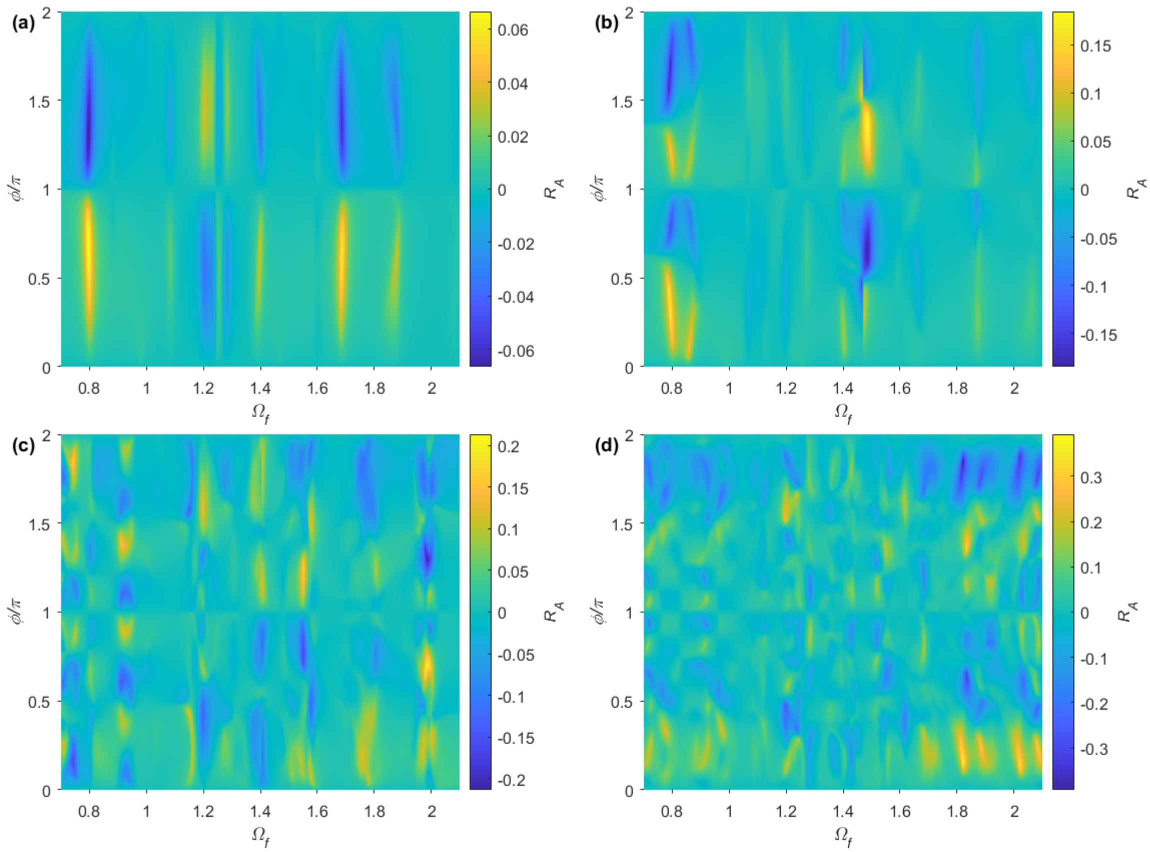

Figure A.3: Plots of R_A with respect to ϕ and Ω_f. (a): $n = 2$, (b): $n = 3$, (c): $n = 5$, (d): $n = 8$.

use $K_c = 0.6$, $\zeta = 0.01$, $K_m = 0.1$, $\Omega_m = 0.2$ and $P = 1$ and calculate R_A as a function of ϕ and Ω_f. The n natural frequencies of the unmodulated system ($k_{g,AC} = 0$) are denoted by $\Omega_{n,\kappa}$, $\kappa = 1, 2, \cdots, n$.

Fig. A.3 shows the amplitude bias, R_A, for systems with different degrees of freedom. In all four panels, regions where the magnitude of R_A is largest occur where Ω_f is nearly centered at $\Omega_{n,\kappa} \pm \Omega_m$, $\Omega_{n,\kappa} \pm 2\Omega_m$, $\Omega_{n,\kappa} \pm 3\Omega_m, \cdots$; these are called sideband resonances. As n increases, the number of sideband frequencies increases and the plot of R_A becomes more and more complex.

Generally, when Ω_f is fixed at a value where R_A changes significantly with ϕ, there are $2(n-1)$ convex and concave regions in the plot of R_A over the range $\phi \in [0, 2\pi]$. But this finding is not valid for a large n, for example, $n = 8$ as shown by Fig. A.3(d). Interestingly, all the three-dimensional (3-D) plots of R_A in Fig. A.3 are odd-symmetric about the line $(\phi, R_A) = (\pi, 0)$.

In Figs. A.3 and A.4, we observe that the magnitude of R_A increases with the number of

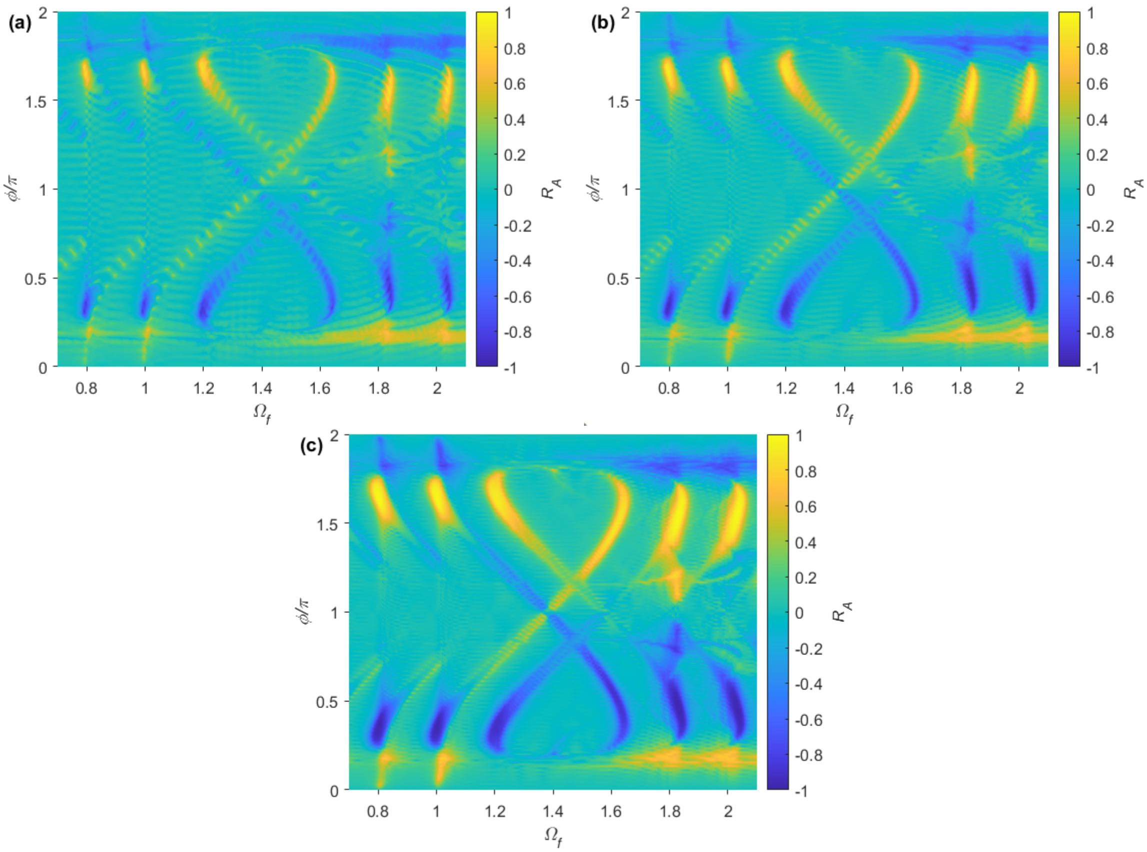

Figure A.4: Plots of R_A with respect to ϕ and Ω_f. (a): $n = 40$, (b): $n = 60$, (c): $n = 100$.

units in the system. Larger difference between the amplitudes of outputs can be therefore realized by adding more units into the modulated system.

Fig. A.4 also shows the limiting behavior of R_A for large values of n in the frequency range $0.7 \leq \Omega_f \leq 2.1$. Regardless of the number of units, however, we have $-1 \leq R_A \leq 1$ by constructions, where the limiting values indicate unidirectional vibration transmission. It implies that there exist two extreme cases: $R_A = 1$ when $A^F_{ev,n} \gg A^B_{ev,1}$, which means vibrations can be transmitted in the forward direction only; $R_A = -1$ when $A^F_{ev,n} \ll A^B_{ev,1}$, which means vibrations can be transmitted in the backward direction only.

The magnitude of amplitude bias, $|R_A|$, can nearly reach 1, as shown in Fig. A.4. Unidirectional vibration transmission can therefore occur in large modulated systems. This agrees with the literature on infinitely-long spatiotemporal modulated materials [5,6]. In contrast, the magnitude of R_A is not very large in short modulated systems (Fig. A.3). This prevents unidirectional vibration transmission from occurring in short systems. Fig. A.4 suggests two ranges of values for the phase difference ϕ where unidirectional transmission may occur: near 0.3π and 1.7π.

A.4. Phase nonreciprocity

For all plots in Fig. A.3, R_A is equal to zero when $\phi = \pi$, regardless of the values of Ω_f and n. However, because R_A is defined based on the envelope equations, it is blind to the phase difference between $x_n^F(\tau)$ and $x_1^B(\tau)$. Therefore, $R_A = 0$ may not correspond to a reciprocal response in the original system. To quantify the degree of nonreciprocity in the response of the original system, we use reciprocity bias R to evaluate nonreciprocity between $x_n^F(\tau)$ and $x_1^B(\tau)$:

$$R = \lim_{T\to\infty} \sqrt{\frac{1}{T}\int_0^T [x_n^F(\tau) - x_1^B(\tau)]^2 d\tau}, \tag{A.5}$$

which is evaluated after the response reaches its steady-state [14]. If $R = 0$, then $x_n^F(\tau) = x_1^B(\tau)$ and the response is reciprocal; otherwise, the response is not reciprocal. R is calculated using the averaging method with the same parameters as the examples in Fig. A.3.

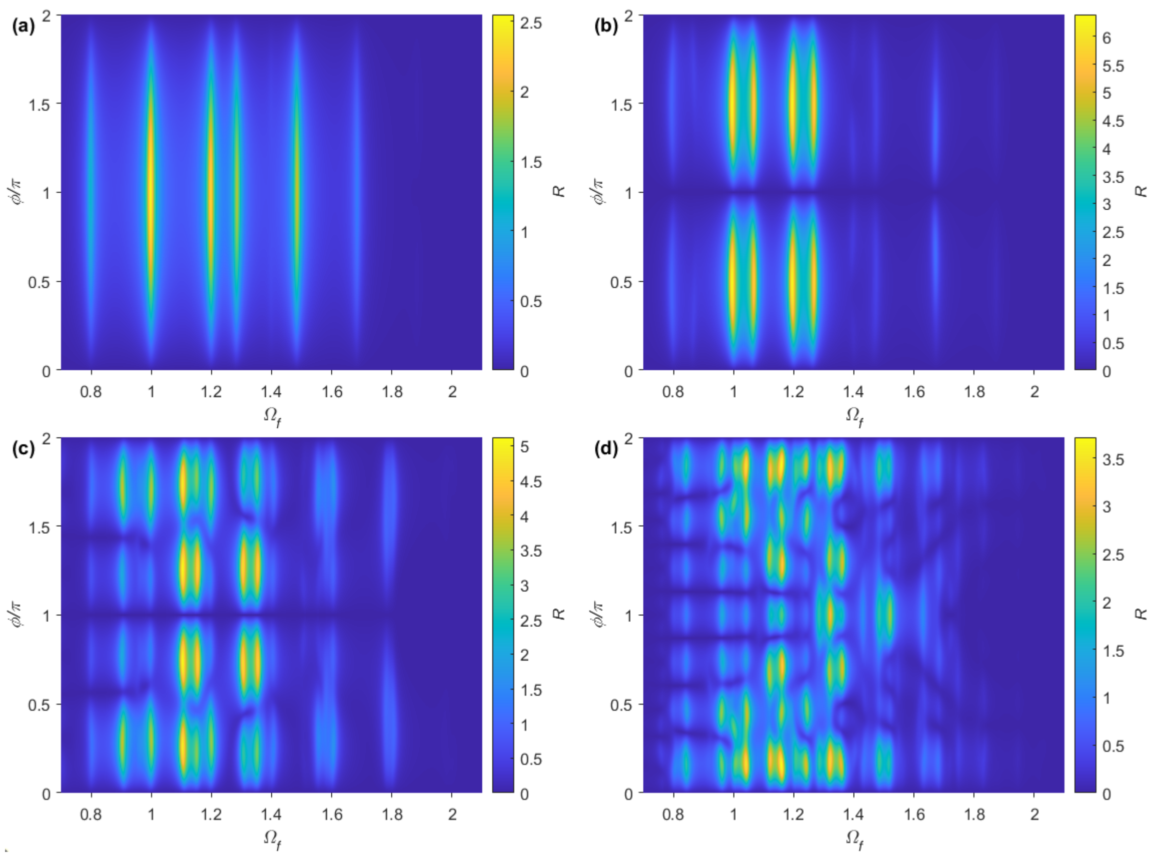

Figure A.5: Plots of R with respect to ϕ and Ω_f. (a): $n = 2$, (b): $n = 3$, (c): $n = 5$, (d): $n = 8$.

Fig. A.5 shows 3-D plots of the reciprocity bias, R, as a function of ϕ and Ω_f for systems of different length. We observe that the 3-D plot of R is symmetric about the plane $\phi = \pi$.

Interestingly, if n is an odd number, regardless of the value of Ω_f , reciprocity invariance holds when $\phi = \pi$, as shown by Figs. A.5(b) and A.5(c). In contrast, if n is an even number, the reciprocity invariance does not hold when $\phi = \pi$, as shown by Figs. A.5(a) and A.5(d).

The results in Figs. A.3 and A.5 indicate the possibility of choosing system parameters such that $R_A = 0$ and $R > 0$. In this state, $R_A = 0$ means that the amplitudes of the output in the forward and backward configurations are the same. Therefore, nonreciprocity ($R > 0$) manifests as different phases in the output displacements. The existence of such regimes of nonreciprocal phase shifts was previously reported in time- independent nonlinear systems [15], but not in modulated systems of the type considered in this work.

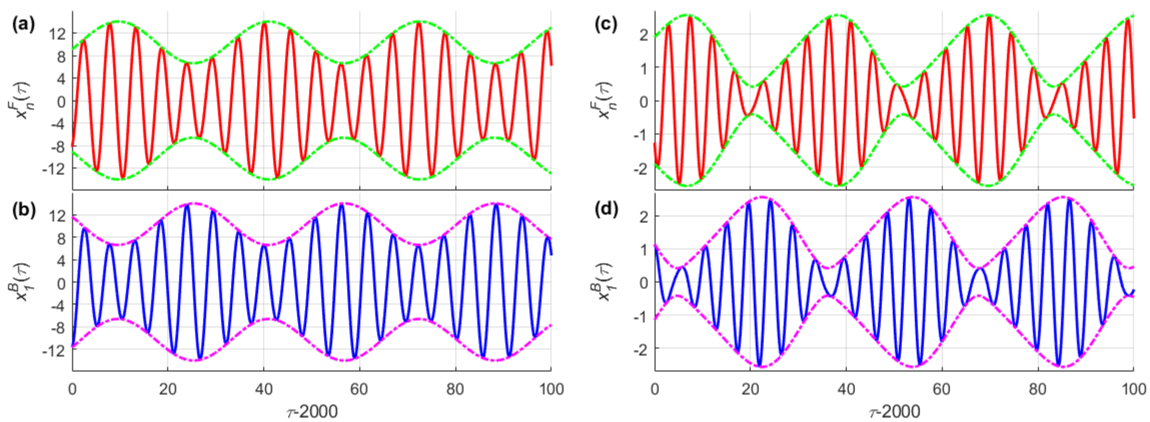

Figure A.6: Plots of outputs and their envelopes, (a) and (b): $n = 4$, $\Omega_f = 1.17$, (c)and(d): $n = 8$, $\Omega_f = 1.51$.

Fig. A.6 shows two examples of phase nonreciprocity obtained at $\phi = \pi$. It is clear from the time-domain response that the response is nonreciprocal. Notice, however, that the difference between the displacements is only in a phase shift. This can be seen more clearly in the response envelopes. For any arbitrary value of Ω_f, when $\phi = \pi$ and n is equal to an even number, besides $R_A = 0$ and $R > 0$, we have $\left|\mathbf{y}_n^F(\tau)\right| = \left|\mathbf{y}_1^B(\tau \pm T_{ev}/2)\right|$. The envelopes in different configurations have the same shape with a temporal shift of τ by half period. However, $x_n^F(\tau)$ is not equal to $x_1^B(\tau + T_{ev}/2)$ or $x_1^B(\tau - T_{ev}/2)$ due to the phase difference between two carrier waves. Here, outputs in forward and backward configurations follow the same envelope profile but at different phases.

A.5. Conclusions

By investigating the envelopes of outputs in forward and backward configurations, we studied nonreciprocal vibration transmission in discrete models of modulated materials. Specifically, we developed equations for the envelopes of the output displacements for this purpose. While the response of modulated systems is quasi-periodic in general, the envelope equations are periodic in time. Thus, studying the envelopes of the nonperiodic response brings convenience in approximating the maximum displacements in the steady-state. We provided a measure for quantifying the degree of nonreciprocity based on the envelope of the response, the amplitude bias. We used the amplitude bias to identify two response regimes in the system. First, we showed that the maximum magnitudes of the amplitude bias correspond to unidirectional vibration transmission in the modulated system. These maximum values were obtained only in systems with many modulated units (long systems). Second, we demonstrated that zero amplitude bias can be used to identify phase nonreciprocity in the system; i.e. response regimes where the difference between the forward and backward output displacements is in their relative phase only. Our results demonstrate that the envelope equations can provide information about nonreciprocity in modulated materials that would be difficult to obtain otherwise. We observed that amplitude bias is not significant in shorter models (with fewer degrees of freedom), and it can become more significant with increasing the number of degrees of freedom. Unidirectional transmission and bandgaps were highlighted in the scenarios with very long models, which agree with the findings of directional bandgaps in infinite-long spatiotemporal modulated systems. Comparing the results of amplitude bias and reciprocity bias for different examples, we identified nonreciprocal response regimes in which the amplitude bias is zero. Furthermore, the envelopes of forward output and backward output can have the same shape and a half-period offset from each other. We presented the conditions leading to this specific form of nonreciprocity.

The analysis based on the envelope of nonperiodic steady-state response provides a new strategy for studying nonreciprocal vibration transmission in linear modulated materials. The methodology presented in this work facilitates parametric studies in the future.

References

[1] S. Andrieux, A. B. Abda, H. D. Bui, "Reciprocity principle and crack identification," *Inverse Problems*, vol. 15, no. 1, pp. 59-65, 1999.

[2] T. Ten Wolde, "Reciprocity measurements in acoustical and mechano-acoustical systems. Review of theory and applications," *Acta Acustica united with Acustica*, vol. 96, no. 1, pp. 1 - 13, 2010.

[3] H. Nassar, B. Yousefzadeh, R. Fleury, M. Ruzzene, A. Alù, C. Daraio, A. N. Norris, G. Huang, M. R. Haberman, "Nonreciprocity in Acoustic and Elastic Materials," *Nature Reviews Materials*, vol. 5, pp. 667-685, 2020.

[4] K. A. Lurie, An Introduction to the Mathematical Theory of Dynamic Materials, Second Edition, Springer Cham, 2017.

[5] H. Nassar, H. Chen, A. N. Norris, M. R. Haberman, "Non-reciprocal Wave Propagation in Modulated Elastic Metamaterials," *Proc. R. Soc. A*, vol. 473, no. 2202, 2017.

[6] G. Trainiti, M. Ruzzene, "Non-reciprocal Elastic Wave Propagation in Spatiotemporal Periodic Structures," *New Journal of Physics*, vol. 18, p. 083047, 2016.

[7] E. Riva, J. Marconi, G. Cazzulani, F. Braghin, "Generalized Plane Wave Expansion Method for Non-reciprocal Discretely Modulated Waveguides," *Journal of Sound and Vibration*, vol. 449, pp. 172-181, 2019.

[8] M. A. Attarzadeh, M. Nouh, "Elastic Wave Propagation in Moving Phononic Crystals and Correlations with Stationary Spatiotemporally Modulated Systems," *AIP Advances*, vol. 8, p. 105302, 2018.

[9] H. Nassar, X. C. Xu, A. N. Norris, G. L. Huang, "Modulated Phononic Crystals: Non-reciprocal Wave Propagation and Willis Materials," *Journal of the Mechanics and Physics of Solids*, vol. 101, pp. 10-29, 2017.

[10] Y. Wang, B. Yousefzadeh, H. Chen, H. Nassar, G. Huang, C. Daraio, "Observation of Nonreciprocal Wave Propagation in a Dynamic Phononic Lattice," *Physical Review Letters*, vol. 121, no. 19, p. 194301, 2018.

[11] S. Wan, L. Cao, Y. Zeng, T. Guo, M. Oudich, B. Assouar, "Low-Frequency Nonreciprocal Flexural Wave Propagation via Compact Cascaded Time-Modulated Resonators," *Applied Physics Letters*, vol. 120, no. 23, p. 231701, 2022.

[12] Y. Chen, X. Li, H. Nassar, A.N. Norris, C. Daraio, G. Huang, "Nonreciprocal wave propagation in a continuum-based metamaterial with space-time modulated resonators," *Physical Review Applied*, vol. 11, no. 6, p. 064052, 2019.

[13] B. L. Kim, C. Daraio, C. Chong, S. Hajarolasvadi, Y. Wang, "Dynamics of time-modulated, nonlinear phononic lattices," *Physical Review E*, vol. 107, p. 034211, 2023.

[14] J. Wu, B. Yousefzadeh, "On Vibration Transmission Reciprocity In Modulated Materials," in *Canadian Society for Mechanical Engineering International Congress*, Edmonton, 2022.

[15] B. Yousefzadeh, "Computation of Nonreciprocal Dynamics in Nonlinear Materials," *Journal of Computational Dynamics*, vol. 9, no. 3, pp. 451-464, 2022.

B. Numerical analysis of phase nonreciprocity in a linear spatiotemporally modulated system

B.1. Introduction

The principle of reciprocity states that vibration transmission between two points in a material remains invariant upon interchanging the locations of the source and receiver. This invariance condition holds for materials with time-independent properties when they operate in the linear response regime. Based on this property, some wave processing techniques are invented and several industrial applications are developed [1-3].However, in reciprocal systems, it is not possible to realize transmission properties that depend on the direction of wave propagation. Recently, in order to realize direction-dependent vibration transmission, theories on breaking reciprocity have drawn the attention of many researchers [4].

Nonreciprocal wave propagation can be realized in a medium that has one or more of its effective properties (*e.g.* effective mass or stiffness) change as a function of time and space [5].The time-varying term in an effective property, which is usually the stiffness of the material, is known as modulation. In such systems, the studies on nonreciprocal wave propagation often use models of discrete and continuous periodic modulated materials. The modulation characteristics such as frequency and wavenumber determine how incident waves disperse as they travel in the periodic materials.

Nonreciprocity in wave propagation can be recognized by the dependence of at least one of the transmission characteristics (amplitude, phase, phase or group velocity, etc.) on the direction of propagation. Unidirectional propagation, in which propagation is prohibited along one direction, was studied in various infinite-long 1-D models with wave-like spatiotemporal modulation in the stiffness coefficient or elastic modulus [5-10].Direction-dependent propagation speed can be identified from the dispersion curve of a two-phase modulated uniform medium, where spatiotemporal modulation is introduced in both the Young's modulus and density [10].

Conversely, experimental studies on nonreciprocal vibration transmission in systems with spatiotemporal modulation were performed on discrete finite setups, where nonreciprocity is identified by differences between the left-to-right and right-to-left transmitted amplitudes [11-14].Nonreciprocity demonstrated by differences in phase was studied in a medium with a synthetic antiferromagnet layer, where the coupling of surface acoustic waves and nonreciprocal spin waves resulted in nonreciprocal phase shifts [15,16].In short periodic systems with spatiotemporal modulations, difference in phase was recognized as the main contributor to nonreciprocity in the steady-state vibration transmission [17].Consequently, it is possible that the left-to-right and right-to-left amplitudes are equal and the difference in the transmitted phase is the only contributor to nonreciprocity. We refer to this transmission scenario as phase nonreciprocity. Phase nonreciprocity was previously shown in a nonlinear passive system [18,19].In this work, we investigate nonreciprocity (in amplitude and phase) in a spatiotemporally modulated system, and study the influence of the modulation strength and the length of the system (number of modulated unit cells) on the vibration transmission properties in the steady-state. A methodology for identifying phase nonreciprocity in the steady-state response is presented. Using the envelope equations of the response, we observe two different types of phase nonreciprocity: one represents that the response envelopes of transmission cases in opposite directions having the same shape; the other one represents the response envelopes with different shapes.

Formulation of the system and solution methodology are introduced in Section B.2. In Sections B.3 and B.4, we investigate the phase nonreciprocity in short modulated systems and long systems, respectively. We summarize our findings in Section B.5.

B.2. Spatiotemporally modulated system

Fig. B.1 shows the schematic of the system we study in this work. The system consists of n identical masses, linear viscous dampers, linear coupling springs and modulated grounding springs. The stiffness coefficient of each grounding spring is composed of two parts: a constant term and a periodic term. For each mass, only the longitudinal rectilinear movement is considered as a degree of freedom (DoF).

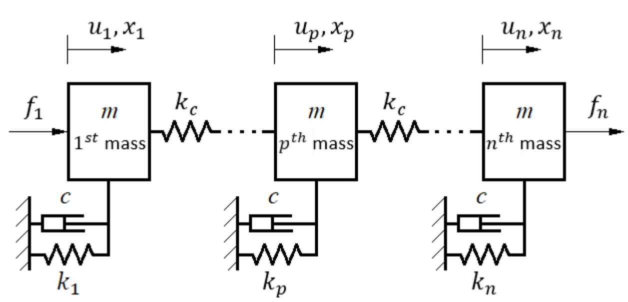

Figure B.1: Schematic of the n DoF system.

In the modulated system shown in Fig. B.1, two external harmonic forces, $f_1(t) = F_1 \cos(\omega_f t)$ and $f_n(t) = F_n \cos(\omega_f t)$, are applied on the first mass and the last mass, respectively. The stiffness coefficient of the p^{th} ($p = 1, 2, \cdots, n$) grounding spring is expressed as $k_p(t) = k_{g,DC} + k_{g,AC} \cos(\omega_m t - \phi_p)$, where $\phi_p = (p-1)\phi$ and ω_m represents the modulation frequency. $k_{g,DC}$, $k_{g,DC}$, ω_m and ϕ are constant. ϕ is the phase shift between modulation in two adjacent units, which is equivalent to the wavenumber in a system with many DoF. The spatial modulation of the grounding stiffness along the length of the system is represented by a non-zero ϕ, which is the key factor in breaking the reciprocity invariance.

B.2.1. Mathematical modeling

Dimensionless variables are defined to replace the dimensional terms in the equations of motion: $\tau = t\omega_0$, $\Omega_m = \omega_m/\omega_0$, $\Omega_f = \omega_f/\omega_0$, $\zeta = c/(2m\omega_0)$, $K_c = k_c/k_{g,DC}$, $K_m = k_{g,AC}/k_{g,DC}$, $P_1 = F_1/(k_{g,DC}a)$, $P_n = F_n/(k_{g,DC}a)$ and $x_p = u_p/a$, where $\omega_0 = \sqrt{k_{g,DC}/m}$ and a is a representative length. The dimensionless governing equations for the system in Fig. B.1 can be written as:

$$\begin{gathered}
\ddot{x}_1 + 2\zeta\dot{x}_1 + [1 + K_m\cos(\Omega_m\tau)]x_1 + K_c(x_1 - x_2) = P_1\cos(\Omega_f\tau), \\
\vdots \\
\ddot{x}_p + 2\zeta\dot{x}_p + [1 + K_m\cos(\Omega_m\tau - \phi_p)]x_p + K_c(2x_p - x_{p-1} - x_{p+1}) = 0, \\
\vdots \\
\ddot{x}_n + 2\zeta\dot{x}_n + [1 + K_m\cos(\Omega_m\tau - \phi_n)]x_n + K_c(x_n - x_{n-1}) = P_n\cos(\Omega_f\tau),
\end{gathered} \tag{B.1}$$

where $\ddot{x}_p$ and $\dot{x}_p$ represent $d^2x_p/d\tau^2$ and $dx_p/d\tau$, respectively.

For this study, we investigate nonreciprocal response in the steady-state, with a focus on phase nonreciprocity: we seek response regimes that are characterized by the same transmitted amplitudes but different (nonreciprocal) phase shifts along opposite directions. Two configurations are defined to distinguish between the two directions of vibration propagation in the 1-D system: (i) the forward (from left to right) configuration with $P_1 = P$, $P_n = 0$ where the output is the steady-state response of the n^{th} mass, $x_n^F(\tau)$; (ii) the backward (from right to left) configuration with $P_1 = 0$, $P_n = P$ where the output is the steady-state response of the first mass, $x_1^B(\tau)$. Vibration propagation through the system is reciprocal if and only if $x_n^F(\tau) = x_1^B(\tau)$ for any τ in the steady-state.

We use reciprocity bias R and output norms N^F and N^B to quantify the degree of nonreciprocity and strength of outputs in the steady-state response of the system [17]. They are defined as:

$$R = \lim_{T\to\infty}\sqrt{\frac{1}{T}\int_0^T [x_n^F(\tau) - x_1^B(\tau)]^2 d\tau} \tag{B.2}$$

$$N^F = \lim_{T\to\infty}\sqrt{\frac{1}{T}\int_0^T [x_n^F(\tau)]^2 d\tau} \tag{B.3}$$

$$N^B = \lim_{T\to\infty}\sqrt{\frac{1}{T}\int_0^T [x_1^B(\tau)]^2 d\tau} \tag{B.4}$$

The norm bias is introduced to quantify the degree of nonreciprocity in terms of the norms only (transmitted vibration energies), without considering the possible difference in phases:

$$R_N = \frac{N^F - N^B}{N^F + N^B}. \tag{B.5}$$

$R_N = 0$ corresponds to equal norms for the forward and backward configurations. We use $R_N = 0$ and $R > 0$ to identify the response regimes where the forward and backward configurations have equal norms but different phases. Such scenarios are recognized as examples of phase nonreciprocity.

B.2.2. Solution methodology

An approximated solution for both outputs can be obtained by using the averaging method, which is based on the quasi- periodic form of the steady-state response:

$$x_n^F(\tau) = \sum_{q=-\infty}^{\infty} [\eta_q e^{i(\Omega_f + q\Omega_m)\tau} + c.c.] \tag{B.6}$$

$$x_1^B(\tau) = \sum_{q=-\infty}^{\infty} [\xi_q e^{i(\Omega_f + q\Omega_m)\tau} + c.c.] \tag{B.7}$$

where η_q and ξ_q are complex amplitudes and *c.c.* represents the corresponding complex conjugate. Using the averaging method, η_q and ξ_q can be calculated for a given Ω_f and other parameters of the modulated system [17].

The approximate solution for each output can be rewritten as a response envelope and a harmonic carrier wave of unit amplitude and the same frequency as the external excitation:

$$x_n^F(\tau) = 2\left|\sum_{q=-\infty}^{\infty} \eta_q e^{iq\Omega_m\tau}\right| \cos(\Omega_f\tau - \varphi_n^F) = E_n^F(\tau)\cos(\Omega_f\tau - \varphi_n^F), \tag{B.8}$$

$$x_1^B(\tau) = 2\left|\sum_{q=-\infty}^{\infty} \xi_q e^{iq\Omega_m\tau}\right| \cos(\Omega_f\tau - \varphi_1^B) = E_1^B(\tau)\cos(\Omega_f\tau - \varphi_1^B), \tag{B.9}$$

$E_n^F(\tau)$ and $E_1^B(\tau)$ are response envelopes for $x_n^F(\tau)$ and $x_1^B(\tau)$, respectively. $x_n^F(\tau)$ and $x_1^B(\tau)$ are not periodic, however, $E_n^F(\tau)$ and $E_1^B(\tau)$ are periodic with the same period $T_E = 2\pi/\Omega_m$. This periodicity of response envelopes brings convenience for investigating nonreciprocity.

The steady-state displacements and response envelopes are calculated for Equation (1) for the following parameters: $K_c = 0.55$, $\Omega_m = 0.3$, $\phi = 0.6\pi$, $\zeta = 0.02$ and $P = 1$. For validating the solution predicted by the averaging method, the response of Eq. (B.1) is computed using the Runge-Kutta method until the steady-state is reached.

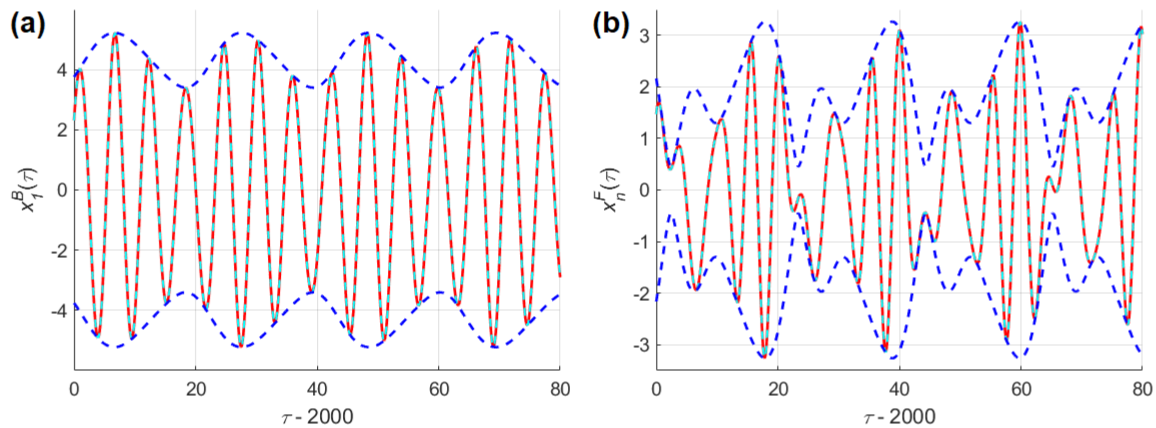

Figure B.2: Comparison between the output displacements computed using the averaging method (red solid curves) and the Runge-Kutta method (cyan dashed curves). (a) $n = 5$, $\Omega_f = 1.06$, $K_m = 0.1$ in backward configuration; (b) $n = 2$, $\Omega_f = 1.27$, $K_m = 0.6$ in forward configuration. Blue curves in panels (a) and (b) are plots of $\pm E_n^F(\tau)$ and $\pm E_1^B(\tau)$, respectively.

Figs. B.2(a) and B.2(b) show that the averaging method predicts the response of the system accurately for these sets of system parameters; this was found to be the case for other parameters used in this work. We further observe that the plots of $\pm E_n^F(\tau)$ and $\pm E_1^B(\tau)$ follow the response envelopes of the outputs in the forward and backward configurations very well. In particular, we note in Fig. B.2(b) that the response envelope is not harmonic. This is an advantage of our formulation over the more conventional methods of computing the response envelope, such as the classical rotating wave approximation that is limited to harmonic envelopes. Thus, results from the averaging method are used hereafter to analyze the steady-state response and nonreciprocity of the system.

B.3. Short modulated systems

B.3.1. Weak modulation

We first investigate phase nonreciprocity ($R_N = 0$) in weakly modulated systems with a small number of degrees of freedom. Specifically, we explore how Ω_f (forcing frequency) and ϕ (phase difference between modulation in two adjacent units, equivalent to modulation wavenumber) influence the difference between the outputs in the forward and backward configurations. In this section, we use $K_c = 0.55$, $K_m = 0.1$, $\Omega_m = 0.3$, $\zeta = 0.02$ and $P = 1$, and compute R and R_N as functions of Ω_f and ϕ.

Fig. B.3 shows the reciprocity bias R and norm bias R_N for systems with 2 DoF and 5 DoF. $\phi = 0$ and $\phi = 2\pi$ represent no spatial modulation in the system, which correspond to a

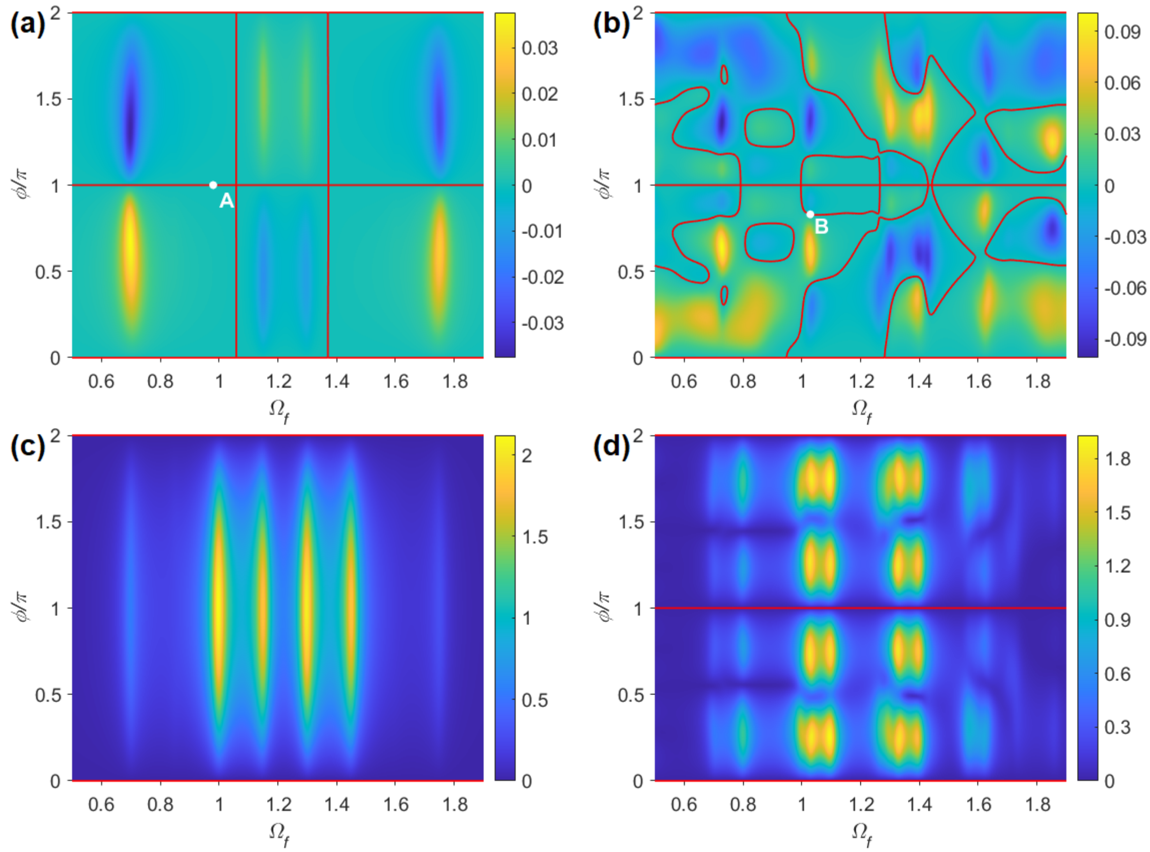

Figure B.3: R_N and R as functions of Ω_f and ϕ. Red curves indicate combinations of Ω_f and ϕ where $R_N = 0$ or $R = 0$ in corresponding plots. (a) Norm bias, R_N, for $n = 2$ and $K_m = 0.1$; (b) norm bias, R_N, for $n = 5$ and $K_m = 0.1$; (c) reciprocity bias, R, for $n = 2$ and $K_m = 0.1$; (d) reciprocity bias, R, for $n = 5$ and $K_m = 0.1$.

reciprocal response ($R = 0$). We observe that the 3-D plot of R_N is odd-symmetric about the red straight line $(\phi, R_N) = (\pi, 0)$, as shown in Figs. B.3(a) and B.3(b); the 3-D plot of R is symmetric about the plane $\phi = \pi$, as shown in Figs. B.3(c) and B.3(d). It means that, regardless of the values of Ω_f and n, $R_N = 0$ if $\phi = \pi$. Interestingly, if n is an odd number, the reciprocity invariance holds only if $\phi = \pi$, regardless of the value of Ω_f, as shown in Fig. B.3(d). However, if n is an even number, reciprocity bias is consistently positive over the range $0 < \phi < 2\pi$, regardless of the value of Ω_f, as shown in Fig. B.3(c). Consequently, phase nonreciprocity occurs when n is an even number and $\phi = \pi$. We refer to this scenario as *Type I* phase nonreciprocity.

Furthermore, if $\phi \neq \pi$, there exist combinations of Ω_f and ϕ which can lead to $R_N = 0$ too. These combinations of Ω_f and ϕ are indicated by the red curves in Figs. B.3(a) and B.3(b) where $\phi \neq \pi$. In contrast to the red straight line $(\phi, R_N) = (\pi, 0)$ which represents

Type I phase nonreciprocity, these curves are determined by K_c, K_m, ζ, Ω_m, Ω_f, ϕ and n. Despite having equal transmitted amplitudes ($R_N = 0$), the response along these red curves are nonreciprocal because $R > 0$, regardless of whether n is even or odd. The response at these points is therefore phase nonreciprocal. We refer to this scenario as *Type II* phase nonreciprocity. The locus of $R_N(\Omega_f, \phi) = 0$ for *Type II* phase nonreciprocity has a complicated shape if n is large; we will see in Section B.4 that this shape becomes even more complicated as n increases.

To better illustrate the difference between *Type I* and *Type II* phase nonreciprocity, we choose two points which are labeled as 'A' (*Type I* phase nonreciprocity) and 'B' (*Type II* phase nonreciprocity) in Figs. B.3(a) and B.3(b). Their coordinates in the (Ω_f, ϕ) plane are: $(0.96, \pi)$ and $(1.209, 0.831\pi)$, respectively. The outputs and envelopes in forward and backward configurations for points A and B are shown in Fig. B.4.

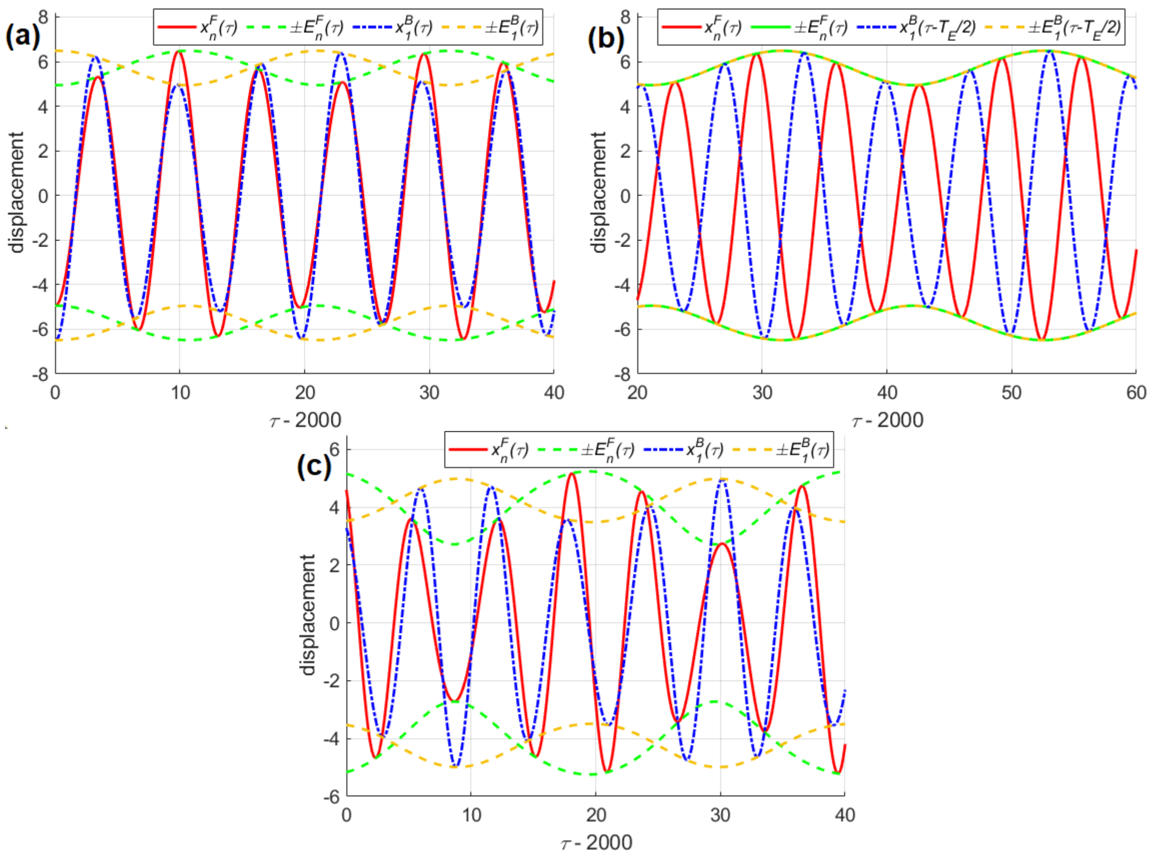

Figure B.4: Displacements and envelopes as functions of time. Red and blue curves indicate plots of $x_n^F(\tau)$ and $x_1^B(\tau)$, respectively. Green and yellow dashed curves indicate plots of $\pm E_n^F(\tau)$ and $\pm E_1^B(\tau)$ respectively. (a) Time-domain response at point 'A'; (b) time-domain response at point 'a' with a temporal shift; (c) time-domain response at point 'B'.

We observe that, the response envelopes in different configurations at point A have the same shape with a temporal shift equal to half a period: $E_n^F(\tau) = E_1^B(\tau \pm T_E/2)$, as shown in Figs. B.4(a) and B.4(b). However, $x_n^F(\tau)$ is not equal to $x_1^B(\tau + T_E/2)$ or $x_1^B(\tau - T_E/2)$ due to the phase different between the two carrier waves, as shown in Fig. B.4(b). At point B, shapes of the envelopes in different configurations are not the same, as shown in Fig. B.4(c).

B.3.2. Strong modulation

We now turn our attention to the case of strong modulations. A critical feature of strong modulations is the appearance of parametric instabilities [20].The response of the system we study here becomes unbounded when this instability occurs. While we postpone a formal stability analysis to future work, we have checked by direct numerical integration that all the results we present here are stable.

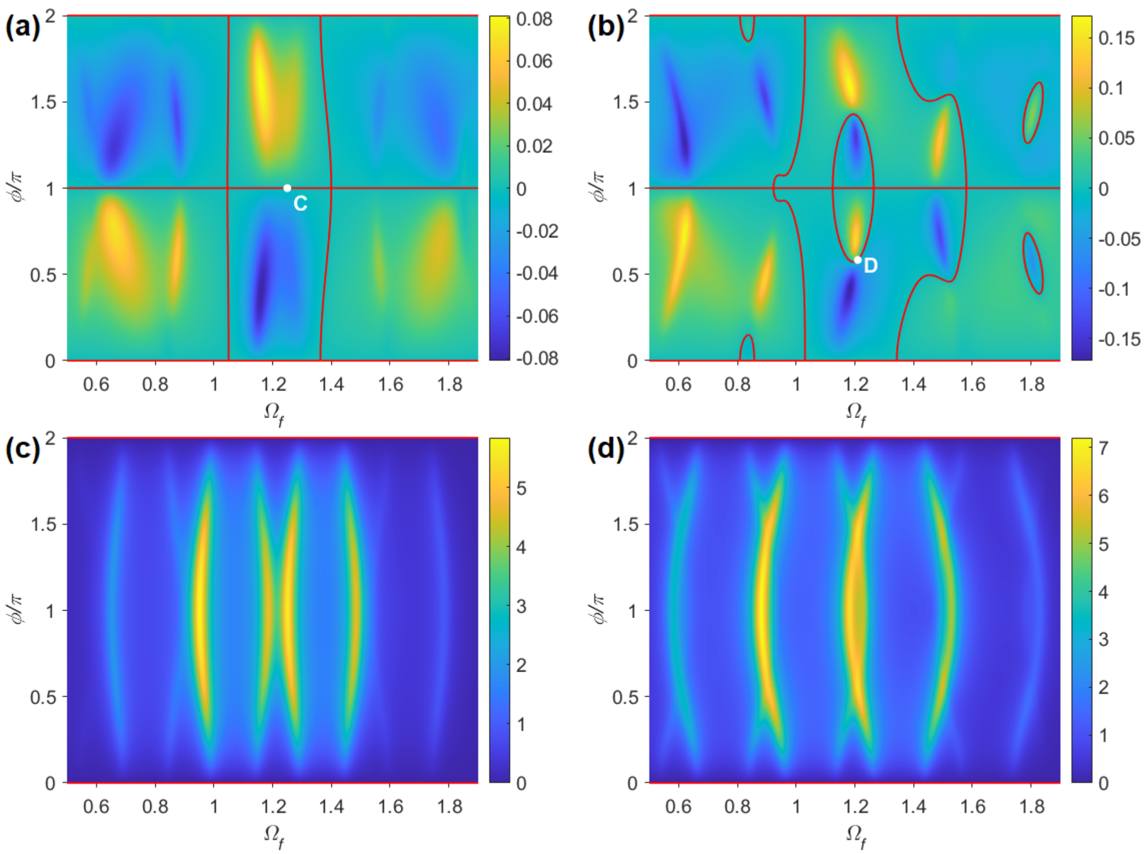

Figure B.5: R_N and R as functions of Ω_f and ϕ. Red curves indicate combinations of Ω_f and ϕ where $R_N = 0$ or $R = 0$ in corresponding plots. (a) Norm bias, R_N, for $n = 2$ and $K_m = 0.4$; (b) norm bias, R_N, for $n = 2$ and $K_m = 0.7$; (c) reciprocity bias, R, for $n = 2$ and $K_m = 0.4$; (d) reciprocity bias, R, for $n = 2$ and $K_m = 0.7$.

Fig. B.5 shows the reciprocity bias R and norm bias R_N for the 2 DoF system with $K_m = 0.4$ and $K_m = 0.7$; the remaining system parameters are the same as the examples in Fig. B.3. We observe in Fig. B.5(a) that the locus of phase nonreciprocity ($R_N = 0$), when compared to Fig. B.3(a), has a higher curvature (looks bent). This is caused by the relatively higher modulation amplitude. Despite the difference between the locus of $R_N = 0$ in Figs. B.3(a) and B.5(a), in both cases the (Ω_f, ϕ) plane is divided into six regions by the contour of $R_N = 0$. If K_m is large enough, the contour of $R_N = 0$ for *Type II* phase nonreciprocity becomes more complex and the (Ω_f, ϕ) plane is divided into more regions, as shown in Fig. B.5(b).

Figs. B.5(c) and B.5(d) show the variation of the reciprocity bias corresponding to Figs. B.5(a) and B.5(b), respectively. Non zero values of the reciprocity norm indicate that the response is indeed nonreciprocal along the locus of $R_N = 0$. We do not expect to encounter $R = 0$ along

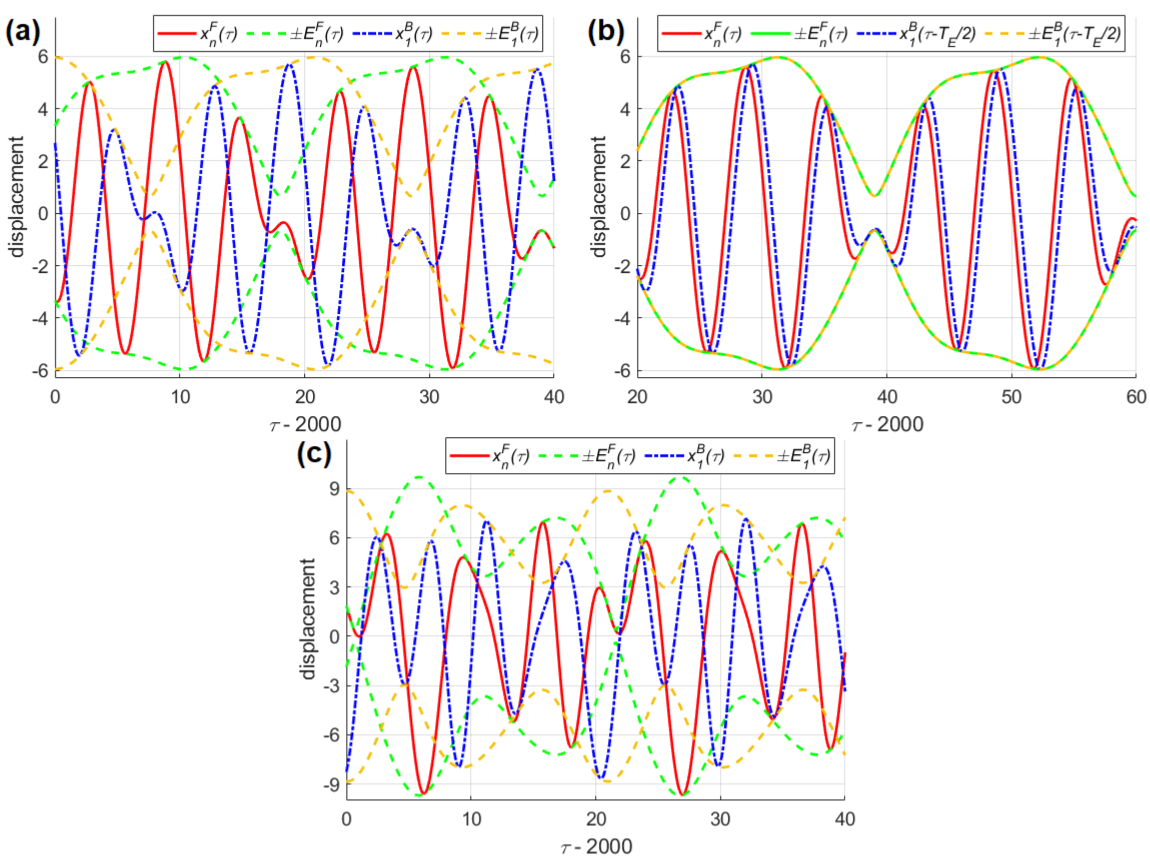

Figure B.6: Displacements and envelopes as functions of time. Red and blue curves indicate plots of $x_n^F(\tau)$ and $x_1^B(\tau)$, respectively. Green and yellow dashed curves indicate plots of $\pm E_n^F(\tau)$ and $\pm E_1^B(\tau)$ respectively. (a) Time-domain response at point 'C'; (b) time-domain response at point 'C' with a temporal shift; (c) time-domain response at point 'D'.

the locus of $R_N = 0$ in this problem because ϕ is the only symmetry-breaking parameter in this problem [19].

We choose two combinations of Ω_f and ϕ in Fig. B.5 to show Type I (point C) and Type II (point D) phase nonreciprocal response in the time domain. Their coordinates in the (Ω_f, ϕ) plane are: $(1.25, \pi)$ for C and $(1.21, 0.584\pi)$ for D. The corresponding outputs and response envelopes in forward and backward configurations are plotted in Fig. B.6.

Figs. B.6(a) and B.6(b) show that $E_n^F(\tau) = E_1^B(\tau \pm T_E/2)$ and $x_n^F(\tau)$ is not equal to $x_1^B(\tau + T_E/2)$ or $x_1^B(\tau - T_E/2)$ at point C. For *Type I* phase nonreciprocity, the response envelopes in different configurations having the same shape is valid not only in weakly modulated systems, but also in strongly modulated systems. For the *Type II* phase nonreciprocal case at point D, the shapes of the envelopes in different configurations are not the same, as shown in Fig. B.6(c).

B.3.3. More on the two types of phase nonreciprocity

Table B.1: Complex amplitudes for points 'A', 'B', 'C' and 'D'.

	Type I phase nonreciprocity		*Type II* phase nonreciprocity	
	Point 'A'	Point 'B'	Point 'C'	Point 'D'
η_{-2}	$0.004 - 0.003i$	$-0.024 + 0.237i$	$0.002 - 0.003i$	$-0.242 + 0.134i$
ξ_{-2}	$0.004 - 0.003i$	$-0.024 + 0.237i$	$-0.004 - 0.001i$	$-0.586 + 0.641i$
η_{-1}	$0.061 - 0.043i$	$-0.046 + 1.947i$	$-0.055 - 0.077i$	$-0.398 - 1.094i$
ξ_{-1}	$-0.061 + 0.043i$	$0.046 - 1.947i$	$0.094 + 0.025i$	$0.583 - 1.207i$
η_0	$2.474 - 1.443i$	$-0.881 + 0.634i$	$-1.983 - 0.315i$	$2.109 - 0.276i$
ξ_0	$2.474 - 1.443i$	$-0.881 + 0.634i$	$-2.030 - 0.358i$	$-2.142 - 0.436i$
η_1	$0.263 - 0.164i$	$0.393 + 0.034i$	$0.543 + 0.367i$	$1.354 - 0.210i$
ξ_1	$-0.263 + 0.164i$	$-0.393 - 0.034i$	$-0.393 - 0.239i$	$-0.138 - 1.476i$
η_2	$-0.011 + 0.005i$	$-0.037 + 0.003i$	$-0.038 + 0.034i$	$-1.328 - 0.091i$
ξ_2	$-0.011 + 0.005i$	$-0.037 + 0.003i$	$-0.023 - 0.047i$	$-0.133 - 0.407i$

To show the outputs of *Type I* and *Type II* phase nonreciprocal cases in more detail, some complex amplitudes (η_q and ξ_q, $q \in [-2, 2]$) of outputs in forward and backward configurations are calculated for points 'A', 'B', 'C' and 'D', listed in Table B.1.

For the outputs of *Type I* phase nonreciprocal cases, we find that: $\eta_q = (-1)^q \xi_q$ for any integer q, which means $|\eta_q| = |\xi_q|$ and the difference between the arguments of η_q and ξ_q is $q\pi$. This leads to the interesting relation between two envelopes: $E_n^F(\tau) = E_1^B(\tau \pm T_E/2)$. This relation is valid for every case of *Type I* phase nonreciprocity. In contrast, we could not find such a straightforward mathematical relation between η_q and ξ_q for the outputs of *Type II* phase nonreciprocal cases.

B.4. Long modulated systems

In this section, we compute the locus of phase nonreciprocity for weakly modulated systems with many DoF (40, 60 and 100). All the system parameters, except the number of units, are the same as those used in Fig. B.3. Fig. B.7 shows that the regions of $R_N > 0$ and $R_N < 0$ on the (Ω_f, ϕ) plane tend to be somewhat independent from n. Therefore, the red curves indicating $R_N = 0$ do not change significantly with n in the examples in Fig. B.7. The zig-zags in the red curves, however, reduce in amplitudes as n increases.

Comparing the magnitudes of R_N in the examples in Figs. B.3 and B.7, we observe that the differences in transmitted amplitudes are very small in short systems compared to long systems; e.g. compare the scales of the color bars in Fig. B.3(b) to Fig. B.7(a). In long

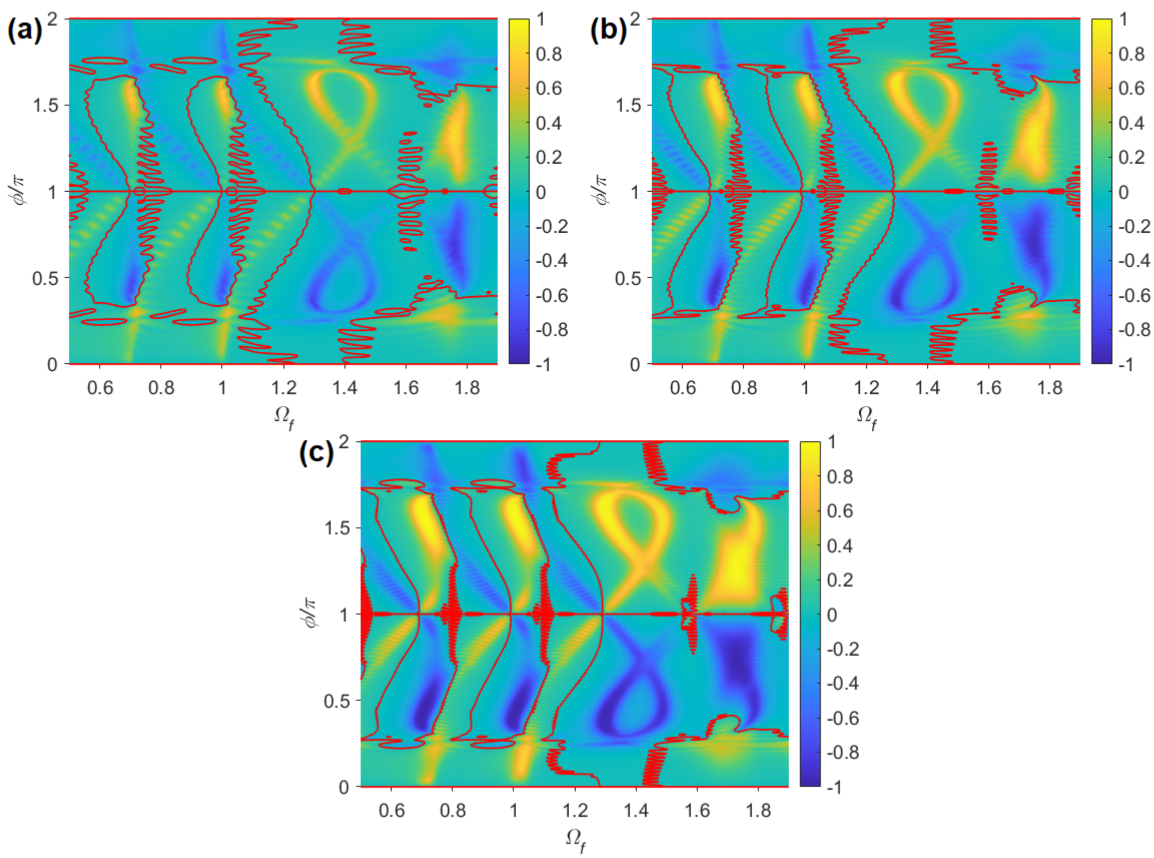

Figure B.7: R_N as a function of Ω_f and ϕ. Red curves indicate combinations of Ω_f and ϕ where $R_N = 0$. (a) Norm bias, R_N, for a 40 DoF system; (b) norm bias, R_N, for a 60 DoF system; (c) norm bias, R_N, for a 100 DoF system.

systems, unidirectional vibration transmission can occur in some regions on the (Ω_f, ϕ) plane, indicated by $|R_N| \approx 1$. Further numerical studies convergence of the patterns in Fig. B.7 are ongoing.

B.5. Conclusions

We presented the application of the response envelopes for analyzing the non-periodic steady-state response of a discrete system with spatiotemporal modulation. Phase nonreciprocity was identified in the numerical analysis of short and long systems. Furthermore, two types of phase nonreciprocity were introduced: *Type I* phase nonreciprocity represents the phase nonreciprocal cases that always happen if the system has an even number of DoF and the phase shift between every two adjacent modulations is $\pm\pi$; *Type II* phase nonreciprocity represents the cases in which nonreciprocal phase shift occur for specific combinations of system parameters and forcing frequencies, when the phase shift between every two adjacent modulations is not $\pm\pi$.

References

[1] J. D. Achenbach, Reciprocity in elastodynamics, Cambridge University Press, Cambridge, UK, 2003.

[2] S. Andrieux, A. B. Abda, H. D. Bui, "Reciprocity principle and crack identification," *Inverse Problems*, vol. 15, no. 1, pp. 59-65, 1999.

[3] T. Ten Wolde, "Reciprocity measurements in acoustical and mechano-acoustical systems. Review of theory and applications," *Acta Acustica united with Acustica*, vol. 96, no. 1, pp. 1 - 13, 2010.

[4] H. Nassar, B. Yousefzadeh, R. Fleury, M. Ruzzene, A. Alù, C. Daraio, A. N. Norris, G. Huang, M. R. Haberman, "Nonreciprocity in Acoustic and Elastic Materials," *Nature Reviews Materials*, vol. 5, pp. 667-685, 2020.

[5] K. A. Lurie, An Introduction to the Mathematical Theory of Dynamic Materials, Second Edition, Springer Cham, 2017.

[6] H. Nassar, H. Chen, A. N. Norris, M. R. Haberman, "Non-reciprocal Wave Propagation in Modulated Elastic Metamaterials," *Proc. R. Soc. A*, vol. 473, no. 2202, 2017.

[7] G. Trainiti, M. Ruzzene, "Non-reciprocal Elastic Wave Propagation in Spatiotemporal Periodic Structures," *New Journal of Physics*, vol. 18, p. 083047, 2016.

[8] E. Riva, J. Marconi, G. Cazzulani, F. Braghin, "Generalized Plane Wave Expansion Method for Non-reciprocal Discretely Modulated Waveguides," *Journal of Sound and Vibration*, vol. 449, pp. 172-181, 2019.

[9] M. A. Attarzadeh, M. Nouh, "Elastic Wave Propagation in Moving Phononic Crystals and Correlations with Stationary Spatiotemporally Modulated Systems," *AIP Advances*, vol. 8, p. 105302, 2018.

[10] H. Nassar, X. C. Xu, A. N. Norris, G. L. Huang, "Modulated Phononic Crystals: Non-reciprocal Wave Propagation and Willis Materials," *Journal of the Mechanics and Physics of Solids*, vol. 101, pp. 10-29, 2017.

[11] Y. Wang, B. Yousefzadeh, H. Chen, H. Nassar, G. Huang, C. Daraio, "Observation of Nonreciprocal Wave Propagation in a Dynamic Phononic Lattice," *Physical Review Letters*, vol. 121, no. 19, p. 194301, 2018.

[12] S. Wan, L. Cao, Y. Zeng, T. Guo, M. Oudich, B. Assouar, "Low-Frequency Nonreciprocal Flexural Wave Propagation via Compact Cascaded Time-Modulated Resonators," *Applied Physics Letters*, vol. 120, no. 23, p. 231701, 2022.

[13] Y. Chen, X. Li, H. Nassar, A.N. Norris, C. Daraio, G. Huang, "Nonreciprocal wave propagation in a continuum-based metamaterial with space-time modulated resonators," *Physical Review Applied*, vol. 11, no. 6, p. 064052, 2019.

[14] B. L. Kim, C. Daraio, C. Chong, S. Hajarolasvadi, Y. Wang, "Dynamics of time-modulated, nonlinear phononic lattices," *Physical Review E*, vol. 107, p. 034211, 2023.

[15] R. Verba, E. N. Bankowski, T. J. Meitzler, V. Tiberkevich, A. Slavin, "Phase Nonreciprocity of Microwave-Frequency Surface Acoustic Waves in Hybrid Heterostructures with Magnetoelastic Coupling," *Advanced Electronic Materials*, vol. 7, no. 8, p. 2100263, 2021.

[16] D. A. Bas, R. Verba, P. J. Sah, S. Leontsev, A. Matyushov, M. J. Newburger, N. X. Sun, V. Tiberkevich, A. Slavin, M. R. Page, "Nonreciprocity of Phase Accumulation and Propagation Losses of Surface Acoustic Waves in Hybrid Magnetoelastic Heterostructures," *Physical Review Applied*, vol. 18, no. 4, p. 044003, 2022.

[17] J. Wu, B. Yousefzadeh, "On Vibration Transmission Reciprocity In Modulated Materials," in *Canadian Society for Mechanical Engineering International Congress*, Edmonton, 2022.

[18] B. Yousefzadeh, "Computation of Nonreciprocal Dynamics in Nonlinear Materials," *Journal of Computational Dynamics*, vol. 9, no. 3, pp. 451-464, 2022.

[19] A. Giraldo, B. Yousefzadeh "Restoring the Reciprocity Invariance in Nonlinear Systems with Broken Mirror Symmetry," *Extreme Mechanics Letters*, p.102008, 2023.

[20] I. Kovacic, R. Rand, S. M. Sah, "Mathieu's Equation and Its Generalizations: Overview of Stability Charts and Their Features," *Applied Mechanics Reviews*, vol. 70, no. 2, p. 020802, 2018.

C. Nonreciprocal dynamics of spatiotemporally varying materials: strong modulations

C.1. Introduction

For a material with time-independent properties, transmission of low-amplitude (linear) vibrations between two points remains unchanged when the locations of the source and the receiver are interchanged. This invariance property is called reciprocity. Reciprocity has led to development of various wave processing techniques and industrial applications, for instance, calibration of hydrophones and crack identification [1-3]. However, vibration transmission properties (speed, amplitude, phase, etc.) that are dependent on the direction of transmission cannot be realized in reciprocal systems. Many researchers have recently focused on developing methods to break reciprocity invariance and realize direction-dependent vibration transmission [4].

Nonreciprocal vibration transmission can occur in a material that has one or more effective properties (*e.g.* effective mass or stiffness) change in both time and space [5]. We refer to a material with such properties as a modulated material. Modulation refers to a time-dependent term (normally periodic) in an effective property, typically the stiffness of the material. Models of discrete and continuous periodic modulated materials are commonly used in the studies on nonreciprocal vibration transmission. The smallest repetitive substructure in a periodic material is a unit cell. The modulation characteristics in each unit cell determine how vibrations transmit differently towards opposite directions in the modulated material.

The difference between transmitted amplitudes in opposite directions (amplitude bias) is an effective way to identify nonreciprocity. As the extreme case of different transmitted amplitudes, unidirectional wave propagation in one-dimensional (1-D) continuous modulated media was recognized by directional bandgaps in their dispersion curves. Such studies were carried out in multiple spatially periodic models with wave-like spatiotemporal modulation in elasticity [5-11]. In contrast, systems of finite length were used to perform experimental studies on nonreciprocal vibration transmission in 1-D spatiotemporally modulated systems, where nonreciprocity is identified by the differences between the left-to-right and right-to-left transmitted amplitudes in the steady state [12-15].

The amplitude bias can be increased by adding more modulated units to the system. For the steady-state vibration transmission in short discrete systems with weak modulations, it is very difficult to observe the difference between the transmitted amplitudes because nonreciprocity is mostly caused by the difference between the transmitted phases [16]. Without changing the length of a discrete system, the difference between the transmitted amplitudes can get higher by increasing the strength of the spatiotemporal modulations [17]. But strong modulations may lead to the system being unstable and result in unbounded response [18]. In this work, we investigate nonreciprocal vibration transmission in the steady state with a focus on the difference between transmitted energies. Based on Floquet theory, we develop a numerical approach to determine the stability of the modulated system and obtain the stability chart. We thus identify modulation parameters that correspond to stable response of the system. This is important for safe and reliable operation of devices with spatiotemporally modulated properties.

We present the problem formulation and solution methodology in Section C.2. In Section C.3, the approach used to determine stability of the modulated system is introduced and a sample stability chart is presented. Nonreciprocal energy transmission in different systems is discussed in Section C.4. The findings of this work are summarized in Section C.5.

C.2. Spatiotemporally modulated systems

C.2.1. Problem setup

Fig. C.1 shows schematically the modulated system we study in this work. Two forces, $f_1(\tau) = P_1 \cos(\Omega_f \tau)$ and $f_n(\tau) = P_n \cos(\Omega_f \tau)$, are applied on the first mass and the last mass, respectively. The modulations in this system are represented by the time-varying terms in

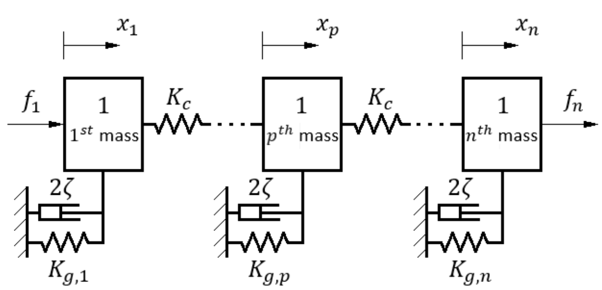

Figure C.1: Scheme of the nDoF system.

stiffness of grounding springs: $K_{g,p} = 1 + K_m \cos(\Omega_m \tau - \phi_p)$, where $p = 1, 2, \cdots, n$ and $\phi_p = (p-1)\phi$. The constant representing a spatial modulation along the 1-D system, ϕ, breaks the mirror symmetry of the system, thus enabling nonreciprocal vibration transmission [16].

The equations of motion for this system are:

$$
\begin{aligned}
\ddot{x}_1 + 2\zeta\dot{x}_1 + [1 + K_m \cos(\Omega_m \tau)]x_1 + K_c(x_1 - x_2) &= P_1 \cos(\Omega_f \tau) \\
&\vdots \\
\ddot{x}_p + 2\zeta\dot{x}_p + [1 + K_m \cos(\Omega_m \tau - \phi_p)]x_p + K_c(2x_p - x_{p-1} - x_{p+1}) &= 0 \\
&\vdots \\
\ddot{x}_n + 2\zeta\dot{x}_n + [1 + K_m \cos(\Omega_m \tau - \phi_n)]x_n + K_c(x_n - x_{n-1}) &= P_n \cos(\Omega_f \tau)
\end{aligned}
\tag{C.1}
$$

where $\ddot{x}_p$ and $\dot{x}_p$ represent $d^2x_p/d\tau^2$ and $dx_p/d\tau$ respectively. All parameters used in this work are dimensionless.

In this study, we investigate nonreciprocal transmission of steady-state vibrations. Two configurations are defined to distinguish between the opposite transmission directions through the 1-D system: (i) the *forward* (from left to right) configuration with $P_1 = P$ and $P_n = 0$ where the output is the steady-state response of the n^{th} mass, $x_n^F(\tau)$; (ii) the *backward* (from right to left) configuration with $P_1 = 0$ and $P_n = P$ where the output is the steady-state response of the 1^{st} mass, $x_1^B(\tau)$.

Output norms N^F and N^B are used to quantify the strength of outputs, which is the transmitted energy in different configurations. N^F and N^B are defined as:

$$N^F = \lim_{T\to\infty} \sqrt{\frac{1}{T}\int_0^T [x_n^F(\tau)]^2 d\tau} \tag{C.2a}$$

$$N^B = \lim_{T\to\infty} \sqrt{\frac{1}{T}\int_0^T [x_1^B(\tau)]^2 d\tau} \tag{C.2b}$$

Norm bias R_N is introduced to quantify the degree of nonreciprocity in terms of the output norms (transmitted vibration energies) only:

$$R_N = \frac{N^F - N^B}{N^F + N^B} \tag{C.3}$$

A zero norm bias, $R_N = 0$, corresponds to equal output norms (transmitted energies) for the *forward* and *backward* configurations. $R_N = 0$ is not equivalent to reciprocal vibration transmission because R_N is unable to identify different transmitted phases in two configurations. By constructions, we have $-1 \leq R_N \leq 1$, where the limit values indicate that the output norm in one of the configurations is much larger than the other one, that is, unidirectional vibration transmission.

C.2.2. Solution methodology

Approximate analytical expressions for outputs in *forward* and *backward* configurations can be obtained by using the averaging method, which is based on the quasi-periodic form of the steady-state response:

$$x_n^F(\tau) = \sum_{q=-\mathcal{F}}^{\mathcal{F}} [y_{n,q}^F e^{i(\Omega_f + q\Omega_m)\tau} + c.c.] \tag{C.4a}$$

$$x_1^B(\tau) = \sum_{q=-\mathcal{F}}^{\mathcal{F}} [y_{1,q}^B e^{i(\Omega_f + q\Omega_m)\tau} + c.c.] \tag{C.4b}$$

where $y_{n,q}^F$ and $y_{1,q}^B$ are complex amplitudes of each harmonic component, and *c.c.* represents the corresponding complex conjugate. For a given Ω_f and other system parameters, $y_{n,q}^F$ and $y_{1,q}^B$ can be calculated by using the averaging method as outlined in [16]. $\mathcal{F}$ determines the number of harmonic components in each output. Increasing $\mathcal{F}$ can improve the accuracy of the approximated solution, particularly when K_m or n is large.

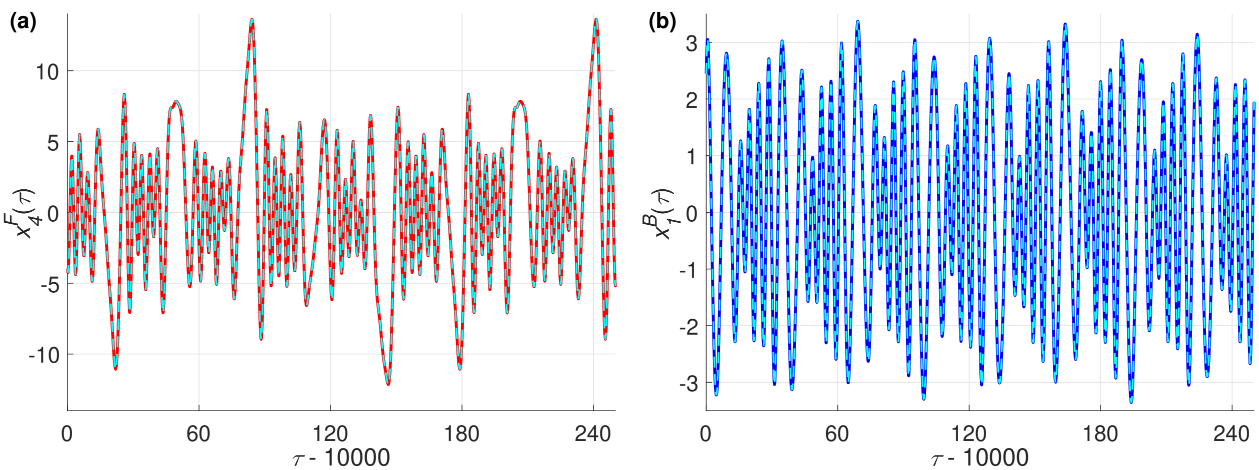

Figure C.2: Comparison between the output displacements computed using the averaging method (solid curves) and the Runge-Kutta method (cyan dashed curves). (a): $n = 4$, $\phi = 0.94\pi$, $K_m = 1.46$, $\Omega_f = 0.96$ and $\mathcal{F} = 25$, in *forward* configuration; (b): $n = 8$, $\phi = 0.41\pi$, $K_m = 0.91$, $\Omega_f = 0.73$ and $\mathcal{F} = 14$, in *backward* configuration.

Displacements in the steady state are calculated for (C.1) for the following parameters: $K_c = 0.6$, $\Omega_m = 0.2$, $\zeta = 0.01$ and $P = 1$, as shown in Fig C.2. To validate the predictions made by the averaging method, the response of (C.1) is computed using the Runge-Kutta method until the steady state is reached. Fig. C.2 shows that the averaging method predicts the steady-state response of the system accurately for these sets of system parameters; the accuracy was also confirmed for other sets of system parameters that lead to the steady-state response in this work.

C.3. Stability analysis

In this work, our investigations on nonreciprocal energy transmission are performed for the steady-state response of the modulated system. However, the response of the modulated system may become unstable and grow without a bound (diverge). Equation (C.1) is a set of coupled Mathieu's equations with external forces. When $K_m \neq 0$, (C.1) contains parametric excitations each of which is the product of a periodic (cosine) function and displacement of a mass. As the result, regardless of $f_1(\tau)$ and $f_n(\tau)$, the response of the modulated system can stay bounded (stable) or the response can become unbounded (unstable). Unbounded response does not reach a steady state in a linear system. Thus, stability analysis for the modulated system is necessary, and unstable scenarios have to be avoided.

C.3.1. Solution methodology

If $P_1 = P_n = 0$, (C.1) can be transformed into a first order differential equation:

$$\frac{\mathrm{d}}{\mathrm{d}\tau}\underline{X} = \underline{\underline{\mathsf{A}}}(\tau)\ \underline{X} \tag{C.5}$$

where $\underline{X} = [\dot{x}_1, \cdots, \dot{x}_n, x_1, \cdots, x_n]^T$ is a $2n \times 1$ vector. $\underline{\underline{\mathsf{A}}}(\tau)$ is a $2n \times 2n$ matrix, it can be rewritten as:

$$\underline{\underline{\mathsf{A}}}(\tau) = \begin{bmatrix} \underline{\underline{\mathsf{D}}} & \underline{\underline{\mathsf{C}}}(\tau) \\ \underline{\underline{I}} & \underline{\underline{O}} \end{bmatrix} \tag{C.6}$$

where $\underline{\underline{\mathsf{D}}}$, $\underline{\underline{\mathsf{C}}}(\tau)$, $\underline{\underline{I}}$ and $\underline{\underline{O}}$ are all $n \times n$ matrices. $\underline{\underline{O}}$ is a zero matrix, $\underline{\underline{I}}$ is an identity matrix and $\underline{\underline{\mathsf{D}}} = -2\zeta\underline{\underline{I}}$. $\underline{\underline{\mathsf{C}}}(\tau)$ can be expressed as:

$$\underline{\underline{\mathsf{C}}}(\tau) = \begin{bmatrix} \mathsf{B}_1(\tau) & K_c & 0 & \cdots & 0 \\ K_c & \mathsf{B}_2(\tau) & K_c & \cdots & 0 \\ 0 & K_c & \mathsf{B}_3(\tau) & \cdots & 0 \\ \vdots & \vdots & \vdots & \ddots & \vdots \\ 0 & 0 & 0 & \cdots & \mathsf{B}_n(\tau) \end{bmatrix} \tag{C.7}$$

where $\mathsf{B}_p(\tau) = -K_c - [1 + K_m \cos(\Omega_m\tau - \phi_p)]$ for $p \in \{1, n\}$, and $\mathsf{B}_p(\tau) = -2K_c - [1 + K_m \cos(\Omega_m\tau - \phi_p)]$ for $p \in \{2, \cdots, n-1\}$ when $n \geq_A ppx_C.3$. In matrix $\underline{\underline{\mathsf{C}}}(\tau)$, the elements in first super diagonal and first subdiagonal are all K_c; with the exception of the elements in its main diagonal, first super diagonal and first subdiagonal, all the elements are zero. Matrices $\underline{\underline{\mathsf{C}}}(\tau)$ and $\underline{\underline{\mathsf{A}}}(\tau)$ are therefore periodic and their period is $T = 2\pi/\Omega_m$.

Next, Floquet theory, the general theory of linear differential equations with periodic coefficients, is applied to determine the stability of the response [18,19]. For a given initial condition $\underline{X}_r(0)$, the transient response at $\tau = T$ is calculated from direct numerical integration of (C.5), denoted by $\underline{X}_r(T)$. The initial condition $\underline{X}_r(0)$ has its r^{th} element equal to 1 and all its other elements equal to zero. By changing r from 1 to $2n$, we obtain a set of solution vectors: $\underline{X}_1(T), \underline{X}_2(T), \cdots, \underline{X}_{2n}(T)$. A square matrix is then constructed from these solution vectors:

$$\underline{\underline{\mathsf{E}}} = \left[\underline{X}_1(T) \quad \underline{X}_2(T) \quad \cdots \quad \underline{X}_{2n}(T) \right] \tag{C.8}$$

If every eigenvalue of $\underline{\underline{\mathsf{E}}}$ has absolute value less than 1, then the response of (C.5) is stable; if any one eigenvalue of $\underline{\underline{\mathsf{E}}}$ has absolute value greater than 1, the response of (C.5) is unstable.

Any external force can be seen as a sum of impulses at various infinitesimal time intervals. An arbitrary impulse on a still system at $\tau = \tau_i$ brings a nonzero motion $\underline{X}_i(\tau_i)$, which is equal to a linear combination of $\underline{X}_1(0)$, $\underline{X}_2(0)$, $\cdots$, $\underline{X}_{2n}(0)$. $\underline{X}_i(\tau_i)$ can be seen as an initial condition starting from $\tau = \tau_i$. All equations in (C.1) are linear equations. According to the principle of superposition, if (C.5) has been proven stable by the approach based on Floquet theory, the initial condition $\underline{X}_i(\tau_i)$ will not lead to unstable motion. Therefore, P_1, P_n and Ω_f have no effect on the stability of (C.1), and the stability of the modulated system shown in Fig. C.1 can be determined by this numerical approach based on Floquet theory.

C.3.2. Stability of n DoF modulated systems

We focus on investigating the effects of the modulation parameters, K_m and ϕ, on the stability of the modulated system shown in Fig. C.1. In this section, we use $n = 4$, $K_c = 0.6$, $\zeta = 0.01$ and $\Omega_m = 0.2$ and determine stability for different combinations of K_m and ϕ. Fig.C.3 shows the stability chart for the modulated system with 4DoF. In Fig. C.3, white regions represent the combinations of K_m and ϕ that result in stable response; grey regions represent the combinations of K_m and ϕ that result in unstable response.

We choose two points which are labelled as 'A' (stable) and 'B' (unstable) in Fig. C.3. Their coordinates in the (K_m,ϕ) plane are $(1.42, 0.9\pi)$ and $(1.1, 0.1\pi)$, respectively. Their displacements in time domain are computed using the Runge-Kutta method, as shown in Fig. C.4. Inside the stable regions of a stability chart, the response of the modulated system is a quasi-periodic function of τ, and it stays bounded, as shown in Fig. C.4(a). In contrast, inside the unstable regions, the response of the modulated system grows exponentially in time, as shown in Fig. C.4(b).

The stability chart is symmetric about the plane $\phi = \pi$. Both K_m and ϕ influence the stability of the response. In general, a larger K_m is more likely to bring instability than a

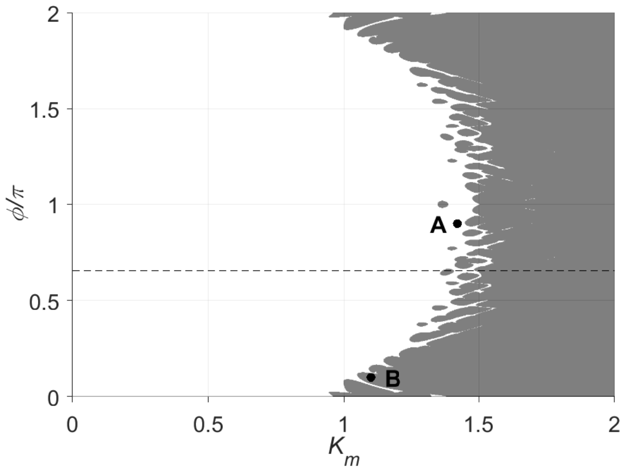

Figure C.3: Stability chart of a 4DoF modulated system with $K_c = 0.6$.

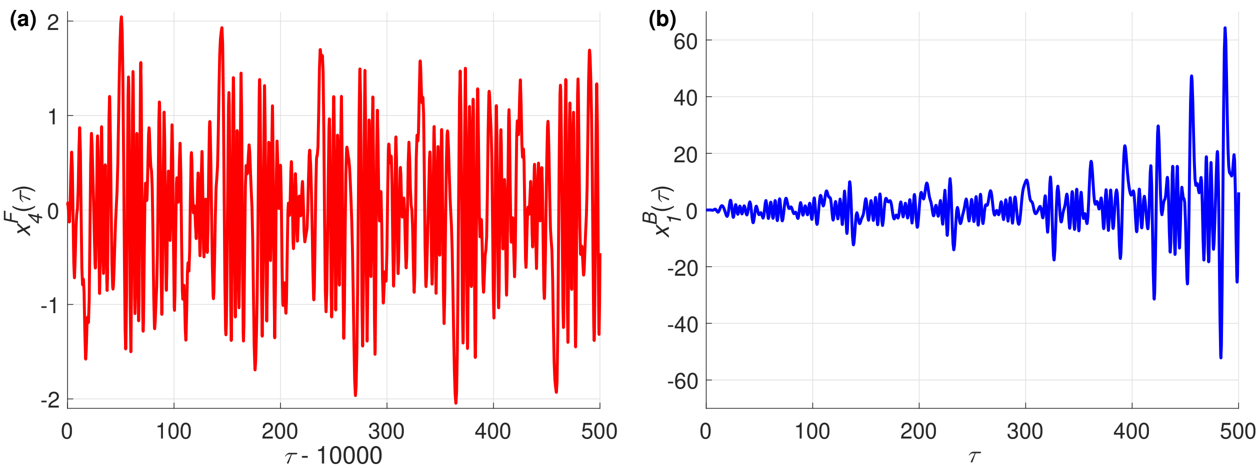

Figure C.4: Time-domain response. (a): $x_4^F(\tau)$ with $\Omega_f = 1.27$ and $P = 1$, at point A; (b): $x_1^B(\tau)$ with $\Omega_f = 1.13$ and $P = 1$, at point B.

smaller K_m, and a modulated system with ϕ closer to π is more tolerant of strong modulations. However, in some scenarios, a larger K_m results in stable response but a smaller K_m does not, although ϕ and other parameters remain unchanged; the horizontal dashed line ($\phi = 0.655\pi$) in Fig. C.3 indicates an example of this scenario: $K_m = 1.37$ is in an unstable region while $K_m = 1.47$ is in a stable region.

In order to ensure the stability of the steady-state response of various modulated systems in *forward* and *backward* configurations, the values of ϕ and K_m should be chosen from the white (stable) regions of corresponding stability charts. Using the approach introduced in this section, we have checked that all the results we present in this work are stable, unless otherwise stated.

C.4. Nonreciprocal energy transmission in modulated systems

In this section, we first investigate nonreciprocal energy transmission by exploring the effects of K_m and n on the magnitude of R_N. We use $K_c = 0.6$, $\zeta = 0.01$, $\Omega_m = 0.2$ and $P = 1$ throughout this section, and calculate R_N as a function of Ω_f and ϕ by using the averaging method.

Fig C.5 shows surface plots of R_N for the modulated systems with different combinations of K_m and n. The values of K_m and n are chosen such that they result in the same range of

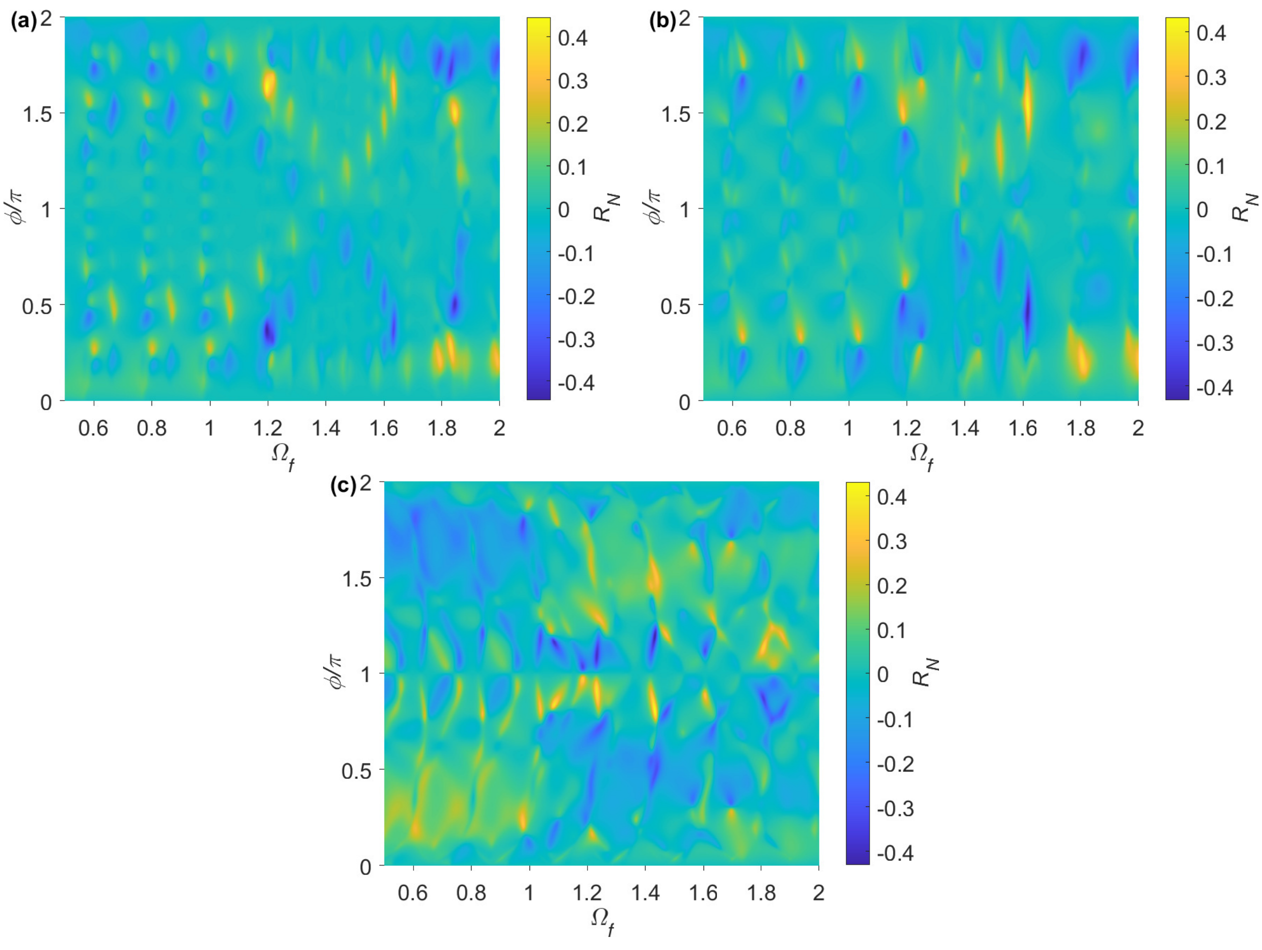

Figure C.5: R_N as a function of Ω_f and ϕ. (a): $n = 12$, $K_m = 0.1$, (b): $n = 7$, $K_m = 0.22$, (c): $n = 4$, $K_m = 0.9$.

values for R_N. These results indicate that to keep the magnitude of R_N unchanged, we can increase the modulation amplitude and reduce the number of unit cells in the system.

Next, we keep increasing the modulation amplitude for the short system with 4DoF. Fig. C.6(a) shows R_N for the short system with $K_m = 1.32$. It is shown in Fig. C.3 that, when $K_m =$

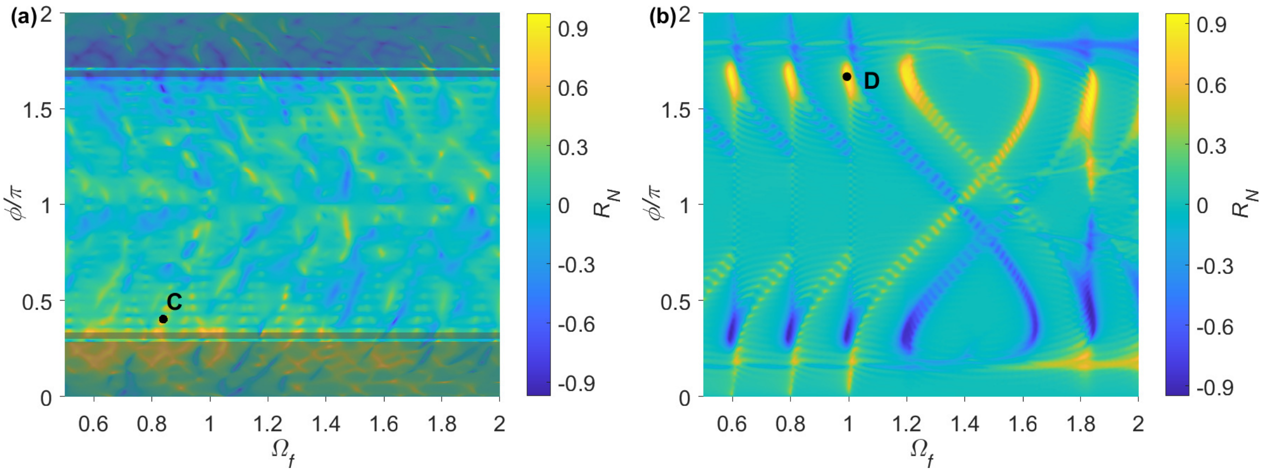

Figure C.6: R_N as a function of Ω_f and ϕ. (a): $n = 4$, $K_m = 1.32$, (b): $n = 55$, $K_m = 0.1$.

1.32, the following parameter ranges of ϕ correspond to an unstable response: $(0, 0.287\pi)$, $(0.299\pi, 0.333\pi)$, $(1.667\pi, 1.701\pi)$ and $(1.713\pi, 2\pi)$; these ranges of unstable response are indicated by the shaded rectangular zones in Fig. C.6(a). In these shaded zones, the results of R_N are invalid, and we must not choose the value of ϕ from them.

Fig. C.6(b) shows R_N for a long system, with $K_m = 0.1$ and $n = 55$ chosen such that R_N varies in the same range as in Fig. C.6(a). Nearly unidirectional vibration transmission ($|R_N| \geq 0.9$) can happen in both modulated systems. The regions of $|R_N| \geq 0.9$ in Fig. C.6(b) are larger and more 'organized' than those in Fig. C.6(a).

To better illustrate the nearly unidirectional vibration transmission cases in these two systems, we choose two points which are labelled as 'C' and 'D' in Fig. C.6(a) and Fig. C.6(b). Their coordinates in the (Ω_f,ϕ) plane are (0.84,0.403π) and (0.994,1.667π), respectively. Point C lies in the stable region of Fig. C.6(a). At both points, $R_N = 0.93$. Outputs in *forward* and *backward* configurations at points C and D are computed, shown in Fig. C.7.

At point C, output norms are $N_C^F = 40.917$ and $N_C^B = 1.515$; at point D, output norms are $N_D^F = 0.7051$ and $N_D^B = 0.0255$. If both systems are time-invariant, i.e. $K_m = 0$, vibration transmission in each of them is reciprocal. In this case, output norms at points C and D are $N_C = 0.2279$ and $N_D = 9.843 \times 10^{-4}$, respectively. Both N_C^F and N_C^B are greater than N_C, and both N_D^F and N_D^B are greater than N_D. Therefore, at points C and D, modulations in both systems acting as inner excitations amplify the transmitted energies in both *forward* and *backward* configurations. Specifically, this amplifying effect is dependent on the direction of transmission, which leads to nonreciprocal energy transmission.

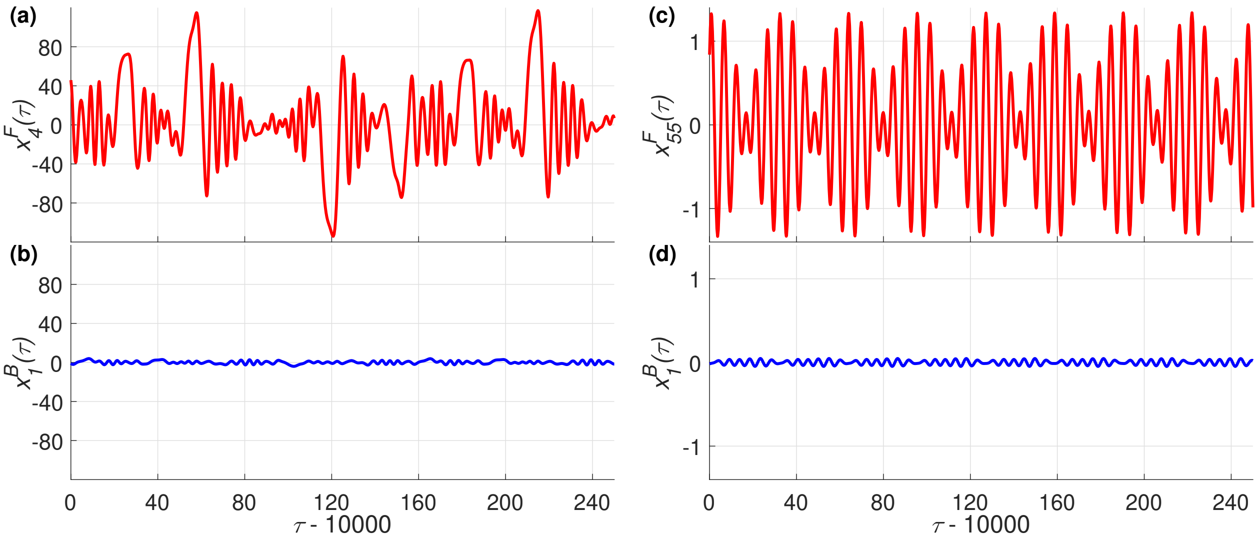

Figure C.7: Time-domain response. (a) and (b): Outputs at point C, (c) and (d): outputs at point D.

C.5. Conclusions

Based on Floquet theory, we developed an approach to determine the stability of motion in discrete models of spatiotemporally modulated materials. We highlighted the effect of the modulation amplitude and modulation phase (wavenumber) on stability, presented graphically by the stability chart. We provided a measure to quantify the degree of nonreciprocity in terms of transmitted energy in the steady state, the norm bias. We used the norm bias to investigate nonreciprocal energy transmission in modulated systems with different length and modulation strength. We showed that a long system with weak modulations and a short system with strong modulations can provide similar values of norm bias. Furthermore, nearly unidirectional vibration transmission can happen not only in very long modulated systems, but also in short systems with very strong modulations. We used the stability chart to identify unstable ranges of modulation phase for a strong modulation amplitude; unstable response must be avoided in operation of devices with spatiotemporally modulated properties.

Stability analysis based on Floquet theory is critical in investigating nonreciprocal vibration transmission in systems with strong modulation because unbounded response is often encountered at higher amplitudes of modulation. It complements the results of the averaging method, which is commonly used to analyze the response of modulated systems. The approach presented in this work motivates further parametric studies on materials with strong modulations.

References

[1] J. D. Achenbach, Reciprocity in elastodynamics, Cambridge University Press, Cambridge, UK, 2003.

[2] S. Andrieux, A. B. Abda, H. D. Bui, "Reciprocity principle and crack identification," *Inverse Problems*, vol. 15, no. 1, pp. 59-65, 1999.

[3] T. Ten Wolde, "Reciprocity measurements in acoustical and mechano-acoustical systems. Review of theory and applications," *Acta Acustica united with Acustica*, vol. 96, no. 1, pp. 1 - 13, 2010.

[4] H. Nassar, B. Yousefzadeh, R. Fleury, M. Ruzzene, A. Alù, C. Daraio, A. N. Norris, G. Huang, M. R. Haberman, "Nonreciprocity in Acoustic and Elastic Materials," *Nature Reviews Materials*, vol. 5, pp. 667-685, 2020.

[5] K. A. Lurie, An Introduction to the Mathematical Theory of Dynamic Materials, Second Edition, Springer Cham, 2017.

[6] B. Goldsberry, S. Wallen and M. Haberman, "Non-reciprocal wave propagation in mechanically-modulated continuous elastic metamaterials," *Journal of the Acoustical Society of America*, vol. 146, pp. 782-8, 2019.

[7] G. Trainiti, M. Ruzzene, "Non-reciprocal Elastic Wave Propagation in Spatiotemporal Periodic Structures," *New Journal of Physics*, vol. 18, p. 083047, 2016.

[8] E. Riva, J. Marconi, G. Cazzulani, F. Braghin, "Generalized Plane Wave Expansion Method for Non-reciprocal Discretely Modulated Waveguides," *Journal of Sound and Vibration*, vol. 449, pp. 172-181, 2019.

[9] M. A. Attarzadeh, M. Nouh, "Elastic Wave Propagation in Moving Phononic Crystals and Correlations with Stationary Spatiotemporally Modulated Systems," *AIP Advances*, vol. 8, p. 105302, 2018.

[10] H. Nassar, X. C. Xu, A. N. Norris, G. L. Huang, "Modulated Phononic Crystals: Non-reciprocal Wave Propagation and Willis Materials," *Journal of the Mechanics and Physics of Solids*, vol. 101, pp. 10-29, 2017.

[11] H. Nassar, H. Chen, A. N. Norris, M. R. Haberman, "Non-reciprocal Wave Propagation in Modulated Elastic Metamaterials," *Proc. R. Soc. A*, vol. 473, no. 2202, 2017.

[12] Y. Wang, B. Yousefzadeh, H. Chen, H. Nassar, G. Huang, C. Daraio, "Observation of Nonreciprocal Wave Propagation in a Dynamic Phononic Lattice," *Physical Review Letters*, vol. 121, no. 19, p. 194301, 2018.

[13] S. Wan, L. Cao, Y. Zeng, T. Guo, M. Oudich, B. Assouar, "Low-Frequency Nonreciprocal Flexural Wave Propagation via Compact Cascaded Time-Modulated Resonators," *Applied Physics Letters*, vol. 120, no. 23, p. 231701, 2022.

[14] Y. Chen, X. Li, H. Nassar, A.N. Norris, C. Daraio, G. Huang, "Nonreciprocal wave propagation in a continuum-based metamaterial with space-time modulated resonators," *Physical Review Applied*, vol. 11, no. 6, p. 064052, 2019.

[15] B. L. Kim, C. Daraio, C. Chong, S. Hajarolasvadi, Y. Wang, "Dynamics of time-modulated, nonlinear phononic lattices," *Physical Review E*, vol. 107, p. 034211, 2023.

[16] J. Wu, B. Yousefzadeh, "On Vibration Transmission Reciprocity In Modulated Materials," *Proceedings of Canadian Society for Mechanical Engineering International Congress*, Edmonton, 2022.

[17] J. Wu, B. Yousefzadeh, "Numerical Analysis of Phase Nonreciprocity in a Linear Spatiotemporally Modulated System," *Proceedings of the International Design Engineering Technical Conferences*, Boston, 2023.

[18] I. Kovacic, R. Rand, S. M. Sah, "Mathieu's Equation and Its Generalizations: Overview of Stability Charts and Their Features," *Applied Mechanics Reviews*, vol. 70, no. 2, p. 020802, 2018.

[19] Rand, R. H., "Lecture Notes on Nonlinear Vibrations (Version 53)," Cornell University, Ithaca, NY, 2017, accessed January 16, 2024, http://dspace.library.cornell.edu/handle/1813/28989.

D. Nonreciprocal dynamics of spatiotemporally varying materials: strong modulations

D.1. Introduction

Propagation of mechanical waves in elastic materials has been studied for about three centuries, dating back to Sir Newton's study of sound propagation in air [1]. For a regular material with constant density and Young's modulus, wave propagation characteristics between two arbitrary points remain invariant after interchanging the locations of the vibration source and receiver. This symmetry property, known as the principle of reciprocity, remains valid for propagation of small-amplitude waves in materials with properties that do not change with time; i.e. linear time-invariant systems. Within this context, it is not possible for waves to have different transmission characteristics (e.g. changes in amplitude and phase) depending on the direction of travel between two points. Such asymmetric wave transmission can be utilized for development of novel vibration mitigation devices and energy harvesting mechanisms, for example. Accordingly, there the physics and engineering of nonreciprocal propagation of elastic waves has recently drawn the attention of many researchers [2].

Nonreciprocal wave propagation has recently been investigated in the context of periodic materials, both for discrete and continuous models. Periodic materials provide an amenable context for this study because their wave propagation characteristics are dictated by the properties of their repeating sub-structure, also known as the unit cell. Nonreciprocal and directional propagation was analyzed in a discrete infinite-long modulated metamaterial, in which a wave-like temporal-spatial modulation was added to stiffness coefficient of the resonant spring in every unit cell [3]. Within the one-dimensional structure, directional scattered waves are generated because of the modulation. The scattered waves are coupled to the incident wave at certain frequencies, resulting in nonreciprocal propagation. For uniform continuous media, researchers found the appearance of nonreciprocity due to temporal-spatial modulation in Young's modulus of the media [4-6], as well as both Young's modulus and density (two-phase modulation) [7]. A similar nonreciprocal wave propagation phenomenon can be realized in elastic metasurfaces by means of temporal-spatial modulation of resonant springs at the surface [8,9].

In experimental demonstration of nonreciprocity due to temporal-spatial modulations, periodic systems naturally comprise only a few units. For example, the temporal-spatial modulations have been realized by means of magnetic forces [10,11]. The spatial modulation, in particular, corresponds to a constant phase shift between the modulated elasticity of adjacent units. This spatial phase shift is as essential in breaking reciprocity as the temporal modulation. To investigate this in more detail, we focus in this work on the special case of a system with two degrees of freedom (2DoF). Our goal is to systematically study the influence of system parameters on the reciprocity of vibration transmission in this system, highlighting the significance of modulation phase shift and nonlinear elasticity. This will be the first building block for investigating the combined effects of modulation and nonlinearity in modulated materials.

In Section D.2, the problem formulation and methodology are introduced. In Section D.3, the effects of system parameters on nonreciprocity are presented in the linear operating range. The influence of nonlinear elasticity on nonreciprocity is described in Section D.4. We conclude in Section D.5 by summarizing our findings and pointing out directions for future work.

D.2. Analysis of a 2DoF system with modulation

We consider a 2DoF system composed of two identical masses, viscous dampers, coupling springs and weakly modulated grounding springs with nonlinearity. On each of the two masses, there is an external force applied. The two external forces have the same frequency. See Fig. D.1.

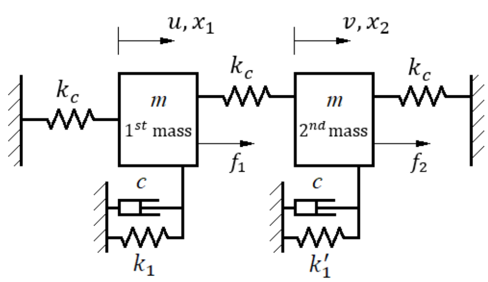

Figure D.1: Scheme of the 2DoF system. Each grounding spring has three components: a constant term, a time-dependent term and a nonlinear (amplitude-dependent) term.

D.2.1. A. Formulation of the problem

The equations of motion for the system in Fig. D.1 are:

$$\begin{aligned} m\ddot{u} + c\dot{u} + (2k_c + k_1)\,u - k_c v &= F_1 \cos(\omega_f t)\,, \\ m\ddot{v} + c\dot{v} + (2k_c + k_1')\,v - k_c u &= F_2 \cos(\omega_f t)\,, \end{aligned} \tag{D.1}$$

where $k_1 = k_L + k_m \cos(\omega_m t) + k_N u^2$ and $k_1' = k_L + k_m \cos(\omega_m t - \phi) + k_N v^2$. The phase shift ϕ represents a spatial modulation in the grounding stiffness of each mass. We introduce the following parameters to non-dimensionalize the governing equations: $t = \tau/\omega_0$, $\omega_0^2 = (2k_c + k_L)/m$, $\omega_m = \Omega_m \omega_0$, $\omega_f = \Omega_f \omega_0$, $c = 2\zeta m \omega_0$, $k_c = K_c(2k_c + k_L)$, $k_m = K_m(2k_c + k_L)$,

$k_N = K_N(2k_c + k_L)/a^2$, $F_1 = a(2k_c + k_L)P_1$, $F_2 = a(2k_c + k_L)P_2$, $u(t) = ax_1(\tau)$ and $v(t) = ax_2(\tau)$, where a is a representative length, The governing equations (D.1) are therefore rewritten as:

$$\begin{aligned} \frac{\mathrm{d}^2}{\mathrm{d}\tau^2}x_1 + 2\zeta\frac{\mathrm{d}}{\mathrm{d}\tau}x_1 + \left[1 + K_m\cos\left(\Omega_m\tau\right)\right]x_1 + K_N x_1^3 - K_c x_2 = P_1\cos\left(\Omega_f\tau\right), \\ \frac{\mathrm{d}^2}{\mathrm{d}\tau^2}x_2 + 2\zeta\frac{\mathrm{d}}{\mathrm{d}\tau}x_2 + \left[1 + K_m\cos\left(\Omega_m\tau - \phi\right)\right]x_2 + K_N x_2^3 - K_c x_1 = P_2\cos\left(\Omega_f\tau\right). \end{aligned} \tag{D.2}$$

Our focus is on investigating the steady-state response of the system. In order to distinguish the two directions of wave propagation (left to right versus right to left), two configurations are defined: (i) the *forward* configuration with $P_1 = P$ and $P_n = 0$ where the output is the steady-state response of the second mass $x_2^F(\tau)$; (ii) the *backward* configuration with $P_1 = 0$ and $P_n = P$ where the output is the steady-state response of the first mass $x_1^B(\tau)$. If and only if $x_2^F(\tau) = x_1^B(\tau)$, vibration transmission through the system is reciprocal. The reciprocity bias R is introduced to quantify the degree of nonreciprocity between the outputs of forward and backward configurations:

$$R = \lim_{T\to\infty}\sqrt{\frac{1}{T}\int_0^T [x_2^F(\tau) - x_1^B(\tau)]^2 d\tau} \tag{D.3}$$

If $R = 0$, the vibration transmission is reciprocal; otherwise, the transmission is nonreciprocal [12]. Output norms N^F and N^B are introduced to represent the response in the forward and backward configurations respectively:

$$\begin{aligned} N^F &= \lim_{T\to\infty}\sqrt{\frac{1}{T}\int_0^T [x_2^F(\tau)]^2 d\tau}, \\ N^B &= \lim_{T\to\infty}\sqrt{\frac{1}{T}\int_0^T [x_1^B(\tau)]^2 d\tau}. \end{aligned} \tag{D.4}$$

In direct numerical simulations, the norms in (D.3) & (D.4) are evaluated after the steady state is reached.

D.2.2. Solution methodology

Approximating the solutions of (D.2) is the key strategy to estimate the displacement output in the steady-state. The steady-state displacement output of the 2DoF system in different configurations is expressed by the expansion in Fourier series:

$$\begin{aligned} x_2^F(\tau) &= \sum_{n=-\infty}^{\infty}\left[\left(\frac{\hat{\xi}_n}{2}e^{in\Omega_m\tau}\right)e^{i\Omega_f\tau} + c.c.\right], \\ x_1^B(\tau) &= \sum_{n=-\infty}^{\infty}\left[\left(\frac{\hat{\eta}_n}{2}e^{in\Omega_m\tau}\right)e^{i\Omega_f\tau} + c.c.\right], \end{aligned} \tag{D.5}$$

where *c.c.* represents the corresponding complex conjugate, $\hat{\xi}_n$ and $\hat{\eta}_n$ are complex-valued amplitudes for a given Ω_f. The representation of the displacement in (D.5) points out an important characteristic of the steady-state response of the systems subject to simultaneous external and parametric excitation: the response contains spectral components not only at the frequency of the external force, Ω_f, but also at $\Omega_f \pm \Omega_m$, $\Omega_f \pm 2\Omega_m$, and so on. To find the amplitudes, $\hat{\xi}_n$ and $\hat{\eta}_n$, we substitute (D.5) into (D.2) and integrate the result over one modulation period. This procedure yields a system of nonlinear algebraic equations for the amplitudes $\hat{\xi}_n$ and $\hat{\eta}_n$, which can be solved numerically. We refer to this procedure as the averaging method.

The transient response is computed by using the Runge-Kutta method [13]. We use the results from direct numerical integration of the governing equations to validate the predictions made by the averaging method.

Fig. D.2 shows the output norms calculated for (D.2) for the following parameters: $\Omega_m = 0.15$, $K_m = 0.1$, $K_c = 0.44$, $\zeta = 0.02$ and $P = 0.1$. There is very good agreement between the analytical and numerical prediction of the steady-state response. Thus, we will use the analytical approach in the remainder of this work. Unless otherwise stated, these parameters are used in examples in other sections as well.

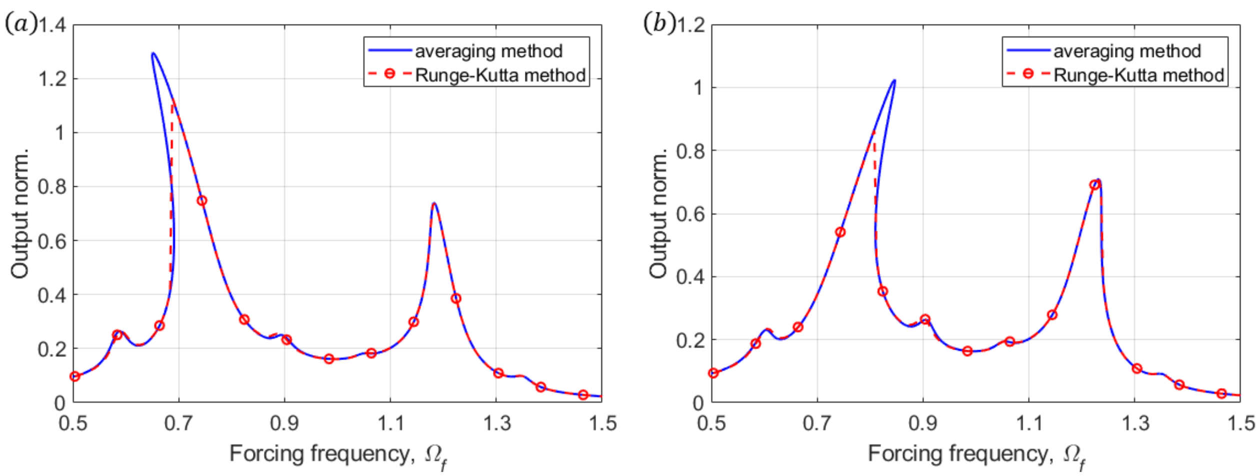

Figure D.2: Comparison between the results of averaging method and numerical simulation. (a): forward configuration with $K_N = -0.05$, $\phi = 0.5\pi$; (b): backward configuration with $K_N = 0.1$, $\phi = 0.5\pi$.

D.3. Nonreciprocal vibration transmission in linear modulated systems

We first investigate nonreciprocity in the linear modulated system; *i.e.* $K_N = 0$ in (D.2). This will establish the importance of linear system parameters on breaking reciprocity. In this work, we only discuss the case of weakly modulated systems ($K_m \leq 0.1$). The methodology presented in Section D.3.2, however, remains valid even for strong modulations.

D.3.1. Effects of K_c and Ω_m in the modulated linear systems

We start by considering the system with temporal modulations only; *i.e.* $\phi = 0$. In this case, the parameter K_c determines the two natural frequencies (dimensionless) of an unmodulated linear system: $\sqrt{1 \pm K_c}$, which are approximately the primary resonant frequencies of a weakly modulated linear system (indicated by the green solid arrows in Fig. D.3). The secondary resonant frequencies of a weakly modulated linear system occur near frequencies $\sqrt{1 \pm K_c} \pm \Omega_m$ (indicated by the green hollow arrows in Fig. D.3), with each pair corresponding to one of the natural frequencies of the unmodulated system. Due to the mirror-symmetry of the system, response is reciprocal.

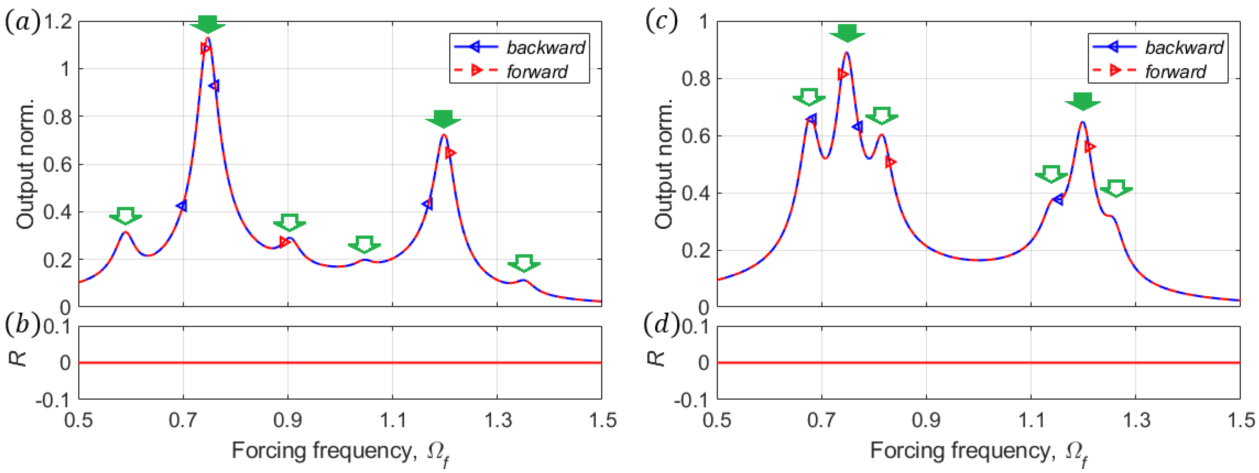

Figure D.3: Effect of K_c and Ω_m on the response of the system with temporal modulation ($\phi = 0$). (a) and (c) are plots of the output norms for forward and backward configurations with respect to forcing frequency. (b) and (d) are plots of reciprocity bias of the systems represent by (a) and (c) respectively. The green solid arrows indicate primary resonances, the green hollow arrows indicate secondary resonances. In both 2DoF systems: $K_N = 0$, (a) and (b): $\Omega_m = 0.15$, (c) and (d): $\Omega_m = 0.05$. In (b) and (d), reciprocity bias is equal to zero over the frequency range, responses of both systems are reciprocal.

D.3.2. Effect of ϕ in the modulated linear system

When $\phi \neq 0$, the modulated system is no longer mirror-symmetric. Thus, the transmission is no longer reciprocal. Fig. D.4 shows the output norms and reciprocity bias of the system at two different values of ϕ. As expected, the degree of nonreciprocity can be controlled by ϕ, the difference in the modulation phases of the two degrees of freedom.

Notice that the output norms in panels (a) and (e) are very similar, but the corresponding reciprocity bias in panels (b) and (f) remain non-zero. This implies that a significant contribution to non-reciprocity is possibly due to the phase difference between the response in the forward and backward configurations. It can be verified in panels (d) and (h). A similar phenomenon may occur when $K_m = 0$ and $K_N \neq 0$ [12].

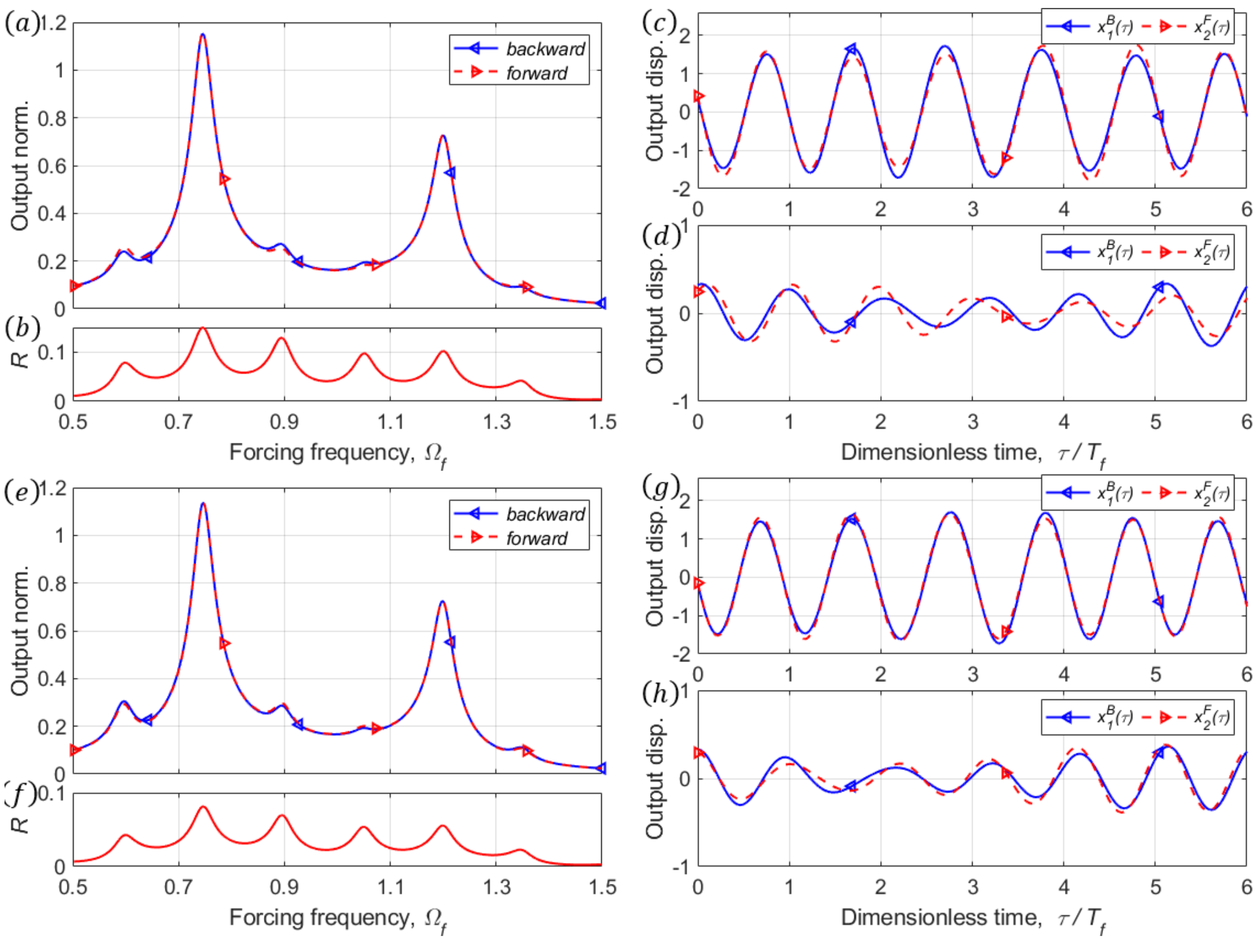

Figure D.4: Effect of ϕ on reciprocity for the linear system, $K_N = 0$. Panels (a)-(d): $\phi = 0.5\pi$, (e)-(h): $\phi = -0.25\pi$. Panels (c), (d), (g) and (h): output displacement at different values of forcing frequency, Ω_f, (c) and (g) $\Omega_f = 0.748$, (d) and (h) $\Omega_f = 1.05$. $T_f = 2\pi/\Omega_f$
.

D.4. Nonreciprocal vibration transmission in nonlinear modulated systems

Although the operation of mechanical systems is traditionally based on their linear response, it is sometimes beneficial or necessary to consider the influence of nonlinear forces, particularly in experiments [10]. Therefore, we investigate the influence of nonlinear elasticity on the nonreciprocity of vibration transmission in our 2DoF system.

We consider both the hardening ($K_N = 0.1 > 0$) and softening ($K_N = -0.05 < 0$) types of nonlinearity. Fig. D.5 shows the output norms of the nonlinear system as a function of forcing amplitude, P. Given that the coupling force is linear, the influence of nonlinearity is larger on the response near the in-phase modes (near 0.75). The steady-state response of (D.2) with $K_N \in \{-0.05, 0.1\}$ and $P \in \{0.06, 0.08, 0.1\}$ is calculated using the averaging method, and the output norms for forward and backward configurations are shown in Fig. D.5. As expected, the primary and secondary resonant frequencies are all amplitude-dependent.

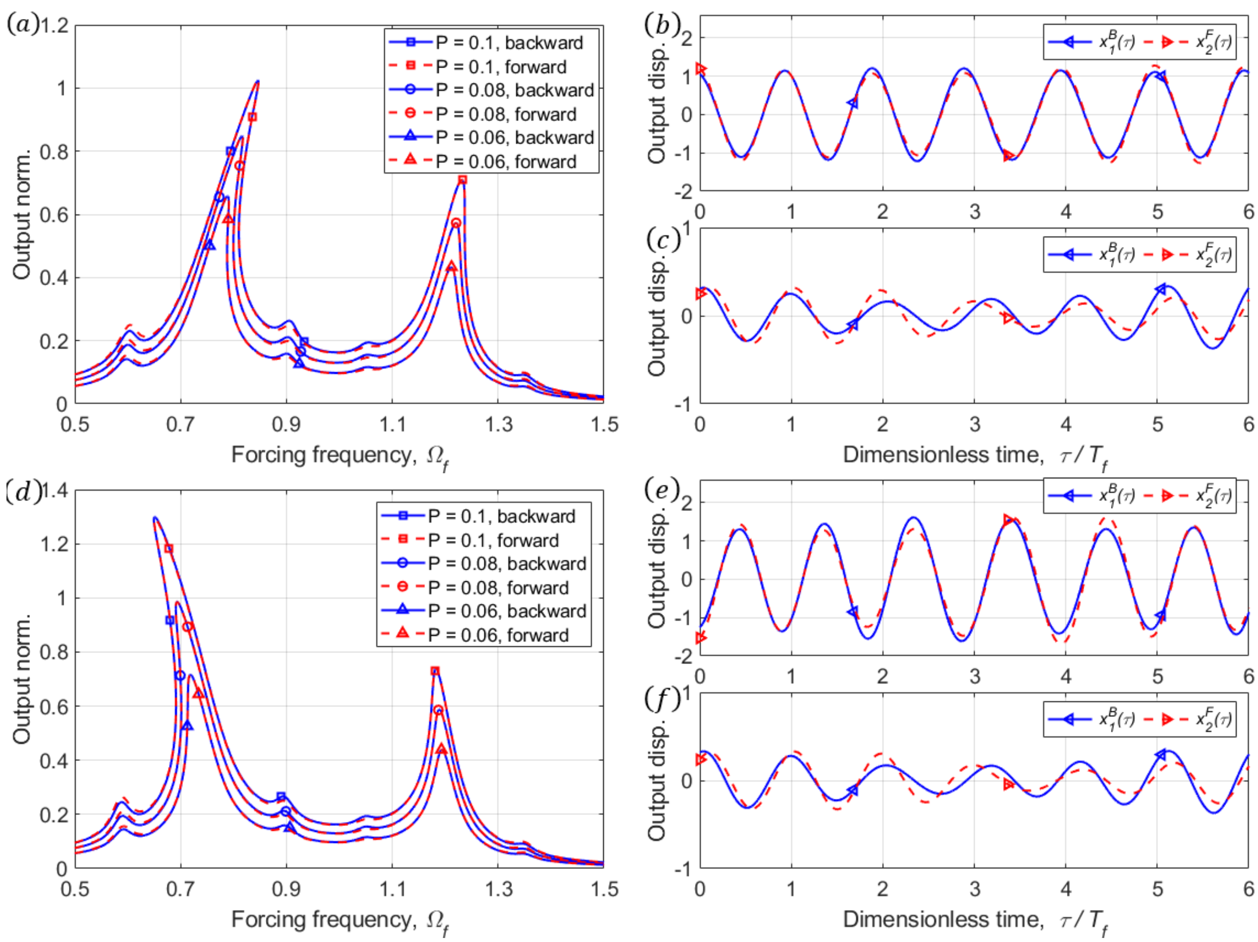

Figure D.5: Steady-state responses of 2DoF nonlinear systems in forward and backward configurations with different excitations, (a)-(c): $K_N = 0.1$, $\phi = 0.5\pi$; (d)-(f): $K_N = -0.05$, $\phi = 0.5\pi$. Panels (b), (c), (e) and (f): output displacement at different values of forcing frequency, Ω_f, (b) $\Omega_f = 0.8$, (c) and (f) $\Omega_f = 1.05$, (e) $\Omega_f = 0.7$.

We use the normalized reciprocity bias, R/P, to study the effect of the forcing amplitude on the degree of nonreciprocity. For the linear system, the degree of nonreciprocity does not depend on the amplitude of motion; this can be inferred by the three overlapping curves in Fig. D.6(a). For the nonlinear system, panels (b) and (c) in Fig. D.6 show that the degree of nonreciprocity depends on the forcing amplitude, as expected. Interestingly, increasing the forcing amplitude increases the normalized reciprocity bias for the system with hardening nonlinearity, while it has the opposite effect in the system with softening nonlinearity. Note that the most significant effect of nonlinearity is observed near the primary in-phase resonance peak in both cases.

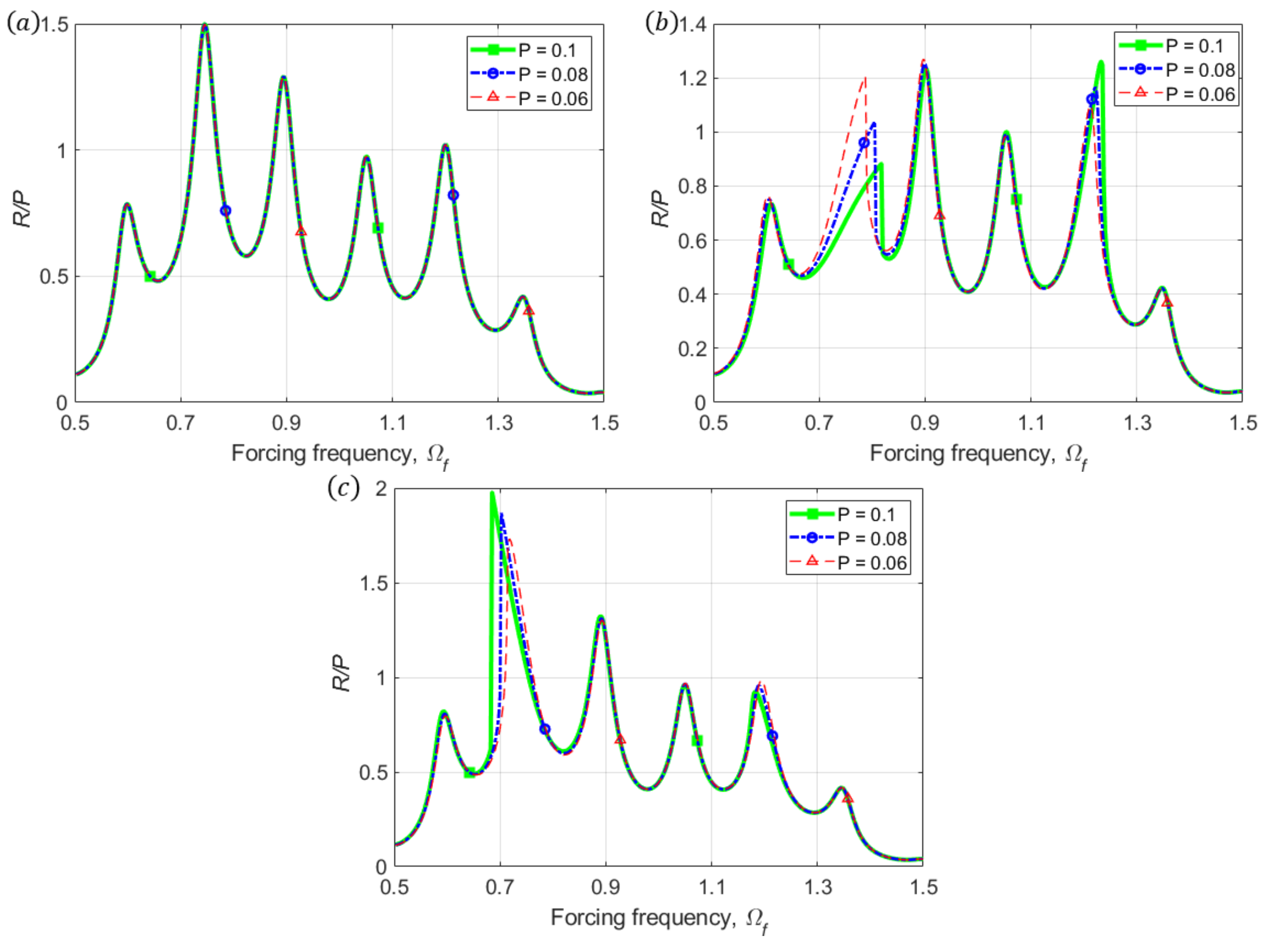

Figure D.6: Plots of normalized reciprocity bias, R/P. (a): a 2DoF linear modulated system, $K_N = 0$ and $\phi = 0.5\pi$. (b): a 2DoF nonlinear modulated system, $K_N = 0.1$ and $\phi = 0.5\pi$. (c): a 2DoF nonlinear modulated system, $K_N = -0.05$ and $\phi = 0.5\pi$.

D.5. Conclusions

We studied the reciprocity of vibration transmission in a discrete model of modulated materials. Temporal-spatial modulation in the stiffness coefficient is the key factor in breaking the reciprocity invariance in coupled systems, within which the phase shift between two adjacent modulations presents the modulation in space. Nonreciprocity in coupled modulated systems can be quantified using the reciprocity bias. We observed that having equal output norms for the forward and backward configurations is not a sufficient test for reciprocity. We presented scenarios in which it is the phase difference that plays a major role in increasing the reciprocity bias. In weakly modulated linear systems, the locus of the primary and secondary resonance can be adjusted by manipulating the coupling stiffness and frequency of modulation. We emphasized the role of the difference in modulation phases of the two units on controlling the reciprocity bias in the linear operating regime. We then reported the influence of cubic (on-site) nonlinearity on the reciprocity bias and highlighted the significance of the type of nonlinearity on how reciprocity depends on the forcing amplitude.

The analysis of coupled modulated systems provides a new perspective on nonreciprocal wave propagation in nonlinear materials. The methodology described in this work facilitates further parametric studies in this context.

References

[1] L. Brillouin, Wave Propagation in Periodic Structures: Electric Filters and Crystal Lattices, Dover Publications, 1953.

[2] H. Nassar, B. Yousefzadeh, R. Fleury, M. Ruzzene, A. Alù, C. Daraio, A. N. Norris, G. Huang, M. R. Haberman, "Nonreciprocity in Acoustic and Elastic Materials," *Nature Reviews Materials*, vol. 5, pp. 667-685, 2020.

[3] H. Nassar, H. Chen, A. N. Norris, M. R. Haberman, "Non-reciprocal Wave Propagation in Modulated Elastic Metamaterials," *Proc. R. Soc. A*, vol. 473, no. 2202, 2017.

[4] G. Trainiti, M. Ruzzene, "Non-reciprocal Elastic Wave Propagation in Spatiotemporal Periodic Structures," *New Journal of Physics*, vol. 18, p. 083047, 2016.

[5] M. A. Attarzadeh, M. Nouh, "Non-reciprocity in Time-periodic Phononic Materials with A Non-zero Moving Velocity," in *Health Monitoring of Structural and Biological Systems XIII*, 2019.

[6] E. Riva, J. Marconi, G. Cazzulani, F. Braghin, "Generalized Plane Wave Expansion Method for Non-reciprocal Discretely Modulated Waveguides," *Journal of Sound and Vibration*, vol. 449, pp. 172-181, 2019.

[7] H. Nassar, X. C. Xu, A. N. Norris, G. L. Huang, "Modulated Phononic Crystals: Non-reciprocal Wave Propagation and Willis Materials," *Journal of the Mechanics and Physics of Solids*, vol. 101, pp. 10-29, 2017.

[8] A. Palermo, P. Celli, B. Yousefzadeh, C. Daraio, A. Marzani, "Surface Wave non-reciprocity via Time-modulated Metamaterials," *Journal of the Mechanics and Physics of Solids*, vol. 145, pp. 104181, 2020.

[9] Q. Wu, H. Chen, H. Nassar, G. Huang, "Non-reciprocal Rayleigh Wave Propagation in Space–time Modulated Surface," *Journal of the Mechanics and Physics of Solids*, vol. 146, pp. 104196, 2021.

[10] Y. Wang, B. Yousefzadeh, H. Chen, H. Nassar, G. Huang, C. Daraio, "Observation of Nonreciprocal Wave Propagation in a Dynamic Phononic Lattice," *Physical Review Letters*, vol. 121, no. 19, p. 194301, 2018.

[11] Y. Chen, X. Li, H. Nassar, A.N. Norris, C. Daraio, G. Huang, "Nonreciprocal wave propagation in a continuum-based metamaterial with space-time modulated resonators," *Physical Review Applied*, vol. 11, no. 6, p. 064052, 2019.

[12] B. Yousefzadeh, "Computation of Nonreciprocal Dynamics in Nonlinear Materials," *Journal of Computational Dynamics*, vol. 9, no. 3, p. 451-464, 2022.

[13] S. S. Rao, Mechanical Vibrations, Sixth Edition, Harlow: Pearson Education, Inc., 2018.